AD NUMBER

ADB064268

NEW LIMITATION CHANGE

TO

Approved for public release, distribution unlimited

FROM

Distribution authorized to U.S. Gov't. agencies only; test and evaluation; Jan. 1982. Other requests shall be referred to AFRPL/[STINFO] TSPR, Edwards AFB, CA 93523.

AUTHORITY

AFRPL ltr, 24 Oct 1984

AFRPL-TR-82-07

UTC/CSD 2632-FR
UTC-United Technologies Corporation
CSD-Chemical Systems Division

HOT BALL AND SOCKET THRUST VECTOR CONTROL

R. A. Ellis
W. J. Kearney

Chemical Systems Division
1050 E. Arques
Sunnyvale, CA 94086

AD B064258

March 1982
Final Report for Period 1 March 1977 - 31 January 1982

Distribution limited to U. S. Government agencies only; test and evaluation; January 1982. Other requests for this document must be referred to AFRPL (STINFO)/TSPR, Edwards AFB, CA 93523.

FOREIGN DISCLOSURE PROHIBITED

Public release or foreign disclosure of this document is prohibited by the United States Department of State Munitions control Newsletter No. 35 dated April 1977 which places carbon-carbon composites technology within the purview of the Munitions List, and therefore subject to the export control requirements of the Department's International Traffic in Arms Regulations.

Prepared for

AIR FORCE ROCKET PROPULSION LABORATORY
DIRECTOR OF SCIENCE AND TECHNOLOGY
AIR FORCE SYSTEMS COMMAND, USAF
EDWARDS AIR FORCE BASE, CA 93523

82 05 07 011

NOTICE

When U.S. Government drawings, specifications, or other data are used for any purpose other than a definitely related government procurement operation, the Government thereby incurs no responsibility nor any obligations whatsoever, and the fact that the Government may have formulated, furnished, or in any way supplied the said drawings, specifications or other data, is not to be regarded by implication or otherwise, or in any manner licensing the holder or any other person or corporation, or conveying rights or permission to manufacture, use, or sell any patented invention that may in any way be related thereto.

FOREWORD

This report was submitted by Chemical Systems Division under contract No. F04611-77-C-0017, job order No. 305909 FI with the Air Force Rocket Propulsion Laboratory, Edwards AFB, CA 93523.

The CSD work was managed by R. A. Ellis, Program Manager. The Project Engineer was W. J. Kearney. The Air Force Project Manager was T. L. Kinsel.

This technical report is approved for release and distribution in accordance with the distribution statement on the cover and on the DD Form 1473.

Thomas L. K[illegible], Project Manager
Ballistic Missile Propulsion Section

Arnold Crelier, Major USAF, Chief
Ballistic Missile and Space Propulsion Branch

FOR THE COMMANDER

Charles R. Cooke, Director
Solid Rocket Division

UNCLASSIFIED

SECURITY CLASSIFICATION OF THIS PAGE (When Data Entered)

REPORT DOCUMENTATION PAGE

READ INSTRUCTIONS BEFORE COMPLETING FORM

1. REPORT NUMBER AFRPL-TR-82-07	2. GOVT ACCESSION NO. AD-B064	3. RECIPIENT'S CATALOG NUMBER 268L
4. TITLE (and Subtitle) Hot Ball and Socket Thrust Vector Control		5. TYPE OF REPORT & PERIOD COVERED Final Technical Report 1 March 1977-31 January 1982
		6. PERFORMING ORG. REPORT NUMBER
7. AUTHOR(s) R. A. Ellis/W. J. Kearney		8. CONTRACT OR GRANT NUMBER(s) F04611-77-C-0017
9. PERFORMING ORGANIZATION NAME AND ADDRESS Chemical Systems Division, United Technologies P.O. Box 358 Sunnyvale, CA 94086		10. PROGRAM ELEMENT, PROJECT, TASK AREA & WORK UNIT NUMBERS 305909 FI
11. CONTROLLING OFFICE NAME AND ADDRESS AFRPL, Director of Science and Technology Air Force Rocket Propulsion Laboratory Edwards Air Force Base, CA 93523		12. REPORT DATE March 1982
		13. NUMBER OF PAGES 159
14. MONITORING AGENCY NAME & ADDRESS (if different from Controlling Office) AFPRO, Chemical Systems Division P.O. Box 358 Sunnyvale, CA 94086		15. SECURITY CLASS. (of this report) Unclassified
		15a. DECLASSIFICATION/DOWNGRADING SCHEDULE

16. DISTRIBUTION STATEMENT (of this Report)

Distribution limited to U.S. Government agencies only. Test and evaluation data, January 1982. Other requests for this document must be referred to the AFRPL/(STINFO) TSPR, Edwards AFB, CA 93523.

17. DISTRIBUTION STATEMENT (of the abstract entered in Block 20, if different from Report)

18. SUPPLEMENTARY NOTES

19. KEY WORDS (Continue on reverse side if necessary and identify by block number)

Solid Rocket; Nozzle; Thrust Vector Control; Carbon-Carbon; Material Evaluation.

20. ABSTRACT (Continue on reverse side if necessary and identify by block number)

Two 7 in. throat diameter hot ball and socket TVC nozzles were designed, fabricated and assembled by CSD for test on the AFRPL SLSH test motor. The first, tested 8 February 1979, experienced an average pressure of 1355 psia over a 60 sec duration with a 90% solids 21% aluminum HTPB propellant. Failure of the 3D C-C exit cone and loss of TVC occurred at 18.7 sec. Up to the time of failure, 16 deg of TVC travel was accomplished. The ball/throat survived the remainder of the firing duration.

DD FORM 1473 1 JAN 73 EDITION OF 1 NOV 65 IS OBSOLETE

UNCLASSIFIED

SECURITY CLASSIFICATION OF THIS PAGE (When Data Entered)

The second nozzle, tested 20 November 1981, incorporated design modifications to the first nozzle and was tested on the SLSH motor at AFRPL under conditions representative of advanced upper stage applications. With a 90% solids, 20% aluminum HTPB type propellant with 12% HMX the average pressure over the 75 sec duration was 688 psia. Due to problems associated with the actuation system, 100% success was not achieved, however, significant accomplishments were recognized.

Results of the development and testing of these two nozzles are prese ed in this final report. Recommendations for further development have also been included.

CONTENTS

CONTENTS (Continued)

ILLUSTRATIONS

ILLUSTRATIONS (Continued)

ILLUSTRATIONS (Continued)

ILLUSTRATIONS (Continued)

ILLUSTRATIONS (Continued)

ILLUSTRATIONS (Continued)

TABLES

BLANK PAGE

1.0 INTRODUCTION

This final technical report is submitted in compliance with contract data requirements list (CDRL) sequence number 6, DD form 1423, contract No. F04611-77-C-0017, "Hot Ball and Socket TVC".

The scope of work covered by the above contract included four phases as follows:

Phase I - Program Plan and Nozzle Design
Phase II - Fabrication and Testing
Phase III - Nozzle Redesign and Supporting Efforts
Phase IV - Fabrication and Testing, Second 7-in. Nozzle

The basic program consisted of phases I and II. The primary objective of the basic two-phase technical effort was to demonstrate the capability of a hot ball and socket (HBS) thrust vector control (TVC) system to perform to the requirements typical of the MX first stage nozzle (1,400 psia for 60 sec with a 90% solids/21% aluminum (Al) hydroxyl-terminated polybutadiene (HTPB) type propellant). The first phase involved the design and analysis of a 7-in. throat diameter (D_t) HBS nozzle TVC system. The second phase encompassed the fabrication and static test firing at the Air Force Rocket Propulsion Laboratory (AFRPL) of one nozzle and TVC system.

Phases III and IV were later added to the basic program following the exit cone failure experienced during test firing of the first 7-in. D_t nozzle. The primary objective of the add-on effort was to correct the problems encountered during the first test and demonstrate successful operation of the 7-in. D_t HBS under conditions representative of advanced upper-stage applications, approximately 750 psia for 75 sec with a propellant of moderate erosiveness.

Phase III covered modification of the design of phase I, analysis of the modified design, laboratory testing and subscale firing to support the redesign effort. Phase IV included fabrication of the second 7-in. D_t nozzle, material property testing, nozzle bench testing, static firing at AFRPL and, subsequent posttest analysis.

The period of performance for phases I and II covered from March 1977 through November 1979. The first nozzle was static test fired 8 February 1979. Phases III and IV covered the period April 1980 through January 1982. The second nozzle was static fired 20 November 1981.

Prior to testing the first 7-in. D_t nozzle, Chemical Systems Division (CSD) experience with the HBS TVC nozzle consisted of two completely successful firing demonstrations of 2-in. D_t nozzles. The first, developed under Independent Research and Development (IR&D) funding and tested May 1976 at AFRPL, demonstrated single plane vectoring of ±8 deg at an average pressure of 850 psia for 11 sec. The second, tested at CSD in August 1978 under Naval Surface Weapons Center (NSWC) contract No. N60921-77-C-0240, successfully demonstrated 15 deg omniaxial vector capability at an average pressure of 1,000 psia for 23 sec. These two tests were successful in all respects.

A major scale-up effort was undertaken in the program reported herein. The challenging degree of scaleup can be seen in Figure 1 which compares the 2-in. D_t ball tested in 1978 with the 7-in. D_t ball tested under this program. The first 7-in. D_t nozzle had a throat area over 12 times larger, a test pressure 35% higher with a more severe propellant and was tested on a motor with 50 times the propellant weight than that associated with the NSWC nozzle, the largest tested to that date.

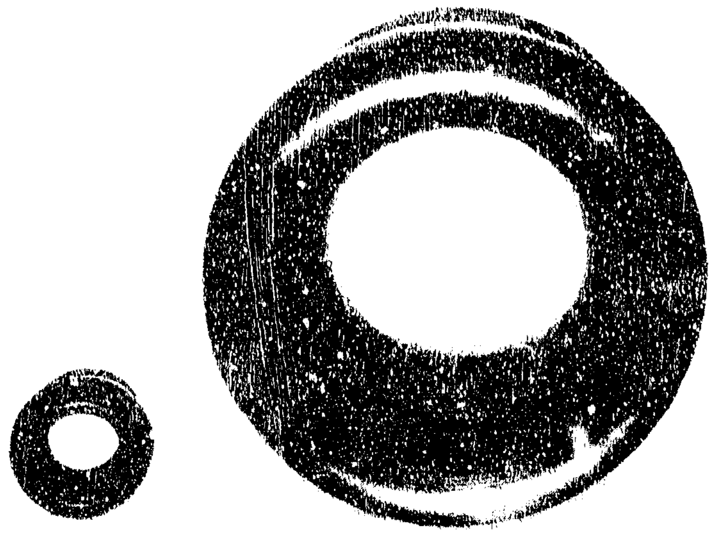

11381-6

Figure 1. C mparison of NSWC 2-in. D_t Ball Tested August 1978 with AFRPL 7-in. D_t Ball Tested February 1979

27259

2.0 SUMMARY

The static test of the first full-scale (7-in. D_t) hot ball and socket (HBS) thrust vector control (TVC) system was planned to demonstrate the integrity of the nozzle system under conditions representative of the MX first stage and to acquire data to define the TVC performance under these conditions. The static test was conducted on the Short Length Super HIPPO (SLSH) motor at test pad 1-52A of the Rocket Propulsion Laboratory, Edwards Air Force Base, California. The propellant was Chemical Systems Division's (CSD) UTP-18803A, a 90% solids, 21% aluminum hydroxyl-terminated polybutadiene (HTPB) formulation. The measured average pressure was 1,355 psia, and the duration was 60 sec.

The system performed as planned up to 10 sec when gas leakage appeared at the threaded interface between the ball extension and the exit cone at an azimuth of about 100 deg. Between 10 and 15 sec the leakage plume grew in size and aft toward the actuator attach ring. A second leakage plume at about 60 deg was observed beginning at 13.9 sec.

At 16.9 sec the leak at the 100 deg azimuth quickly opened up aft to the compliance ring. At 17.3 sec the nozzle began moving as programmed from 8 deg back toward null, but stalled at a 7.5 deg vector angle. The ball remained intact at this angle throughout the remainder of the 60 sec propellant burn.

At 18.6 sec an additional leakage plume was seen at the 330 deg azimuth. A flash was observed at about 190 deg, and the apparent crack at 60 deg opened greatly. At 18.7 sec the exit cone broke up and was extruded through the steel actuator attach ring and ejected. The actuator attach ring was ejected at 19.9 sec.

Essentially all of the ejected nozzle components were recovered. The nozzle was reconstructed to assess the failure, and contour measured to determine material erosion. The ballistic throat erosion rate was 11.0 mils/sec. Key recovered components were forwarded to Southern Research Institute (SoRI) and Atlantic Research Corporation (ARC) for further analysis.

Upon nozzle disassembly and posttest analysis, the socket was found to be cracked. The crack in the socket may have been related to the loss of the exit cone and actuators. The loss of the contribution of the exit to thrust and the loss of the forward actuator bias load (pull-only actuators) nearly tripled the bearing load on the socket.

The following significant problems were observed in the test and posttest analysis:

- Thread leakage, exit breakup, and ball extension loss
- Excessive forward splitline erosion
- Aluminum oxide-deposition leading to TVC system stall
- Cracked socket.

The following was accomplished in the test of nozzle S/N 1:

- Demonstration of survival of the ball and socket at an average pressure of 1,355 psia for the entire planned 60 sec duration
- Successful vectoring through 16 deg of travel for the first 17.3 sec, including deflection to the planned maximum angle of 8 deg
- Command to position accuracy of better than 0.1 deg.

The design of nozzle S/N 1 was modified for nozzle S/N 2 to correct the problems identified in the first test. Laboratory scale testing and a subscale verification firing were conducted to evaluate the modifications planned for nozzle S/N 2. The design modifications included an improved exit cone and joint, a sacrificial entrance extension, carbon-carbon (C-C) surface treatment and a carbon-phenolic lockring as a replacement for the C-C.

The static test of nozzle S/N 2 was conducted on the SLSH motor at the Air Force Rocket Propulsion Laboratory (AFRPL) under conditions representative of advanced upper stage applications. The propellant was CSD's UTP-19687, a 90% solids, 20% aluminum (HTPB) type with 12% cyclotetramethylene tetranitramine (HMX). The measured average pressure over the 75 sec duration was 688 psia.

The nozzle experienced severe annular flow around the ball for 5 sec after ignition. The flow resulted from the inability of the ball to instantaneously translate 0.30-in. from the forward locking to the socket due to the inability of the pull-only actuators to instantaneously backflow hydraulic fluid and allow motion. The actuators held the ball off the socket until the actuator cylinders bled down, at which point the ball sealed on the socket. Aluminum oxide deposition from this temporary flow was extensive on the ball, socket and lockring surfaces, and led to nozzle stall after the first vector event.

Upon posttest disassembly the components were found to be in excellent condition considering the unexpectedly severe conditions to which they were subjected. In fact, the socket, exit cone, metallic structures, and actuation hardware are virtually reusable.

The problems associated with nozzle S/N 2 are summarized as follows:

- The actuation system was unable to instantaneously relieve hydraulic fluid from the actuator cylinders, and prevented the ball from translating 0.30-in. and sealing on the socket for about 5 sec
- During nearly 5 sec of annular flow around the ball, aluminum oxide liberally plated on the ball, socket, and lockring
- The aluminum oxide solified after one successful vector event, stalling the system.

Significant accomplishments recognized include:

- Demonstration of the capability of a large (7-in. D_t) HBS nozzle to survive the thermal/structural environment associated with advanced upper stage conditions
- Demonstration of the tenacity of 3D C-C as evidenced by survival in an unexpectedly adverse environment during the 5-sec of annular flow around the ball, and under subsequent stall forces experienced during the remaining planned duration
- Demonstration of a large C-C ball and socket to provide a non-leaking interface once sealed.

- Demonstration of the effectiveness of the sacrificial entrance to reduce entrance and splitline erosion.
- Acquisition of significant data and experience to enable incorporation of improvements in C-C materials and subsequent HBS TVC designs.

3.0 NOZZLE S/N 1 CONFIGURATION

The first 7-in. D_t nozzle conformed to Chemical Systems Division (CSD) drawing C13179-01-01, "Static Test Assembly - Hot Ball and Socket 8 Deg. TVC Capability". Physical characteristics of the nozzle assembly depicted in Figure 2 included an overall length of 49 in. and a diameter of 40 in. at the interface with the Short Length Super Hippo (SLSH) test motor. The initial throat diameter was 7 in., and the exit plane diameter was 26 in., providing an initial expansion ratio of 13.8.

The ball/integral throat and entrance (ITE), socket, lockring (forward socket) and exit cone were all 3D carbon-carbon (C-C). The billets from which these components were machined were fabricated by Fiber Materials, Inc. (FMI) with Union Carbide T-300 fiber. The ball preform design (Figure 3) was modeled to the 7 in. billets, fabricated by FMI for the AFWAL/ML 7-in. MANTECH program*, except that reinforcement spacing was reduced to 0.080 in. at the throat.

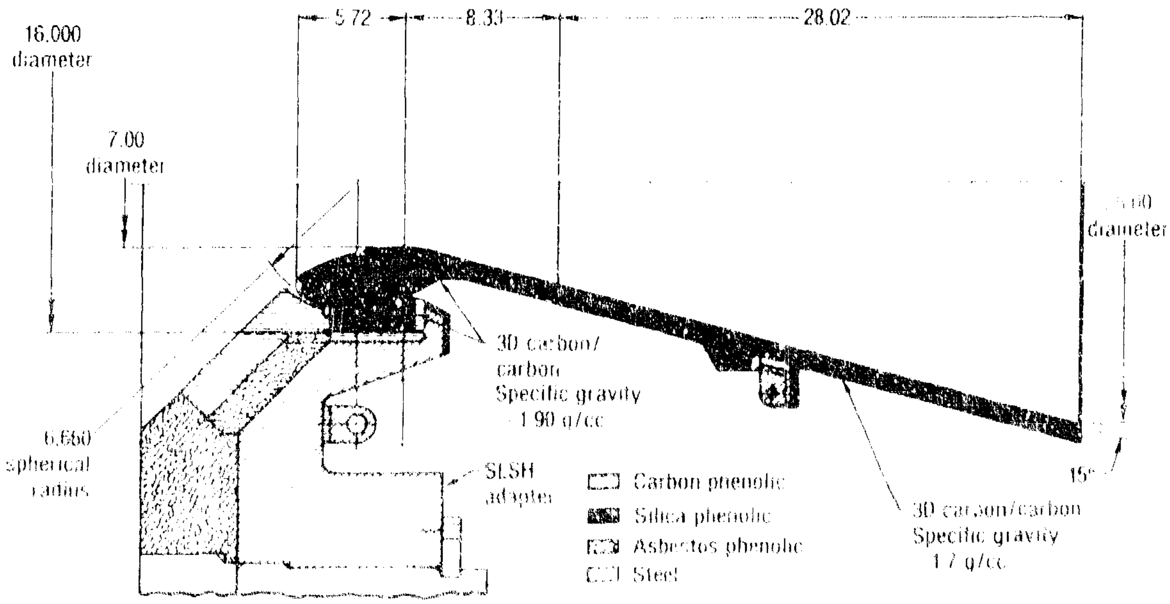

Note: All dimensions are in inches.

Figure 2. Hot Ball and Socket Nozzle and TVC Configuration

21084

* Reference: Contract F33615-77-C-5252

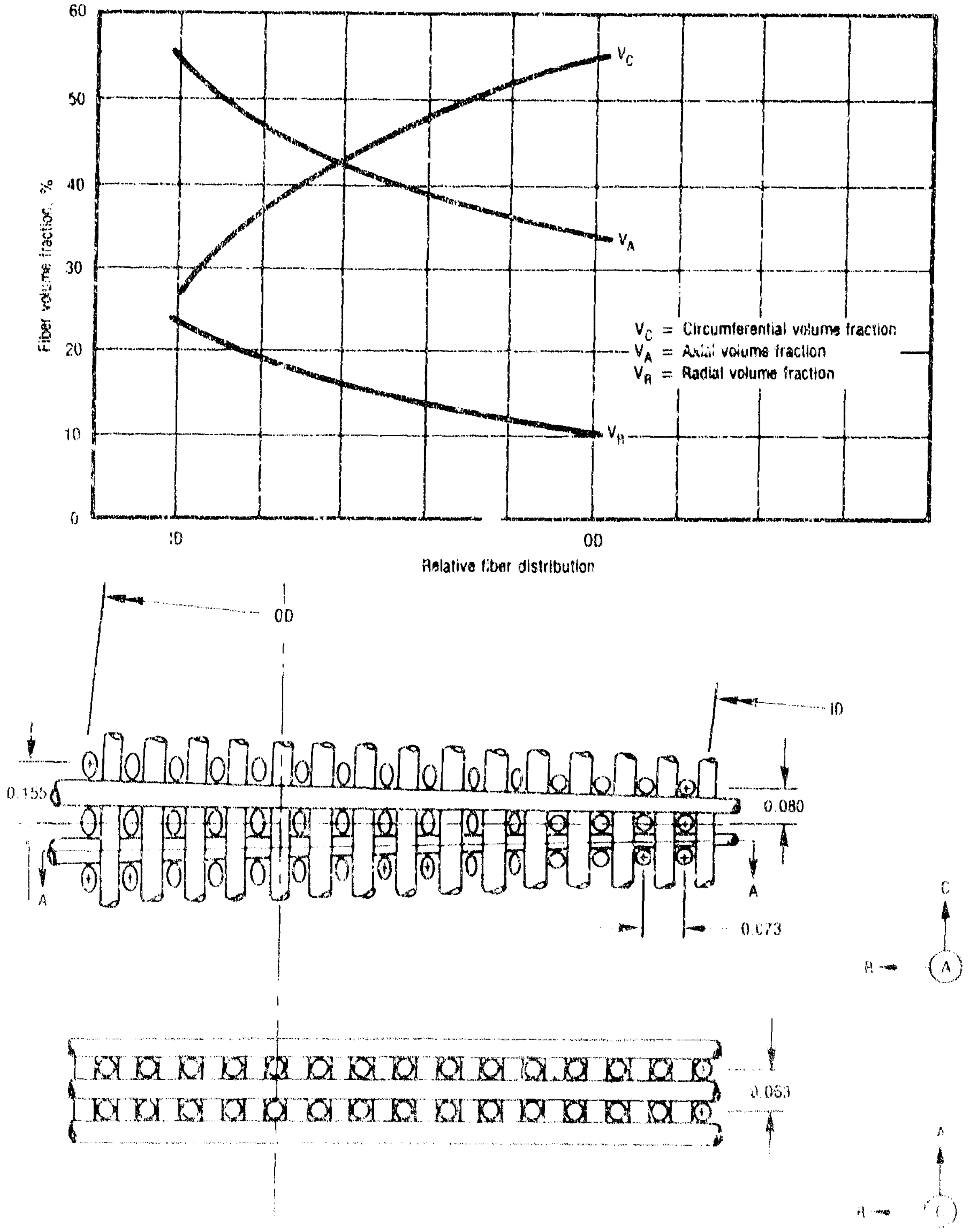

Figure 3. S/N 1 Throat/Ball Preform Design

27260

The socket preform included both the socket and lockring. The socket preform design (Figure 4) reflected an attempt to increase the axial shear-out capability of the finished parts. A 15 deg frustra design was used to enable the axial fiber bundles to contribute to the axial plane shear strength. Weaving the socket preform as a frustra required an increase in the number of axial and radial bundles as the diameter increased to prevent the axial and radial volume fractions from decreasing from the forward to aft end.

The exit cone preform design (Figure 5) contained a 40-40-20 axial, circumferential and radial volume fraction distribution. The exit cone design required a step at about mid-length to accommodate a shear lip for the actuation compliance ring. In addition to increasing the quantity of axial and radial yarn bundles as the diameter increased, the axial bundles were tapered to provide a more uniform volume fraction distribution. This preform presented a major challenge to 3D weaving technology in that it is the largest 3D C-C frustra ever fabricated, and many of the innovations to provide a uniform part had never been attempted on any previous part.

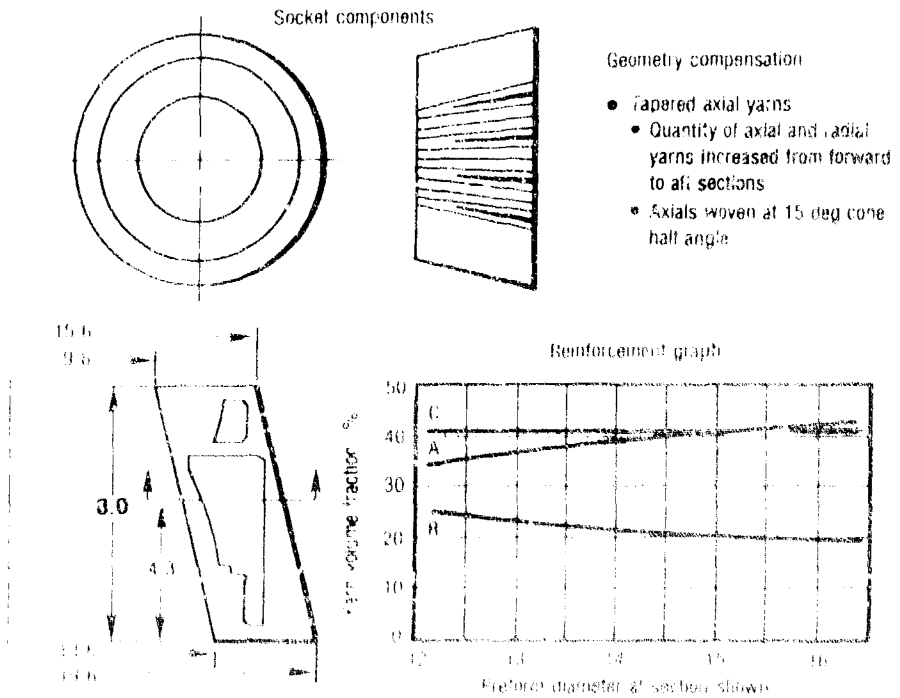

Figure 4. S/N 1 Socket Preform Design

27261

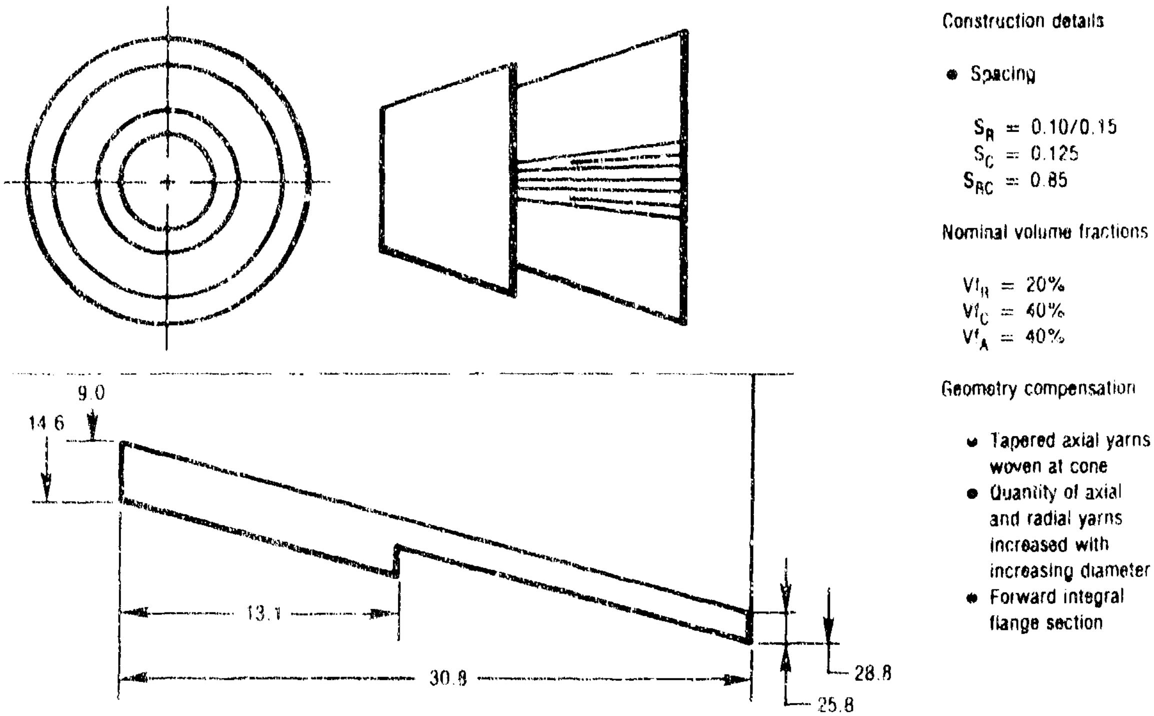

Preform overlay — 3D C-C exit cone

Figure 5. S/N 1 Exit Cone Preform Design

27156

All billets were densified using FMI's 5 ksi pressure-impregnation-carbonization (PIC) process. The impregnant used during densification of the ball and socket billets was allied 15V coal tar pitch. The socket and lockring were subsequently machined from one billet. The final density of the ball and socket billets was 1.9 gm/cc. Ashland A240 petroleum pitch was used for the densification of the exit cone. A summary of the densification process for each billet is summarized in Table 1.

The exit cone also presented a major challenge in densification because of its size and shape. The first two low-pressure cycles were each followed by graphitization. During the initial cycle a problem developed. The cone buckled locally in three locations at the large diameter. Lack of proper frame support during the initial carbonization apparently caused these buckles. During subsequent processing the buckles, or undulations, reduced in severity, but the final machined part still exhibited wrinkles. Following the two low-pressure cycles, the billet was subjected to two 5 ksi PIC cycles, bringing the density to 1.5 to 1.6 gm/cc. At this point low pressure impregnation and atmospheric

TABLE 1. DENSIFICATION PROCESS SUMMARY, NOZZLE S/N 1 BILLETS

20434

	Pitch Impregnant	Low Pressure Impregnation and Carbonization Cycles	Pressure,† psi	PIC* Cycles	Resin Cycles	Graphitization Cycles
Throat	15V	1	5,000	5	2	8
Socket	15V	1	5,000	5	1	7
Exit cone	A240	2	5,000	2	2	5

* PIC = pressure impregnation and carbonization
† For PIC cyles

carbonization with resin was incorporated to increase the density to 1.7 gm/cc. After final machining, the ball and socket were CVD infiltrated with pyrolytic graphite.

Figure 6 depicts the final machined ball, socket and lockring. Figure 7 shows the exit cone as part of the nozzle assembly with the actuators attached to the compliance ring. The lockring exhibited in Figure 6 was not used in the static test assembly since it failed in bench testing. The lockring failure and subsequent recovery are discussed in section 4.1.

The actuation system consisted of four pull-forward-only hydraulic actuators installed between the nozzle adapter ring and exit cone compliance ring. Opposing pairs of actuators were controlled by a pitch and yaw servovalve that responded to commands originating in a duty cycle generator and processed by an electronic control unit, completing the closed-loop control. One potentiometer installed in each actuator provided nozzle position feedback. In the pull only configuration the nozzle blowoff load is reduced by the amount of the pull load of the actuators, resulting in reduced bearing loads and torque. The actuator assembly configuration is presented in Figure 8.

The nozzle/SLSH motor adapter and compliance ring were made of 4340 and 4130 steel respectively. Carbon and silica-phenolic insulators protected the metallic structures from the high temperature of the [illegible].

11391-7

Figure 6. Final Machined Ball, Socket and Lockring, Nozzle S/N 1

27262

Figure 7. [illegible] Cone and Actuator Attach Configuration, Nozzle S/N 1

[illegible]

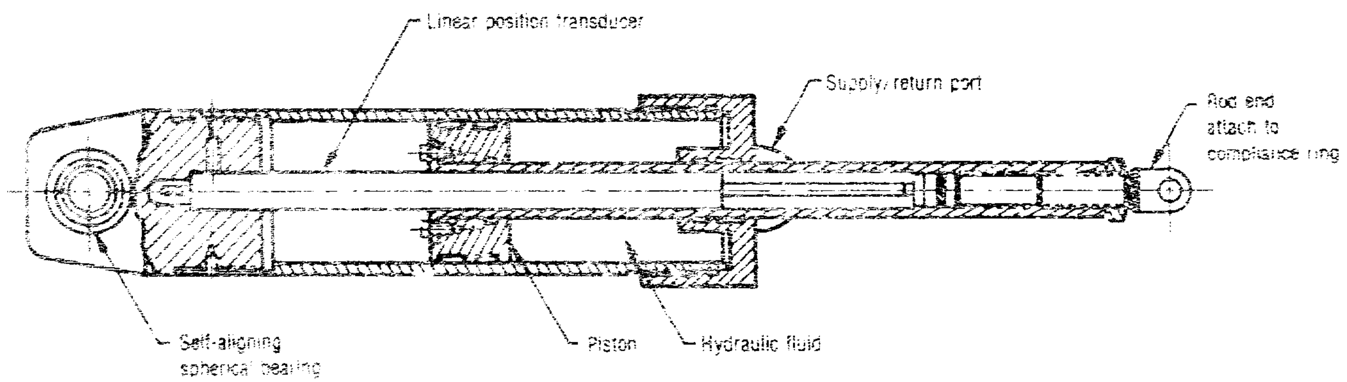

Figure 6. Actuator Assembly

27254

4.0 RESULTS - NOZZLE S/N 1

4.1 BENCH TEST

Prior to assembly of the carbon-carbon (C-C) nozzle, the steel adapter ring was assembled with a steel ball, socket, and exit cone. The steel assembly was mated with the actuation system in the exact configuration planned for the static test assembly. This preliminary bench test configuration, shown mated to the bench test fixture in Figure 9, enabled the verification and fine tuning of the actuation system prior to checkout of the static test assembly. Upon completion of the actuation system checkout, the static test assembly components were assembled and bonded by Chemical Systems Division (CSD). The assembled nozzle is presented in Figure 10.

The nozzle was assembled to the same test fixture shown in Figure 9 for bench test checkout. The objective of the bench testing was to subject the assembly to every load it was to see in firing, except of course, thermally-induced loads. The imposed loads include those seen on the forward lockring during prefire steering checks and motor pressure tailoff due to the forces resulting from the pull-forward actuators. During these times there is no

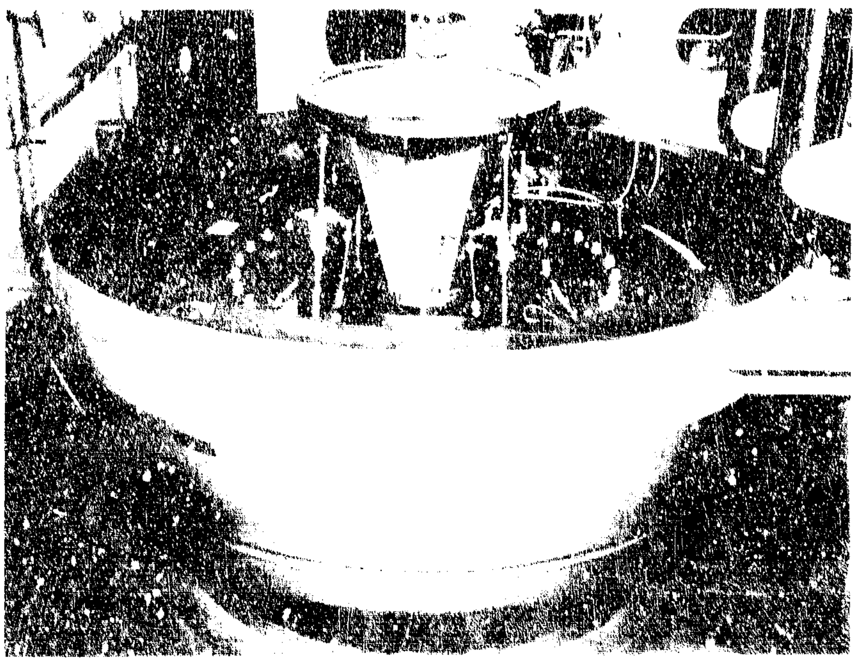

Figure 9. Actuation System Bench Test Assembly

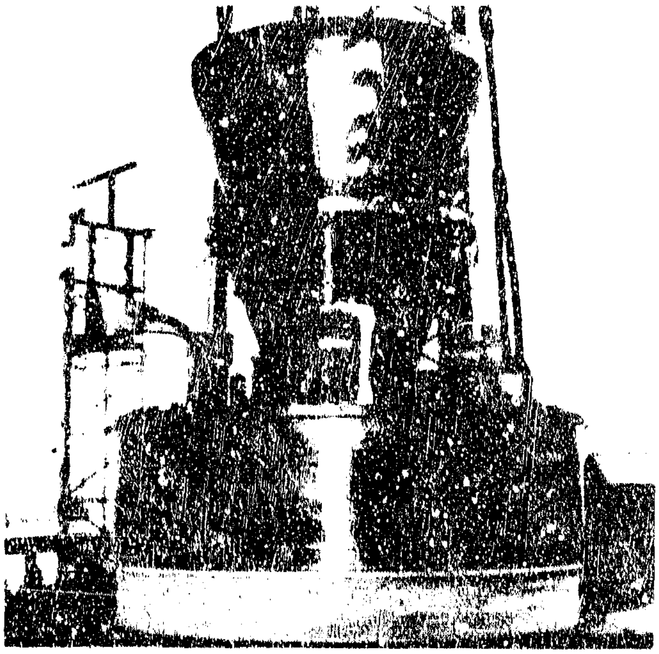

14187-5

Figure 10. Hot Ball and Socket Nozzle and TVC Assembly, Nozzle S/N 1

27266

blowoff load, so the forward actuator load is unopposed. These are the only times in the firing sequence that there is a load on the lockring.

Failure of the lockring occurred during simulation of the pre-ignition steering check when there was no internal pressure (blowoff load). The load during this part of the test was 30,000 to 40,000 lbf forward, all from the actuators. The lockring threaded to the socket failed in hoop tension, breaking into 3-120° segments while vectored over 8 deg. The axial load was then taken by one segment that sheared the forward lip of the socket along a meridional (slanted "axial" or conical reinforcement). The failed lockring is shown in Figure 11. The forward entrance insulators that provide some load carrying support to the lockring were not assembled to the nozzle at this time. Also, there was no adhesive in the threads between the lockring and socket, as was typical of two earlier successful tactical-size designs, so there was some clearance and some ability to deflect although the threads were "tight". The occurrance of two independent failures was concluded: 1) hoop failure of the lockring and 2) shear failure of the socket forward lip.

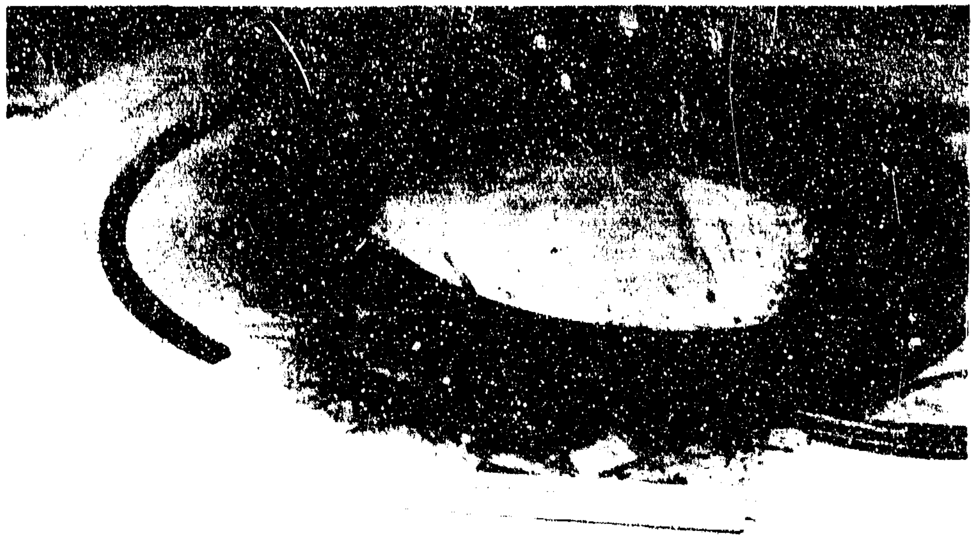

11480-6

Figure 11. Lockring Failure which Occurred during Bench Testing, Nozzle S/N 1

27267

The design modification implemented for the forward end of the nozzle is presented in Figure 12. The socket and phenolic ring on the outside diameter (OD) were left bonded in the adapter ring, but machined back to the "equator", which removed the damaged portion of the socket. The lockring and grafoil were replaced with a ring from a 7-in. "MANTECH"-type billet made of HM fiber, wound by Haveg and densified at Fiber Materials, Inc. (FMI). Threads were eliminated and a steel ring and insulators were added to give more rigid support in both radial and axial (forward) directions. Bearing area of the lockring was substantially increased.

Upon completion of the design modification the nozzle was again mated to the bench test fixture. The nozzle was successfully subjected to the full forward actuator load of 36,000 lbf. Attempts to pressurize the plugged nozzle and vector at a blowoff load equivalent to 1,900 psi motor chamber pressure were unsuccessful. Leakage of GN_2 through the cold 3D C-C prevented full pressurization. The high permeability of 3D C-C at room temperature is well known, however, it approaches zero at about 2,000°F, so leakage during firing is negligible. The problem was one of facility limitations. The 3D C-C surfaces were

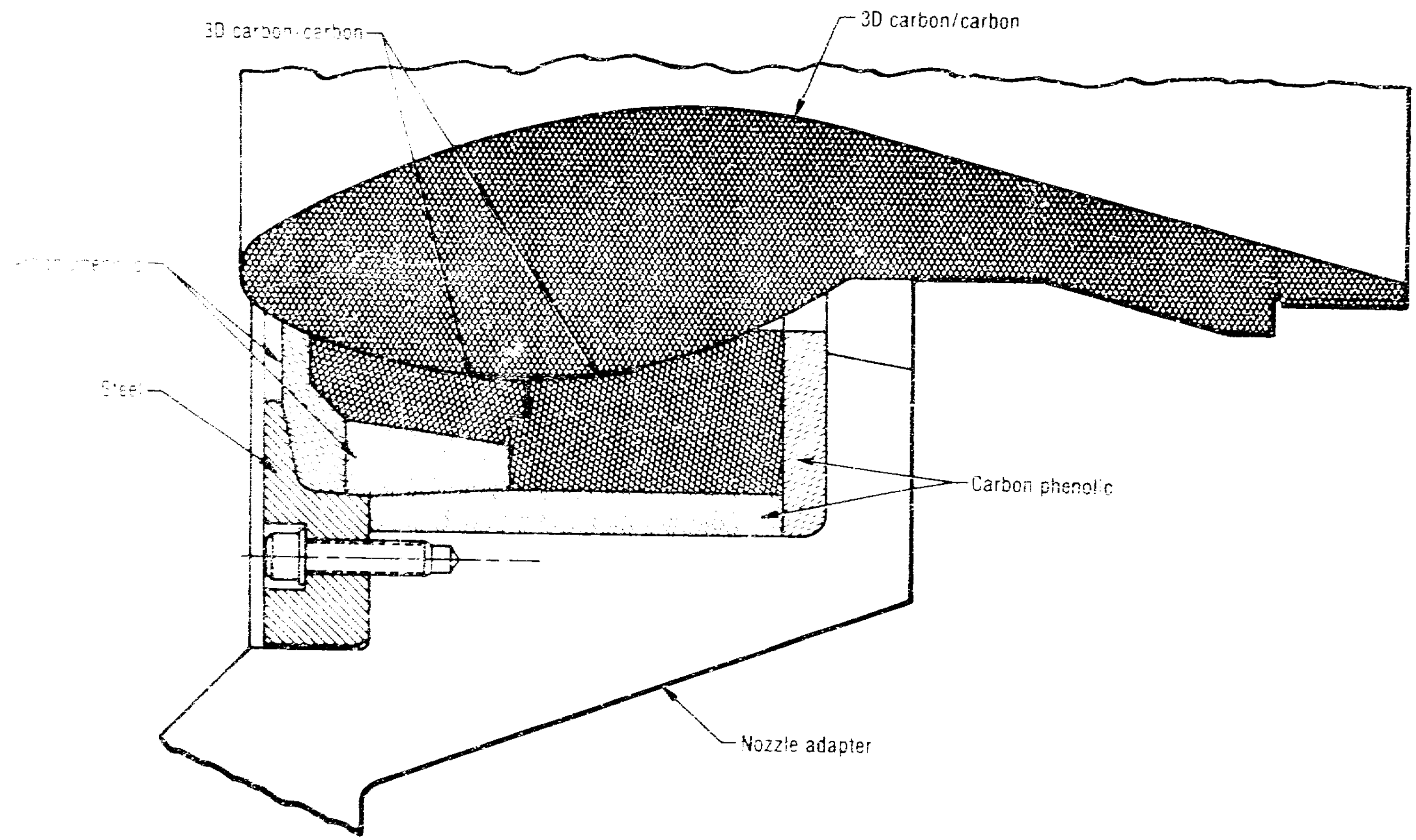

Figure 12. Nozzle Subassembly as Redesigned Following Bench Test Failure

21652

subsequently sealed with RTV rubber enabling successful loading of the ball and socket. The RTV rubber, however, prevented vectoring of the ball while loaded.

4.2 STATIC TEST

4.2.1 General

The static test of the full-scale (7-in. D_t) hot ball and socket (HBS) thrust vector control (TVC) system was planned to demonstrate the integrity of the nozzle system and acquire data to define the TVC performance under static firing conditions. The 8 February 1979 static test was conducted on the Short Length Super HIPPO (SLSH) motor at test pad 1-52A of the Rocket Propulsion Laboratory, Edwards Air Force Base, California. The motor was assembled by Air Force Rocket Propulsion Laboratory (AFRPL) personnel in accordance with CSD drawing C12413. The nozzle as installed on the motor is shown in Figure 13. The propellant was CSD's UTP-18803A, a 90% solids, 21% aluminum hydroxyl-terminated polybutadiene (HTPB) type. The igniter, a phenolic cartridge type, was in accordance with CSD P/N C00631-07-01. The predicted average pressure was 1,235 psia over the planned 60 sec duration. The planned duty cycle is shown in Figure 14.

14187 1

Figure 13. Nozzle S/N 1 as Installed on SLSH Motor

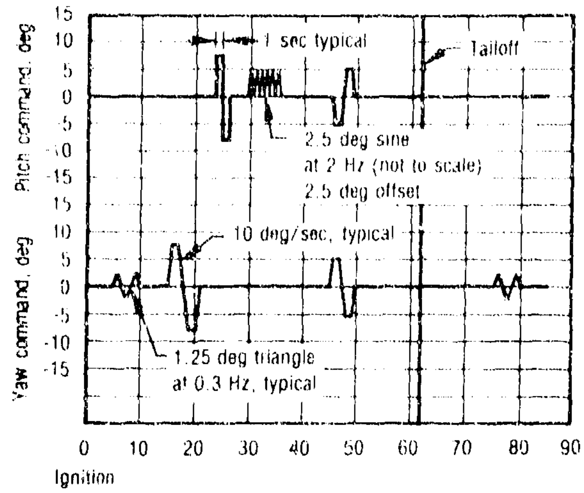

Figure 14. Planned Static Firing Duty Cycle, Nozzle S/N 1

27158

Two minutes before ignition the nozzle was vectored 8 deg in the pitch and yaw axes to verify the readiness of the system. The nozzle/TVC system responded as expected. Upon ignition, the system performed as planned up to 10 sec. Between 5.3 and 9.3 sec the nozzle successfully executed a 1-1/2 deg vectoring sequence with torque levels as expected. At 10.0 sec gas leakage was observed at the threaded interface between the ball extension and the exit cone at an azimuth of about 100 deg. The downward angle of the leakage plume (back toward the motor), as shown in Figure 15 suggests the leak followed the threaded boundary between the exit and the ball extension. Between 10 and 15 sec the leakage plume grew in size and aft toward the actuator attach ring. A second leakage plume, at about 60 deg, was observed beginning at 13.9 sec.

At 15 sec the nozzle began vectoring to 8 deg in the yaw plane, completing this event as programmed at 16.3 sec and holding at 8 deg (for a one-sec hold). At 16.9 sec the leak at the 100 deg azimuth quickly opened up aft to the compliance ring, (Figures 16 and 17). At 17.3 sec the nozzle began moving as programmed from 8 deg back toward null, but stalled at 7.5 deg. The ball remained at this angle throughout the remainder of the 60 sec duration.

At 18.6 sec an additional leakage plume was seen at the 330 deg azimuth, a flash was observed at about 190 deg, and the apparent crack at 60 deg opened greatly. At 18.7 sec the exit cone broke up and was extruded through the steel

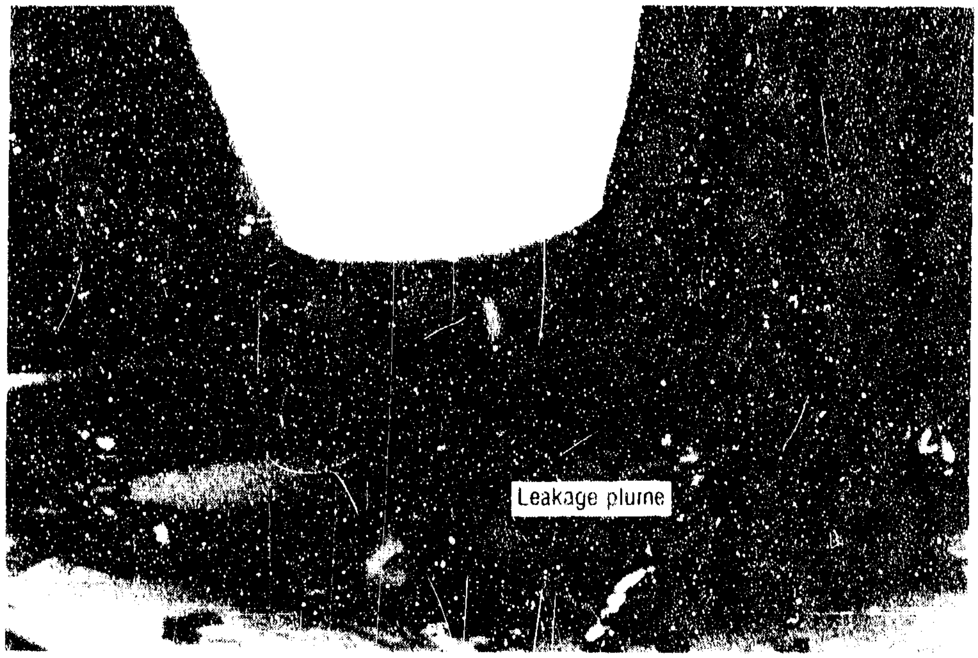

Figure 15. Initial Leakage Plume

27269

actuator attach ring and ejected. The actuator attach ring was ejected at 19.9 sec.

A crack was observed in the ball extension shortly after the actuator attach ring was lost. The ball extension subsequently came off in three pieces, at three different times. The section from 90 to 220 deg was lost at 20.8 sec, the 220 to 270-deg piece was lost at 26.0 sec, and the remaining piece (270 to 90 deg) at 40.5 sec. The sequence of events is summarized in Table 2.

As noted, the ball - which includes the throat - and the socket remained in place, but with the ball at a 7-1/2 deg vector, throughout propellant burn. Tailoff was at 58.8 sec. Figure 18 compares the predicted and measured chamber pressure. Chamber pressure was substantially higher (14%) than predicted at the maximum, but was not determined to be cause of the failure. The maximum measured pressure was 1,630 psia; average pressure was 1,355 psia.

2072-5

Figure 16. Leak at 100-deg Azimuth at about 17 sec, Side View

2072-3

Figure 17. Leak at 100-deg Azimuth at about 17-sec, Front View

27270

TABLE 2. SEQUENCE OF EVENTS, NOZZLE S/N 1

20435

Approximate Time, sec	Event
0	Motor ignites, firing proceeds as planned
5.3 - 9.3	Nozzle vectors as planned in yaw plane, one and one-half cycles with 1-1/4-deg amplitude
10.0	Small leakage plume observed at threads at the 100-deg azimuth
10.0 - 13.9	Plume grows in size, extends aft
13.9	A second leakage plume begins at about 60 deg
15.0	Nozzle begins vector to 8-deg in yaw; leakage plume at 100 deg extends forward
15.3	Leakage plume at 100 deg extends aft
16.3	Nozzle completes vector to 8 deg as planned, begins 1-sec planned hold
16.9	Leak at 100 deg quickly opens up in aft direction all the way to the compliance ring
17.3	Nozzle begins planned return to null, but stalls at 7.5 deg
18.6	Additional leakage plume appears at 300 deg; flash seen at 190 deg; and crack at 60 deg opens
18.7	Exit cone breaks up and is extruded through the steel actuator attach ring. Ball remains in place at 7.5 deg angle of yaw plane
19.9	Actuator attach ring is ejected
20.8	Ball extension section from 90 to 220 deg ejected
26.0	Ball extension section from 220 to 270 deg ejected
40.5	Ball extension section from 270 to 90 deg ejected
40.5 - 68.8	Ball, which includes throat, remains in place; propellant burn continues as planned
68.8	Motor tailoff occurs near expected time

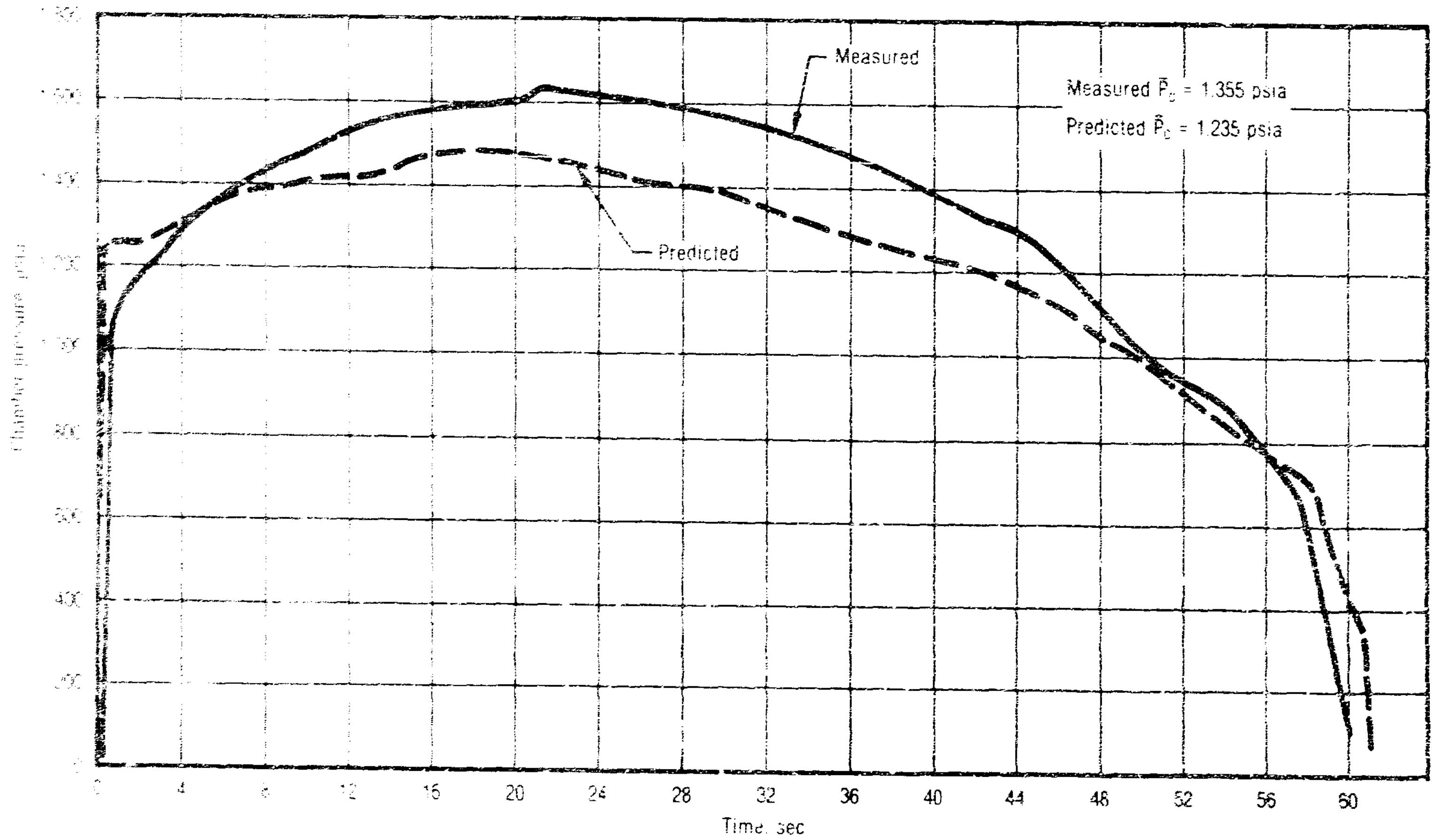

Figure 18. Predicted vs Measured Chamber Pressure, Nozzle S/N 1

21654

4.2.2 TVC Data

The HBS TVC nozzle performed the ±8 deg trapezoidal wave form in both the pitch and yaw axis during ambient pre-ignition steering checks as expected. During this prefire sequence, the ball was vectored against the forward lock-ring. During firing the nozzle accomplished 17 deg of vector travel in the yaw plane up to 18 sec, the time of exit cone ejection (no vectoring was planned in the pitch plane during this time period). The achieved angular movement during the test firing is shown in the plot of yaw position versus time (Figure 19). Movement of the nozzle as expected was recognized during the 1.25 deg triangular commands between 5 and 9 seconds at a chamber pressure of 1,400 psia. An 8 deg vector position was achieved at 16 sec when chamber pressure was 1,580 psia.

Measured torque is plotted against time in Figure 20. Figure 21 presents a cross-plot of nozzle torque versus nozzle deflection angle for vectoring to the point of failure. The hysteresis torque determined from the full loop achieved between 5 and 9 sec is equivalent to one-half the width of the loop, or 126,000 in.-lb. The friction coefficient determined from the data was 0.11, comparable to previous subscale test data.

The offset torque is the difference between the center of the measured torque loop and the axis, and is equal to 34,000 in.-lb. Since no offset torques were seen during bench test or prefire steering checks, the origin of the offset is aerodynamic in nature. Industry data indicate that the magnitude is typical for nozzles of this size. The HBS aerodynamic spring torque was essentially zero.

The measured torque for the vector event to +8 deg is significantly higher than earlier events and ultimately reached stall conditions before exit failure. The increasing torque and subsequent stall torque was attributed to increased friction due to aluminum oxide deposition in the forward splitline.

4.2.3 Thermocouple Data

Nineteen thermocouples were instrumented to the aft ball, socket, exit cone and one actuator (pitch + at top dead center (TDC)). The locations are depicted in Figure 22. The temperature response of thermocouples TC-1 through TC-19 is presented in Figures 23 through 41. Note that 120 sec corresponds with ignition.

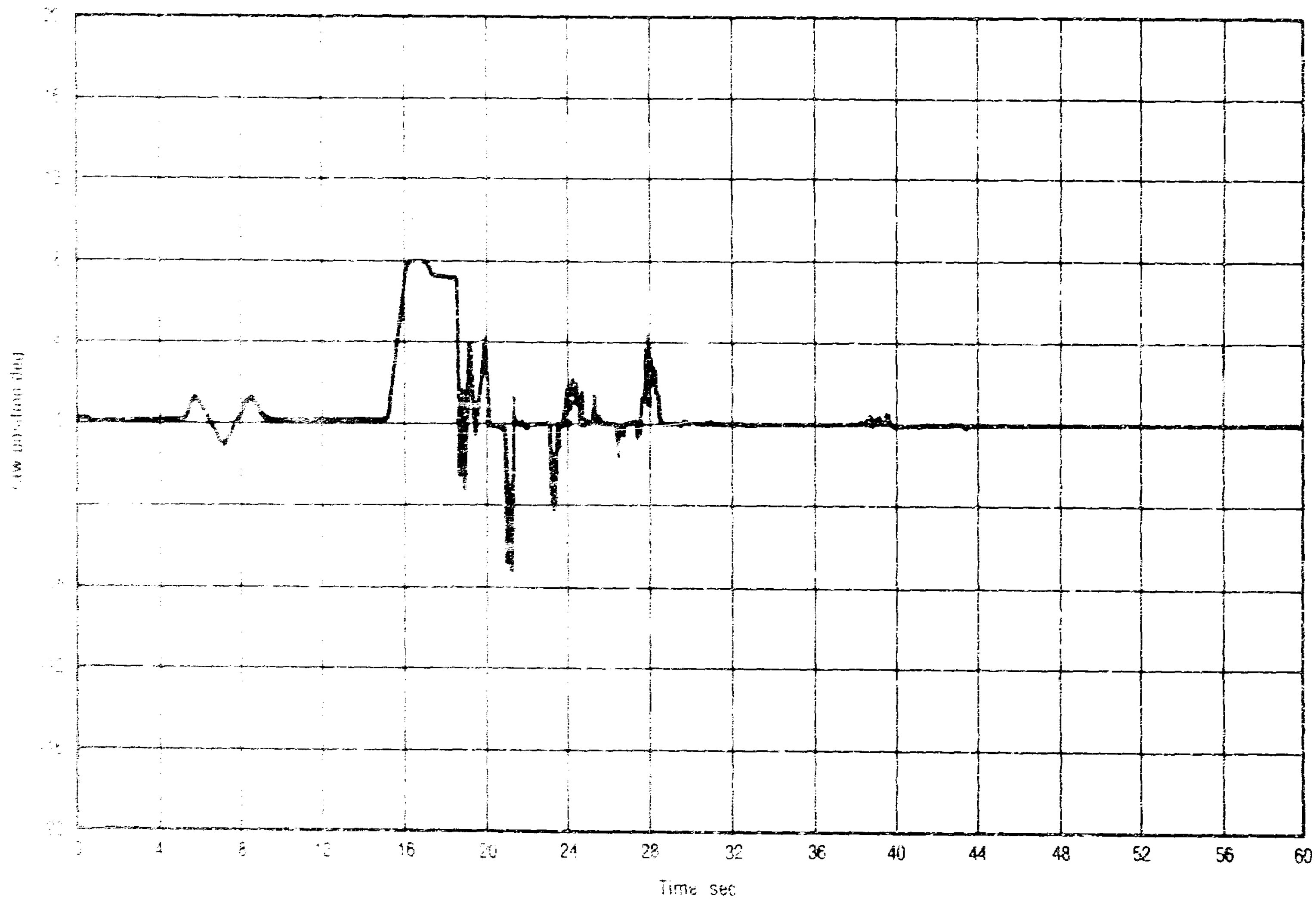

Figure 19. Measured Yaw Position vs Time, Nozzle S/N 1

21653

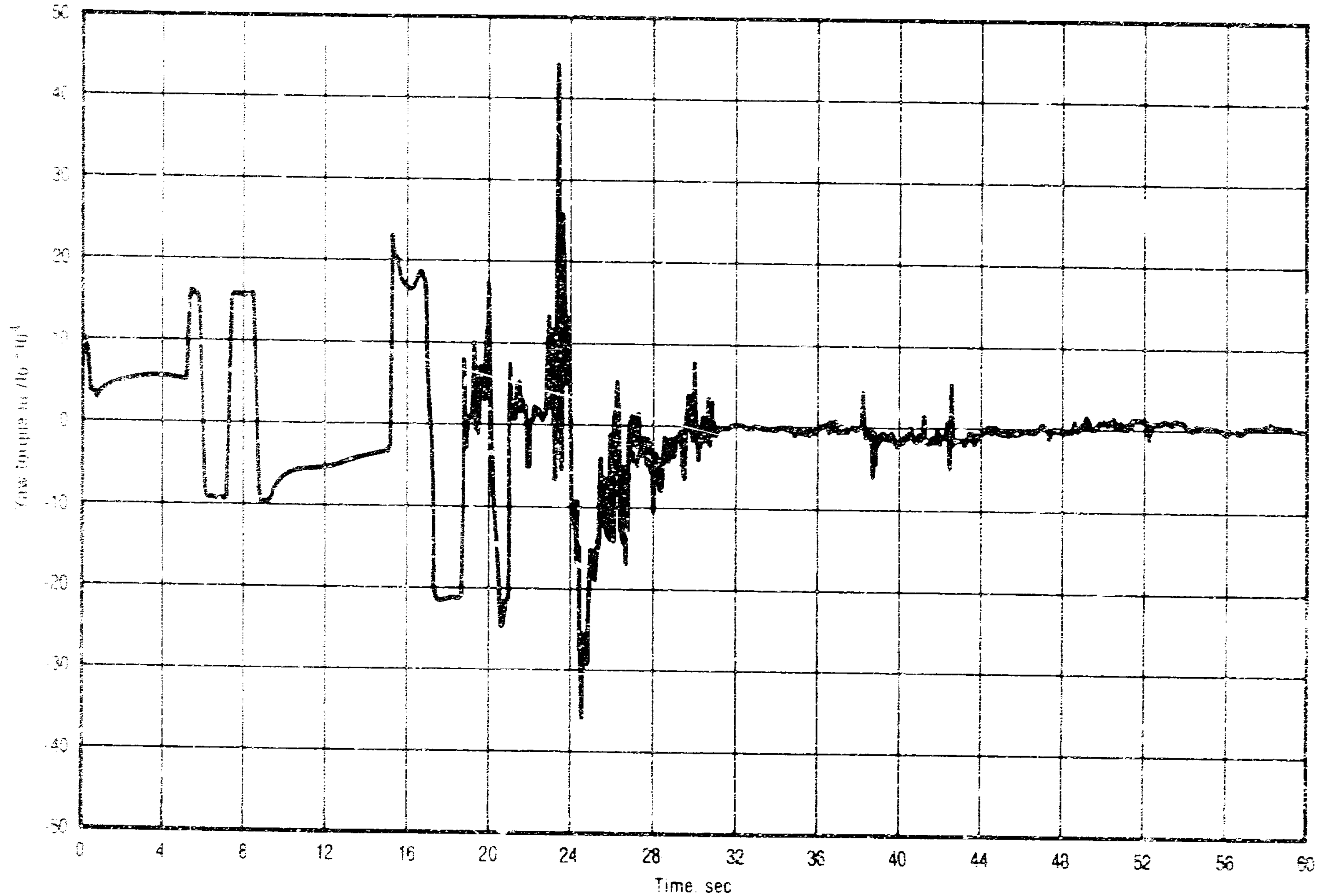

Figure 20. Measured Yaw Torque vs Time, Nozzle S/N 1

21656

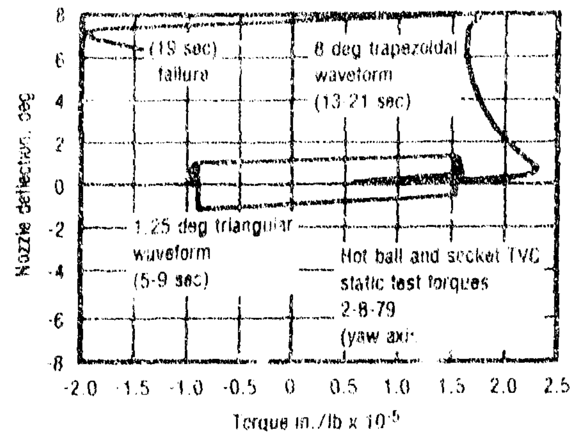

Figure 21. Measured Yaw Torque   Deflection Angle, Nozzle S/N 1

27159

Review of these thermocouples indicate all were responding normally except for TC-8 which was not reading at ignition. Thermocouples 1 through 4, monitoring the backface of the socket, were recording temperatures of 100°F or less, as expected, up to 16 sec when the leakage and subsequent exit cone ejection resulted in loss of data. TC's 5 through 10 (at the ball aft end and forward exit cone) except for the non-functioning TC-8 did not show anomalous behavior under the circumstances of severe flow experienced in this region. TC's 6 and 10, closest to the major flow, exhibited a significant change in thermal response at 10 sec, when the initial flow started, until loss of data coinciding with exit ejection. Thermocouples 11 through 14 in the compliance ring region exhibited only a slight (approximately 20°F) temperature rise at 10 sec. Two thermocouples near the exit plane (TC's 15 and 16) were not significantly affected by the conditions between 10 sec and exit ejection. Thermocouples 17 and 18 on the 0 deg actuator cylinder under a 1/8-in. thick silicone rubber layer remained at approximately 60°F for the entire time up to exit ejection. Thermocouple 19 on the actuator shaft rose only 15°F at the time of the initial leak.

4.2.4 Strain Gage Data

Four strain gages were located on the compliance ring 90° apart as shown in Figure 22. Plots of strain versus time for these four gages are presented in Figures 42 through 45. One significant indication exhibited is at 15.25 sec corresponding to the time the nozzle and actuators experienced a stall force of

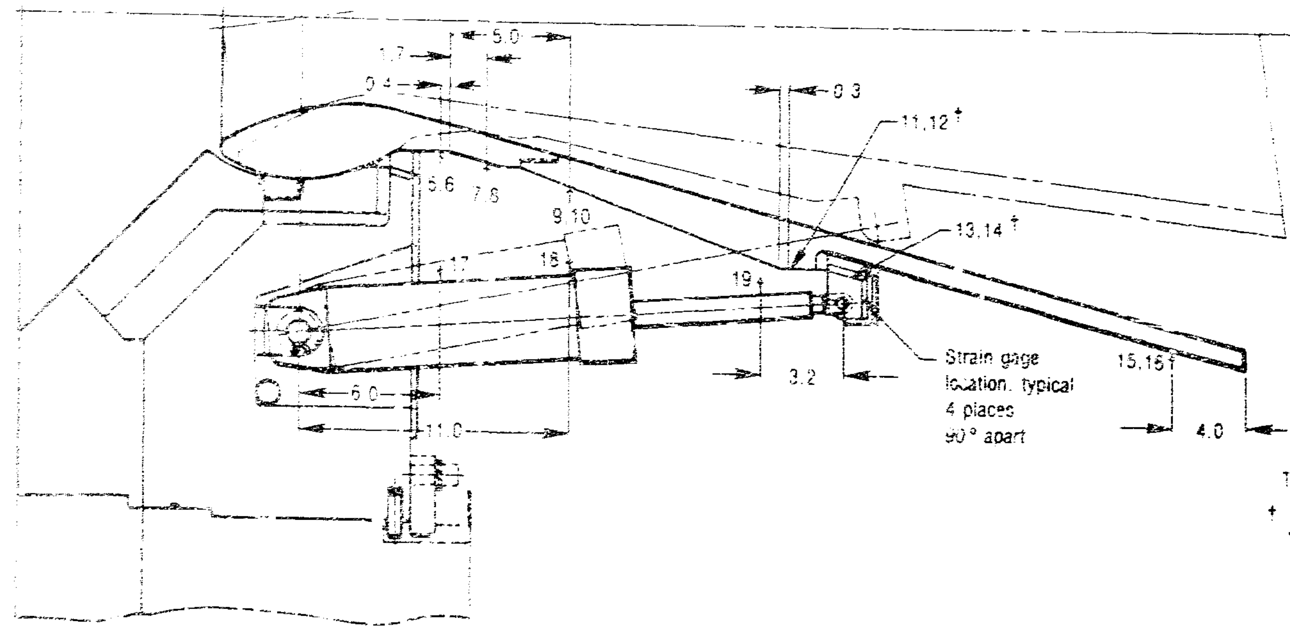

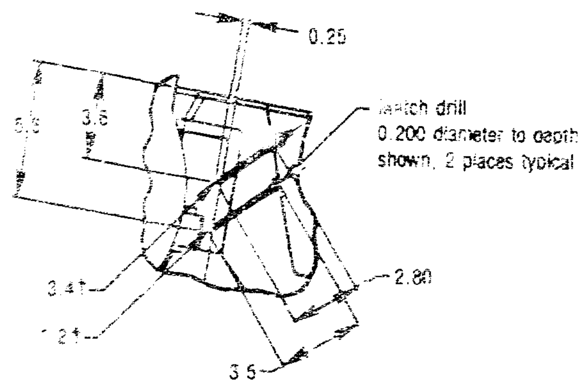

Thermocouple Data

† No.	Location, °
1	10
2	100
3	10
3	10
4	100
5	TDC
6	90
7	TDC
8	90
9	TDC
10	90
11	TDC
12	90
13	TDC
14	45
15	TDC
16	90
17	Pitch + actuator
18	Pitch + actuator
19	Pitch + actuator

Figure 22. Location of Thermocouples and Strain Gages, Nozzle S/N 1

18381

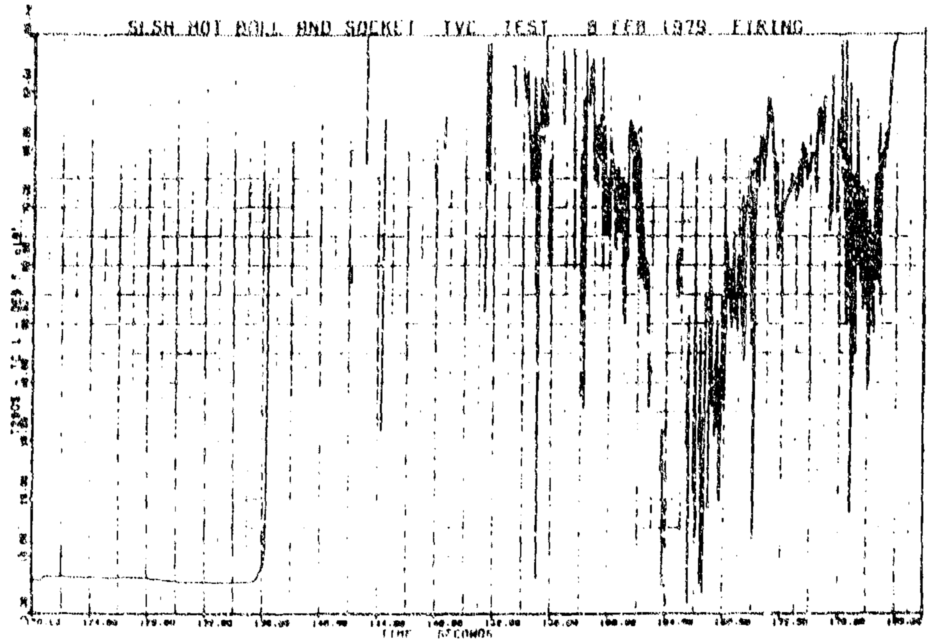

Figure 23. TC1 vs Time

27271

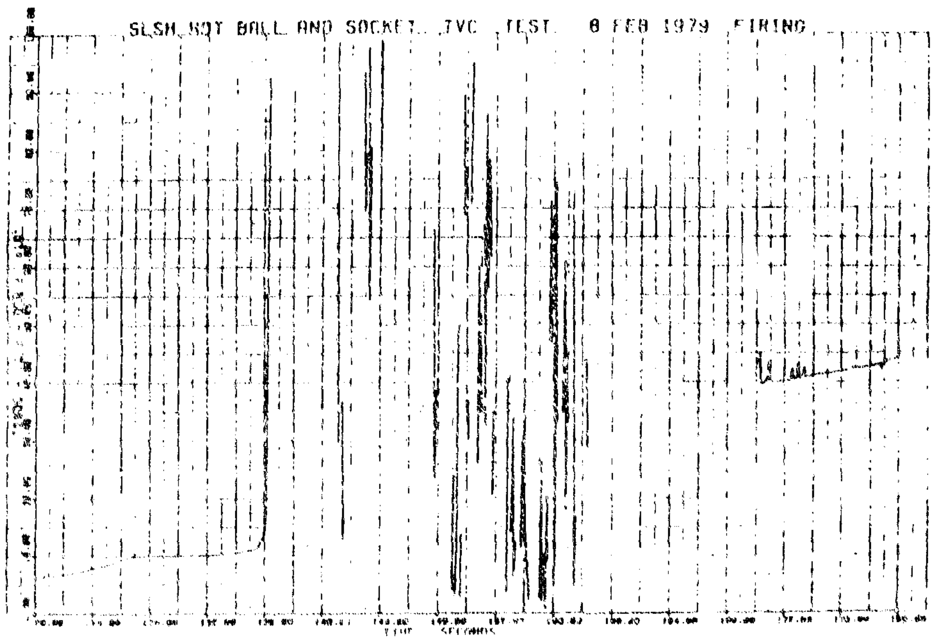

Figure 24. TC2 vs Time

27272

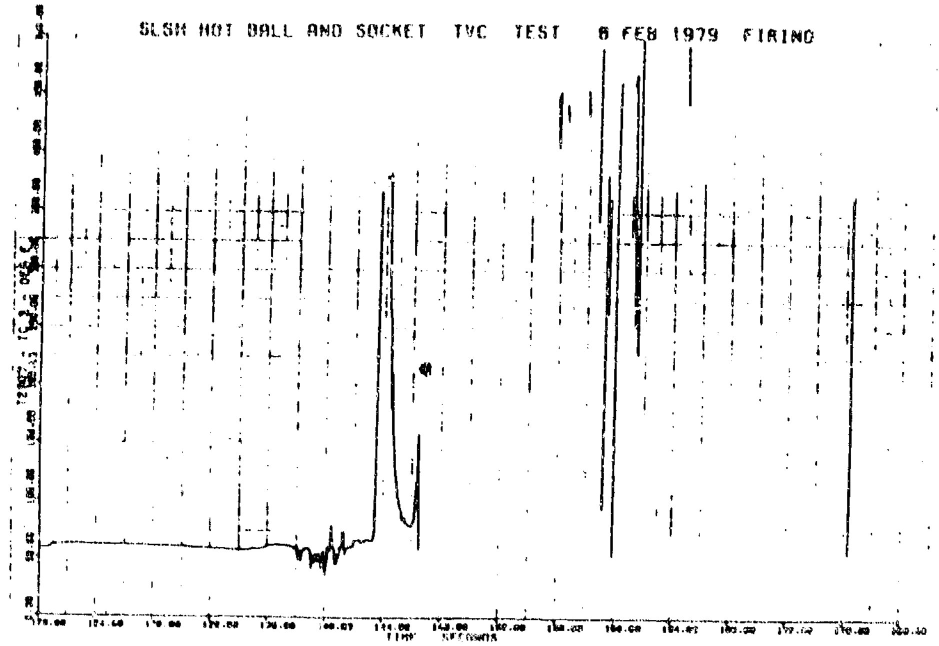

Figure 25. TC3 vs Time

27273

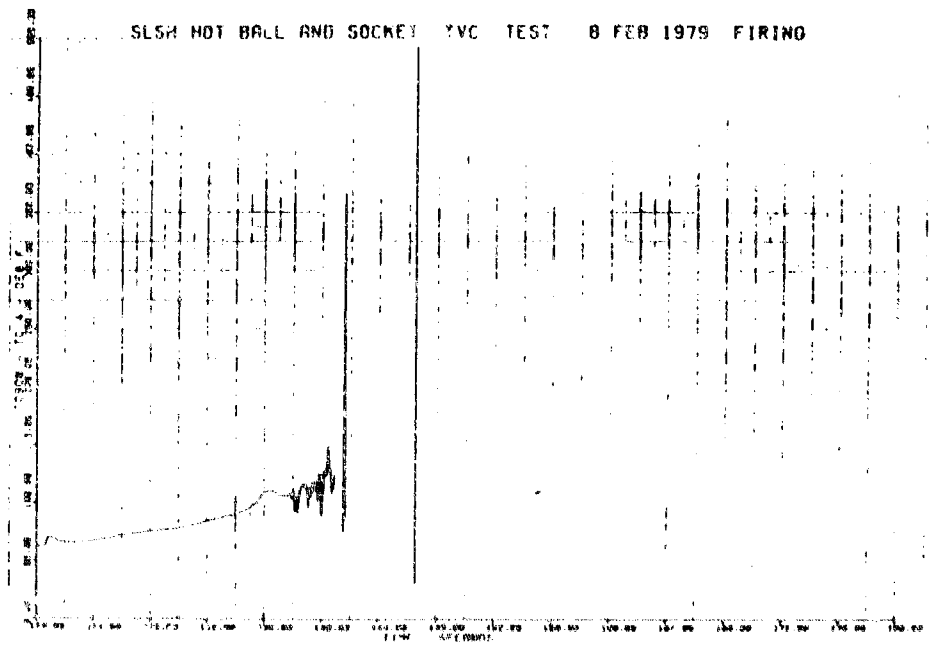

Figure 26. TC4 vs Time

27274

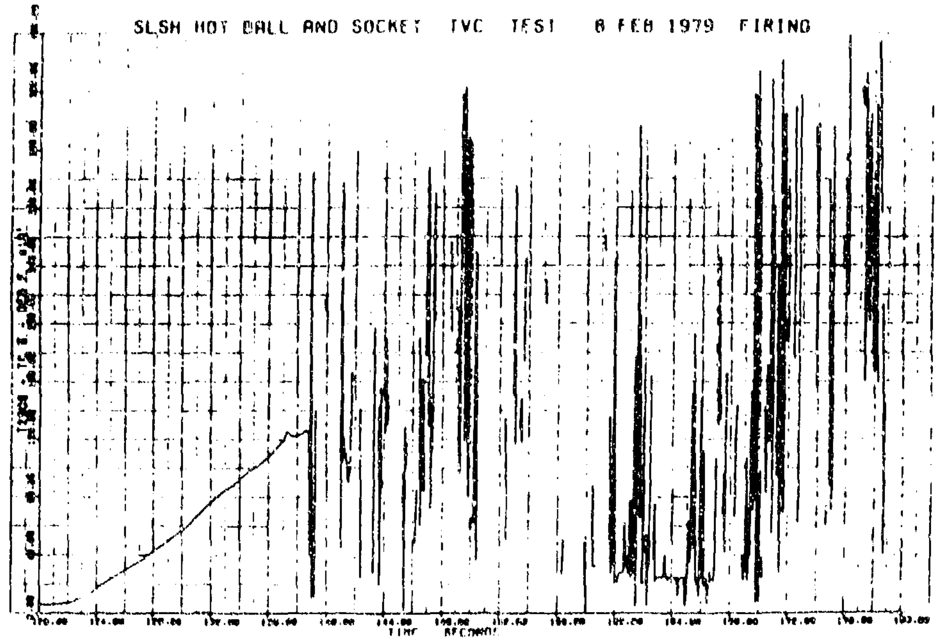

Figure 27. TC5 vs Time

27275

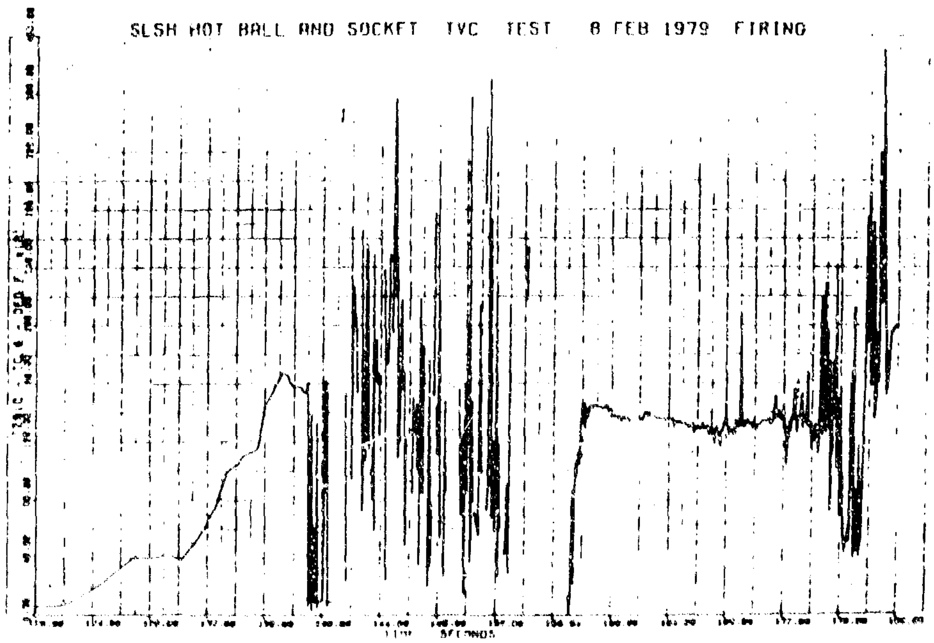

Figure 28. TC6 vs Time

27276

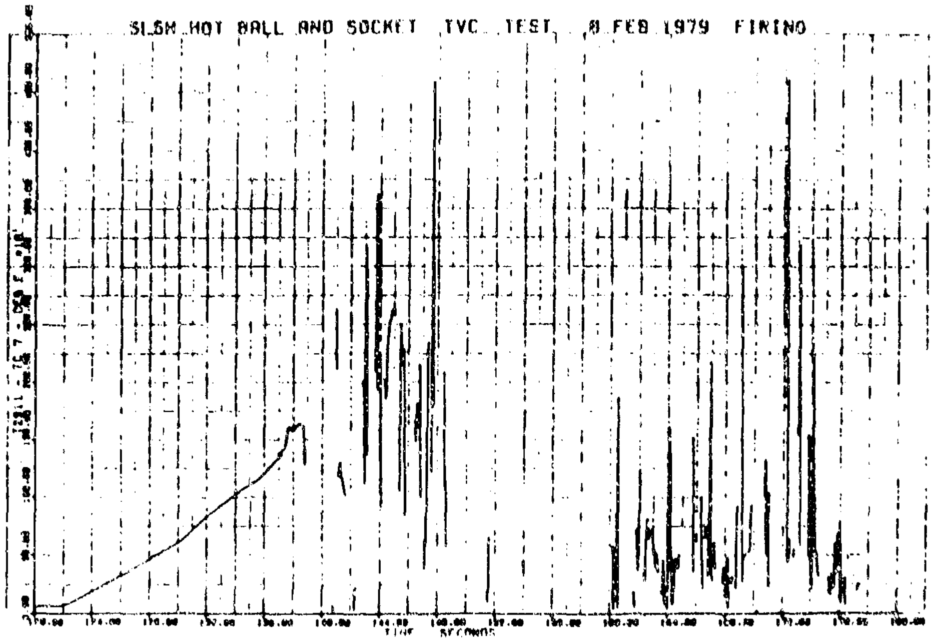

Figure 29. TC7 vs Time

27277

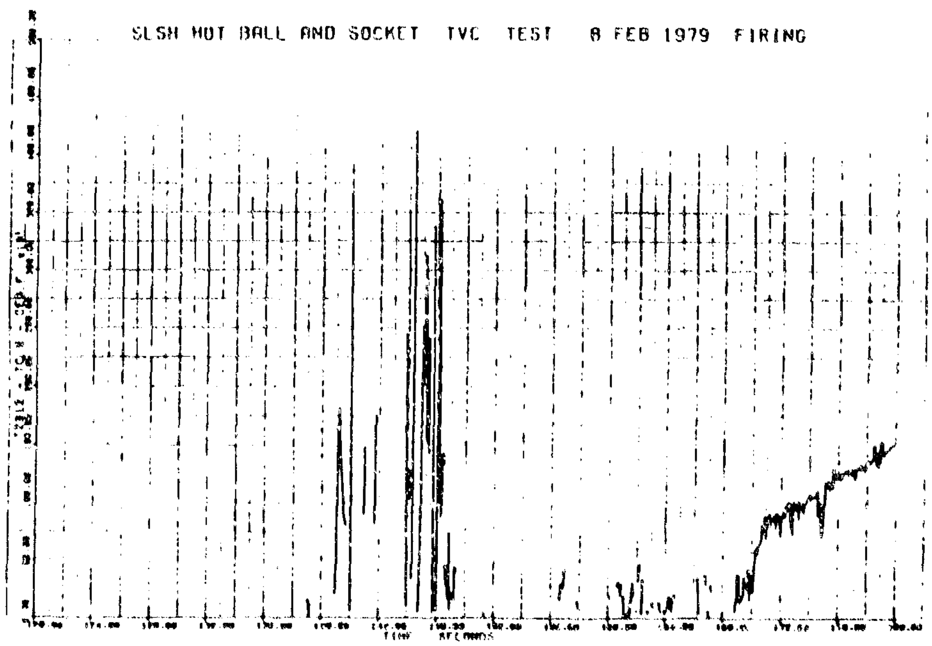

Figure 30. TC8 vs Time

27278

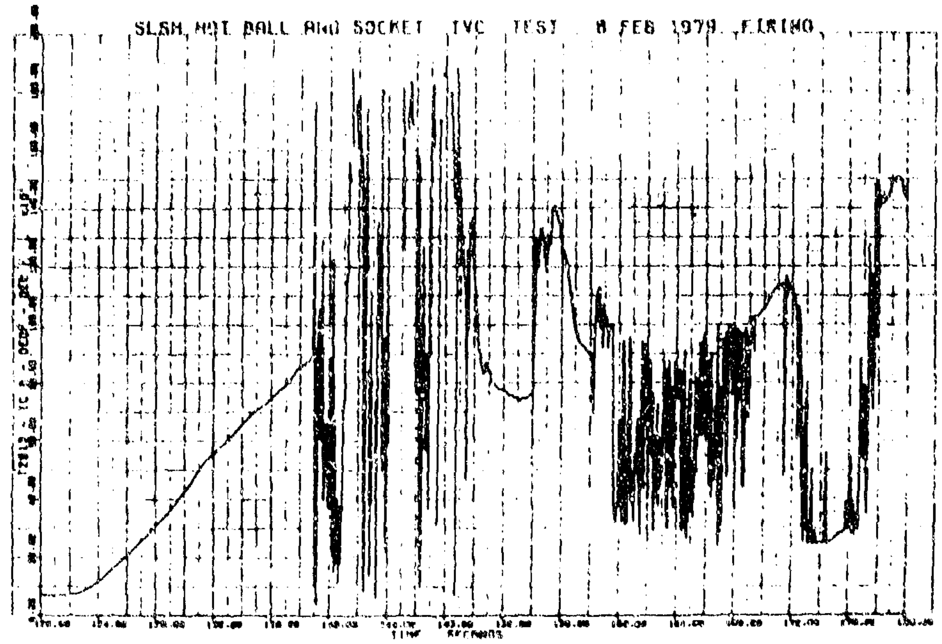

Figure 31. TC9 vs Time

27279

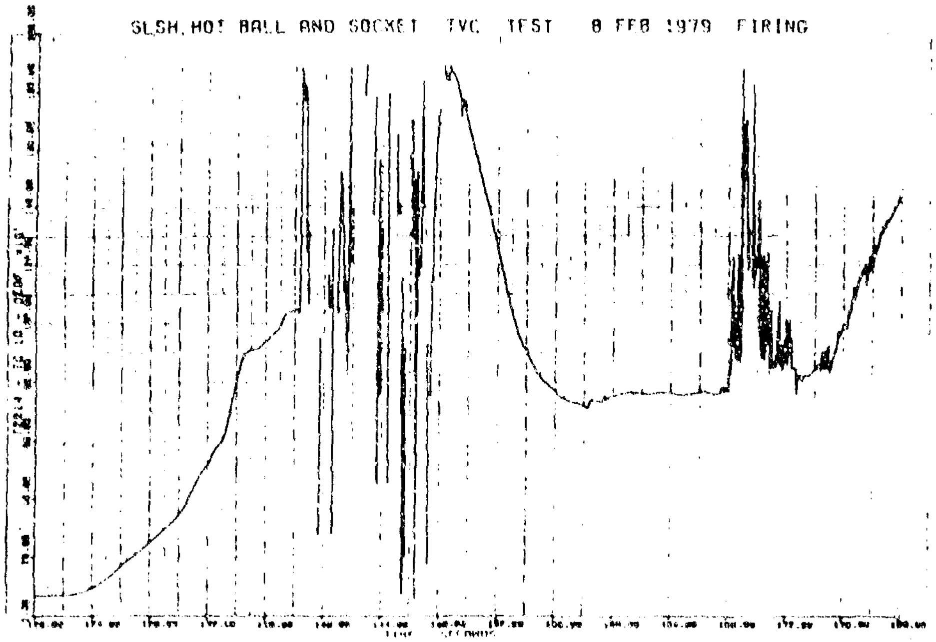

Figure 32. TC10 vs Time

27280

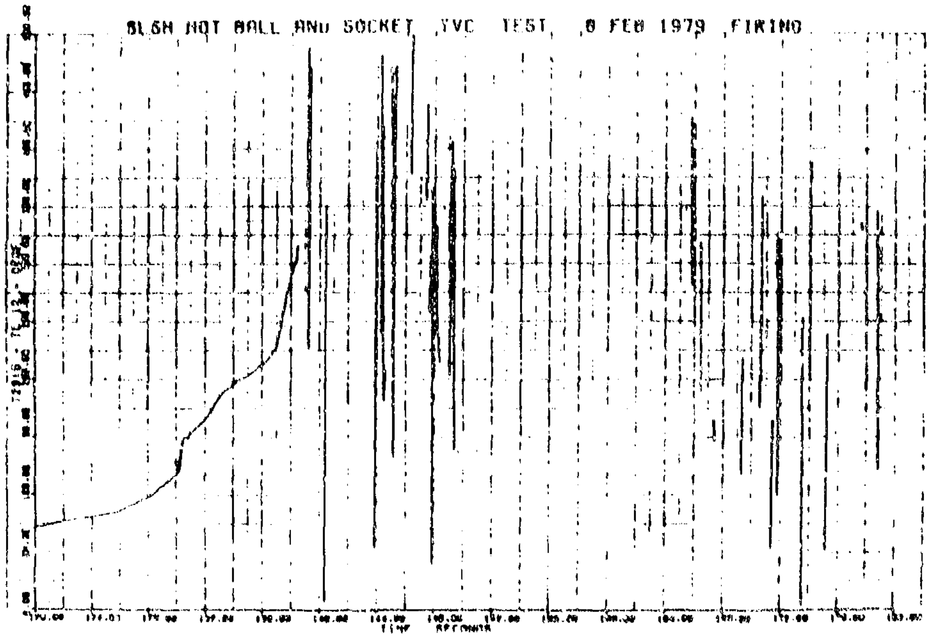

Figure 33. TC11 vs Time

27281

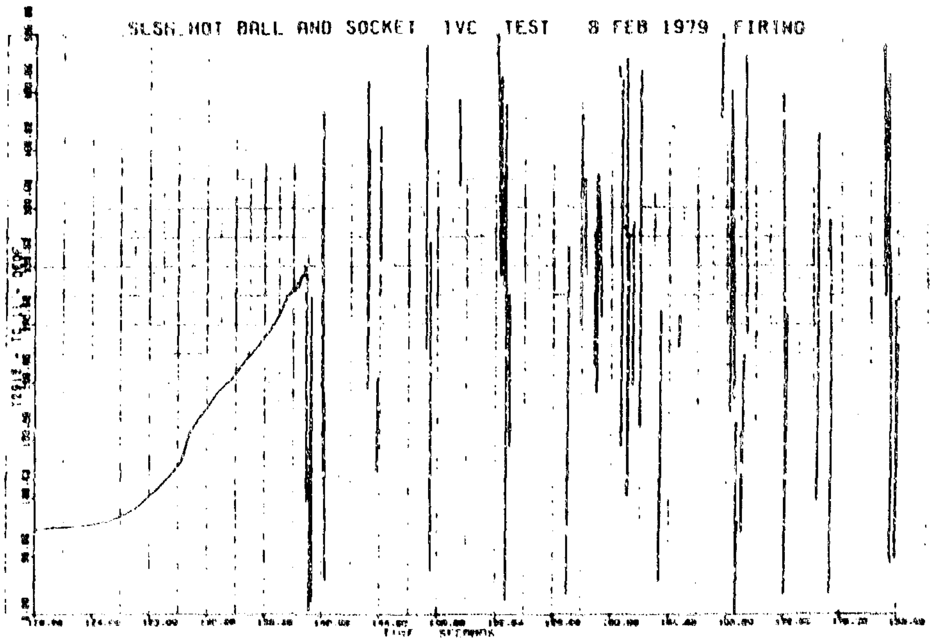

Figure 34. TC12 vs Time

27282

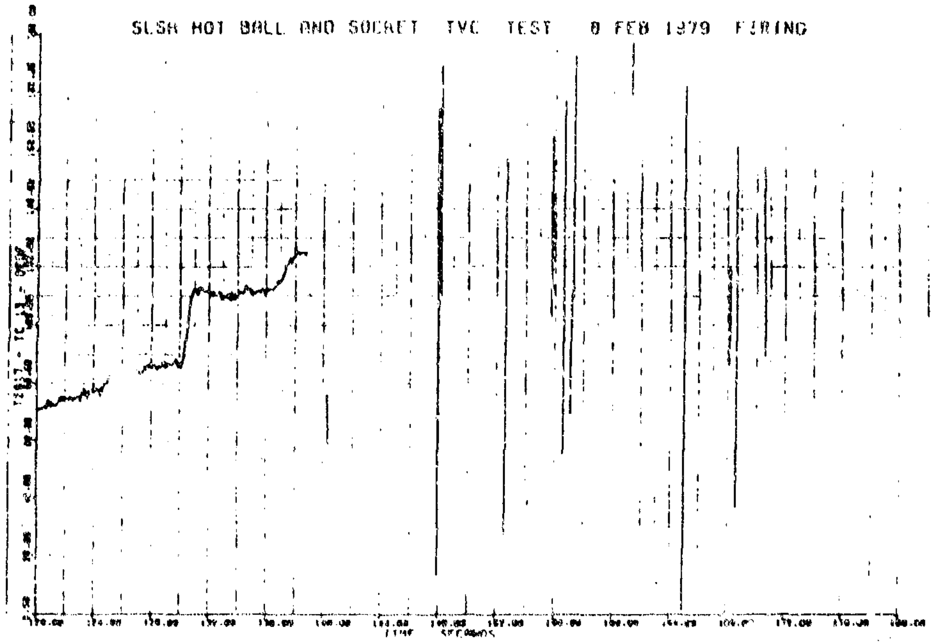

Figure 35. TC13 vs Time

27283

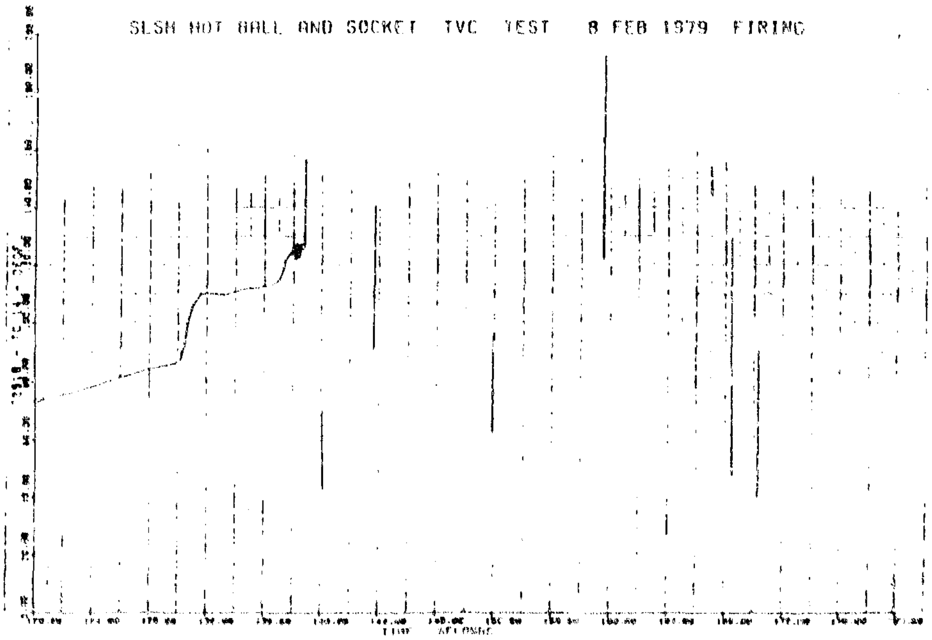

Figure 36. TC14 vs Time

27284

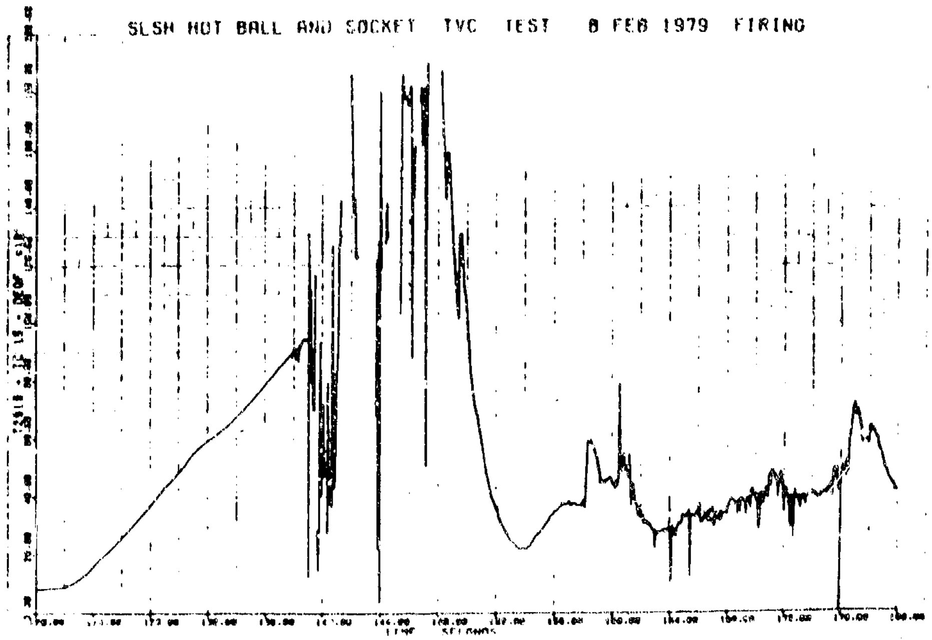

Figure 37. TC15 vs Time

27285

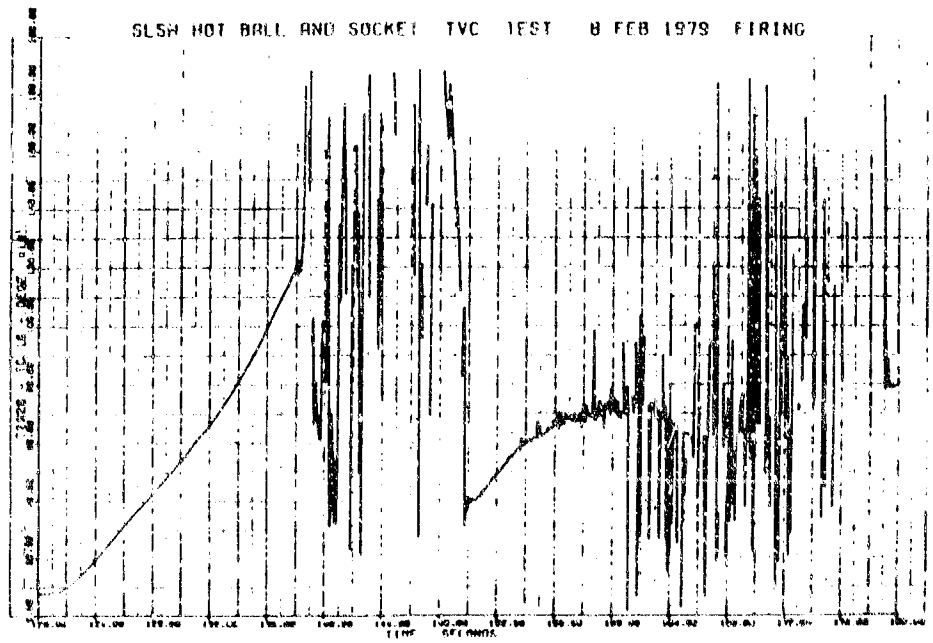

Figure 38. TC16 vs Time

27286

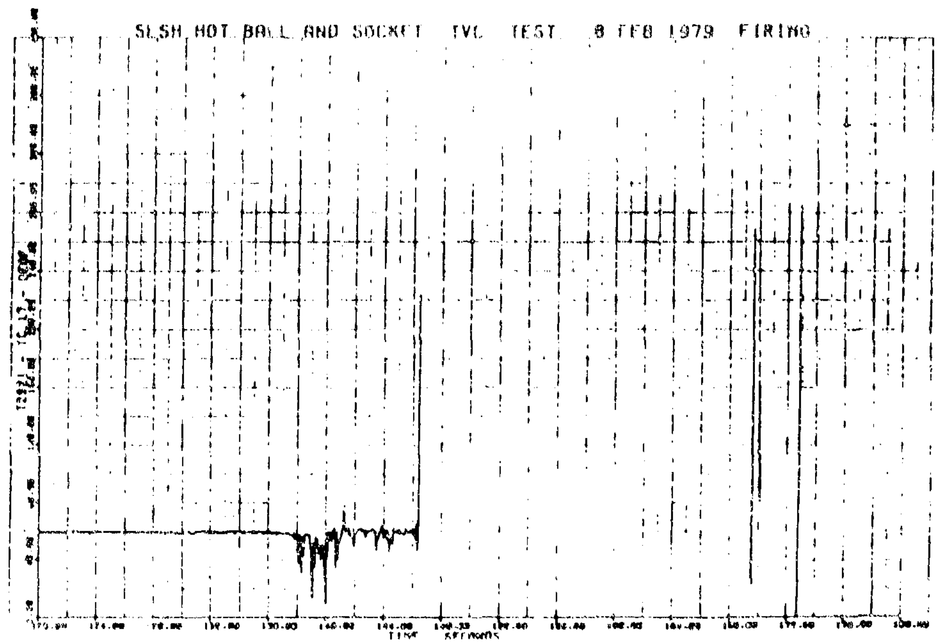

Figure 39. TC17 vs Time

27287

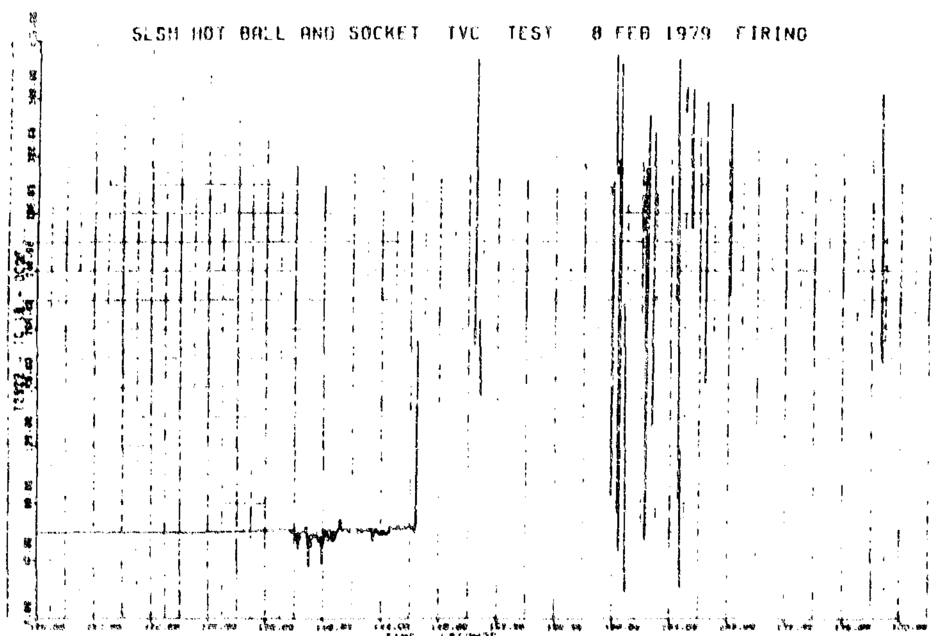

Figure 40. TC18 vs Time

27288

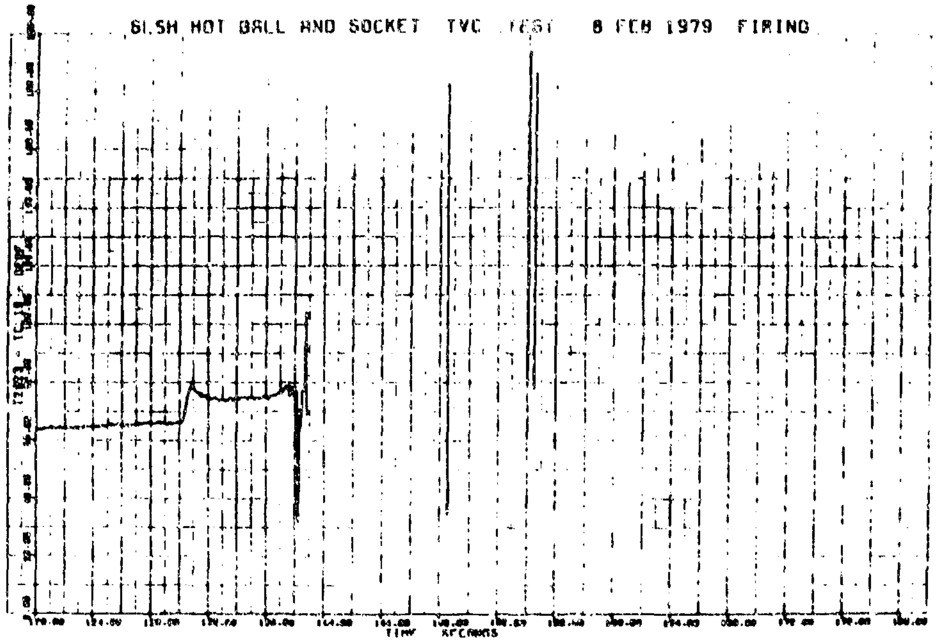

Figure 41. TC19 vs Time

27289

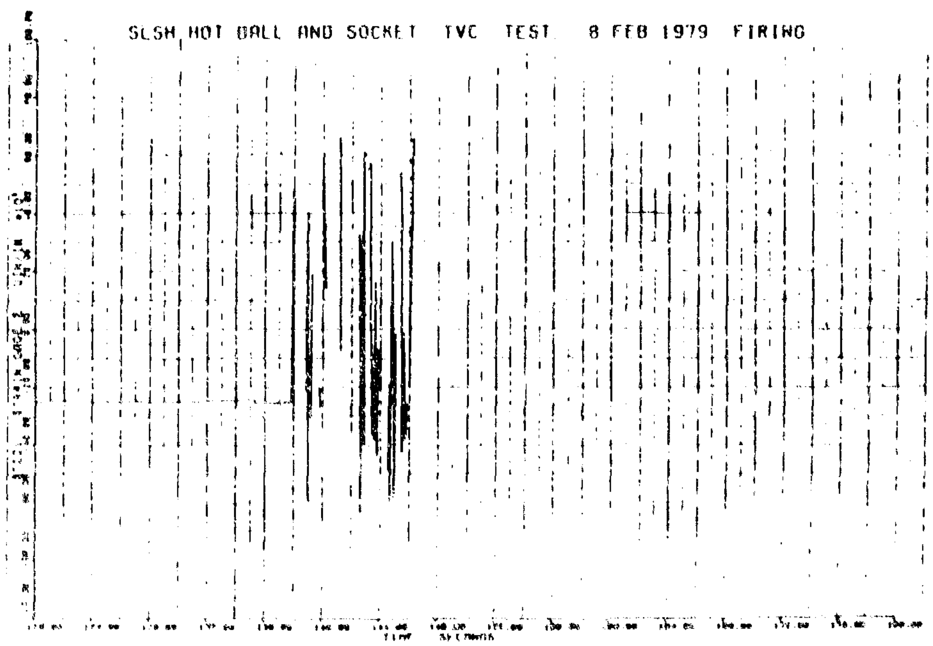

Figure 42. Strain Gage 1, 0 deg from TDC

27290

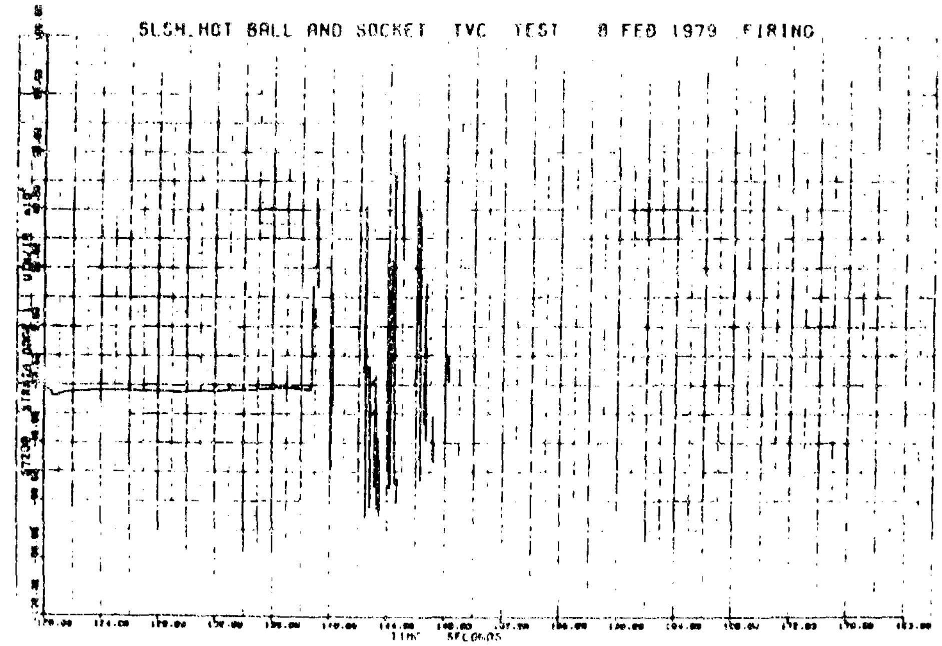

Figure 43. Strain Gage 2, 90 deg from TDC

27291

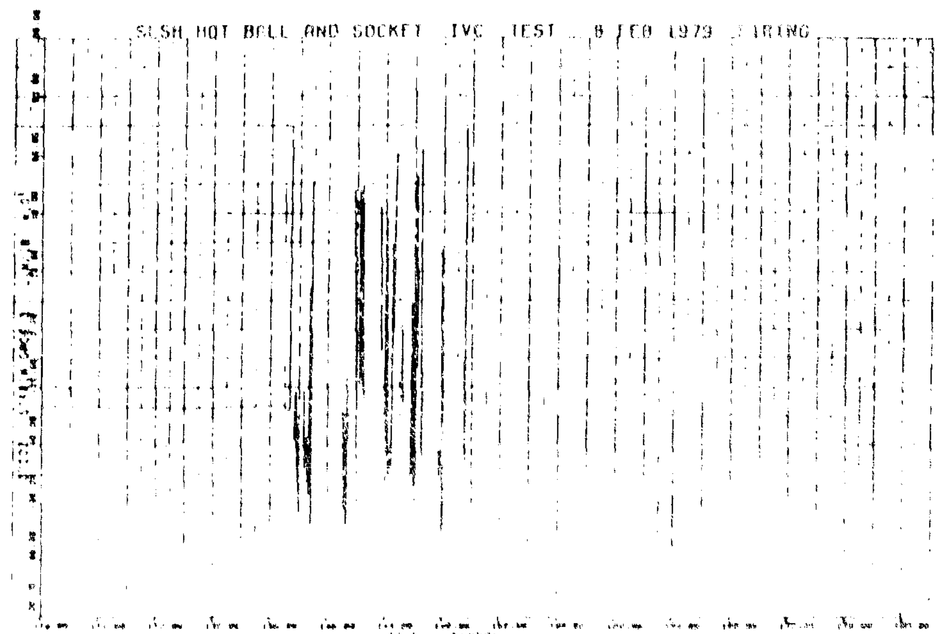

Figure 44. Strain Gage 3, 180 deg from TDC

27292

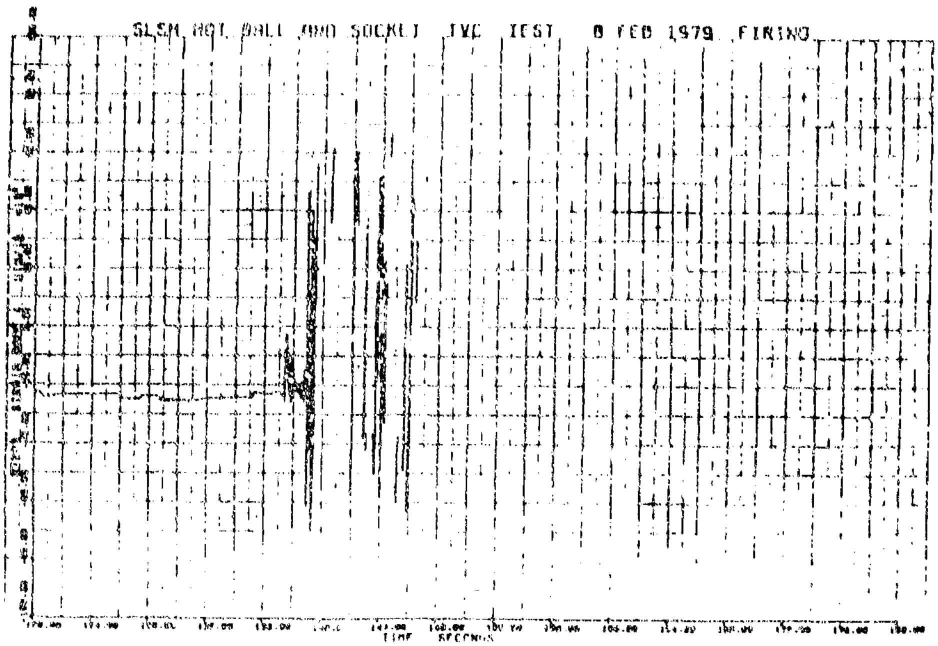

Figure 45. Strain Gage 4, 270 deg from TDC

27293

over 18,000 lbf. Another indication at the 270 deg azimuth (SG 4) between 6 and 10 sec corresponds to TVC actuator forces exerted during this period.

4.2.5 Recovered Hardware Studies

The nozzle hardware which remained intact was disassembled and studied along with the recovered ejected hardware. The three pieces of the ball extension and the exit (which separated into 14 large pieces) are shown reassembled in Figure 46. The 100 deg location where leakage was first observed is closest to the camera. Some key pieces of the exit at the threaded forward end which are seen to be missing were not recovered.

The postfire ball and nozzle ring are seen in Figure 47 and with the recovered aft ball extension reconstructed in Figure 48. The ball is shown in Figure 49 after removal from the socket, but with the forward lockring still in place. The notch at 0 deg is a saw cut from insulator removal. Aluminum oxide deposits (verified by chemical analysis) are seen between the ball and forward lockring surfaces near the 320 deg azimuth and around to about the 60 deg azimuth. Additional aluminum oxide deposits are seen on the aft face of the forward lockring.

Figure 46. Reconstructed Exit Cone and Ball Extension, Nozzle S/N 1

21091

There was, by design, a gap during firing be ween the aft face of the forward lockring and the forward face of the socket. In contrast, the mating (sealing) surface between the ball and socket (the shiny band on the ball) is free of contamination and any signs of leakage. The ball entrance shown in Figure 50 depicts the high, nonuniform erosion experienced during the firing.

The surface of the socket is seen in Figure 51. The shiny, mating surface with the ball is, like the ball, free of contamination and leakage indications. Aluminum oxide deposits are evident, however, in the annular gap that existed during test forward of the sealing, load-carrying mating surface. The posttest socket was cracked at about the 230 deg azimuth. Upon ejection of the exit cone and simultaneous loss of actuation, the forward biased thrust and actuator forces, offsetting the blowoff load, were also lost. The result was a 300% increase in the bearing load on the socket, causing hoop tensile failure of the socket. Note that the crack edges are sharp and there is no sign of flow through or near the portion of the crack extending into the sealing surface. Note also that the aluminum oxide deposit over the portion of the crack forward of the sealing surface is cracked correspondingly, indicating the socket cracked after the aluminum oxide solidified.

The measured erosion profiles from the recovered components are presented in Figure 52. The effects on entrance erosion of the 7-1/2 deg cant of the ball for the last 42-1/2 sec of firing are clear, with maximum erosion in the plane of cant. The side of the entrance vectored into the flow (so that impingement was likely: the 90 deg azimuth) was eroded bluntly and to a maximum depth of 0.97 in., and the opposite side (where the majority of the flow presumably

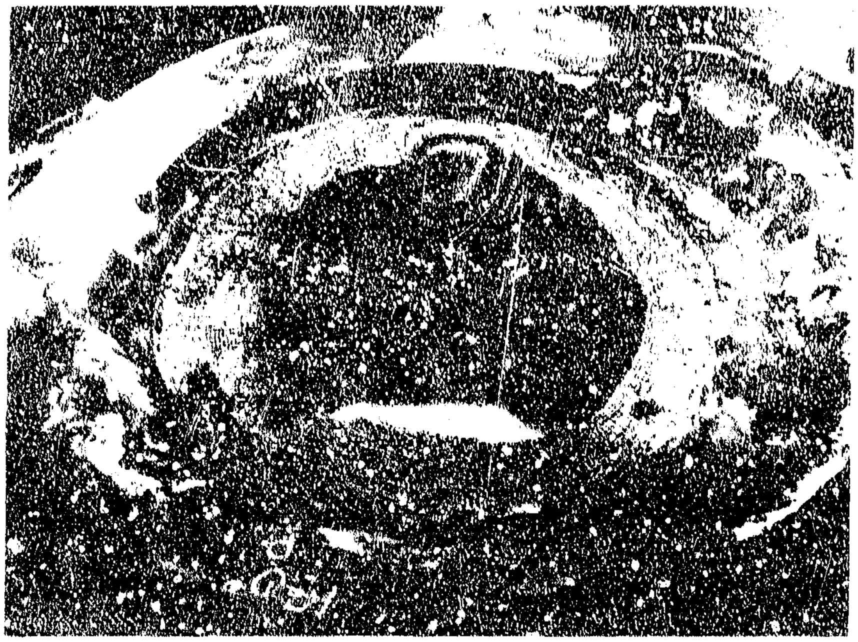

11784-2

Figure 47. Aft View of Posttest Ball and Nozzle Ring, Nozzle S/N 1

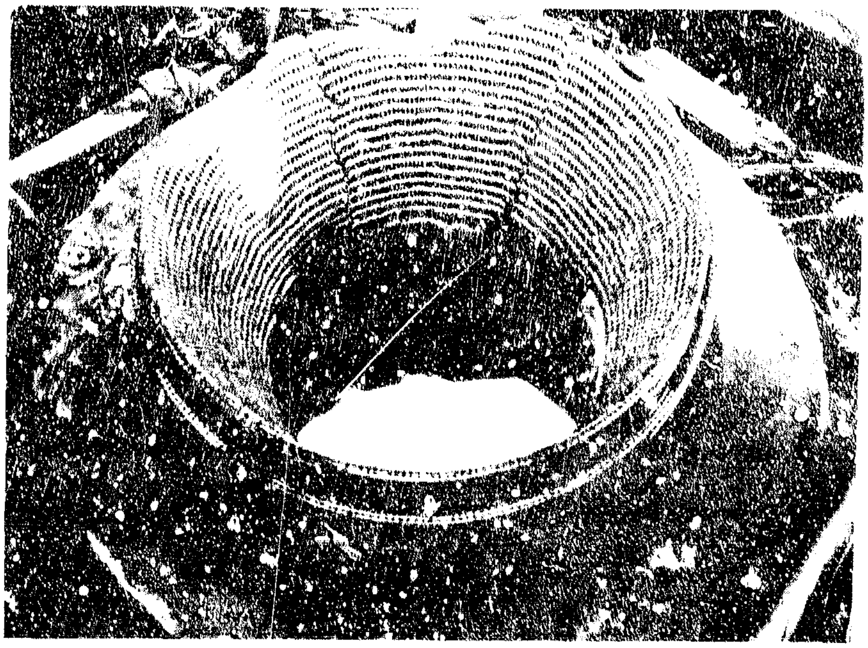

11784-4

Figure 48. View of Posttest Ball with Reconstructed Aft Extension, Nozzle S/N 1

27498

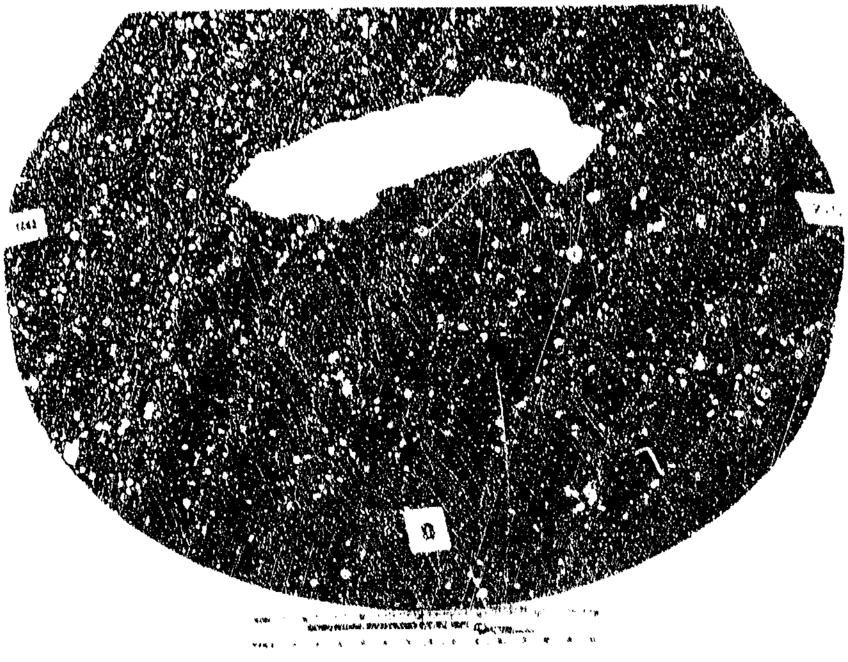

Figure 49. Postfire Ball, Nozzle S/N 1

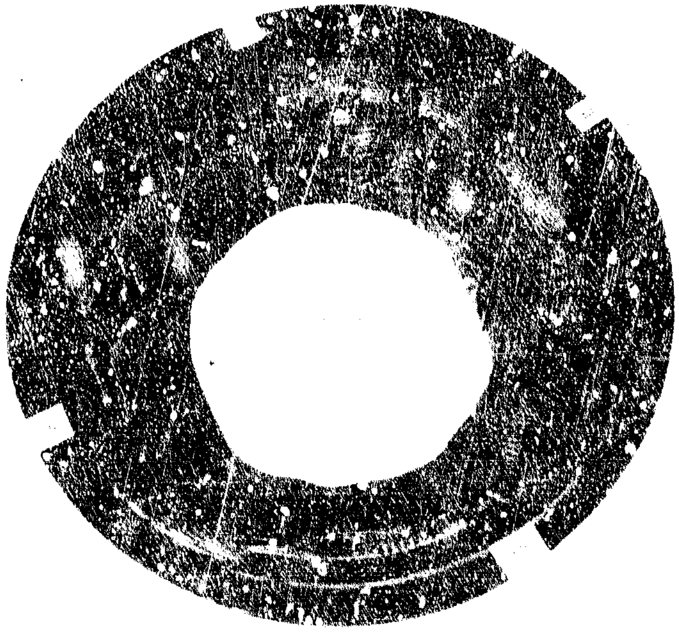

Figure 50. Postfire Ball Throat/Entrance, Nozzle S/N 1

21098

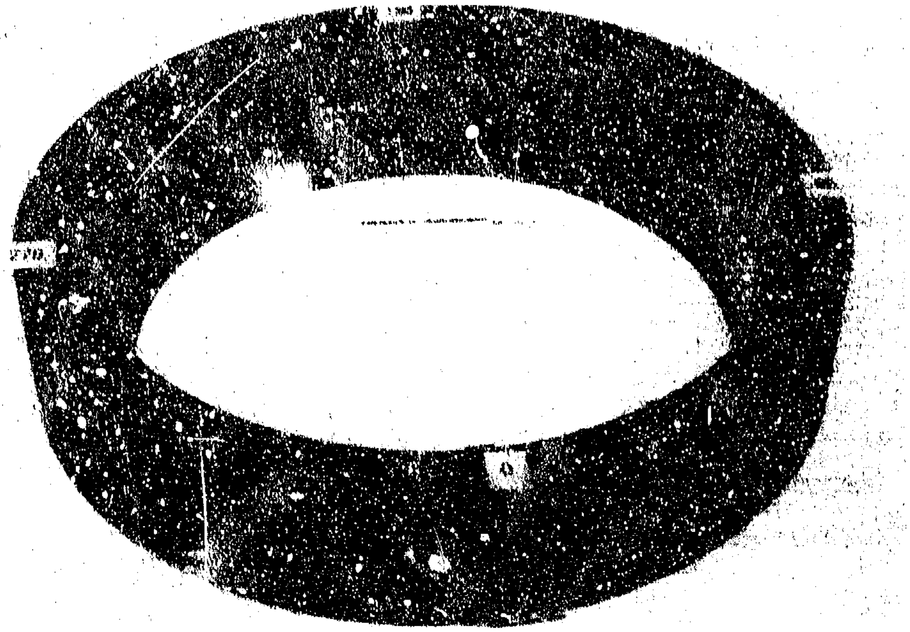
12072-5

Figure 51. Postfire Socket, Nozzle S/N 1

21097

entered the nozzle) was eroded 1.24 in. The locations 90 deg from these were eroded 0.43 in. and 0.85 in. The average ballistic throat erosion rate was 11.0 mils/sec, which is surprisingly low for a 58.7 sec test of this severity.

The erosion of the ball entrance and the surrounding forward lockring insulators was severe and higher than expected had the firing gone as planned. Flow was severe enough to cause local melting of the steel ring that retained the lockring, as shown in Figure 53. At least part of the flow severity can be linked to the canted position of the entrance during the last 42.5 sec of the test.

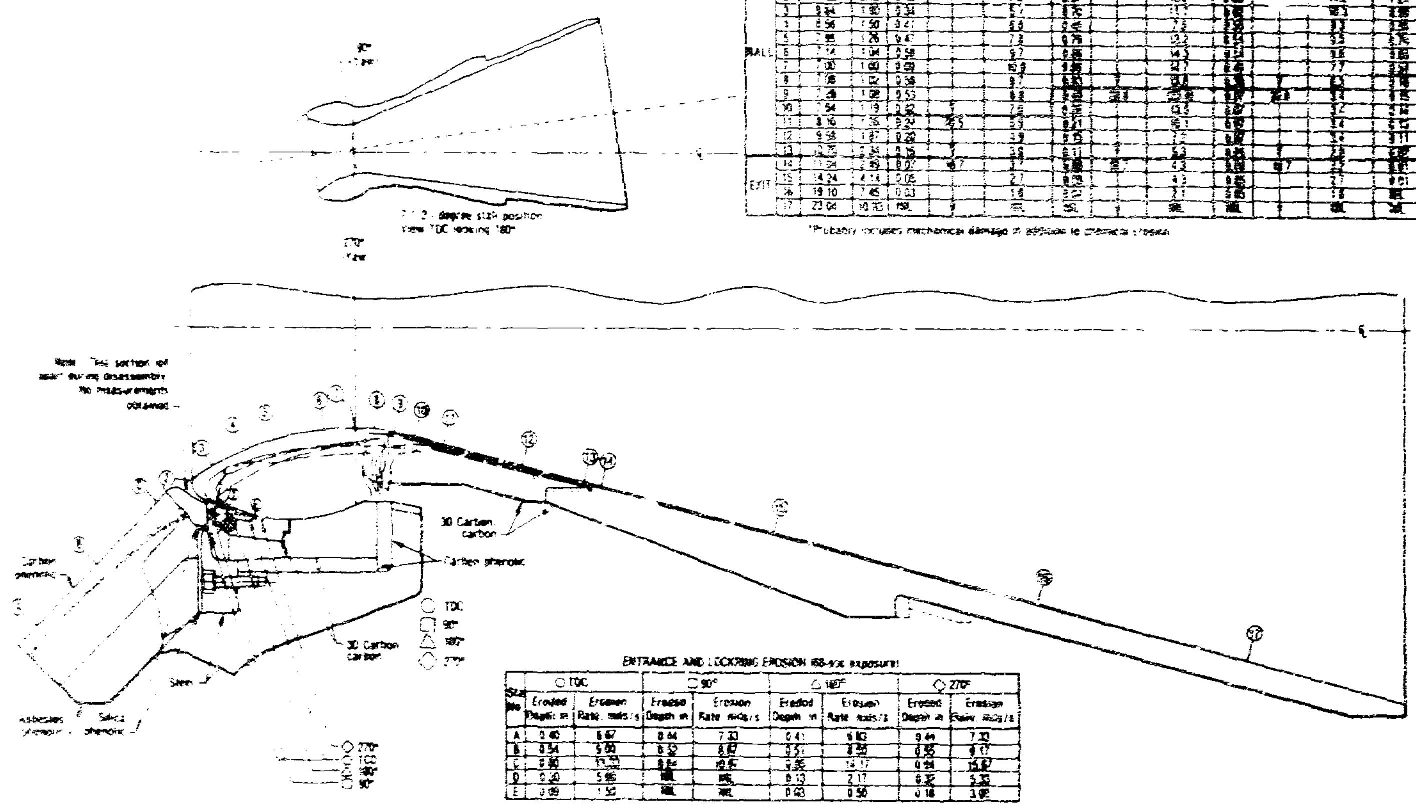

BALL AND EXIT EROSION

	Sta No	Initial Diameter in	Initial Area Ratio	○ TDC Eroded Depth in	○ TDC Time of Exposure sec	○ TDC Estimated Erosion Rate mils/s	□ 90° Eroded Depth in	□ 90° Time of Exposure sec	□ 90° Estimated Erosion Rate mils/s	△ 180° Eroded Depth in	△ 180° Time of Exposure sec	△ 180° Estimated Erosion Rate mils/s	◇ 270° Eroded Depth in	◇ 270° Time of Exposure sec	◇ 270° Estimated Erosion Rate mils/s
BALL	1	12.26	3.27	2.06	92.2	1.9	0.23	59.0	6.5	0.13	69.3	2.2	0.18	69.6	3.8
	2	10.68	2.42	0.43		7.2	0.07		[illegible]	[illegible]		14.2	1.24		[illegible]
	3	9.34	1.90	0.34		5.7	0.76		11.7	[illegible]		10.3	[illegible]		10.5
	4	8.56	1.50	0.41		5.8	0.45		7.5	[illegible]		[illegible]	[illegible]		14.2
	5	7.95	1.26	0.47		7.3	0.79		13.2	[illegible]		3.5	[illegible]		[illegible]
	6	7.14	1.04	0.58		9.7	[illegible]		14.5	[illegible]		1.8	[illegible]		11.3
	7	7.00	1.00	0.59		10.8	[illegible]		12.7	[illegible]		7.7	[illegible]		8.5
	8	7.08	1.02	0.58		9.7	[illegible]		[illegible]	[illegible]		6.3	[illegible]	[illegible]	6.3
	9	7.28	1.08	0.53		8.8	[illegible]	[illegible]	[illegible]	[illegible]	[illegible]	[illegible]	[illegible]		5.5
	10	7.54	1.19	0.42		7.6	[illegible]		13.5	[illegible]		3.2	[illegible]		3.4
	11	8.16	1.35	0.34	29.5	5.9	0.21		5.1	[illegible]		3.4	[illegible]		3.5
	12	9.38	1.87	0.28		3.9	[illegible]		[illegible]	[illegible]		3.0	0.11		4.2
	13	10.75	2.34	0.15		3.8	0.11		5.3	[illegible]		2.8	[illegible]		2.4
EXIT	14	11.04	2.49	0.07	18.7	3.7	[illegible]	[illegible]	4.3	[illegible]	18.7	2.5	[illegible]	18.7	8.5
	15	14.24	4.14	0.05		2.7	0.08		4.1	0.05		2.7	0.01		8.5
	16	19.10	7.45	0.03		1.8	0.02		2.1	0.03		1.8	[illegible]		[illegible]
	17	23.04	10.93	NIL		NIL	NIL		NIL	NIL		NIL	NIL		NIL

*Probably includes mechanical damage in addition to chemical erosion

ENTRANCE AND LOCKRING EROSION (60-sec exposure)

Sta No	○ TDC Eroded Depth in	○ TDC Erosion Rate mils/s	□ 90° Eroded Depth in	□ 90° Erosion Rate mils/s	△ 180° Eroded Depth in	△ 180° Erosion Rate mils/s	◇ 270° Eroded Depth in	◇ 270° Erosion Rate mils/s
A	0.40	6.67	0.44	7.33	0.41	6.83	0.44	7.33
B	0.54	9.00	0.52	8.67	0.51	8.50	0.55	9.17
C	0.80	13.33	0.64	10.67	0.85	14.17	0.94	15.67
D	0.20	5.66	NIL	NIL	0.13	2.17	0.32	5.33
E	0.09	1.50	NIL	NIL	0.03	0.50	0.18	3.00

Figure 52. Measured Erosion, Nozzle S/N 1

27195

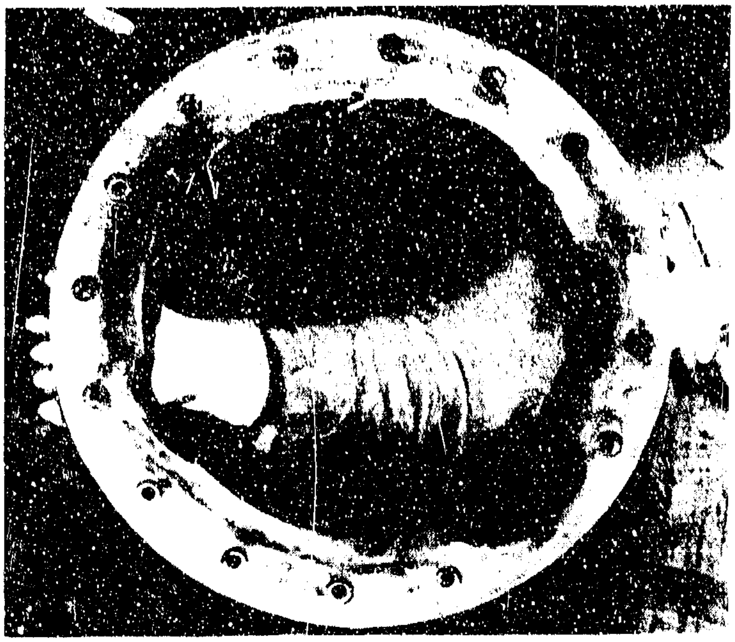

C 11805-1

Figure 53. Postfire Steel Support for Lockring, Nozzle S/N 1

21093

5.0 PROBLEM ASSESSMENT - NOZZLE S/N 1

Four significant problems were observed in the test and posttest analysis of nozzle S/N 1:

- Thread leakage, exit breakup, and ball extension loss.
- Excessive forward splitline erosion.
- Aluminum oxide deposition leading to thrust vector control (TVC) system stall.
- Cracked socket.

The following discussion reflects Chemical Systems Division's (CSD) observations in conjunction with the characterization studies performed on posttest parts and remnants by Atlantic Research Corp. (ARC) (reference 2).

5.1 THREAD LEAKAGE, EXIT BREAKUP, AND BALL EXTENSION LOSS

It was concluded that these problems were related, since the exit breakup and ball extension loss are believed to have resulted from the flame-cutting effects of the exhaust leakage. The primary cause of the leakage was believed to be a bad decision on CSD's part to densify the exit to only 1.7 g/cc (for the purpose of saving weight), whereas the data base with woven 3D carbon-carbon (C-C) materials such as this was primarily with materials densified to about 1.9 g/cc. Density and porosity characteristics of the posttest exit and ball extension were examined by ARC. The results showed a 1.6 g/cc density for the exit, which is even lower than the reported 1.7 g/cc. The open porosity of the exit was determined to be over 21%, compared to 7 to 8% with typical 1.9 g/cc 3D C-C material. This represents 75% of the total porosity in the exit and results in a specific open pore volume for the exit, which is more than double that of the ball extension. These results, coupled with a mismatch in thermal expansion between the exit and ball extension and the numerous zones of weave anomalies, contributed to the problems associated with this test. In addition, the ball-to-exit thread design was not the best choice. As discussed in section 6.0, the 4-acme thread utilized did not accommodate, in some thread forms, a full unit cell of radial and circumferential bundles. The lack of reinforcements in some thread teeth probably resulted in a significant reduction in shear capability.

5.2 EXCESSIVE FORWARD SPLITLINE EROSION

This problem may or may not have been caused by the 7-1/2 deg canted position of the entrance during the final 42.5 sec of the test. It was therefore assumed that the stubiness of the entrance was at fault in that it induced high circulatory flow similar to that experienced in subsonic splitline nozzles. Lengthening the entrance and increasing the contraction ratio to create a relatively quiescent separated flow region near the splitline was the proposed solution to this problem.

5.3 ALUMINUM OXIDE DEPOSITION LEADING TO THRUST VECTOR CONTROL SYSTEM STALL

The posttest analysis concluded that deposition of aluminum oxide in the annulus between the forward part of the ball and the lockring caused actuator stall.

5.4 CRACKED SOCKET

The crack in the socket was most likely caused by the exit and actuator loss. The loss of the contribution of the exit to thrust and the loss of the forward actuator bias load (pull-only actuators) nearly tripled the load on the socket. However, for future designs it was determined best to retain the socket more positively (on a ramp instead of a cylinder, and with tighter tolerances) and to change the socket weave design from a conical frustra to a high-hoop fraction cylindrical construction, which has more predictable characteristics.

6.0 REDESIGN OF NOZZLE S/N 1

Nozzle S/N 1 (Figure 54), was later modified to correct the problems identified in that test and discussed in sections 4.0 and 5.0. Design changes were made only where necessary so that performance in the test of the second nozzle could be correlated to the changes. The actuation system design remained unchanged since it performed without problems during the 8 February 1979 test. The potential solutions considered in the nozzle redesign are summarized in Table 3.

6.1 DESIGN CRITERIA

6.1.1 Ballistics

The revised design was to be tested on the short length super HIPPO (SLSH) motor at the Air Force Rocket Propulsion Laboratory (AFRPL). The test conditions selected were those representative of advanced upper stage conditions, approximately 750 psia for 75 sec with a propellant of moderate erosiveness. The Government-furnished equipment (GFE) grain was fabricated by Chemical Systems Division (CSD) under AFRPL contract No. F04700-79-C-0080. The propellant was CSD's UTP-19,687, a 90% solids/20% Al/12% cyclotetramethylene tetranitramine

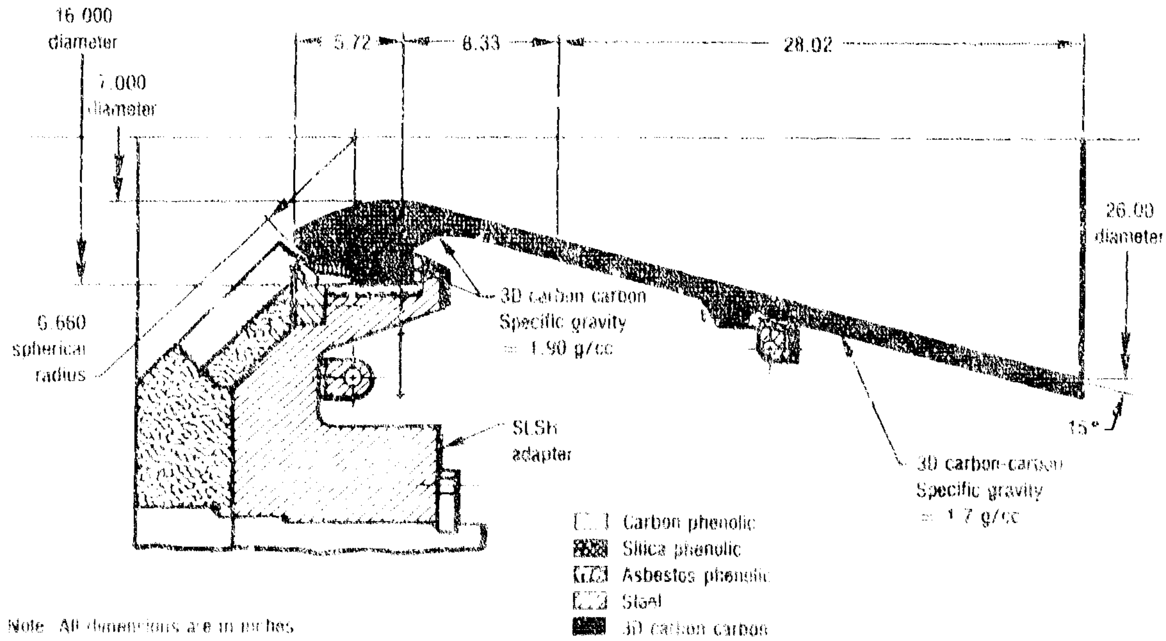

Figure 54. Hot Ball and Socket TVC Nozzle S/N 1

27196

TABLE 3. SUMMARY OF POTENTIAL SOLUTIONS CONSIDERED IN NOZZLE S/N 1 REDESIGN

T6825

Thread leakage, exit breakup, and throat extension loss	1. Increase exit density to 1.9 g/cc 2. Lengthen the threaded joint 3. Add a stepped-joint seal at forward end of threads 4. Improve graphite cement application and cure 5. Improve ball-to-exit joint
Excessive forward splitline erosion	1. Lengthen entrance and increase contraction ratio to create separated flow region at splitline
Aluminum oxide deposition leading to system stall	1. Change forward lockring to carbon phenolic 2. Treat forward surface of ball to prevent deposition
Cracked socket	1. Retain socket on ramp 2. Tighten tolerances 3. Change socket weave from conical frustra to cylinder with high hoop volume fraction

(HMX) hydroxyl-terminated polybutadiene (HTPB). This propellant was successfully demonstrated in the Jet Propulsion Laboratory (JPL) high energy performance nozzle firing, and the CSD/Societe Europeene de Propulsion (SEP) advanced apogee motor fired at AFRPL on 15 November 1979.

The physical dimensions and properties of the center-perforated grain are presented in Table 4. The predicted ballistic conditions were as follows:

Maximum pressure, psia	803
Average pressure, psia	746
Action time, sec	74.6

The design maximum expected operating presure (MEOP) was 1,004 psia (1.25 x maximum pressure).

6.1.2 TVC

The thrust vector control (TVC) requirements were identical to those of nozzle S/N 1:

Maximum deflection, deg	8 omniaxial
Maximum slew rate, deg/sec	40
Minimum acceleration, deg/sec	300
Pivot point	Forward throat pivot

Since no problems were encountered with the TVC actuation system design used with nozzle S/N 1, it remained unchanged. The actuation system again consisted of four pull-only hydraulic actuators with an integral feedback potentiometer control system. The actuator assembly configuration is per CSD drawing C13134. The pull-only nature of the actuators provided a constant forward load reducing the net blowoff load due to chamber pressure, and hence torque.

TVC performance calculations were made to determine the expected nozzle response and required actuator hydraulic supply pressure. The design parameters and expected response of the TVC system are presented in Table 5.

TABLE 4. DIMENSIONS AND PROPERTIES OF UTP-19,687

T8271

Grain	
Weight	13,504 lbs
Length	61.7 in.
Bore diameter	45.7 in.
Web	16.3 in.
Propellant	
Burning rate at 1,000 psia	0.2623 in./sec
Burning rate exponent	0.305
Propellant density	0.0653 lb/sec.^{3}
C*	5,076 ft/sec
Flame temperature	6538°R

The torque for nozzle S/N 2 would be lower than that for nozzle S/N 1 because of the reduced average chamber pressure (746 versus 1,355 psia). Since the torque would be lower for the conditions of S/N 2, the hydraulic supply pressure to the actuators was reduced from 3,000 psi (used for S/N 1) to 2,000 psi. The reduced supply pressure provides a reduction in the bending loads imposed on the exit.

6.2 DESIGN MODIFICATIONS

A major effort of the design modification included an investigation

TABLE 5. TVC DESIGN PARAMETERS AND EXPECTED RESPONSE, NOZZLE S/N 2

T8272

Actuation moment arm	12.9 in.
Piston area, actuator	6.045 in.^{2}
Maximum actuator pull force	12,090 lbf
Maximum torque capability of actuator	156,000 in.-lb
Forward bias load, actuators	24,121 lbf
Ball spherical radius	6.66 in.
*Design friction coefficient	0.12
Calculated response at MEOP (1004 psia):	
†Net blow off load	48,000 lbf
Blowoff torque	84,231 in.-lb
Aerodynamic torque	5,500 in.-lb
Offset torque	1,000 in.-lb
Total torque	90,733 in.-lb
Safety factor, actuator capability	1.72:1

* Maximum measured on successful Navy Launch Vehicle Materials firing August 1978

† Includes forward bias load contribution from pull-only actuators

of alternative ball-to-exit joint concepts. Evidence from the first 7-in. hot ball and socket (HBS) firing indicated that the exit cone failure initiated at the threaded joint. Although the exact cause had not been isolated, confidence in threaded joints was of concern.

Threaded joint concerns included: (1) uncertainty of load transfer under bending loads, (2) uncertainty of sealing under bending loads due to a possible gap, either mechanically induced and/or from differential thermal expansion between the ball and exit, and (3) uncertainty of the load-carrying capability of individual thread teeth under shear loads. The shear strength uncertainty arises from the primary dependence of local thread shear strength on the number of local radial reinforcements. With a fine thread design (near the unit cell size or less) the probability of an adequate number of radial bundles at a given location in each tooth is reduced, and hence confidence in the thread shear capability is correspondingly reduced.

Several joint candidates were evaluated on the basis of structural integrity, fabricability, and cost and compared to the four-per-inch Acme threads incorporated in nozzle S/N 1 (reference 3). The candidate concepts included: pins, keys, breech lock, and collar. Overall disadvantages were identified with each concept for this application.

The study concluded that for this particular design the candidate non-threaded joints did not offer an overall advantage over an improved threaded joint. A coarser, modified Acme thread was selected as the best replacement for the four-per-inch Acme threads of S/N 1. The selected 1-1/2 thread per in., 10-deg-modified stub Acme allows an average of three radial bundles per tooth cross-section. This thread design provides a better shear capability than with the finer four-per-in. Acme threads in which an average of only one radial bundle was present in each tooth cross-section. The included angle of each thread form was reduced from 29 deg to 10 deg resulting in an almost square tooth, to reduce the radial load component under TVC bending. Figure 55 clearly compares the differences between the 4 Acme and 1-1/2 Acme threads.

Additional changes incorporated to preclude leakage at the joint included increasing the exit density from the 1.5 - 1.7 range to 1.9 g/cc, matching the weave design of the aft throat extension with the forward exit cone, and improving the application and cure of graphite cement. Increasing the exit density to 1.9 g/cc reduces the open porosity of the exit from 21% or more to the 8 to 9% range, similar to that of the throat and socket. By better matching the weave spacing, fiber volume fraction, and density between the forward exit and aft throat extension, more nearly similar properties can be expected, reducing the potential for thermal expansion and/or mechanically induced mismatch.

To reduce the severe erosion encountered in the first test at the forward splitline between the ball and lockring, the entrance was lengthened and the entrance expansion ratio was increased. This provided a sacrificial entrance and a separated flow region eliminating direct impingement at the splitline.

Changing the forward lockring from 3D carbon-carbon (C-C) to carbon phenolic was intended to help prevent Al_2O_3 deposition. Alumina is less likely to deposit on carbon phenolic because of (1) outgassing as the surface chars and

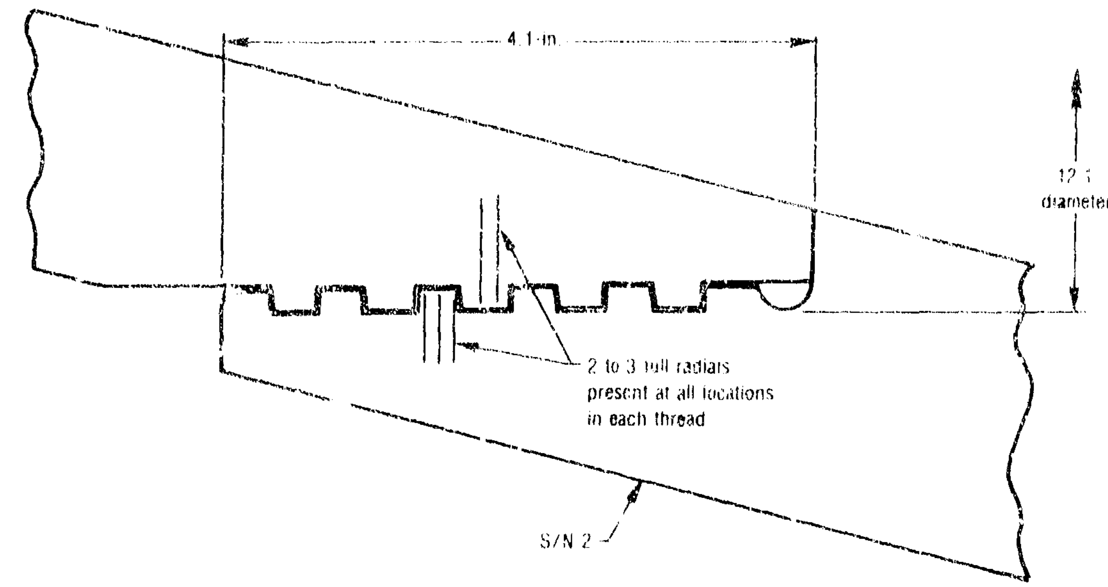

1.500 stub acme thread modified 10°

≈ 3 radial fiber bundles per tooth

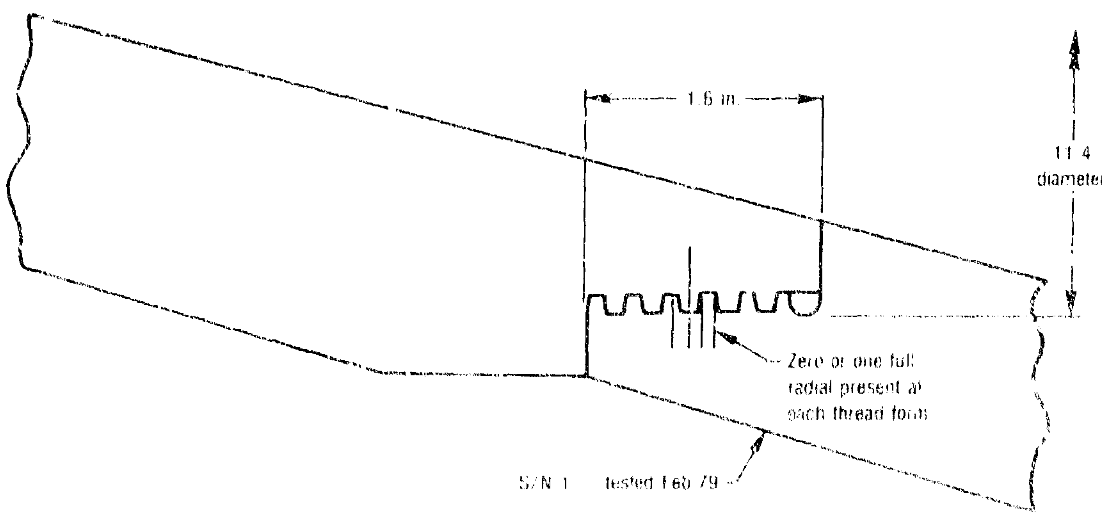

4 acme thread

≈ 1 radial fiber bundle per tooth

Figure 5[illegible]. Comparison of the 1-1/2 Stub Acme Thread with the 4 Acme Thread Tested on Nozzle S/N 1

27249

(2) the higher surface temperature which results from the low conductivity of the phenolic. Secondly, the ball surface was to be treated to help prevent deposition. The surface treatment candidates were evaluated under laboratory testing.

The problem of the cracked socket, observed upon posttest disassembly, was most likely associated with (1) the loss of the actuator forward bias load and (2) the exit cone's thrust contribution. These two effects nearly tripled the blowoff load on the socket. However, for conservatism, the weave plan for the socket was changed from a conical construction to a cylindrical construction, and a ramp retention was introduced. The response of a cylindrical billet to loading can be more confidently estimated than that of a conical billet. The socket was supported on a 3-deg ramp and tolerances were tightened to better ensure positive support.

The revised design (nozzle S/N 2) is presented in Figure 56 and compared to the tested S/N 1 design in Figure 57. Note that the exit cone was truncated to

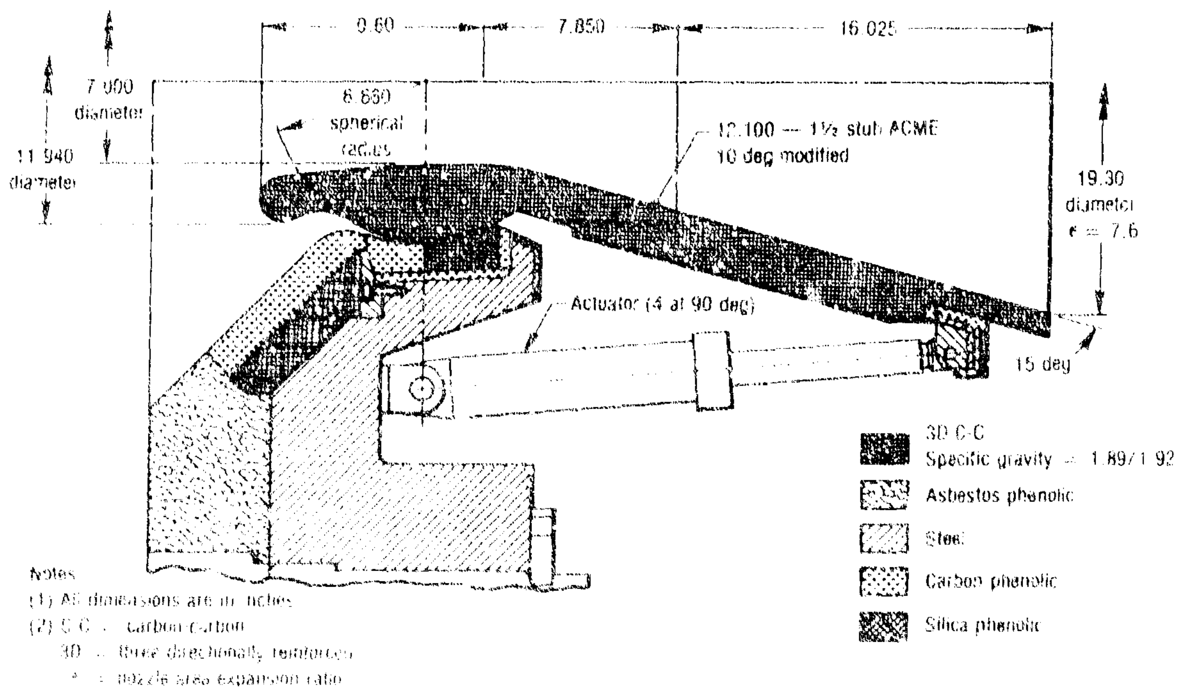

Figure 56. Hot Ball and Socket TVC Nozzle, Revised Design (S/N 2)

27147

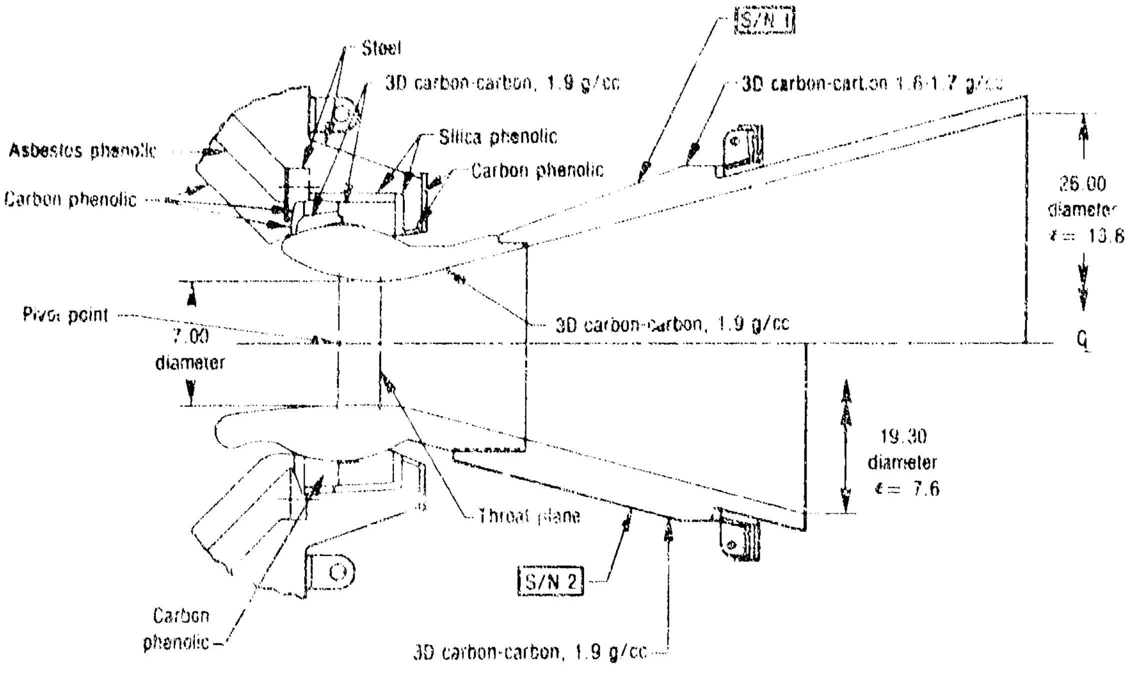

Note: All dimensions are in inches

Figure 57. Comparison of Nozzle S/N 1 to Redesigned Nozzle

27198

reduce the expansion ratio and prevent flow separation at the lower pressure of the second test. Aerothermal and structural analysis results reported in reference 3 indicate no design deficiencies. While C-C billet fabrication for the full-scale nozzle was underway, parallel efforts were on-going to select a C-C surface treatment and prepare for a subscale verification firing.

6.3 SUPPORTING LABORATORY EFFORTS

The purpose of this task was to develop a surface treatment for the spherical surfaces of the 3D C-C ball and socket which ideally meet the following objectives:

- Reduce the friction coefficient to reduce torque
- Reduce or eliminate alumina deposition
- Seal the surface (reduce permeability) to permit bench testing with gas pressure providing the axial load.

A survey of numerous surface treatment candidates was conducted including a literature search and industry contacts. Candidates were screened on the basis of cost, reported friction coefficient, processibility, and high temperature capability. Table 6 lists those candidates subsequently considered for laboratory scale testing.

The various surface treatments were applied to 3.92-in. spherical diameter C-C ball and socket test rings such as those shown in Figure 58. Each test bearing set was tested in the bench test assembly shown in Figures 59, 60, and 61. Friction and relative permeability data were obtained with this test configuration.

Each ball and socket set was subjected to plus and minus 5-deg single axis, triangular wave commands totaling 20 deg of travel for each event. Vectoring was performed over a range of ball to socket bearing pressures up to a nominal value of 5,500 psi. The maximum slew rate achieved was 10-deg/sec.

The friction coefficient results for the variety of surface treatments examined are summarized in Table 7. The most promising candidate appeared to be the 50% Sermetel/50% Teflon mixture. Sermetel (type W), a corrosion inhibiter for steel, consists of an aqueous ceramic binder solution with aluminum filler. Sermetel is capable of withstanding temperatures of at least 1,200°F. The combination of Sermetel and Teflon apparently provides the relatively low friction coating characteristics of Teflon while the hard Sermetel aids in preventing cold flow and high breakaway friction typically associated with Teflon.

TABLE 6. CANDIDATE CARBON-CARBON SURFACE TREATMENTS

T8273

Candidate	Comments
Dylon TL	Graphite powder in Trichloroethylene carrier
Teflon	Low friction characteristics
Sermetel	Inorganically bonded aluminum
Teflon/Sermetel	Combination may increase service temperature of Teflon
Tin	Remains liquid between 450 and 4230 °F
Everlube	MO_2S and resin
Microseal 100	Impinged graphite and resin
Microseal 200	Impinged graphite and MO_2S

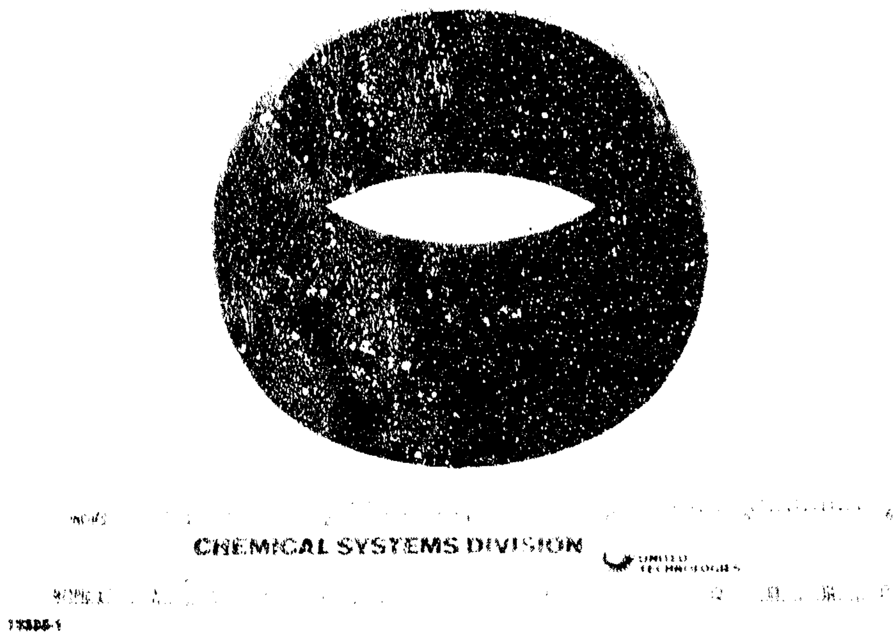

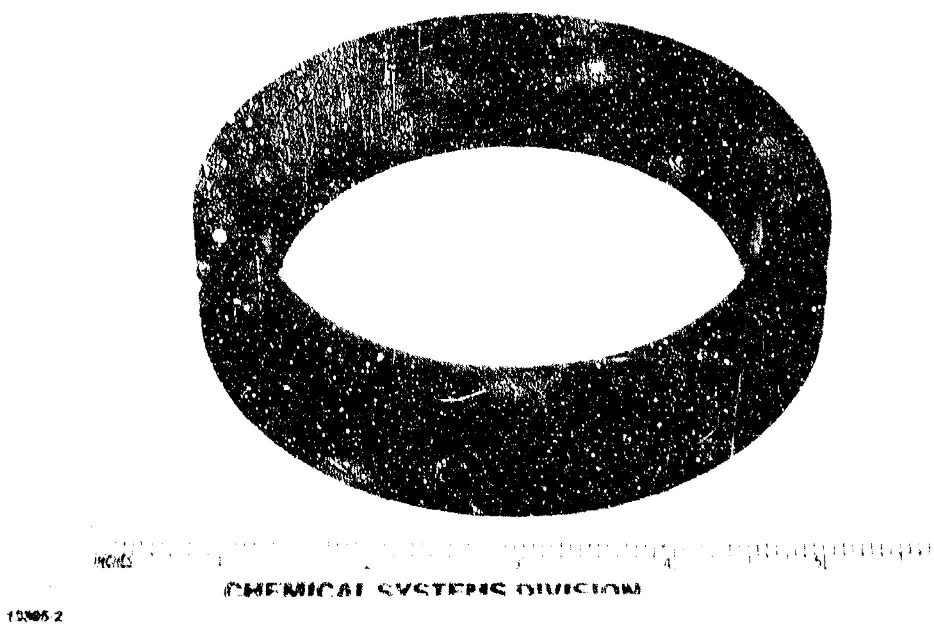

Figure 58. Ball and Socket Test Rings Used for Surface Treatment Studies
27199

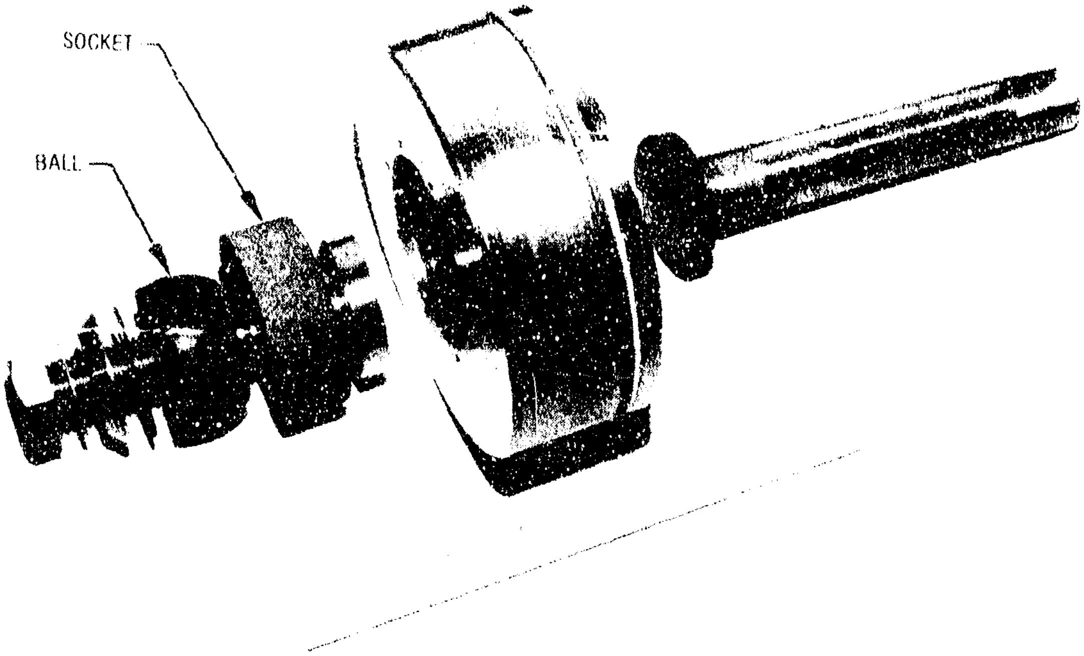

9662-13

Figure 59. Laboratory Bench Test Configuration

10000

The 7-in. HBS interface is expected to experience temperatures up to 1,200^{o}F as shown in Figure 62. The ball and socket test rings treated with the Sermetel/Teflon mixture were placed in an oven to 1,200^{o} F for 5 min. Upon removal the coating appeared unaffected and, when retested, the friction coefficient was unchanged (0.07 to 0.08).

The permeability of the C-C with the Sermetel/Teflon was also somewhat reduced compared to previous experience as evidenced by monitoring pressure decay in the test rig. The ability of the surface treatments to inhibit alumina deposition can be truly evaluated only in a static test firing; however, it was believed that the properties of Teflon might reduce the alumina problem.

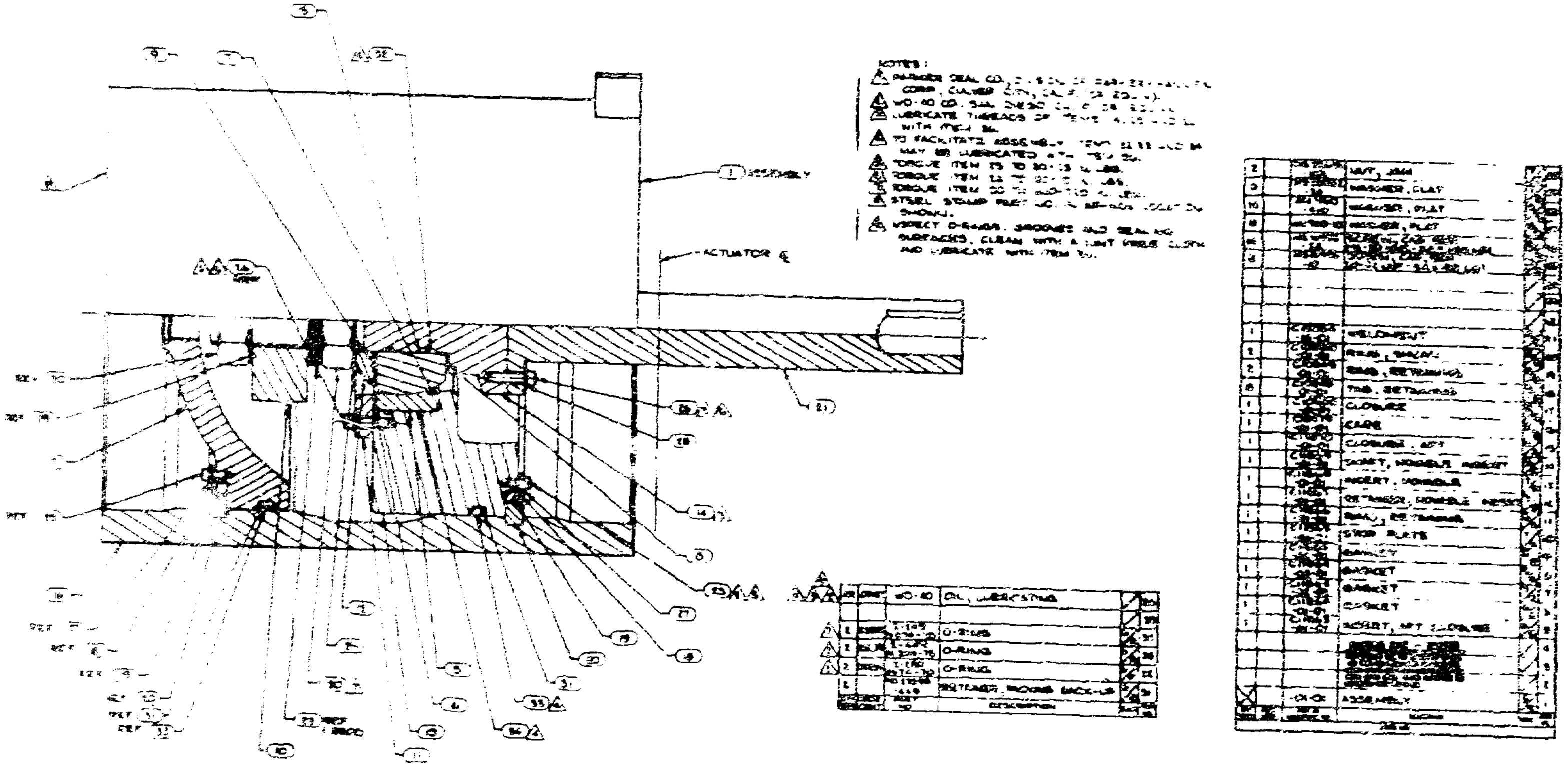

Figure 60. Laboratory Bench [illegible] figuration

09988

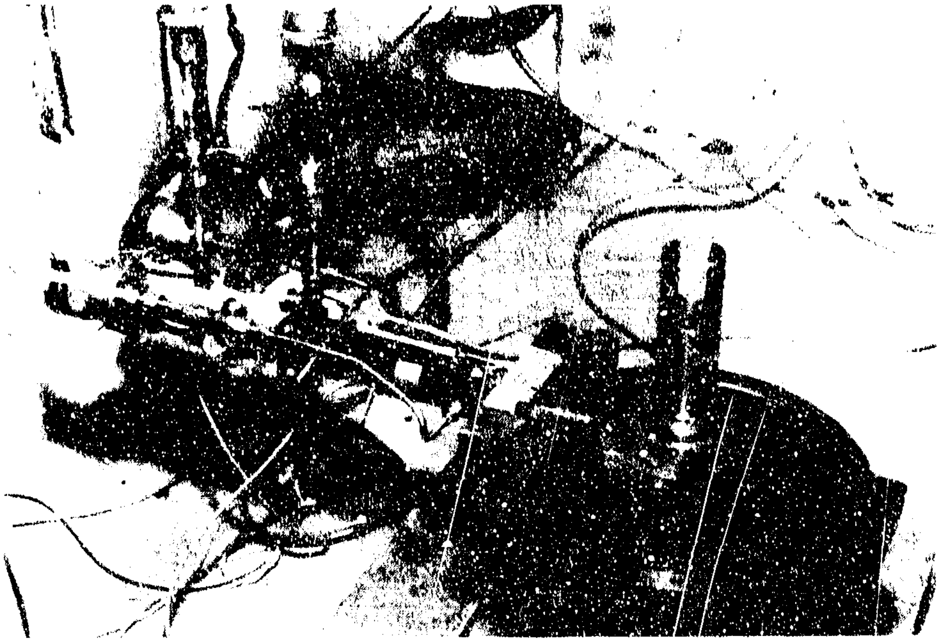

13323-2 Figure 61. Assembled Bench Test Rig

27200

TABLE 7. LABORATORY SCALE FRICTION COEFFICIENT RESULTS

T8274

Surface Treatment	*Friction Coefficient (μ)
Untreated	0.09 - 0.12
Dylon TL	0.08 - 0.11
Teflon	0.06 - 0.10
Microseal 200 overcoated with microseal 100	0.11 - 0.15
Everlube	0.10 - 0.13
30% Sermetel/70% Teflon	0.06 - 0.08
50% Sermetel/50% Teflon	0.06 - 0.08
Ion plated tin on socket w/untreated ball	0.11 - 0.13
Ion plated tin on socket w/50% Sermetel / 50% Teflon on ball	0.08 - 0.10

* Range of μ may be due to variation of loads, slew rate and wearing of surfaces. The maximum coefficient measured is the driver for design considerations.

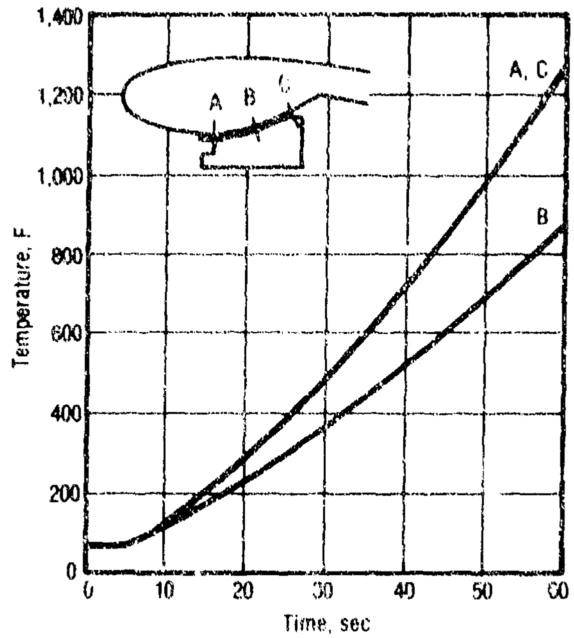

Figure 62. Expected Temperature History for 7-in. Ball-to-Socket Interface

18142

7.0 SUBSCALE NOZZLE VERIFICATION FIRING

7.1 OBJECTIVE

The objective of the subscale (2-in. D_t) firing was to verify the performance of modifications planned for the full-scale (7-in. D_t) hot ball and socket (HBS) nozzle. The design modifications planned for the full-scale nozzle which were evaluated in subscale were:

- Sacrificial entrance - was intended to split the flow and provide a separated flow region to protect forward splitline components from excessive erosion
- Carbon phenolic lockring - replaced the previously used carbon-carbon (C-C); intended to reduce deposition of aluminum oxide in the splitline
- Ball/socket surface treatment - intended to (1) provide a low friction bearing surface to reduce torque; and (2) inhibit alumina deposition.

In addition, the test was intended to acquire additional data on the HBS nozzle and further demonstrate its thermostructural integrity.

7.2 NOZZLE DESIGN

The nozzle assembly configuration (CSD P/N 13397-02-01) is depicted in Figure 63. Assembled and exploded views of the major subscale components are presented in Figures 64 and 65, respectively. This design is similar to that of HBS nozzle tested in August 1979 under Naval Surface Weapons Center (NSWC) contract No. N60921-77-C-0240 (reference), except for the following:

- A lengthened, sacrificial entrance was incorporated in the Air Force Rocket Propulsion Laboratory (AFRPL) design.
- The lockring material was changed from C-C to carbon-phenolic.
- A friction-reducing surface treatment was applied to the AFRPL ball and socket spherical surfaces.
- The threads at the ball-to-exit joint were lengthened and the included angle of the threads was reduced from 29 deg to 10 deg to reduce the radial load component (which tends to open up the thread gap).

- The fiber bundle spacing of the AFRPL ball was coarser than that of the NSWC ball (0.090 versus 0.050-in.) to reflect current practice and reduce cost.

A summary of the similarities and differences between the NSWC and AFRPL nozzles is presented in Table 8. A comparison of the prefire NSWC ball and prefire AFRPL ball incorporating the sacrificial entrance is presented in Figure 66.

The actuation system used in the NSWC test was refurbished for cost effectiveness for reuse in the AFRPL test. The system consisted of four pull-only hydraulic actuators with position feedback sensors in a closed-loop configuration and one servovalve per axis. Refurbishment included thoroughly cleaning all components, nondestructive evaluation (NDE), and replacement of O-rings, hydraulic hoses, and position transducers. Also, the exit cone fired in the NSWC nozzle was reused in the AFRPL nozzle with refurbishment in the threaded region only.

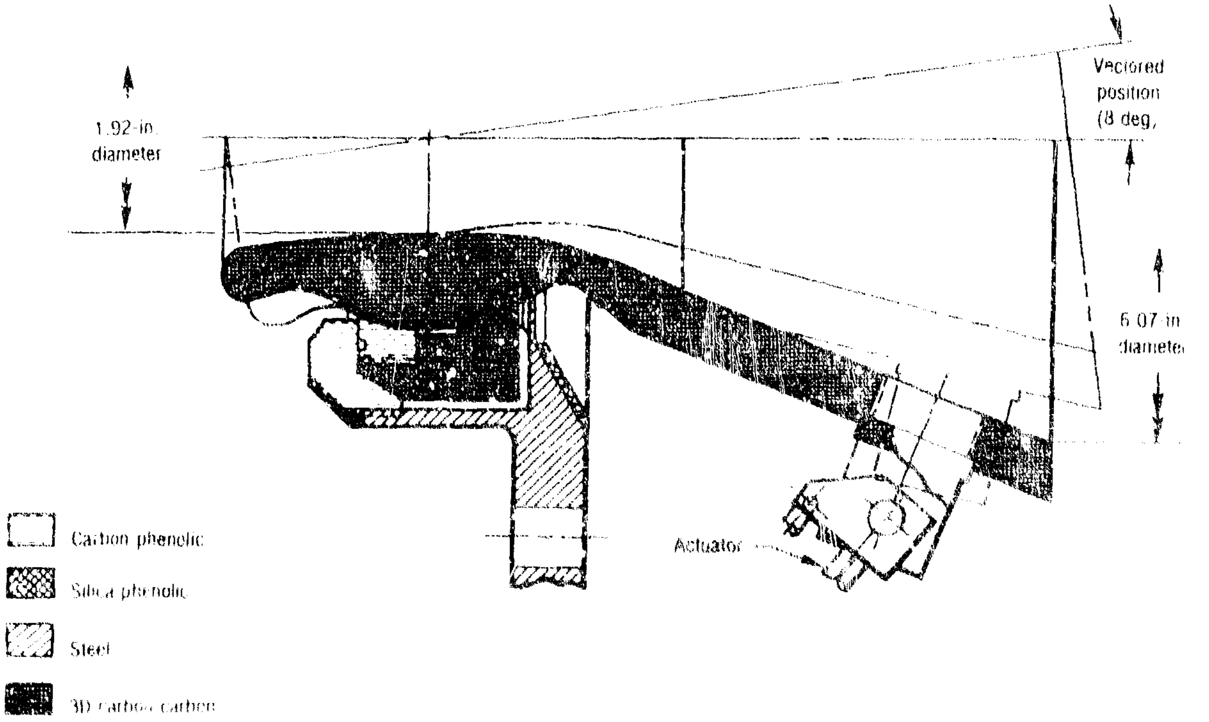

Figure 63. AFRPL Subscale Hot Ball and Socket Nozzle Configuration

13538-2

Figure 64. AFRPL Subscale Hot Ball and Socket Nozzle, Exploded View (Prefire)

27202

Figure 65. AFRPL Subscale Hot Ball and Socket Nozzle, Assembled View (Prefire)

TABLE 8. COMPARISON OF THE AFRPL SUBSCALE DESIGN WITH THE NSWC DESIGN

T8275

	NSWC	AFRPL
Throat diameter (in.)	1.92	1.92
TVC angle (deg)	15	8
Sacrificial entrance	No	Yes
Lockring material	Carbon-carbon	Carbon-phenolic
Surface treatment	CVD	Sermetel/Teflon
Ball fiber type	HM	HM
Ball fiber spacing (in.)	0.050	0.090
Included angle of ball-to-exit cone thread shape (deg)	29	10

Note: The exit cone fired in the NSWC nozzle was reused in the AFRPL nozzle with new threads machined at the forward end.

7.3 BENCH TESTING

Upon assembly of the nozzle and integration with the actuation hardware the system was subjected to extensive bench testing. Two of Chemical Systems Division's (CSD) TM-3 motor closures with a spacer ring between them were bolted together providing a cost-effective bench test pressure vessel. The nozzle housing was mated directly to the open port, and a plate with pressure fittings closed off the port of the opposite closure. The nozzle was subjected to numerous blowoff loads and hydraulic supply pressure while executing commanded vector events. The nozzle was eventually loaded to the blowoff load expected at the predicted maximum pressure of 861 psi. Hydraulic supply pressure was 3,000 psi, the maximum planned for the static firing.

The maximum torques measured during vector events to 8 deg in the pitch and yaw planes were 1,600 and 1,700 in.-lb, respectively, while at the maximum blowoff load. The measured torque values correspond to a friction coefficient between 0.075 and 0.08 (35% less than that nominally observed without the applied surface treatment). Figures 67 and 68 present the measured torque loops for vector events in the pitch and yaw planes, respectively, at the expected maximum blowoff load of 4,600 lbf.

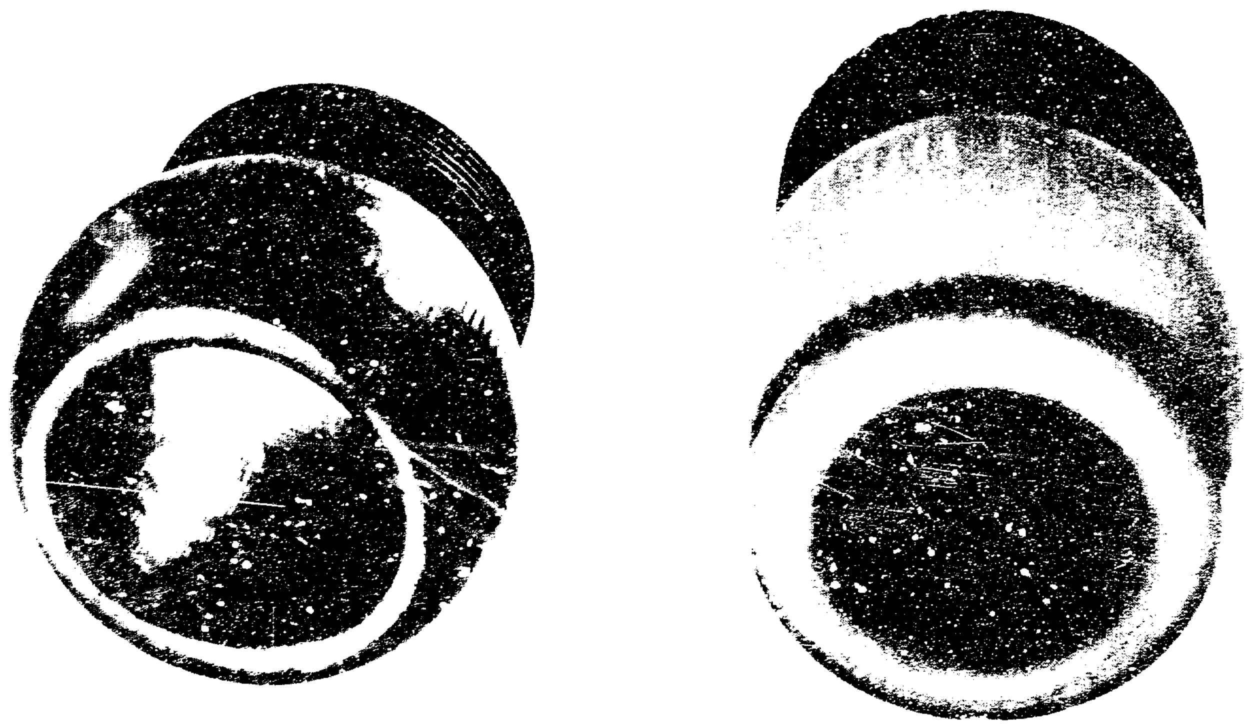

NSWC Ball AFRPL Ball

Figure [illegible]. Comparison of Prefire NSWC Ball with Prefire AFRPL Subscale Ball

27204

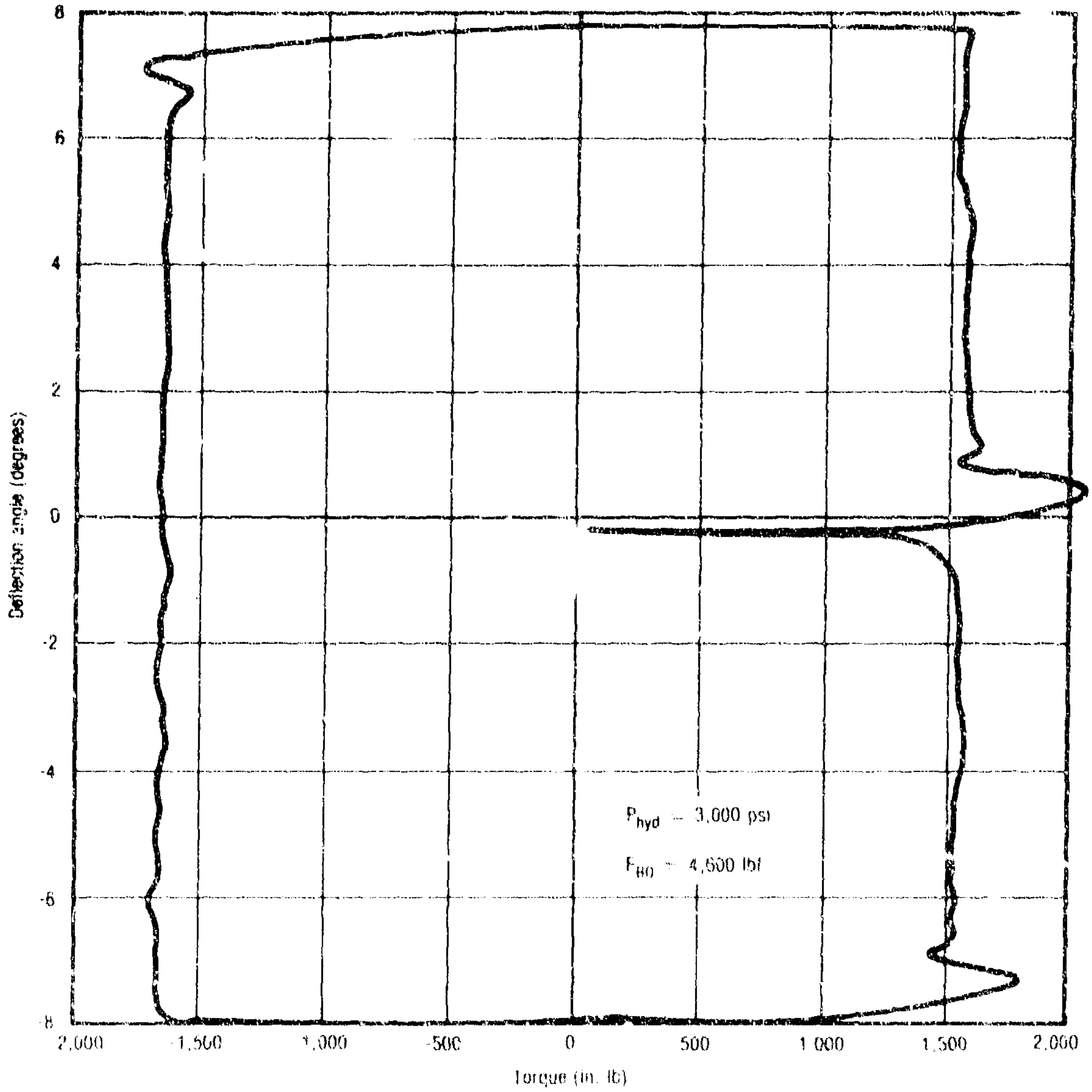

Figure 67. Torque vs Deflection Angle, Pitch Axis, Bench Test

27250

7.4 TEST RESULTS

The static test firing of the HBS nozzle on 18 March 1981, utilized CSD's TM-3 motor on pad ST-3 at CSD's Coyote development center. The loaded case configuration was per CSD drawing C11992-03-01. The center-perforated grain consisted of 441 lb of CSD's UTP-19,687 propellant, a 90% solids/20% Al hydroxyl-terminated polybutadiene (HTPB) type with 12% cyclotetramethylene tetranitramine (HMX).

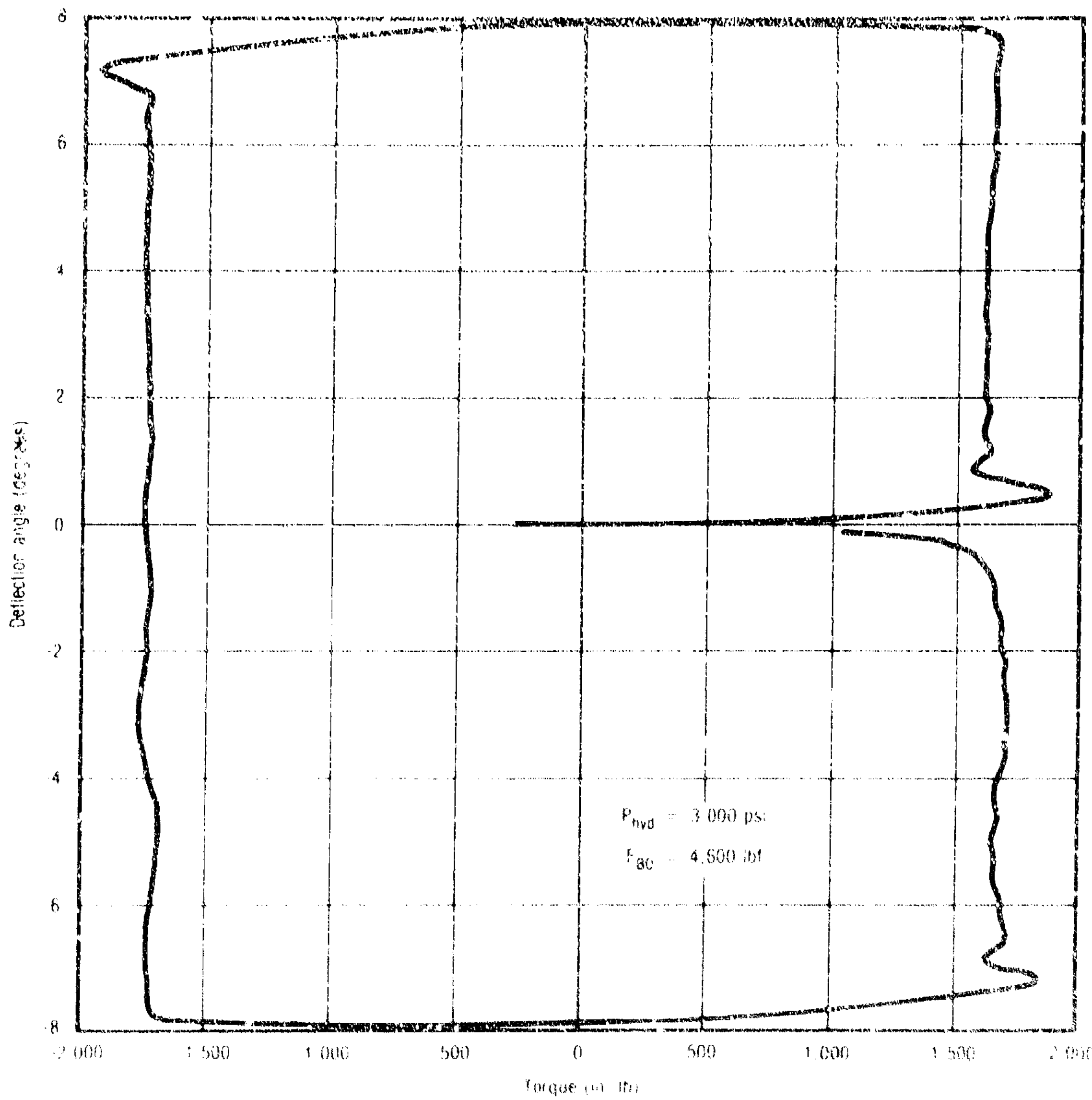

Figure 68. Torque vs Deflection Angle, Yaw Axis, Bench Test

27251

The pressure-time trace measured during the 28-sec firing is shown in Figure 69. The maximum pressure was 935 psia, and the average pressure was 779 psia. The maximum and average axial thrust was 3,371 and 3,652 lbf respectively. 150 deg of vector travel were commanded during the static firing.

Upon disassembly, the nozzle was found to be in excellent posttest condition as shown in the posttest exploded view in Figure 70. No leakage between

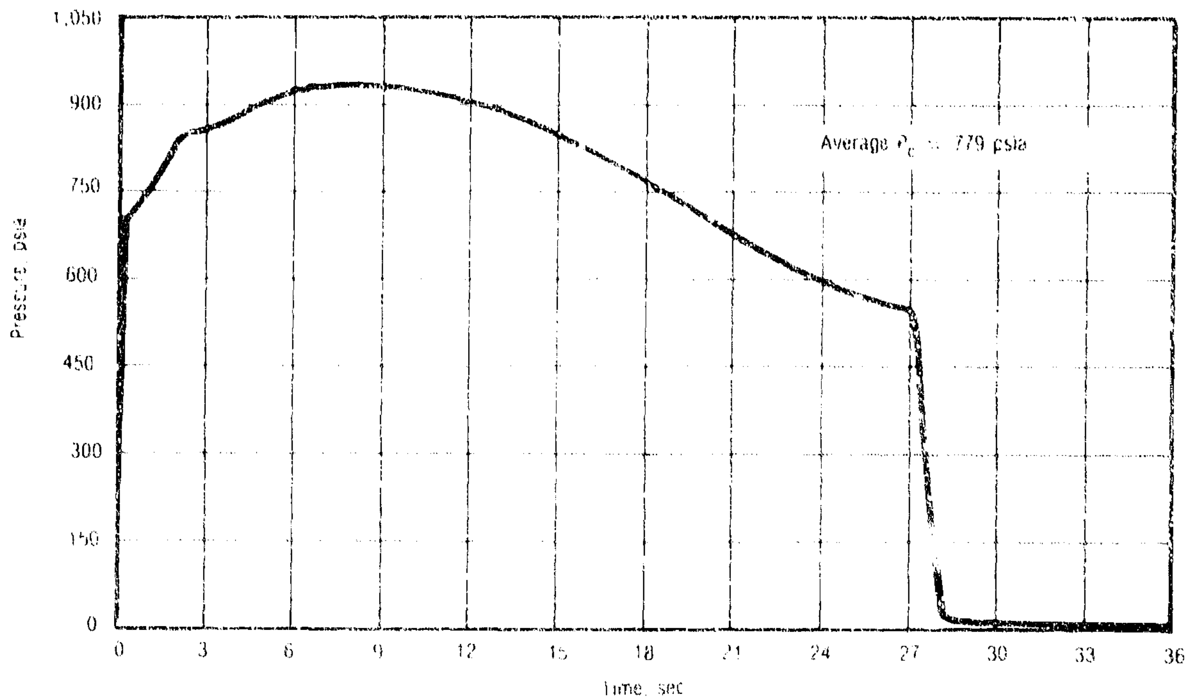

Figure 69. AFRPL Subscale Hot Ball and Socket Nozzle, Pressure vs Time

27205

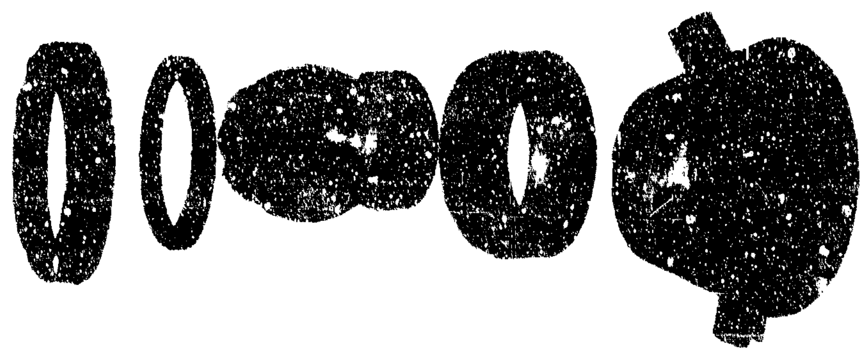

Figure 70. Posttest AFRPL Subscale Hot Ball and Socket Nozzle, Exploded View

27206

the ball and socket occurred as evidenced by the excellent condition of the mating ball and socket surfaces. The erosion profile of the ball was smooth, cylindrical, and tubular. The measured average ballistic throat erosion rate was 5.8 mils/sec. The posttest erosion profile is shown in Figure 71.

The posttest ball is compared with the prefire condition in Figure 72. The sacrificial entrance performed well preventing erosion of the splitline components. The reduced entrance erosion is clearly seen when compared to the posttest NSWC ball in Figure 73 which did not incorporate the sacrificial entrance. In fact, it performed too well since, unexpectedly, no erosion occurred on the carbon-phenolic lockring which was found to have swelled into the ball preventing execution of some thrust vector control (TVC) events. The design gap between the ball and lockring was inadequate and was subsequently modified for the full-scale assembly. The phenolic lockring otherwise performed well. No aluminum oxide was observed on the ball, socket, or in the splitline.

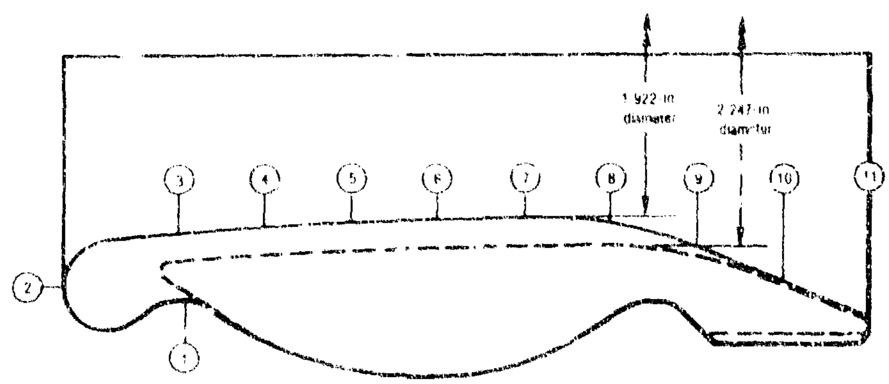

Station No.	Initial Radius in.	Initial Area Ratio	Measured Erosion: Minimum Depth, in.	Minimum Rate, mil/sec	Maximum Depth, in.	Maximum Rate, mil/sec	Average Depth, in.	Average Rate, mil/sec
1	1.425	2.20	0.026	0.9	[illegible]	3.0	0.063	2.3
2	1.340	[illegible]	0.395	14.1	0.561	20.0	0.485	17.3
3	1.050	1.20	0.126	4.5	0.186	6.6	0.154	5.5
4	1.000	1.05	0.182	[illegible]	0.212	7.6	0.191	6.8
5	0.980	1.04	0.162	5.8	0.200	[illegible]	0.180	6.4
6	0.965	[illegible]	0.164	[illegible]	0.189	6.8	0.171	6.1
7	0.961	1.00	0.155	5.5	0.174	6.7	0.165	5.9
8	0.995	[illegible]	0.118	4.2	0.135	[illegible]	0.125	4.5
9	1.130	[illegible]	0.022	0.8	0.069	[illegible]	0.048	1.7
10	[illegible]	1.87	0.014	0.5	0.059	2.1	0.035	1.3
11	[illegible]	[illegible]	0.008	[illegible]	0.039	[illegible]	0.025	0.9

Propellant — [illegible] HMX) Average ballistic throat erosion
Average pressure — [illegible] psia rate — 5.8 mil/sec
Burn time — [illegible] sec

Figure 71. AFRPL Subscale Ball Erosion Profile

27207

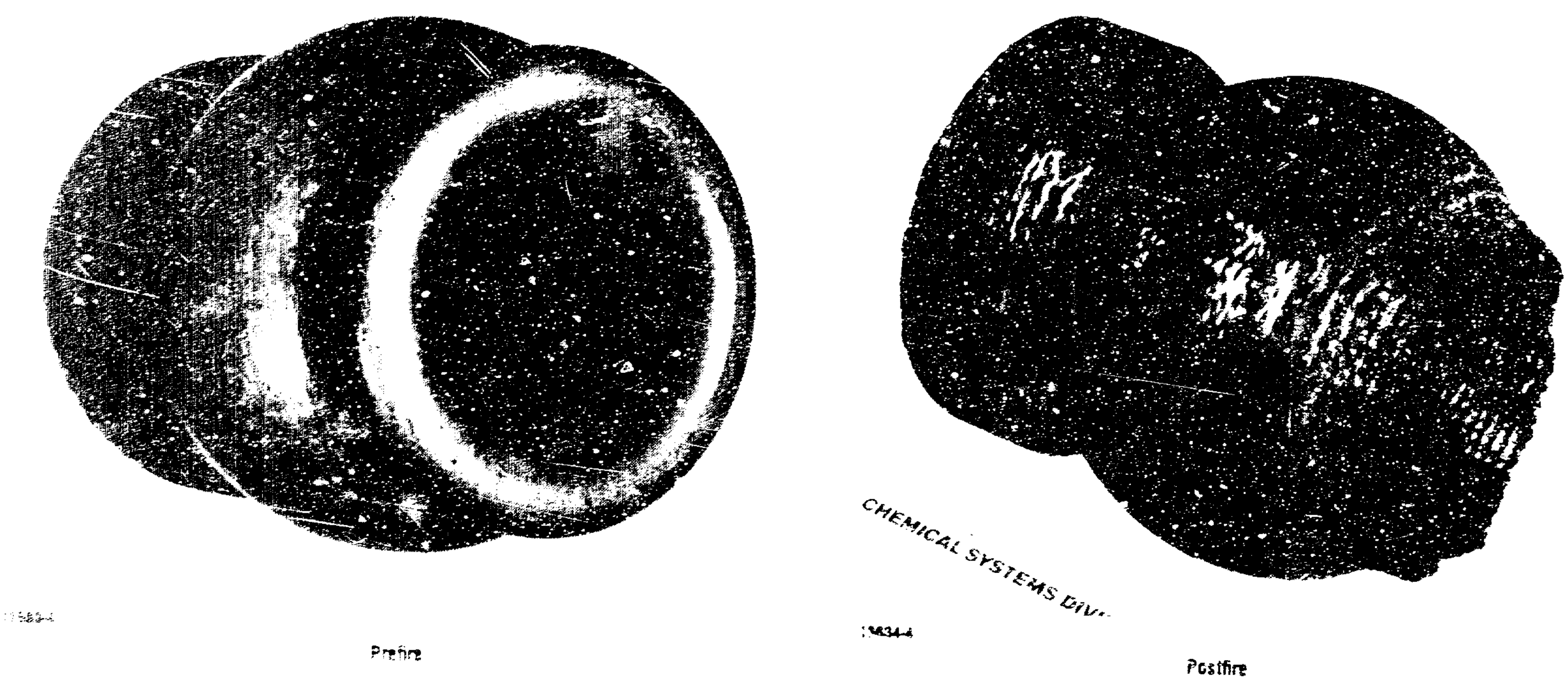

Figure 72. Comparison of AFRPL Subscale Ball, Prefire vs Postfire

27208

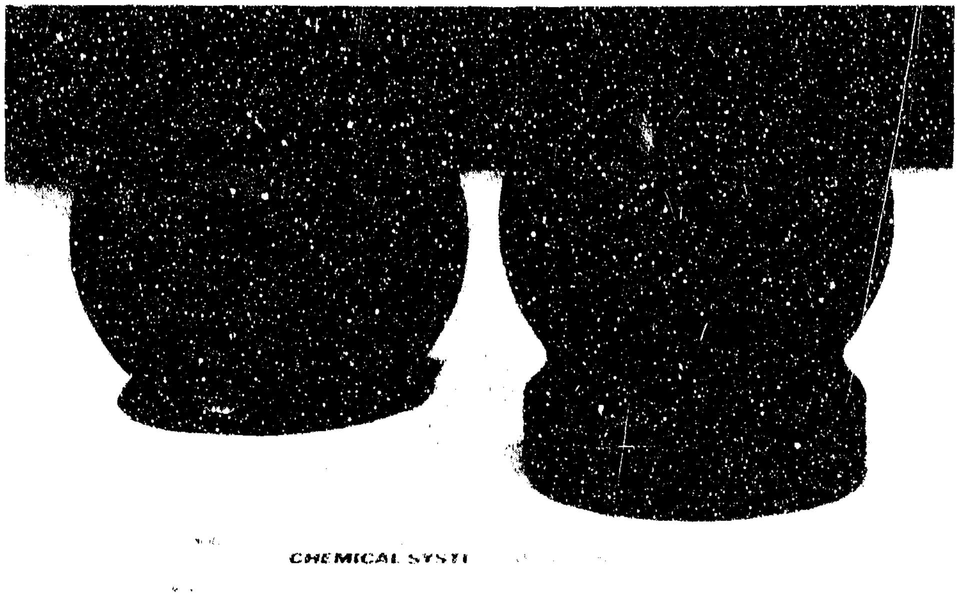

13634-7

Figure 73. Comparison of Postfire NSWC Subscale Ball (Left) (Tested 29 August 1978) With Postfire AFRL Subscale Ball (Tested 18 March 1981)

27209

Since interference of the lockring with the ball occurred from a few seconds past ignition through the duration of the firing, isolation of the performance of the surface treatment during the firing is impossible. However, because of the excellent low torque results achieved with the surface treatment during bench testing with no evidence of any detrimental effect, it was selected for the full-scale test.

An overlay of the TVC position commands and measured response is shown in Figure 74. Three-quarters of the total vector travel commanded was performed including vectoring in the cross plane to 8 deg. At 4 sec into the firing the nozzle achieved 1.5 deg of a 4-deg command in the minus yaw plane when the torque exceeded the capability of the actuator (3,850 in.-lb). Again at 18 through 23 sec the nozzle was unable to respond to the 8-deg step commands in the yaw plane. TVC events at tailoff in the yaw plane were performed, however, with higher than expected torque. Events in the pitch and cross-axis planes were performed, but also with higher than expected torques. Analysis of the prefire steering checks showed that, compared with the bench test results, the

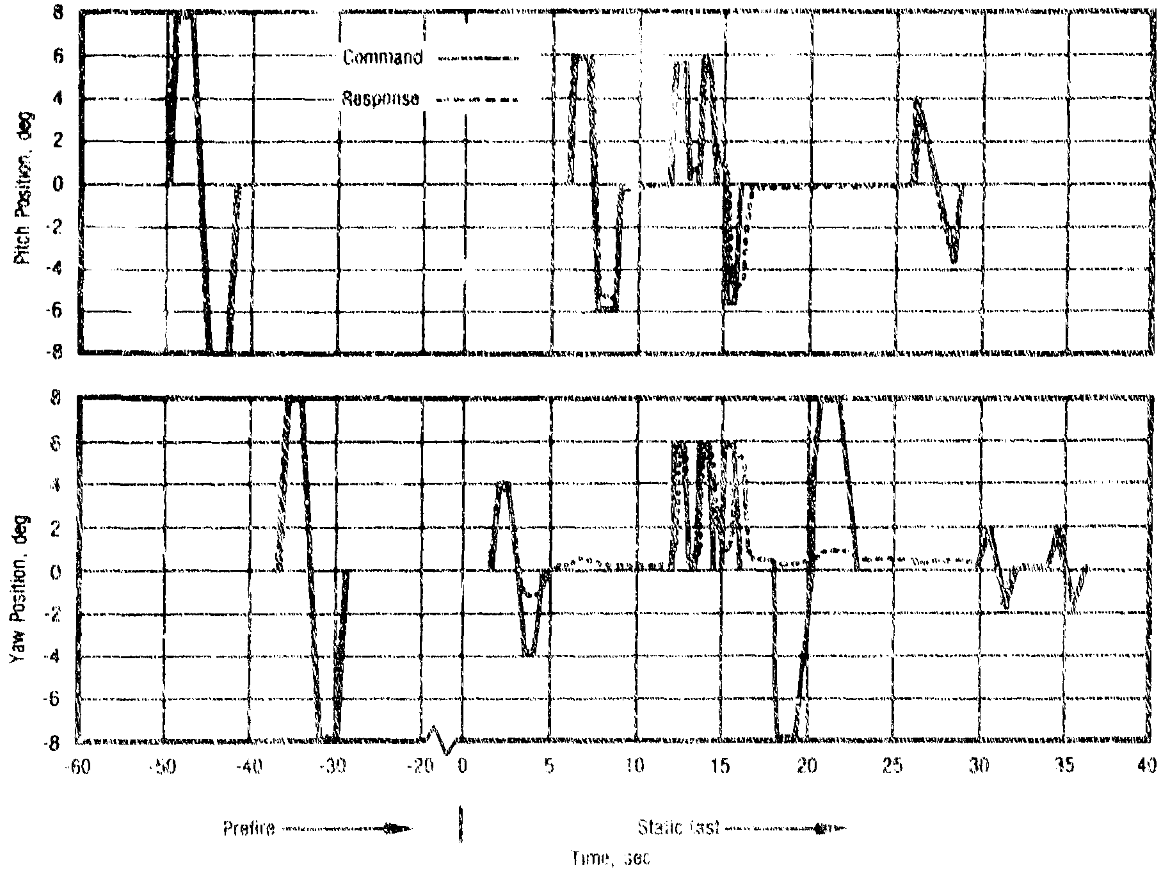

Figure 74. AFRPL Subscale Hot Ball and Socket Nozzle TVC Duty Cycle (Measured Response Overlayed on Commands)

27210

system was performing properly before motor ignition. This data, including the response to commands at tailoff and analysis of the acquired actuator control data monitored during the firing, shows that no fault existed within the actuation system. The high torque measured is attributed to the inadequate gap provided between the ball and carbon-phenolic lockring.

The following observations were made:

- The sacrificial entrance was effective in protecting the forward splitline components by providing a separated flow region.
- The carbon phenolic lockring was not sufficiently gapped from the movable ball resulting in interference when it charred and swelled.

- The applied surface treatment demonstrated, in bench testing, a 35% reduction in torque from that nominally measured in previous tests. The phenolic swelling problem precluded confirmation of torque reduction during firing.
- The surface treatment did not detrimentally affect performance of the nozzle in firing.
- Aluminum oxide deposition was not apparent in the splitline or on the ball and socket surfaces.

All of the modifications demonstrated in the subscale test were incorporated in the full-scale assembly. An increase in the radial gap between the phenolic lockring and ball was incorporated in the full-scale design. This test and a survey of industry experience with carbon phenolic in splitlines was the basis for the change in the full-scale design. The spherical radius of the full-scale S/N 2 nozzle lockring was subsequently modified to provide a 0.10-in. radial gap between the ball and lockring while the ball is seated on the socket. This gap results in 0.30 in. of axial translation by the ball from the seated position on the lockring to the socket.

8.0 NOZZLE S/N 2 - FABRICATION AND TESTING

8.1 NOZZLE FABRICATION

The second 7-in. D_t hot ball and socket (HBS) nozzle conformed to Chemical Systems Division (CSD) drawing C13179-02-01. Nozzle S/N 2 maintained the same basic physical characteristics and short length super HIPPO (SLSH) motor interface as nozzle S/N 1 except that the exit was truncated reducing the expansion ratio to 7.6 (versus 13.8) and the overall length to 37.9 in. (versus 49 in.).

The 3D carbon-carbon (C-C) ball, socket, and exit cone were fabricated by Fiber Materials, Inc. (FMI) with Union Carbide T300 fiber. The preform weave spacing for the ball at the 7-in. reference diameter was $\Delta R = 0.090$ in., $\Delta C = 0.100$ in., and $\Delta A = 0.080$ in. The fiber volume distribution for the ball is presented in Figure 75. The socket preform was woven as a cylinder (axial fibers running parallel to the centerline) as opposed to the frustra design of

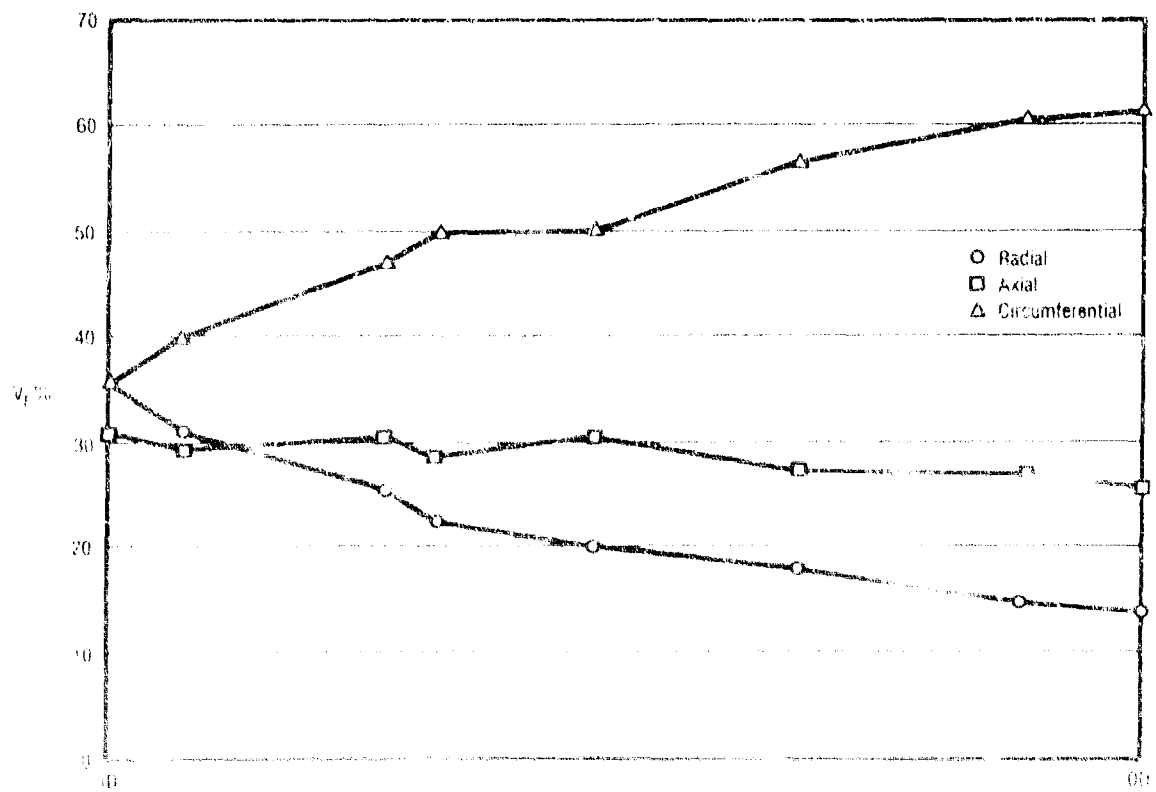

Figure 75 Ball Preform Fiber Volume Distribution, S/N 2

27252

the S/N 1 socket. The spacing at the spherical diameter of the socket was ΔR = 0.090 in., ΔC = 0.200 in., and ΔA = 0.080 in. The fiber volume distribution for the socket is presented in Figure 76. The exit, woven as a frustra, maintained a constant spacing between bundles of 0.090 in. in the radial direction. The spacing in the axial (meridional) direction increased from 0.080 in. at the forward end to 0.120 in. at the aft end. The circumferential spacing of the exit preform varied from 0.070 in. at the forward and inside diameter (ID) to 0.300 in. at the aft end outside diameter (OD). The fiber volume distributions for three zones of the exit cone as depicted in Figure 77 are presented in Figures 78 through 80.

Allied 15V coal tar pitch was used during densification of all three billets up to the final resin impregnation stage. The ball and socket were each processed through one low pressure rigidization cycle, five pressure-impregnation carbonization (PIC) cycles at 5 ksi, and one final resin cycle. The

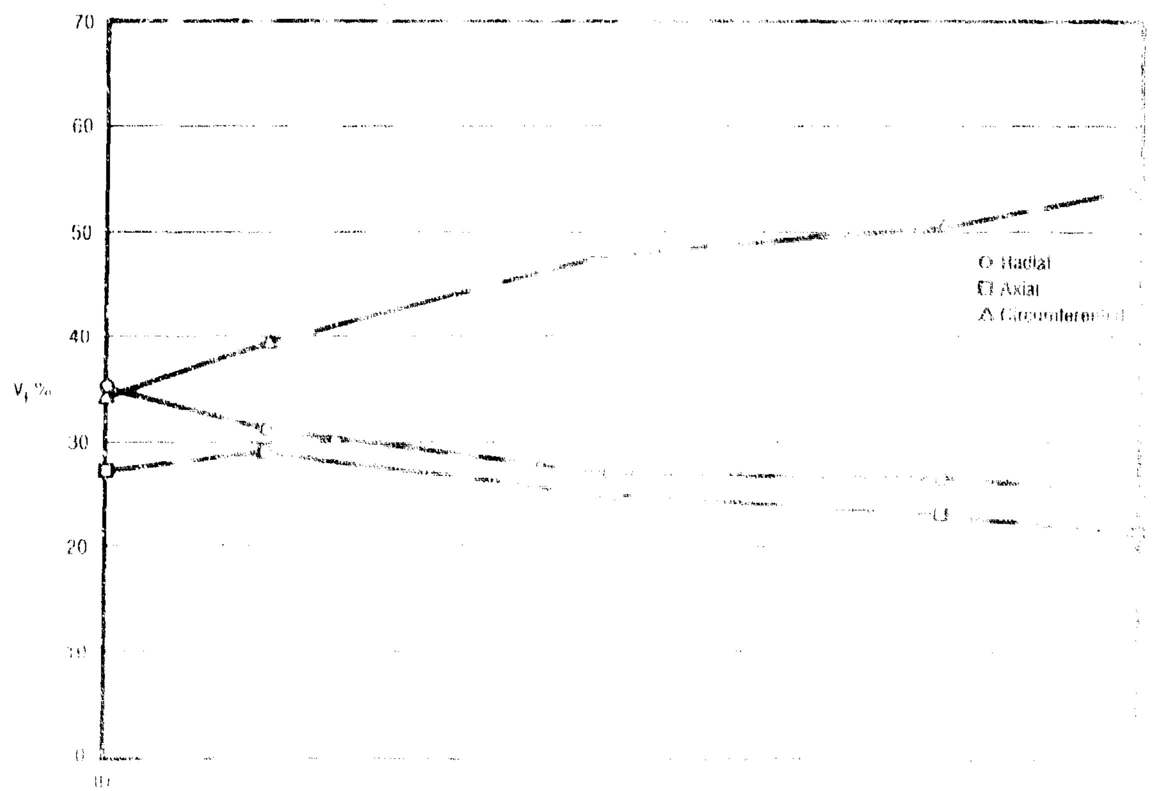

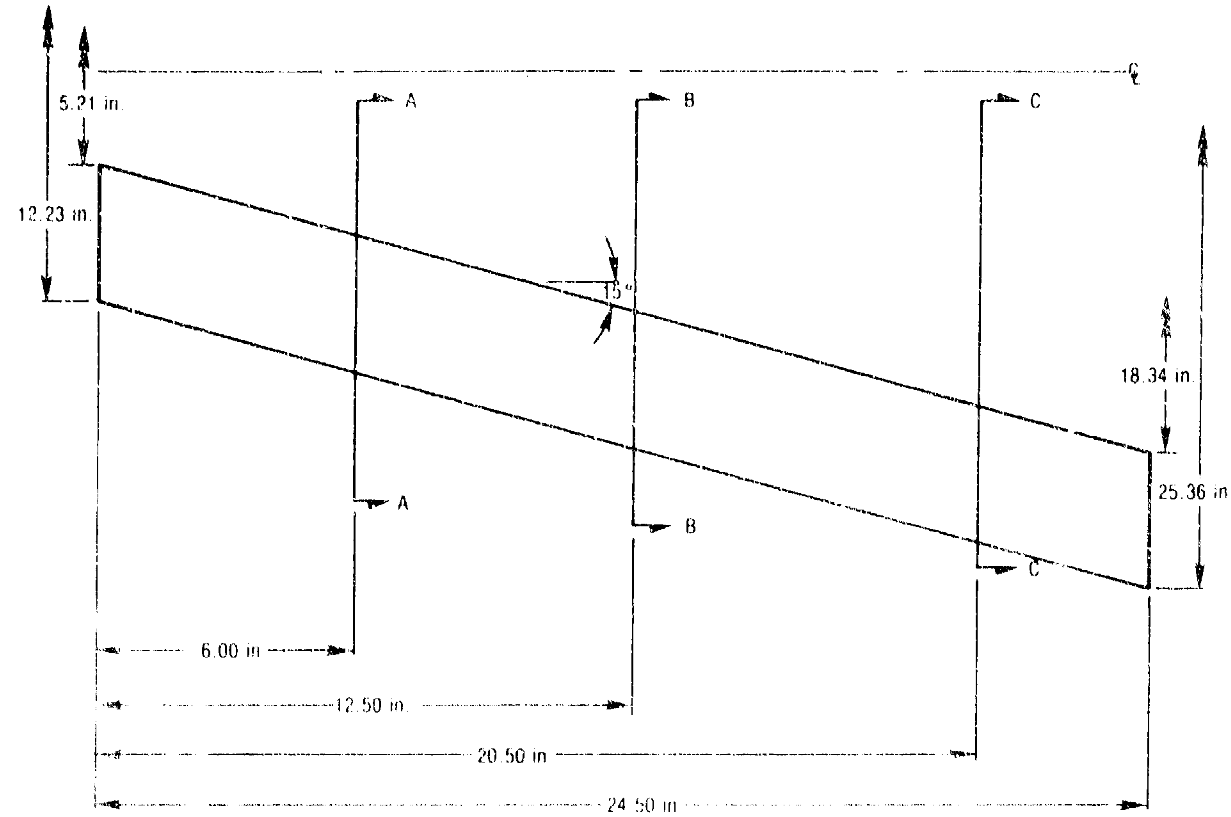

Figure 77. Exit Cone Preform Dimensions, S/N 2

27254

exit cone was processed through three-low pressure impregnation cycles, three -ksi PIC cycles, and three resin impregnations. All graphitization runs were 2,400°F.

The ball and exit cone were processed through densification without any major difficulties or anomalies. However, distortion of the nominal weave geometry was apparent in the socket billet following the initial atmospheric carbonization. Upon skin machining, the circumferential yarns on the OD were slumped (equally displacing the radials) in the axial direction. The maximum amplitude of the undulations was nearly 1 in. After continued processing, skin machining revealed the anomaly was a surface condition only, and would not extend into the final machined part. The distortion was most likely the result of improper preform framing. In addition to the distorted weave anomaly, the socket experienced an aborted cycle during the fifth PIC run. The conditions at

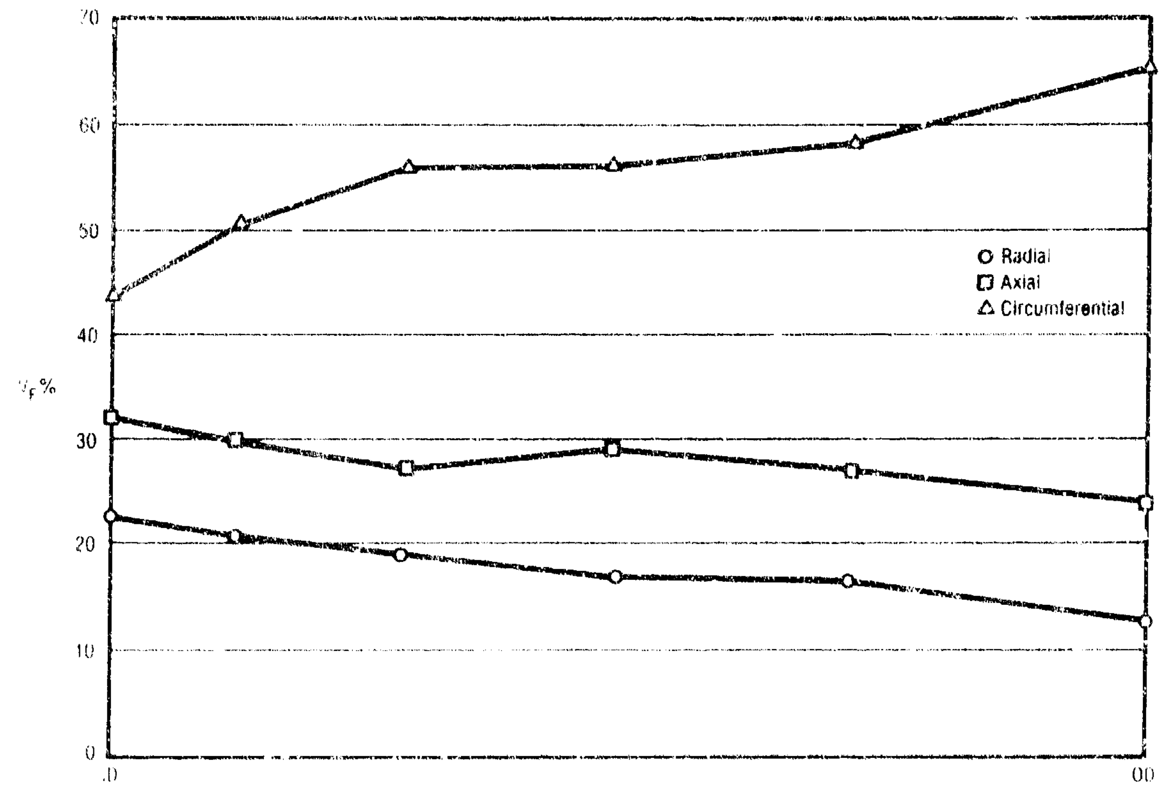

Figure 78. Exit Cone Preform, Fiber Volume Distribution at Section A-A (Reference Figure 77), S/N 2

27255

shutdown were approximately 450 C and 5,000 psi. The billet was subsequently reprocessed through another pressure carbonization cycle. Final machined densities achieved were 1.90 g/cc for the ball and socket and 1.83 g/cc for the exit cone.

Machining of the final parts was done by FMI. The finish machined ball, socket, and exit cone are shown in Figures 81, 82, and 83, respectively. The groove milled into the OD of the socket was incorporated to accommodate access for strain gage instrumentation during nozzle assembly. The carbon-phenolic overwrap on the socket seen in Figure 82 was added following a machining error whereby the 3-deg OD taper was running backwards. Hence, the OD at the aft end was oversize while the forward end was undersize. Carbon phenolic was laid up on the socket, cured in place, and machined correctly to the print. A close-up

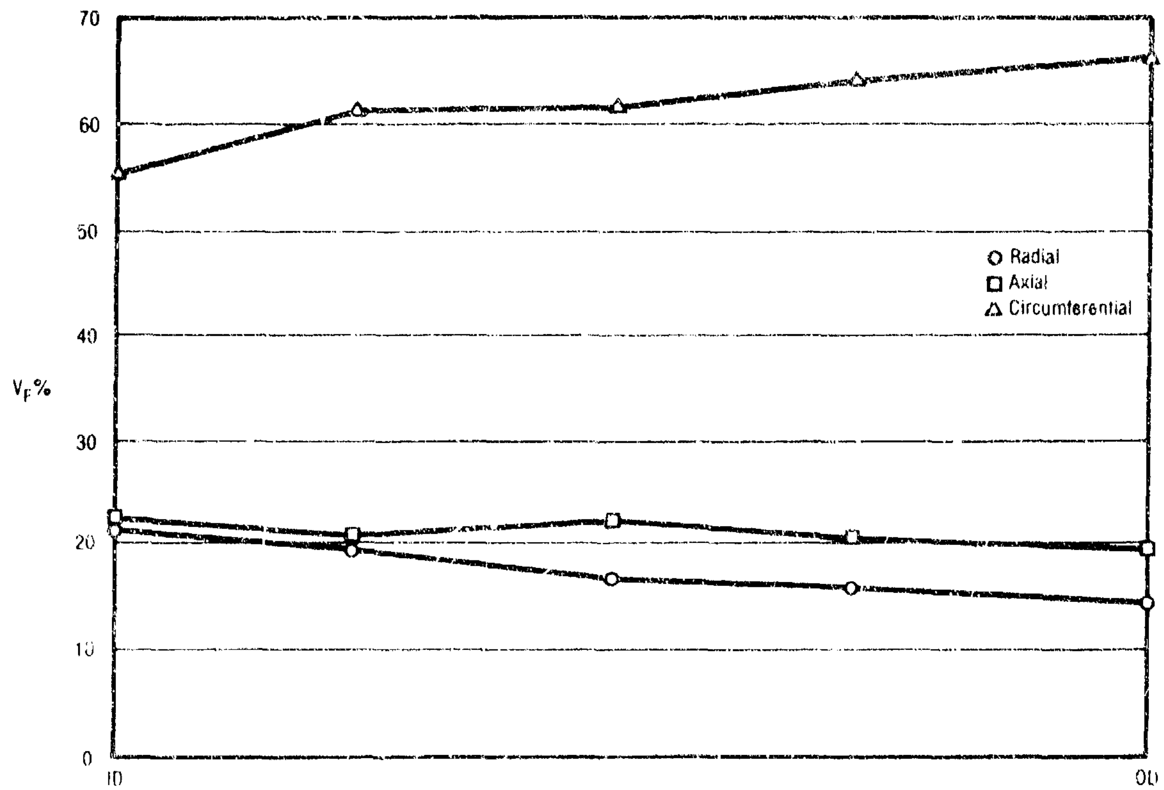

Figure 79. Exit Cone Preform, Fiber Volume Distribution at Section B-B (Reference Figure 77), S/N 2

27256

view of the 1-1/2 stub Acme threads of the ball is pictured in Figure 84. Note that three to four radial fiber bundles are evident in each thread form.

No hardware from the S/N 1 nozzle firing was salvageable for reuse on nozzle S/N 2. The actuation system, steel nozzle components (including the nozzle adapter and compliance ring), and the phenolic insulators were identical to the S/N 1 counterparts. The phenolic insulators including the flat-laminated carbon-phenolic lockring were fabricated by Edler Industries. Assembly of the nozzle was also performed by Edler. Upon delivery to CSD, the assembly was integrated with the actuation system and instrumented with thermocouples and strain gages. The locations of thermocouples and strain gages are depicted in Figure 85. The instrumented nozzle and actuation assembly is shown in Figure 86.

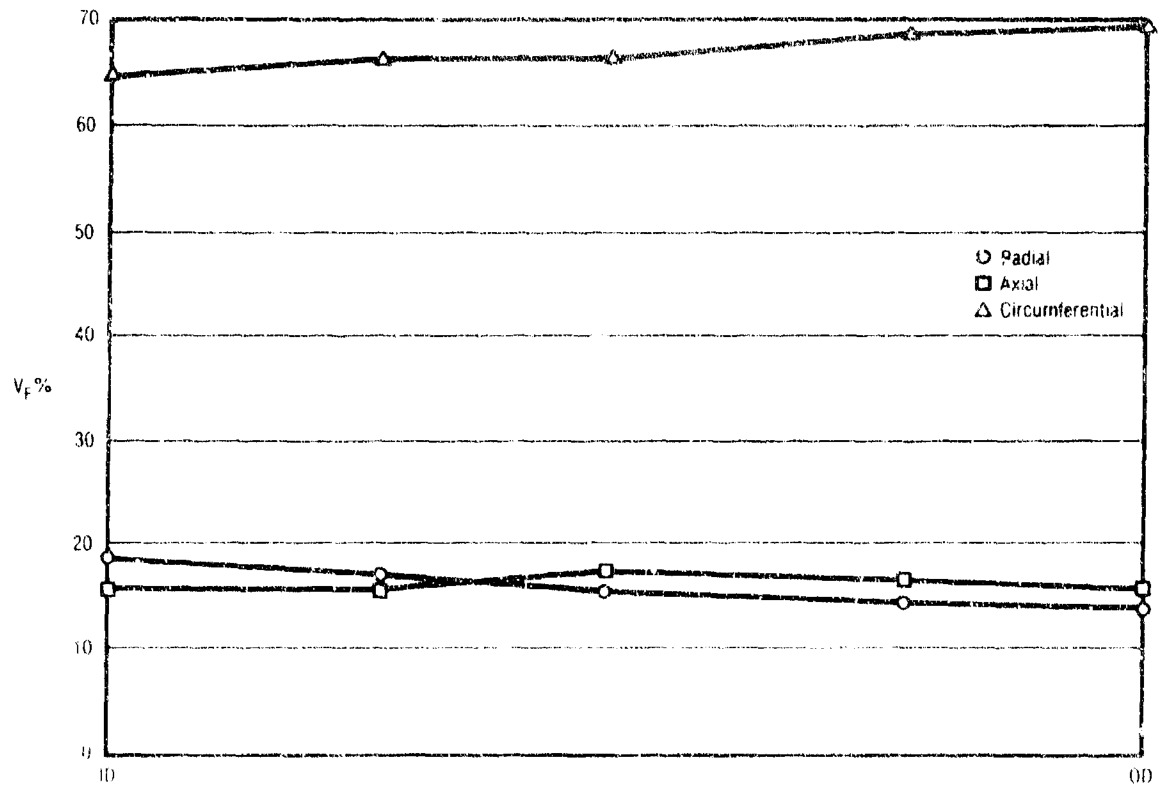

Figure 80. Exit Cone Preform, Fiber Volume Distribution at Section C-C (Reference Figure 77), S/N 2

27257

8.2 C-C MATERIAL PROPERTY TESTING

FMI conducted extensive mechanical and thermal tag-end property testing on the ball, socket, and exit cone (reference 5). The acquired property data was reviewed by CSD and used to update margins of safety for critical failure modes. Tables 9 and 10 respectively present the thermal and mechanical test matrix performed. The measured property data indicated an insignificant decrease in the shear strength of the socket from that assumed in analysis. All other values exceeded the assumed allowables used in analysis. Table 11 presents the revised margins of safety (all of which remained positive) for key failure modes updated with the measured property values.

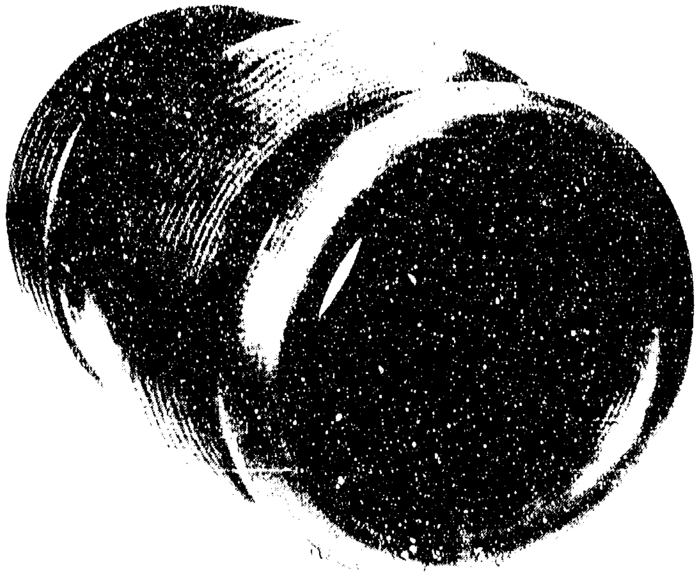

13013-5

Figure 81. Ball, 7-in. Hot Ball and Socket Nozzle S/N 2

27211

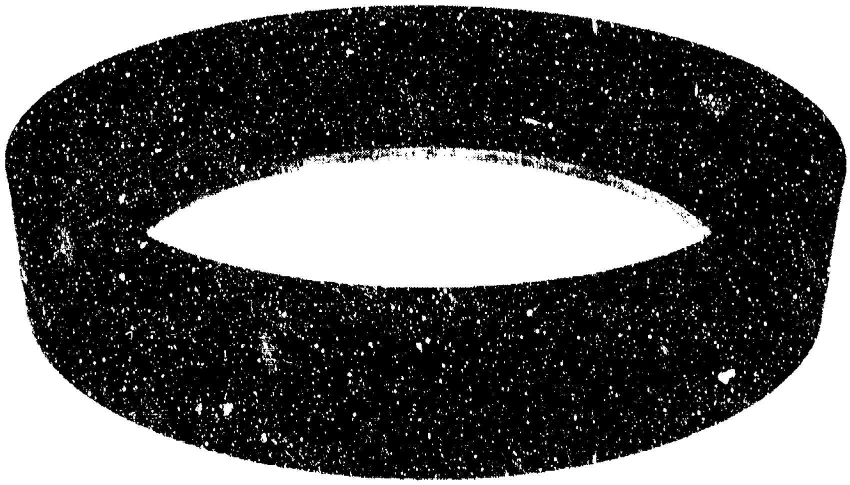

13848-1

Figure 82. Socket, 7-in. Hot Ball and Socket Nozzle S/N 2

27212

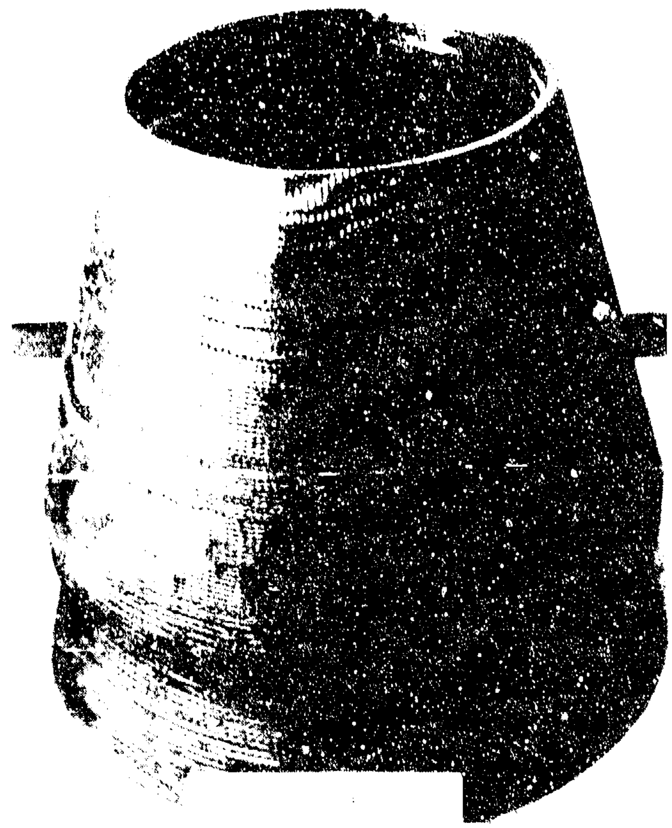

14075-1

Figure 83. Exit Cone, 7-in. Hot Ball and Socket Nozzle S/N 2

27213

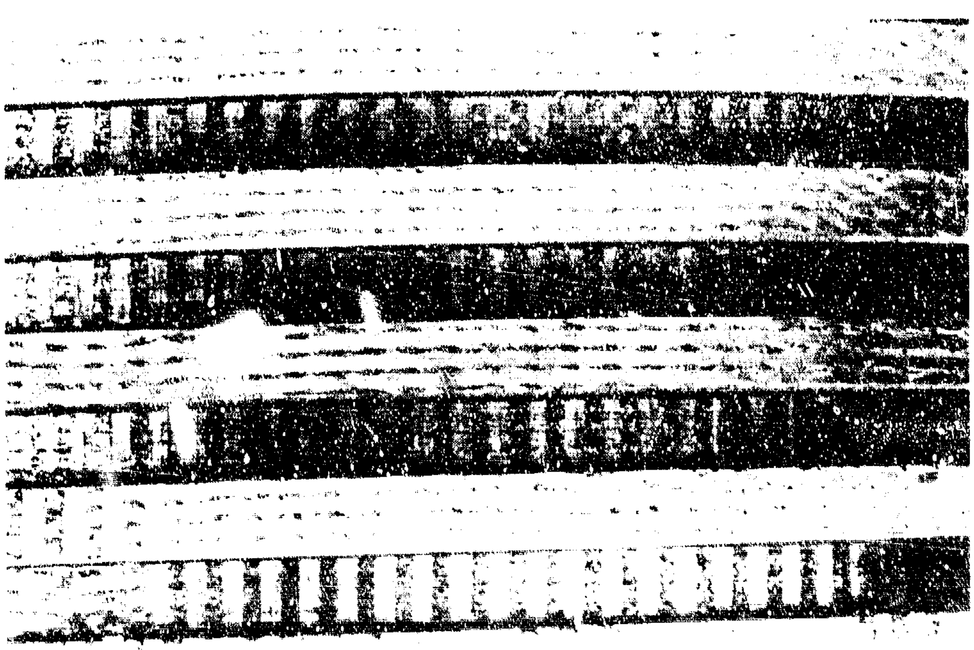

13813-3

Figure 84. Close-Up View of Ball Threads Showing at Least Three Radial Bundles Per Thread Form

27214

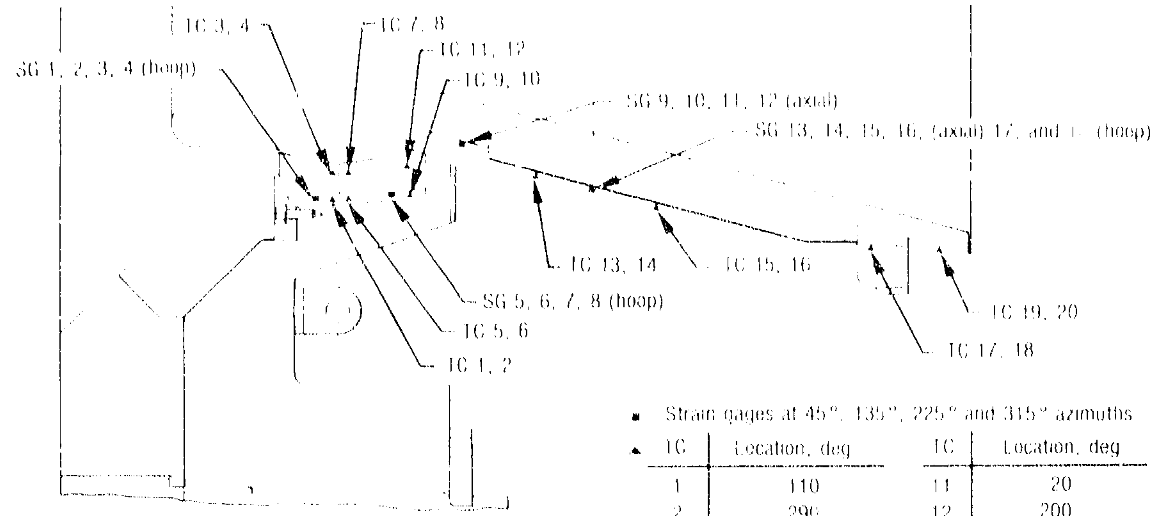

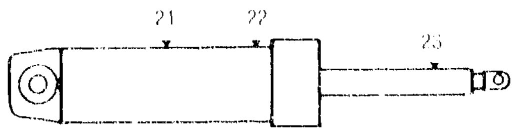

■ Strain gages at 45°, 135°, 225° and 315° azimuths

▲

TC	Location, deg	TC	Location, deg
1	110	11	20
2	290	12	200
3	20	13	TDC
4	200	14	90
5	110	15	TDC
6	290	16	90
7	20	17	TDC
8	200	18	90
9	110	19	TDC
10	290	20	90

Figure 85. Thermocouple and Strain Gage Locations, Nozzle S/N 2

18145

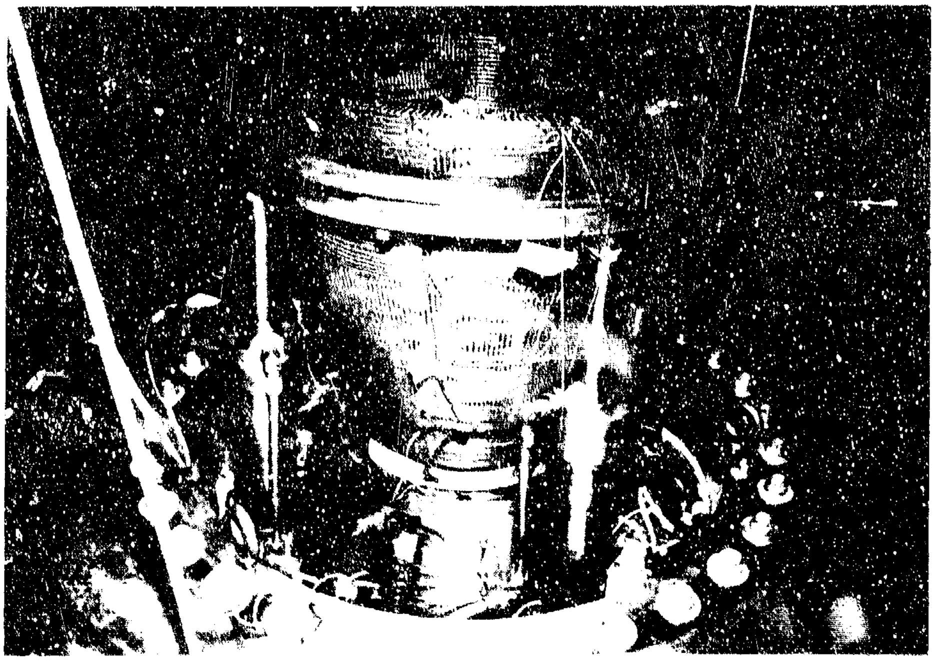

14057-01

Figure 86. Instrumented Nozzle and Actuation Assembly, Nozzle S/N 2

27?15

TABLE 9. THERMAL TAG-END PROPERTY TEST MATRIX

T5058R

Priority and Test No.	Thermal Diffusivity, 70 to 4,500 F		Type of Billet			Specimen Location in Billet		Specimens per Test
	Radial	Axial	Ball	Socket	Exit Cone	Radial	Axial	
1	x		x			ID	Any	2
2		x	x			ID	Any	2
3	x			x		ID	Any	2
4		x		x		ID	Any	2
5	x				x	Mid	Fwd	2
6		x			x	Mid	Fwd	2

8.3 BENCH TESTING

Before the steel nozzle adapter ring was delivered to Edler Industries for final assembly, the steel nozzle mock-up was assembled with the actuators for actuation system checkout and verification as was done with nozzle S/N 1 (described in section 4.1). Following checkout and disassembly, the adapter ring was shipped to Edler for final assembly.

The assembled nozzle was returned to CSD and bench tested with the same test fixture as was used for nozzle S/N 1. The throat was plugged and a rubber diaphragm was fastened to the forward end of the steel adapter. The cavity between the diaphragm and nozzle was pressurized with GN_2 through the throat plug while the bench test vessel was filled with water up to the diaphragm.

Difficulties were experienced when attempting to pressurize the nozzle to the full blowoff load expected during firing. The porosity of the C-C prevented achievement of pressure corresponding to loads higher than 50% of the blowoff load expected. The surface treatment provided an improvement in reducing open porosity compared to that experienced with nozzle S/N 1, but was not sufficient to enable full pressurization. The open porosity is essentially reduced to zero

TABLE 10. MECHANICAL TAG-EN

Priority and Test No.	Exit Cone (Frustum)	Type of Billet: Ball (3D C/C)	Socket (3D C/C)	Type of Test: Radial	Axial	Hoop	Radial Core Shear	Axial† Core Shear	Hoop Core Shear	Shear*	Loading Cor: Tension	Com
1	X					X					X	
2	X					X						
3	X									X		
4	X						X					
5	X				X						X	
6	X				X						X	
7	X				X							
8	X				X							
9	X			X								
10	X				X							
11	X					X						
12		X				X					X	
13		X				X					X	
14		X		X								
15		X		X								
16		X			X							
17		X				X						
18		X					X					
19		X					X					
20		X						X				
21			X	X								
22			X			X					X	
23			X			X						
24			X	X								
25			X		X							
26			X									
27		X										
28		X				X						
29		X				X						
30		X				X						
31	X							X				
32	X								X			
33	X									X		
34	X						X					
35		X			X						X	
36		X			X						X	
37			X				X					
38	X			X							X	
39	X			X								
40		X		X							X	

Notes:

* Specimens to be cut perpendicular to exit wall, pot nozzle axis

† The test methods specified are:

(1) Compression ring segment test
(2) Standard thermal expansion test
(3) Full ring specimen test with bag pressure
(4) Core shear test
(5) Axial tension compression test

‡ Specimens to be cut parallel to exit wall

Data Acquisition:

The following information will be provided:

(1) Complete load deflection history, including compressive ring segment test
(2) Locations of specimens relative to original location in billet)
(3) Actual dimensions of specimens
(4) Number of fiber bundles and filaments (axia
(5) Modulus
(6) Ultimate stress
(7) For thermal expansion tests, heat-up curves

CAL TAG-END PROPERTY TEST MATRIX

T5057R

Loading Condition		Temperature, F				Specimen Location In Billet		Kind of Test			
Tension	Compression	70	1,000	1,500	2,500	Radial	Axial	Modulus and Strength	Thermal Expansion	Test† Method	Specimens per Test
X		X				Any	Fwd	X		(3)	2
	X	X				Any	Fwd	X		(3)	2
		X				Any	Fwd	X		(4)	3
		X				Any	Fwd	X		(4)	5
X		X				Any	Fwd	X		(5)	3
X					X	Any	Fwd	X		(5)	3
	X	X				Any	Fwd	X		(5)	3
	X				X	Any	Fwd	X		(5)	3
						Any	Fwd		X	(2)	3
						Any	Fwd		X	(2)	3
						Any	Fwd		X	(2)	3
X		X				OD	Any	[illegible]		(3)	2
X					X	OD	Any	X		(3)	3
	X	X				OD	Any	X		(1)	3
						ID	Any		X	(2)	3
						ID	Any		X	(2)	3
						[illegible]	Any		X	(2)	2
		X				Any	Aft	X		(4)	5
		X				Any	Fwd	X		(4)	5
		X				OD	Any	X		(4)	5
	X	X				Any	Any	X		(5)	3
X		X				Any	Any	X		(3)	2
	X	X				Any	Any	X		(3)	2
						Any	Any		X	(2)	3
						Any	Any		X	(2)	3
						Any	Any		X	(2)	2
	X	X				ID	Any	X		(3)	2
	X				X	ID	Any	X		(3)	2
	X			X		ID	Any	X		(3)	2
	X	X				OD	Any	X		(3)	2
		X				Any	Aft	X		(4)	5
		X				Any	Aft	X		(4)	5
		X				Any	Aft	X		(4)	5
		X				Any	Aft	X		(4)	3
X		X				OD	Any	X		(5)	3
X					X	OD	Any	X		(5)	3
		X				Any	Any	X		(4)	5
X		X				Any	Any	X		(5)	3
	X	X				Any	Any	X		[illegible])	3
X		X				OD	Any	X		[illegible])	3

provided:

ory, including lateral compensation load used in the

ve to original billet (radial, axial, and circumferential

filaments (axial, radial, and hoop bundles) in specimens

heat up curves and cooldown curves are required

TABLE 11. KEY FAILURE MODES AND MARGIN OF SAFETY UPDATED WITH MEASURED PROPERTIES, NOZZLE S/N 2

T8276

Failure Mode	Calculated Stress, psi	Assumed Allowable psi	M.S. with* Assumed Allowable	Measured† Allowable psi	Revised* M.S.	% Change in M.S.
1 Ball/socket hoop compression blow off load w/o actuator bias	7685	9400	0.22	B) 12400 S) 10200	0.61 0.33	+177 +50
2 Aft ball, axial tension actuator stall	2456	4400	0.79	6200	1.52	+92
3 Throat hoop tension	1995	8220	3.1	16000	7.0	+126
4 Ball/exit thread shear	1232	1500	0.22	B) 2400 E) 2300	0.94 0.87	+327
5 Socket shear blow off load w/o actuator bias	2306	2820	0.22	2560	0.11	-50
6 Socket [illegible] strain (in./in.) press[illegible] temperature	0.0019	0.0020	0.05	0.0024	0.26	+420
7 Exit, [illegible]al tension at threads bending under actuator stall	1786	4400	1.5	8750	3.89	+159

* All marg[illegible] are positive
† Room temperature properties

at operating temperatures; therefore, this is not a problem during static firing. Successful vectoring was accomplished at the 50% load expected while demonstrating torque values predicted for those loads. Vectoring was also demonstrated on the lockring under the full load of the actuators as is typical during prefire steering checks.

8.4 STATIC TEST FIRING

8.4.1 General

Nozzle S/N 2 was static test fired on 20 November 1981, on the SLSH test motor at the Air Force Propulsion Laboratory (AFRPL) test pad 1-52A. The motor was loaded with 13,410 lb of CSD's UTP-19,687 propellant, a 90% solids, 20% aluminum hydroxyl-terminated polybutadiene (HTPB) type with 12% cyclotetramethylene tetranitramine (HMX). The igniter, a phenolic cartridge type, was in accordance with CSD P/N C00631-07-01. The design average pressure was 743 psia over a planned 75-sec duration. The planned duty cycle is presented in Figure 87. The first thrust vector control (TVC) event was planned at 5 sec into the firing.

The nozzle was actuated by four pull-only actuators operating at a hydraulic supply pressure of 2,000 psi. The system was controlled in a continuous

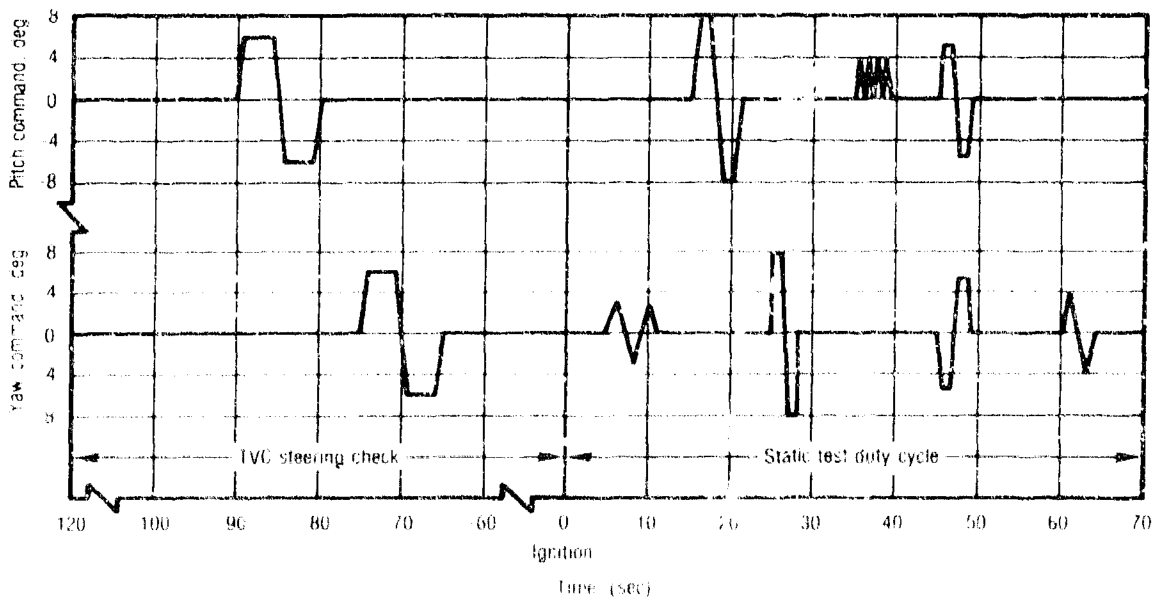

Figure 87. Planned Duty Cycle, Nozzle S/N 2

27153

closed-loop feedback configuration by two servovalves, one each controlling the pitch and yaw axis, and four linear position transducers, each integral with an actuator. Two differential pressure transducers and two absolute pressure transducers monitored the actuator cylinder pressures for determining torque. Additional instrumentation included two motor chamber pressure tranducers, 23 thermocouples, 18 strain gages, and five movie cameras. Facility limitations prevented acquisition of axial thrust or side force measurements.

Ninety sec before ignition, during prefire steering checks, the nozzle successfully performed the commanded trapezoidal wave form in the pitch and yaw axes. The nozzle was seated on the forward lockring at this time under 24,000 lb force contributed solely by the pull-only actuators. When the chamber pressure rose to 300 psi, the ball was expected to shift from the lockring to the socket, a distance of 0.30 in. From ignition to 1.9 sec the ball was seated on the lockring. At 1.9 sec into the firing, annular flow was observed around the ball as it moved off the lockring. The flow was predominatly over an area of 180 deg (0 to 180 deg) as seen in Figure 88. At 6.5 sec, the ball seated on the socket and sealed off the flow in the annulus between the ball and socket. Between 1.9 and 6.5 sec, the ball was suspended by the actuators

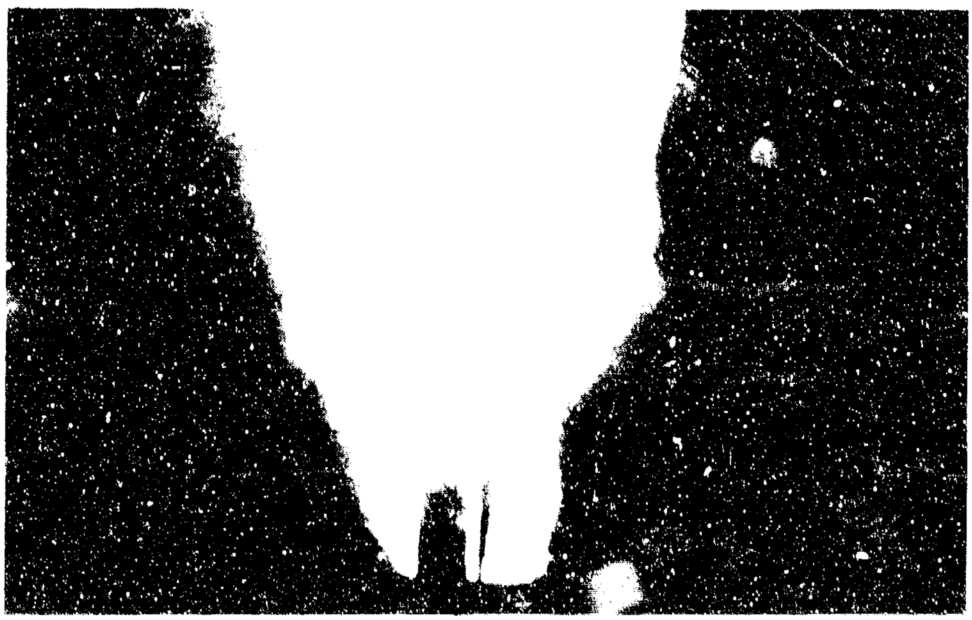

14108-3

Figure 88. View of Flow Around Ball Between 2 and 6 sec, Nozzle S/N 2
27154

between the lock ring and the socket, allowing annular flow. The annular flow impinged on the outside of the exit and on the actuators. Thermocouple and strain gage wires were severed by the flow, so no exit instrumentation data was recorded later in firing. Rubber insulation was partially peeled off the actuators. Plating of aluminum oxide was observed where the annular flow impinged on the outside of the exit and compliance ring.

Table 12 lists the sequence of events during the ignition to 6.5 sec period. The sequence was derived from analysis of the high-speed (1,000 frames per sec) cameras and the other instrumentation.

Between 5 and 11 sec the first vector event (yaw plane + 3 deg) was successfully accomplished; however, torque values increased significantly as the event progressed. The nozzle did not respond to subsequent commanded

TABLE 12. SEQUENCE OF EVENTS, NOZZLE S/N 2 (FROM IGNITION TO 6.5 SEC.)

T8277

Approximate Time, sec	Event
0	Motor ignites
1.1	P_c is sufficient to create aft blow-off load higher than forward force of actuators
1.88	First sign of fl[illegible] observed around ball
2.0	Thermocouples [illegible] strain gages along aft ball and exit cone no longer functional
2.39	Silicone rubber starts to peel away from 90° actuator
2.65	Silicone rubber starts to peel away from 0° actuator
4.5	Burst of alumina observed in plume of "secondary" flow
5.0	First vector event in yaw plane begins
6.2	Flow around ball diminishing (begins to seal)
6.5	No flow (sealed)

events. The measured torques after 11 sec were of stall values (about 150,000 in.-lb).

The nozzle remained intact for the 75-sec duration while experiencing stall forces of 12,000 lbf for single axis events and 17,000 lbf in the cross axis. Chamber pressure versus time is plotted in Figure 89. The maximum pressure was 841 psia, while the average pressure was 688 psia over the 74.6-sec action time. The ballistic throat erosion rate was 4.7 mils/sec. Significant data related to the test of nozzle S/N 2 is presented in Table 13.

8.4.2 TVC Data

Translation of the nozzle 0.30 in. axially from the lockring position to the socket required an eo al amount of stroke by all four actuators. During this period (within 1 sec after ignition) when the blowoff load due to chamber pressure was increasing above the forward load due to the actuators and the thrust contribution, the nozzle was in the null position. Stroking the actuator piston 0.30-in. aft required the displacement of 1.8 in.^{3} of hydraulic fluid from

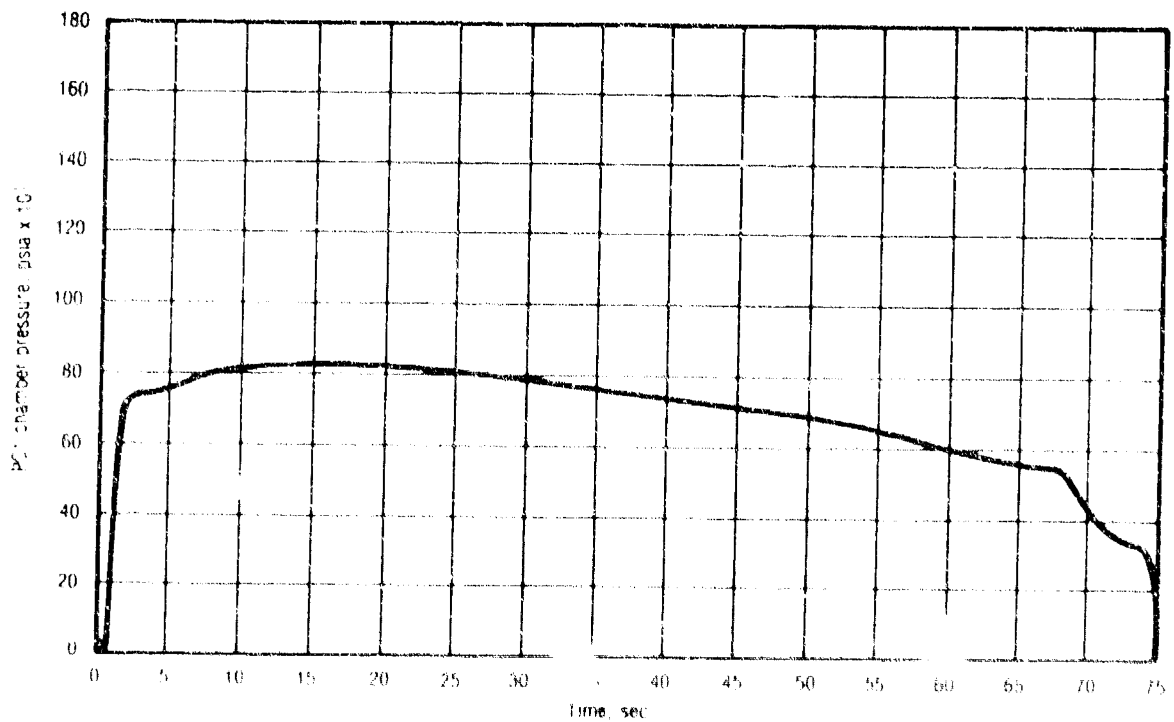

Figure 89. Pressure vs Time, Nozzle S/N 2

27155

TABLE 13. SIGNIFICANT DAT , HOT BALL AND SOCKET NOZZLE S/N 2

T8278

Test date	20 November 1981
Propellant	90% solids, 20% Al, 12% HMX
Action time (sec)	74.6
Maximum pressure (psia)	841
Average pressure (psia)	688
Ballistic throat erosion rate (mils/sec)	4.7
Accomplished TVC travel (deg)	29
Maximum vector angle (deg)	3

each of the four actuators. The two servovalves (one for each axis) were ot capable of instantaneously displacing this volume while in the null position with nearly zero current supplied to the servovalve. The actuators were essentially experiencing hydraulic lock.

The flow capability of the servovalve is a function of input current as presented in Figure 90. The measured current on the pitch and yaw servovalves obtained from the test data was 0.25 and 0.06 mA, respectively, up to the time of the first vector event (5 sec). The flow rate capability of the two servovalves was hence approximately 2 and 0.5 $in.^3$/sec for the pitch and yaw axis respectively As chamber pressure and hence blowoff load was increasing, the pressure in the actuator cylinders was increasing, until at 1.9 sec the ball was pulled off the lockring by the actuators. Before this time the ball was seated and sealed on the forward lockring under loads imposed by the actuators. As fluid was slowly relieved, the nozzle slowly shifted aft off the lockring. The fact that the pitch actuators were displacing fluid approximately four times faster than the yaw actuators, and the yaw plus actuater at 90 deg was experiencing hydraulic pressures approximately 15 to 20% higher than the opposite yaw minus actuator, may have led to asymmetrical movement of the ball, which would explain the observed flow only from 0 to 180 deg with the maximum occurring at 90 deg. Considering the low leakage rate of the yaw servovalve (0.5 $in.^3$/sec)

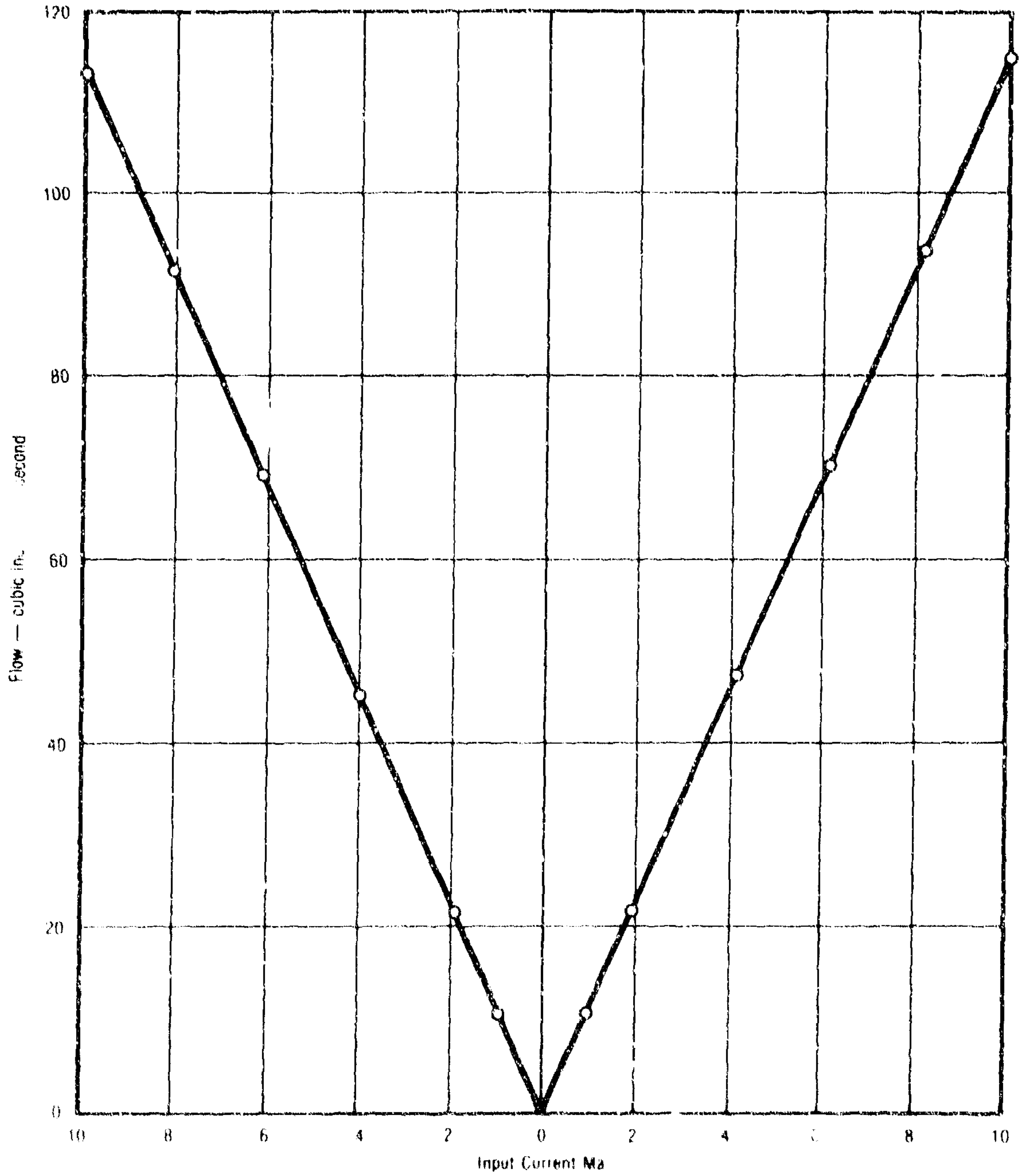

Figure 90. Servovalve Flow Rate vs Inp t Current

27258

it would have taken over 7 sec to displace the total 3.8 in.^{3} of fluid had the yaw axis not been commanded through a vector event at 5 sec. At this time the current input to the yaw servovalve increased to 0.6 mA significantly increasing the flow capability of the valve. Within 1 sec the flow around the ball began to diminish. Plots of cylinder pressure versus time for each of the four actuators are presented in Figures 91 through 94.

The first event (±3-deg triangular wave form) at 5 sec was accomplished, however, torque increased as the event progressed. The doubling of the torque values through this event from 5 to 11 sec resulted from the alumina which plated on the ball and socket surfaces during the 4 sec of flow around the ball as evidenced upon posttest disassembly and documentary movies. A plot of torque versus time is presented in Figure 95.

The second planned event to 8 deg in the pitch axis at 15 sec and all subsequent vector events were not achieved. Stall torques of 150,000 in.-lb measured during these periods were attributed to the solidified alumina between the ball and socket. The angular position achieved during each planned event is overlayed on the planned duty cycle in Figure 96. Twenty-seven degrees of the

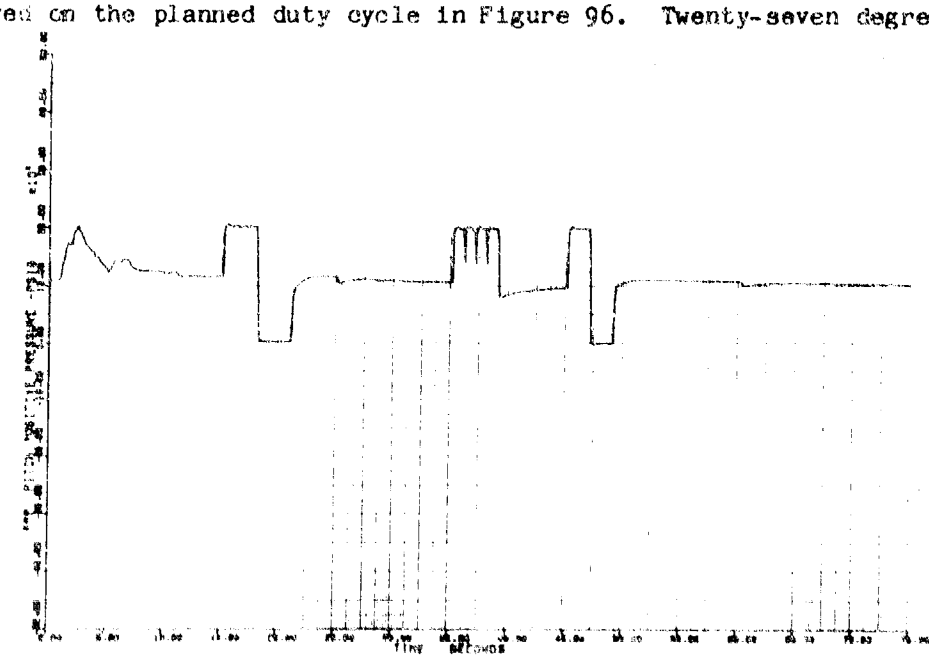

Figure 91. Pitch Plus Cylinder Pressure vs Time, S/N 2

27216

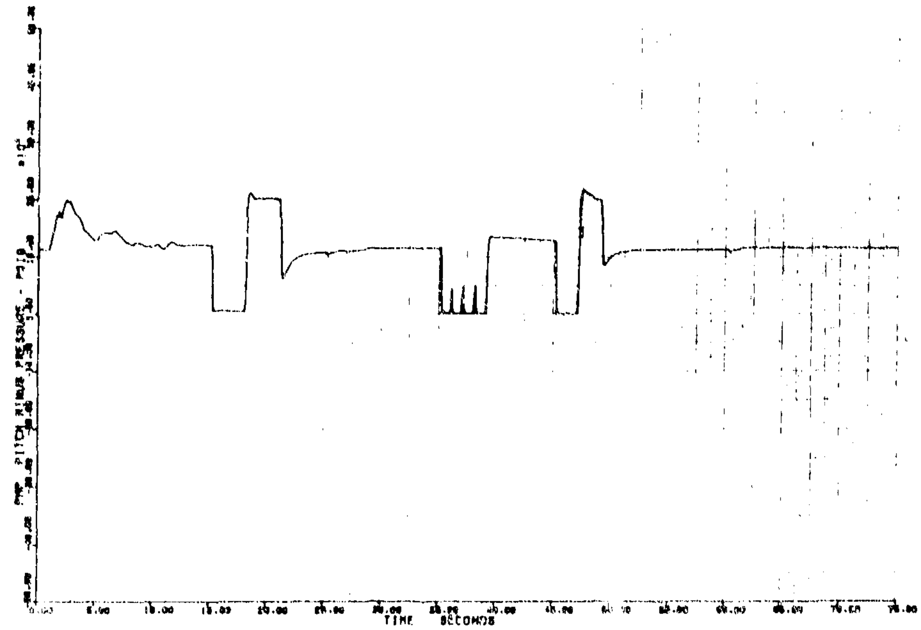

Figure 92. Pitch Minus Cylinder Pressure vs Time, S/N 2

27217

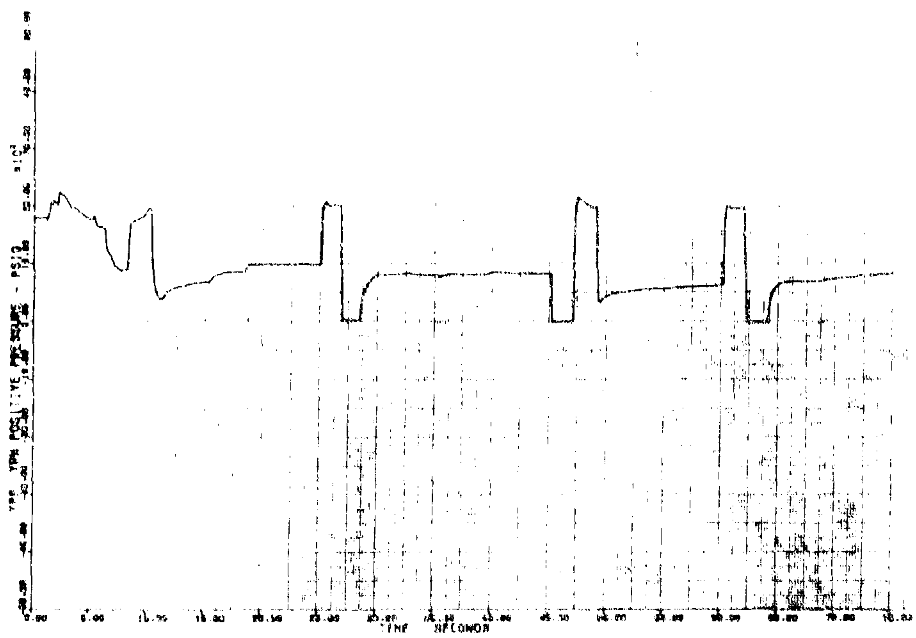

Figure 93. Yaw Plus Cylinder Pressure vs Time, S/N 2

27218

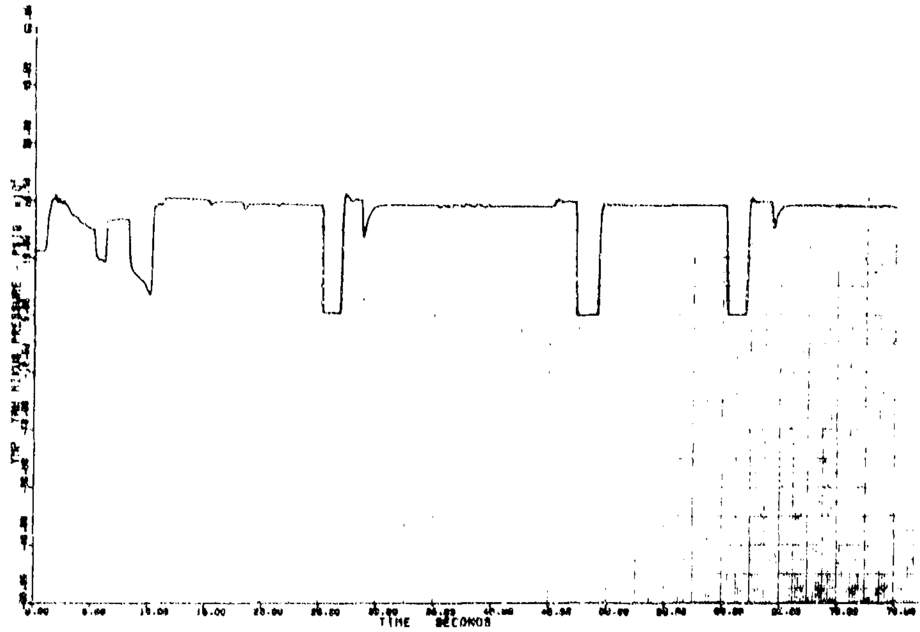

Figure 94. Yaw Minus Cylinder Pressure vs Time, S/N 2

27219

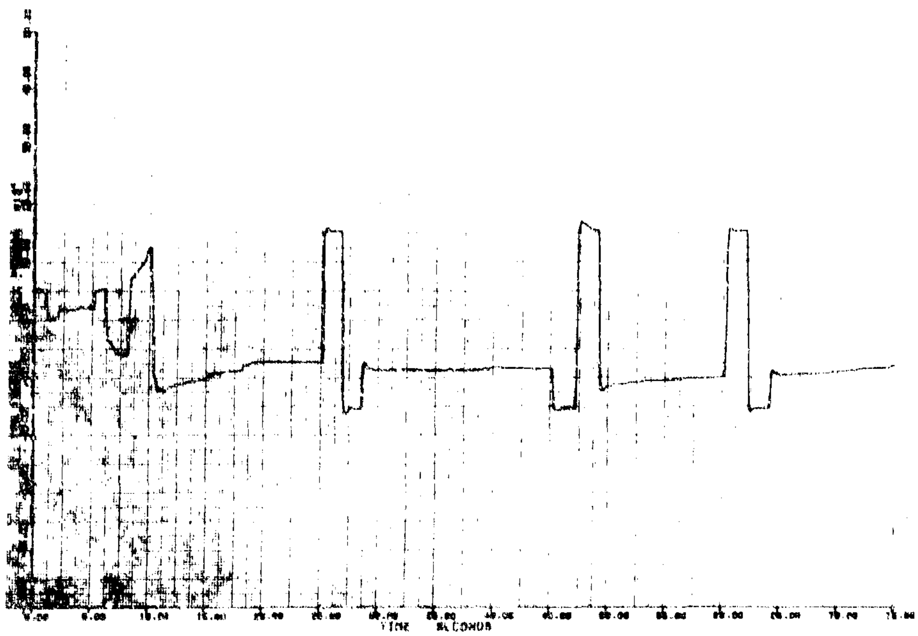

Figure 95. Yaw Torque vs Time, S/N 2

27160

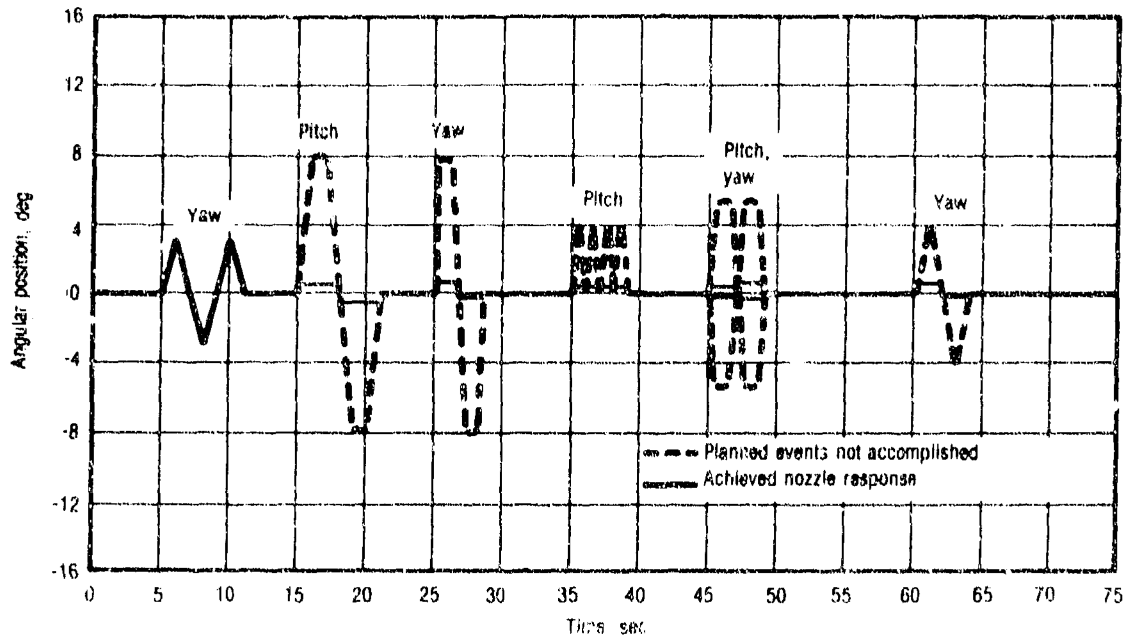

Figure 96. Hot Ball and Socket Nozzle S/N 2 Duty Cycle, Planned and Achieved

27220

planned 162 deg of vector travel were accomplished. Additional TVC plots for nozzle S/N 2 are presented in appendix A.

8.4.3 Thermocouple Data

Twenty-three thermocouples were instrumented to the nozzle as shown in Figure 85. Two tungsten/rhenium thermocouples were attached near the exit plane. Three of the 21 chromel-alumel types were located on the pitch-plus actuator at 0 deg. Four were located indepth into the socket, two indepth into the lockring, six at the backface of the socket and lockring, and six were instrumented along the length of the exit cone including the compliance ring. Each of the three axial locations on the lockring and socket was instrumented with a pair of thermocouples 180 deg apart.

Thermocouples 1 through 12 (indepth and backface thermocouples on the lockring and socket) responded for the full 75-sec duration. Plots of temperature versus time for these 12 thermocouples are presented in Figures 97 through 108. The effect of annular flow around the ball, for 5 sec, on the thermocouple

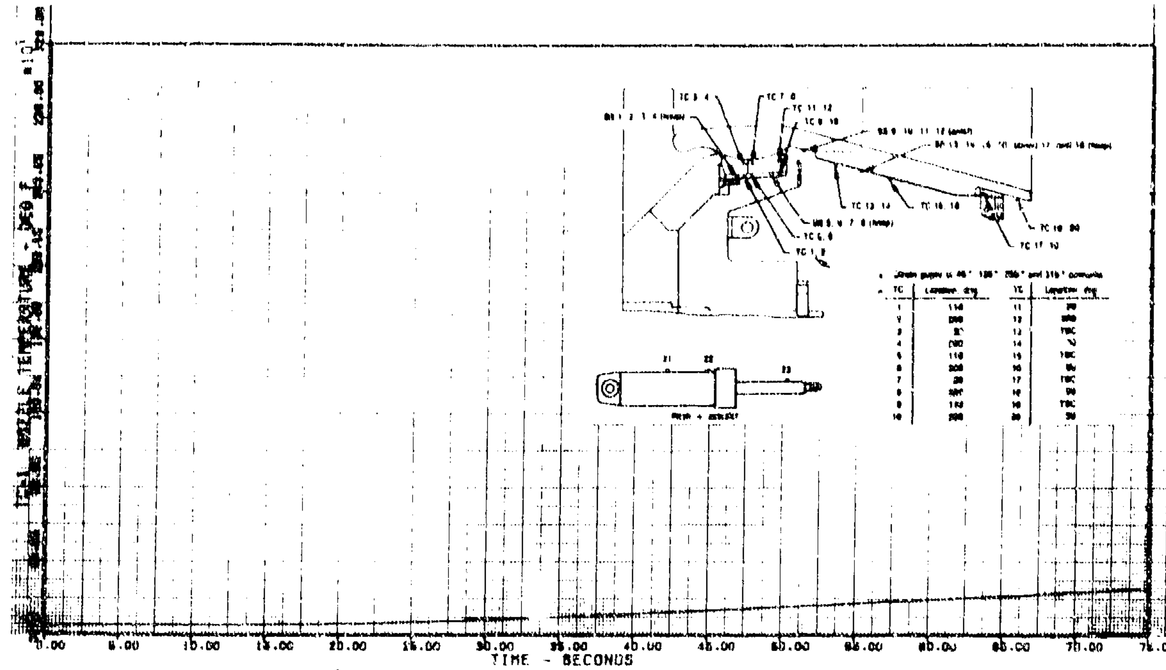

Figure 97. Temperature vs Time, TC1

27221

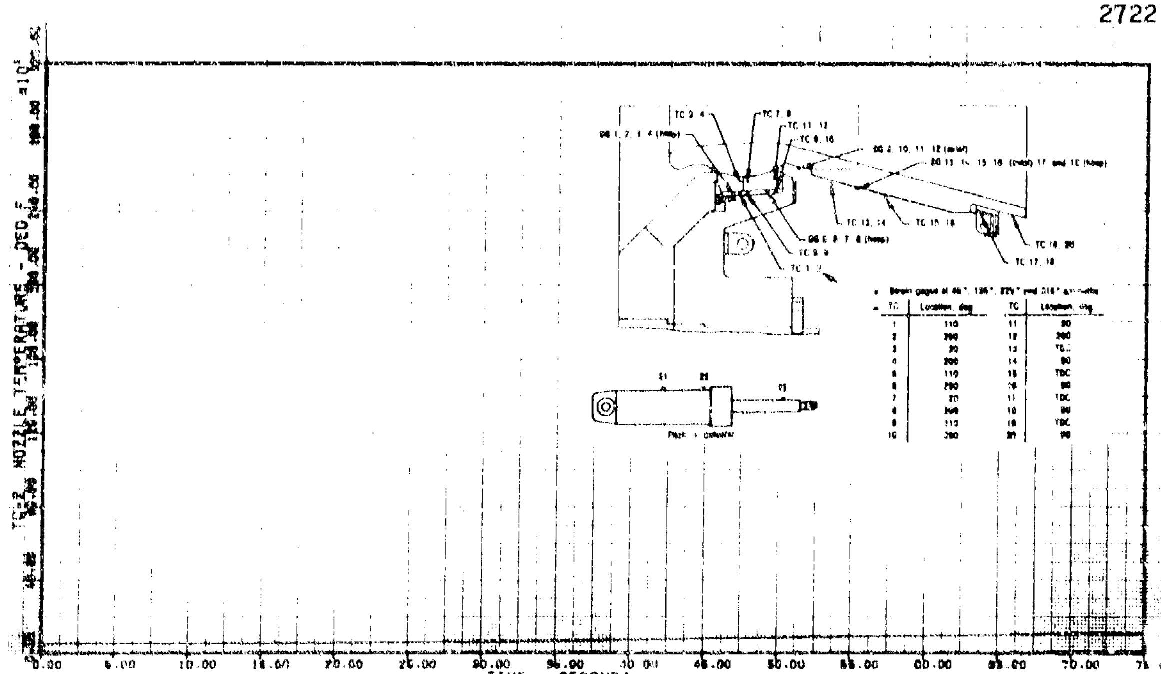

Figure 98. Temperature vs Time, TC2

27222

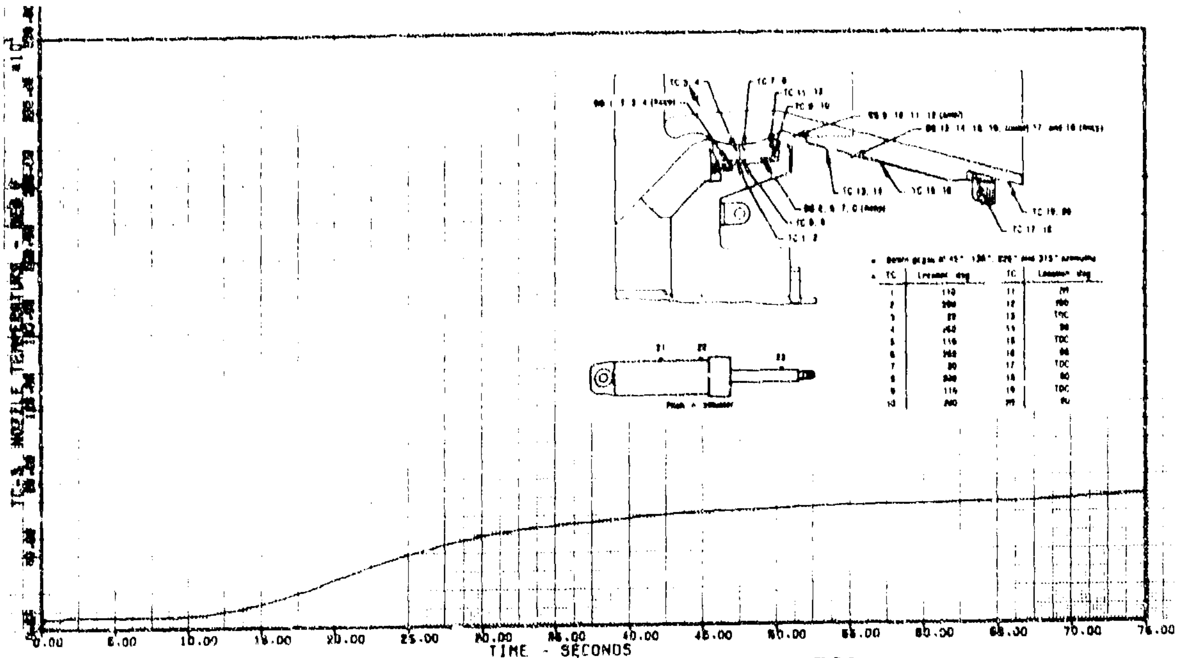

Figure 99. Temperature vs Time, TC3

27223

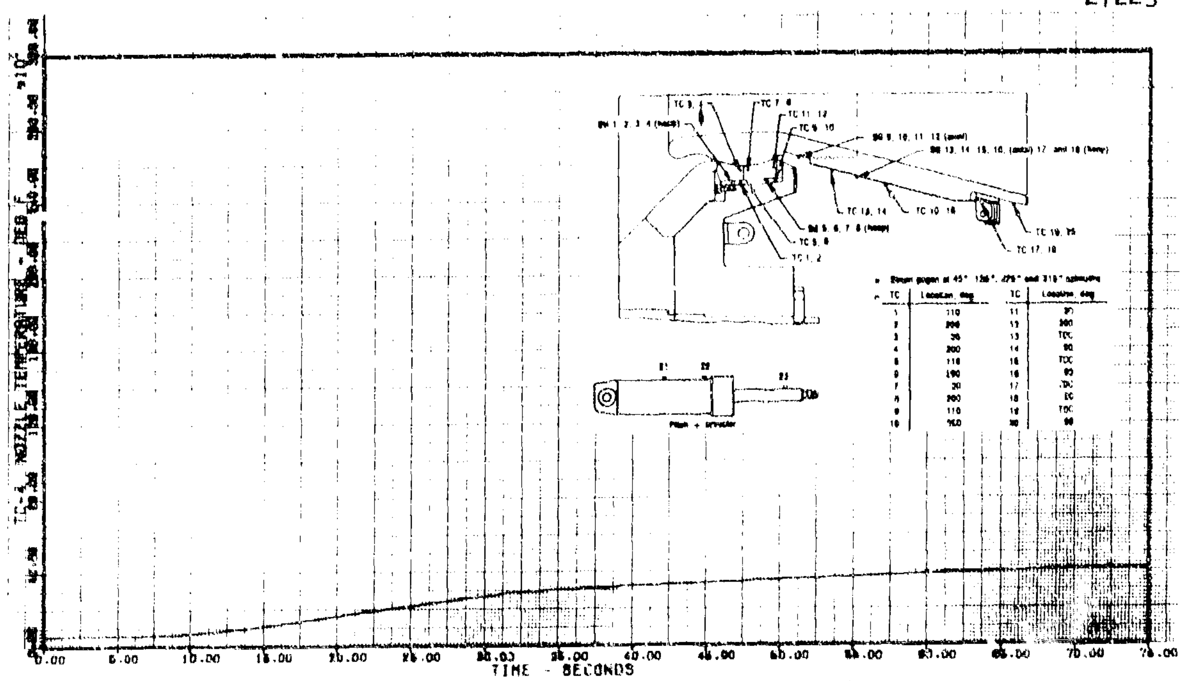

Figure 100. Temperature vs Time, TC4

27224

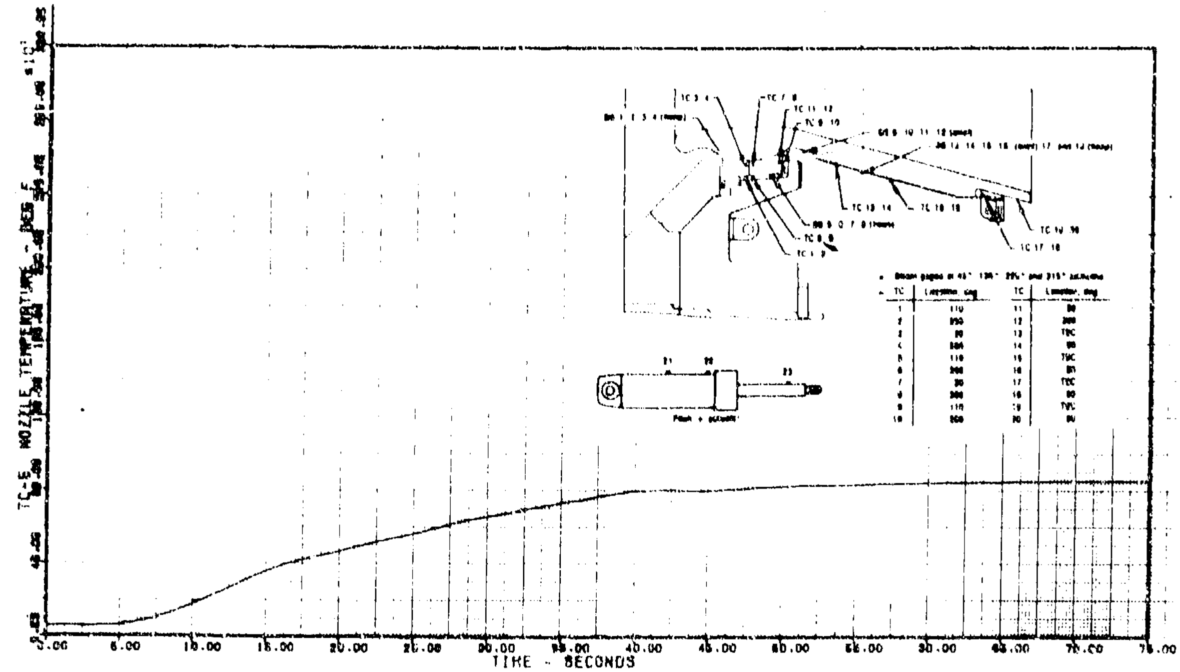

Figure 101. Temperature vs Time, TC5

27225

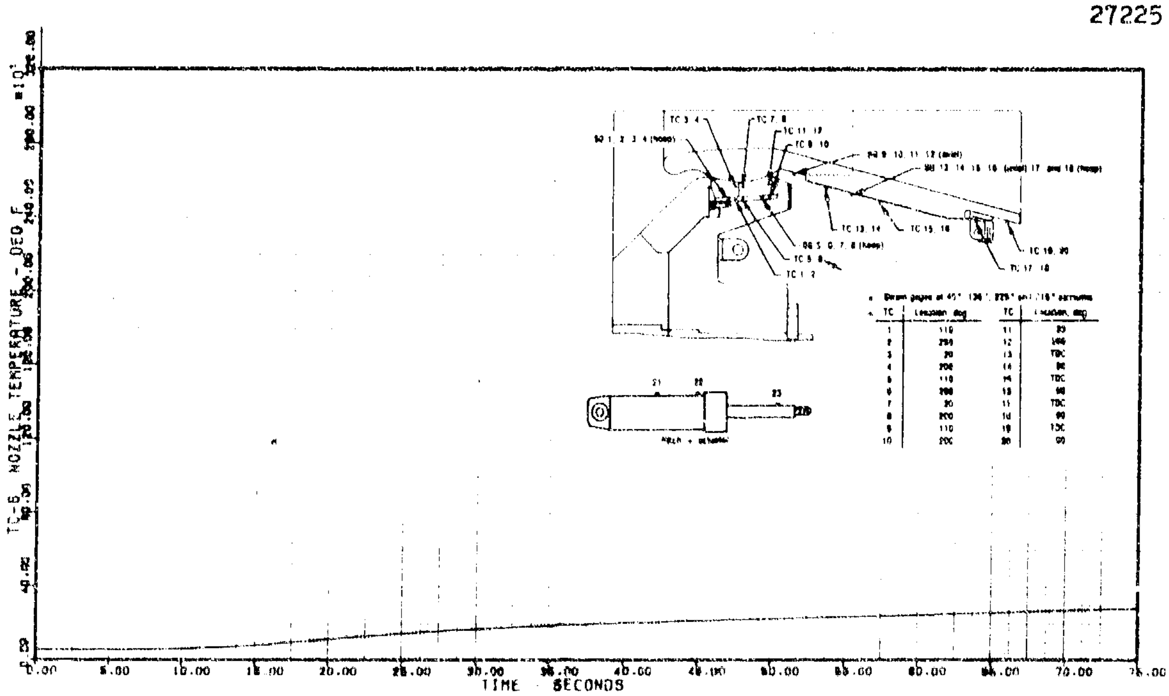

Figure 102. Temperature vs Time, TC6

27226

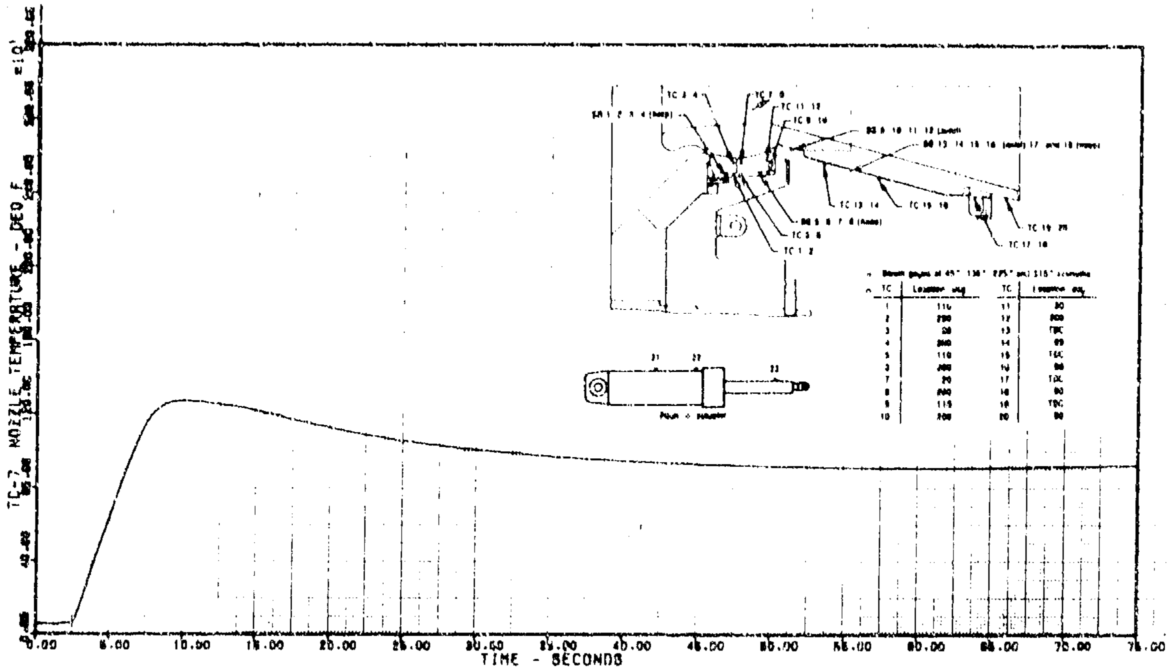

Figure 103. Temperature vs Time, TC7

27227

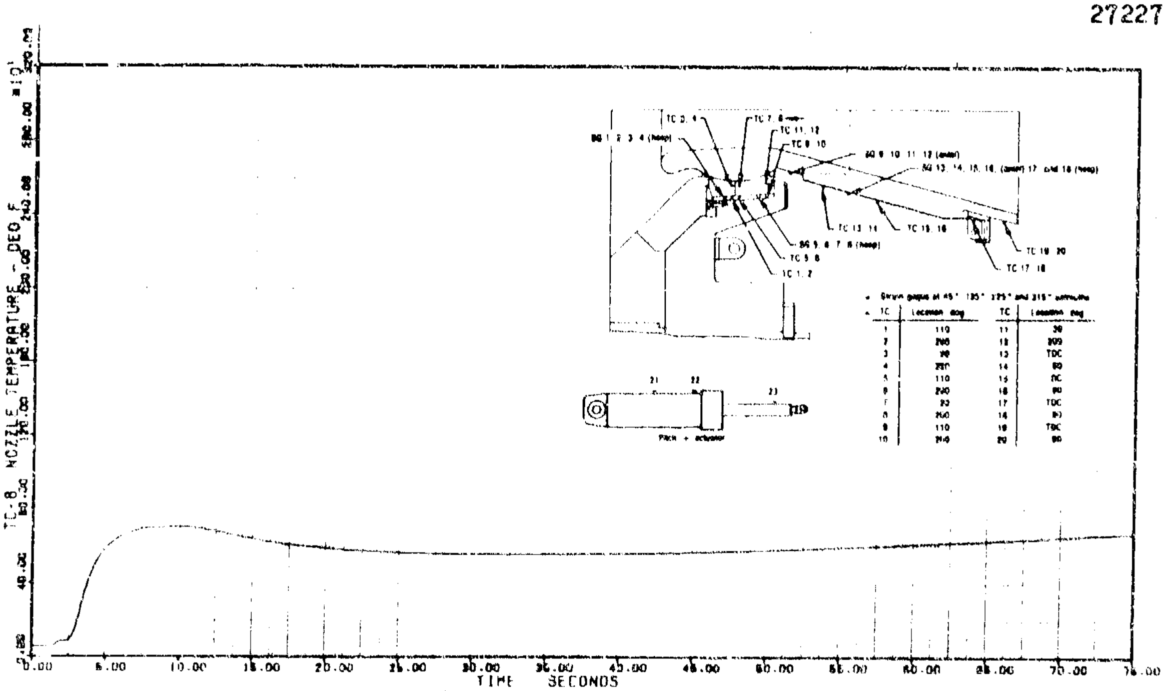

Figure 104. Temperature vs Time, TC8

27228

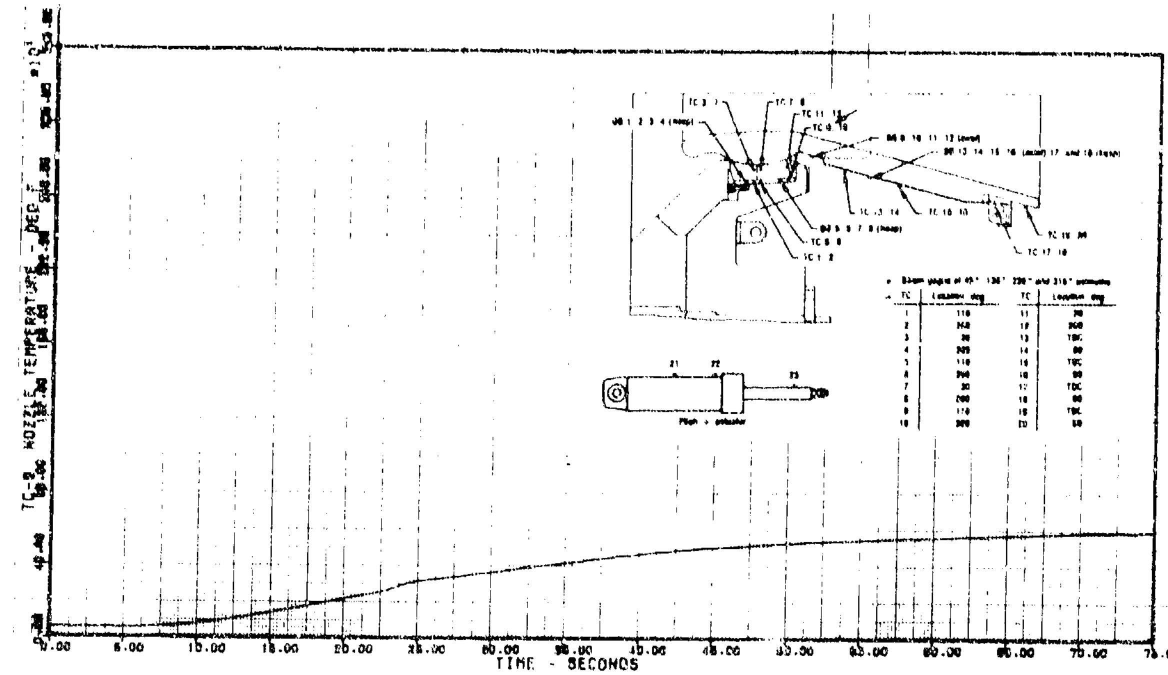

Figure 105. Temperature vs Time, TC9

27229

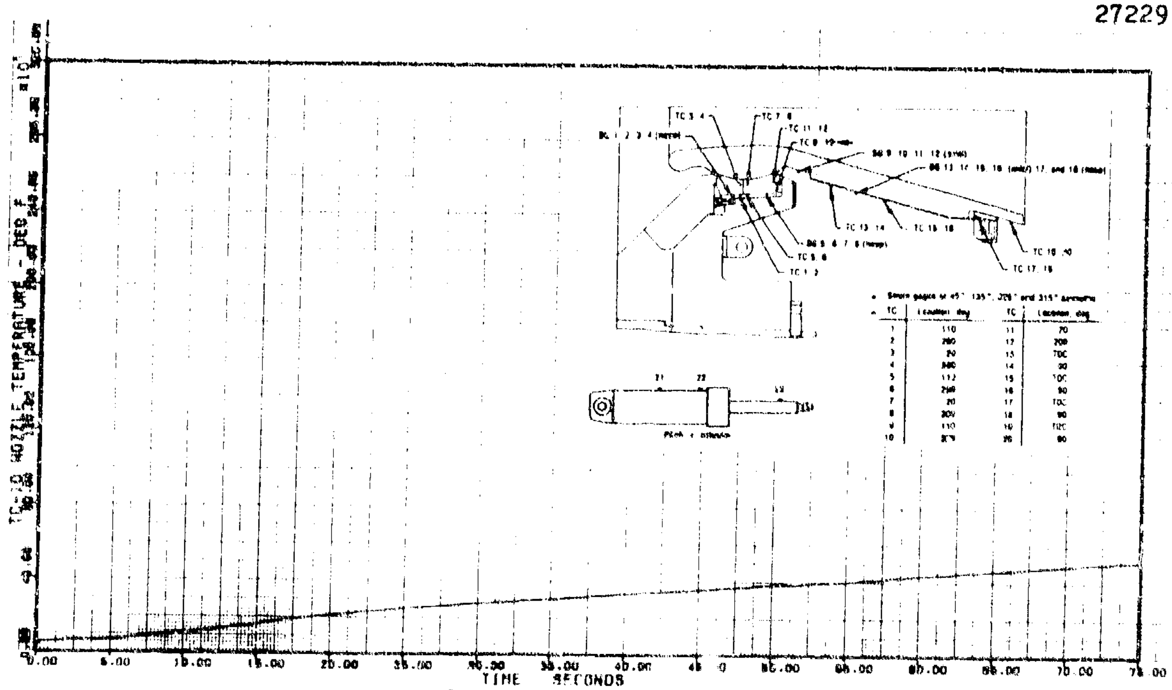

Figure 106. Temperature v Time, TC10

27230

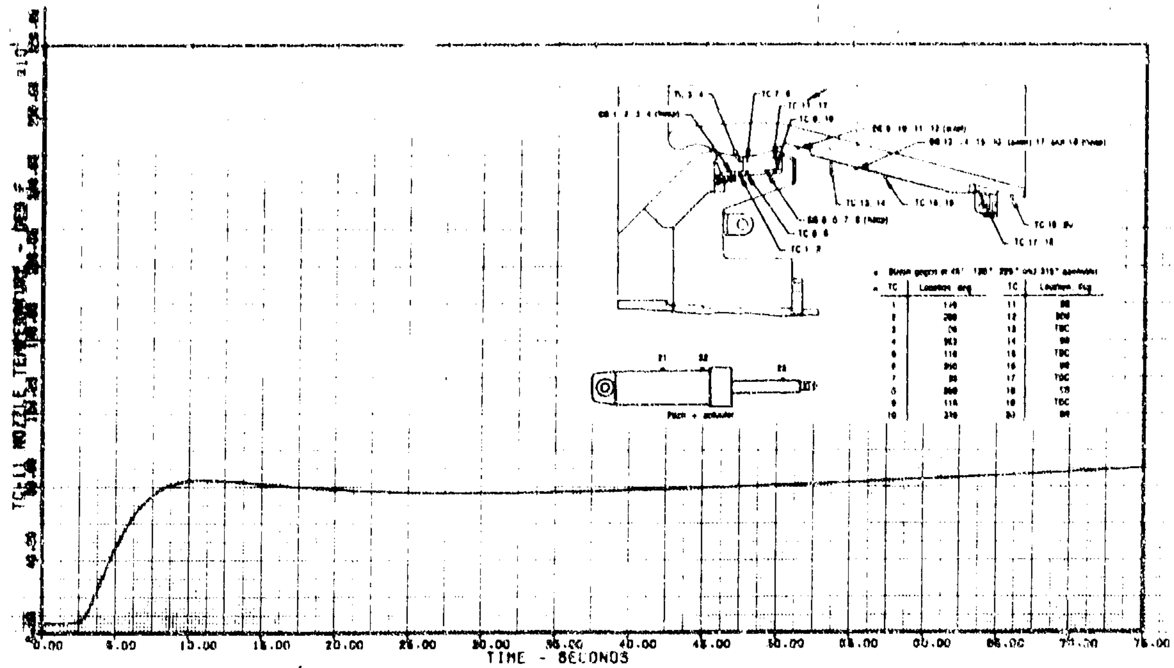

Figure 107. Temperature vs Time, TC11

27231

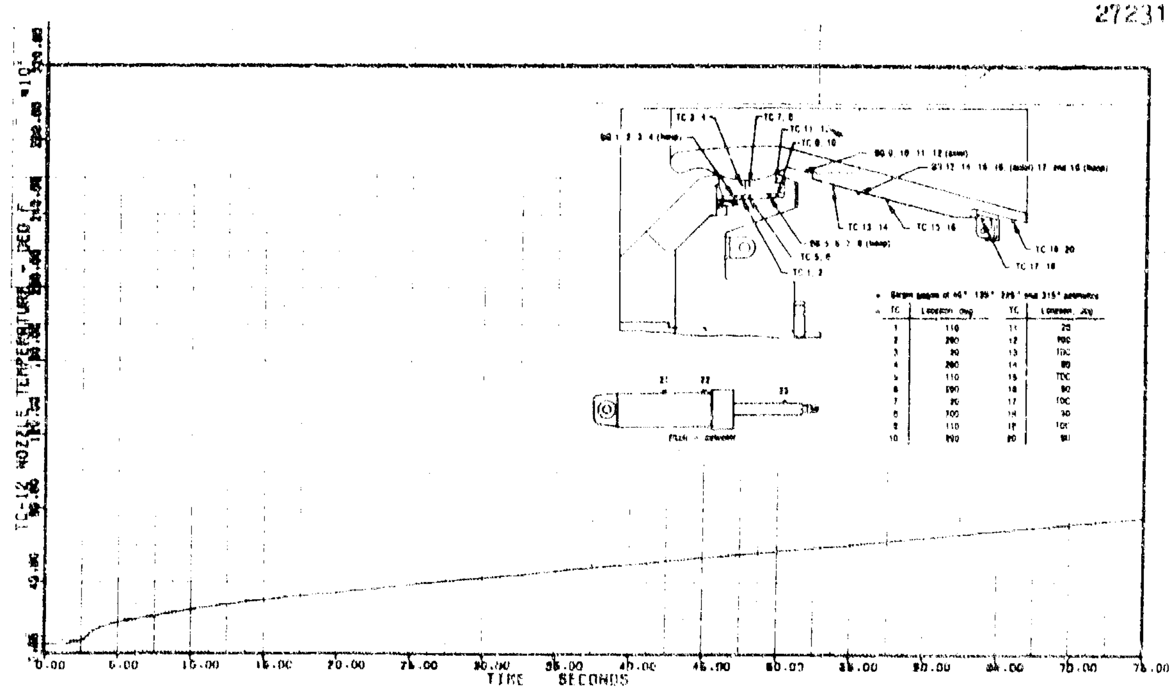

Figure 108. Temperature vs Time, TC12

27232

response at the lockring and socket is apparent in the data. Higher temperatures were measured by thermocouples 1, 3, 5, 7, 9, and 11, which were within the 0- to 180-deg area of observed maximum flow, than by those at the same respective axial station, but 180 deg away. As expected, the most significant difference within each pair was for those indepth in the socket and lockring. The two thermocouples (7 and 8) indepth into the forward end of the C-C socket rose significantly at 2.5 sec because of the flow around the ball. TC7 within the 180-deg area of flow rose to 1,280°F within 7 sec, then dropped to 920°F at tailoff. TC8, 180 deg away, peaked at 700°F within 5 sec and measured 680°F at tailoff. An overlay of the temperature time history for TCs 7 and 8 is presented in Figure 109.

Thermocouples 13 through 20, along the exit cone, were no longer functional after 2 sec into the firing. All of these thermocouples were located at either 0 or 90 deg (within the region of flow). Plots of temperature versus time for these eight thermocouples are presented in appendix B.

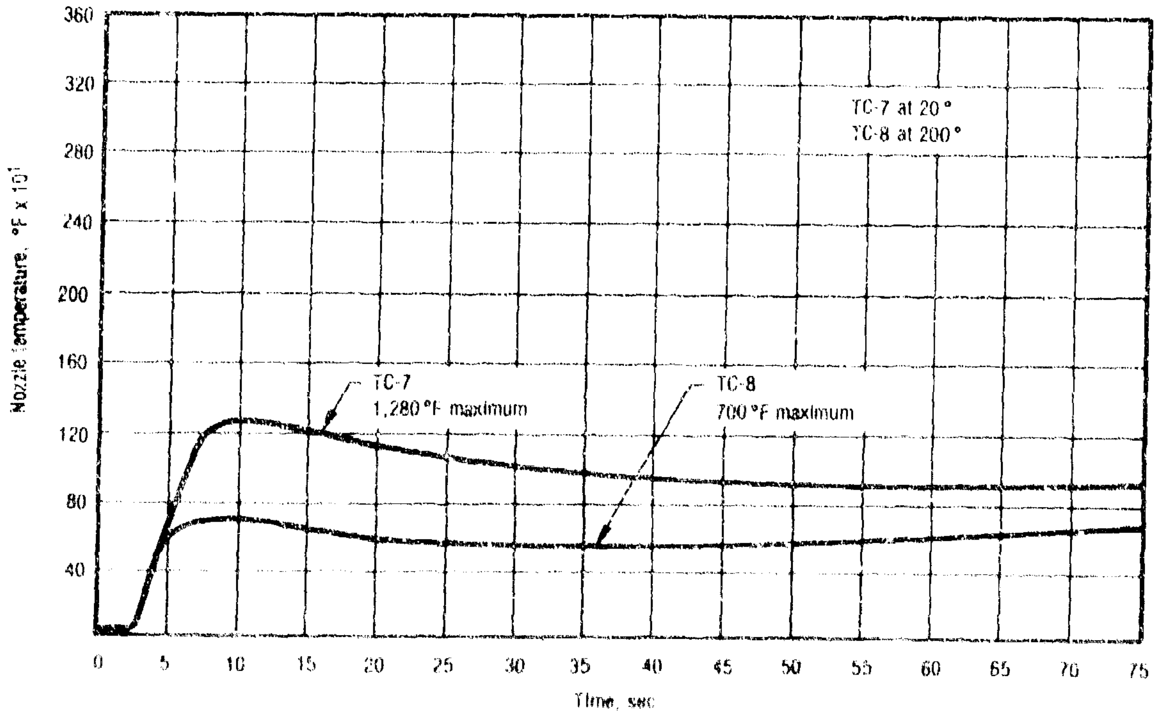

Figure 109. Temperature vs Time, In-Depth Thermocouples at Forward End of Socket

27157

Thermocouples 21 and 22, located behind 1/8-in.-thick rubber on the pitch-plus actuator cylinder, and TC 23 on the actuator shaft responded for the full firing duration. This actuator was within the region of flow experienced for 5 sec. Temperature versus time for these three thermocouples is presented in Figures 110, 111, and 112. The maximum temperatures measured on the cylinder were 110 and 200°F for TCs 21 and 22, respectively. TC 22, further aft than TC 21, showed a rise of about 75°F at the time of flow (2 sec) whereas TC 21 was unaffected. TC 23 on the actuator shaft quickly rose at 2 sec to 610°F before dropping, and then rising again to 610°F at tailoff. These measured temperatures were not high enough to have caused thermal expansion binding of the actuator.

8.4.4 Strain Gages

Eighteen strain gages (10 hoop and eight axial) were instrumented to the nozzle as shown in Figure 85. Four hoop gages were instrumented on the OD of the lockring and four hoop gages were placed on the socket OD. All ten gages (two hoop and eight axial) on the exit cone were lost at 2 sec because of impingement of the annular flow. Two gages on the socket (SG 5 and 6) were not functional at ignition. Because of the anomalous events which occurred at the

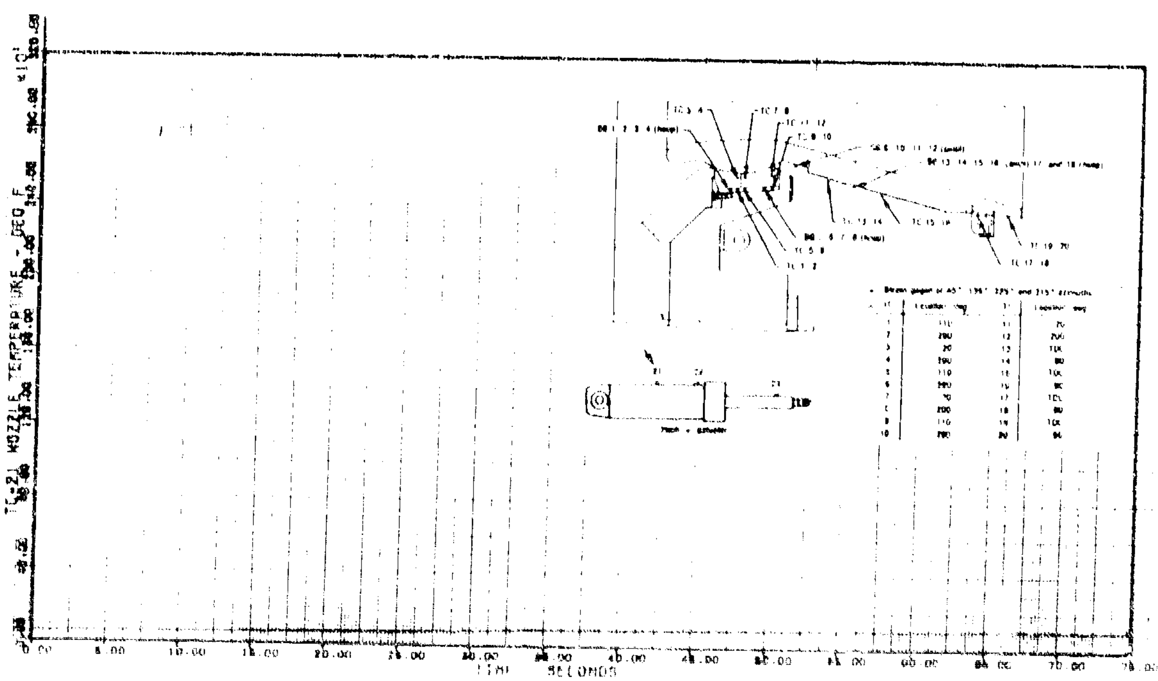

Figure 110. Temperature vs Time, TC21

27233

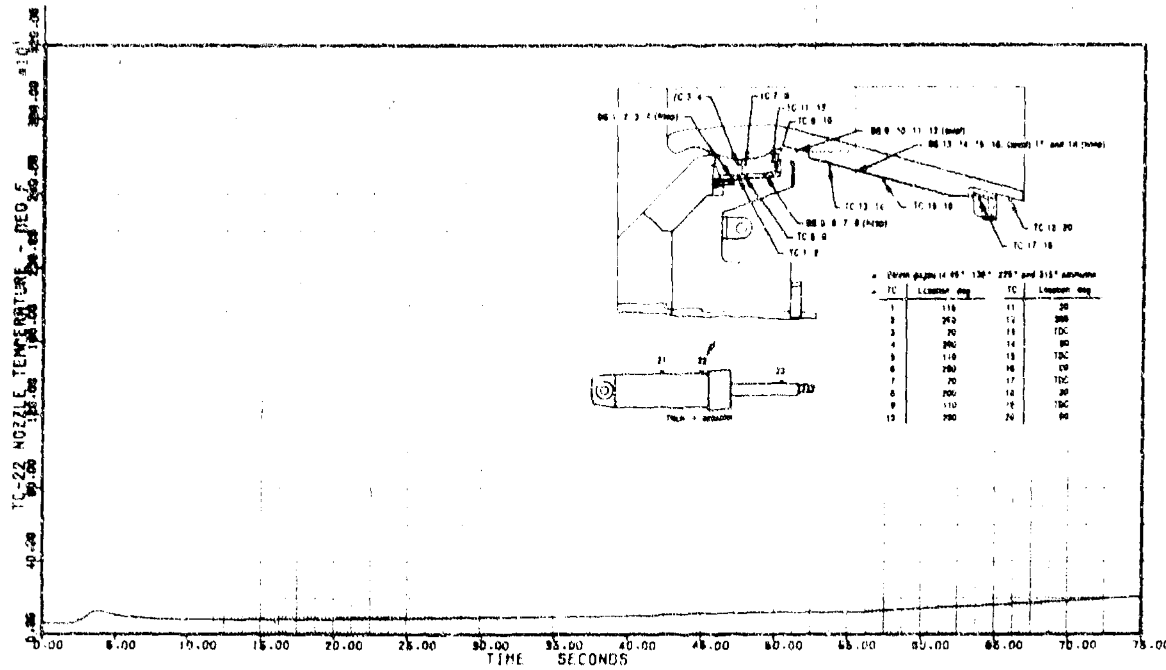

Figure 111. Temperature vs Time, TC 22

27234

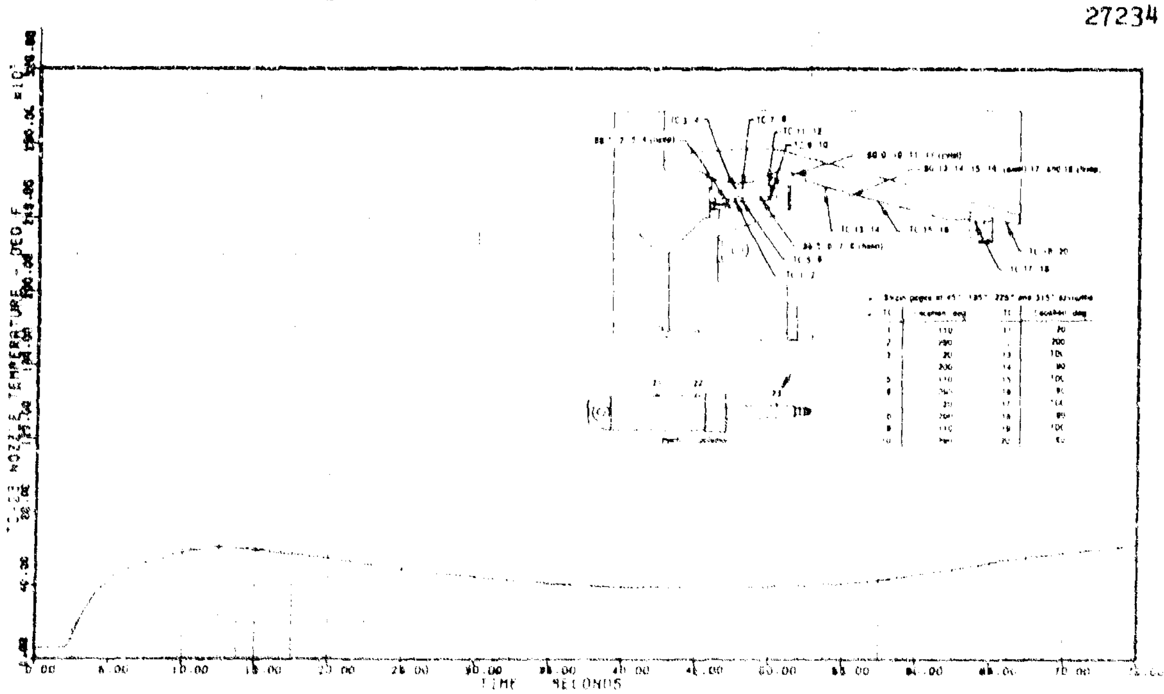

Figure 112. Temperature vs Time, TC23

27235

beginning of the firing and uncertainties in the bearing geometry resulting from extensive alumina deposition, clean interpretation of the data is difficult. However, indications on gages 1 through 4 (Figures 113 to 116) of the lockring at 2 sec support the sequence of events established from the TVC data and high speed movies. Two gages (3 and 4) on the lockring exhibit events at 25, 47, and 60 sec, when vectoring in the yaw plane was attempted, indicating interference with the lockring. Extensive deposition of alumina between the ball and lockring found upon disassembly verified that interference did indeed occur. Plots of strain versus time for strain gages 7 to 18 are presented in appendix B.

8.4.5 Posttest Hardware Assessment

The posttest assembly is compared to the prefire condition in Figure 117. The fired nozzle was in very good condition especially when considering that (1) the ball was subjected to nearly 5 sec of unexpected annular flow near the beginning of the firing and, (2) the exit cone was subjected to stall loads imposed by the actuators during most of the firing duration. The extensive alumina seen plated on the outside of the exit cone indicates the severity of the annular flow experienced.

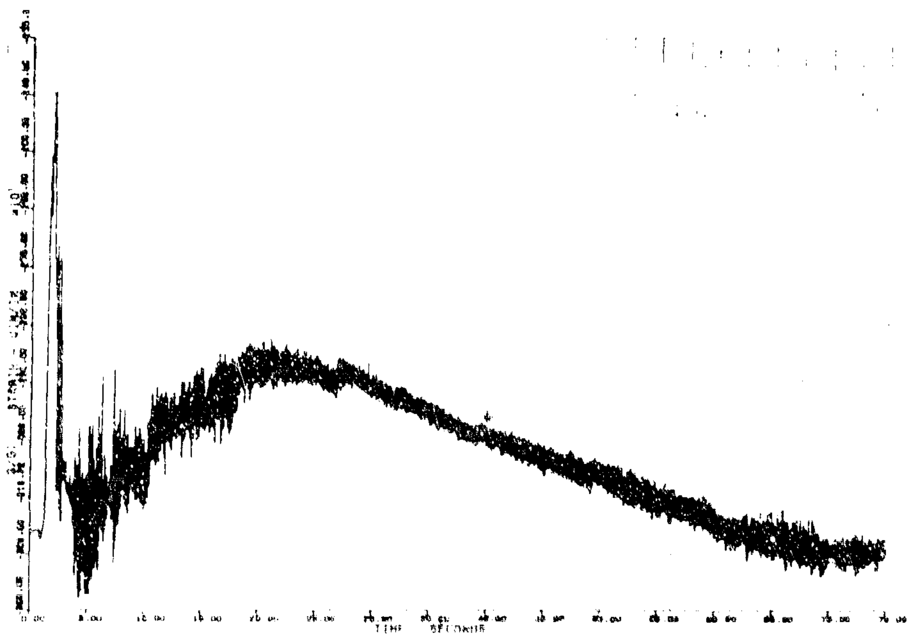

Figure 113. Hoop Strain vs Time, S/G 1 (Lockring, 45°)

27236

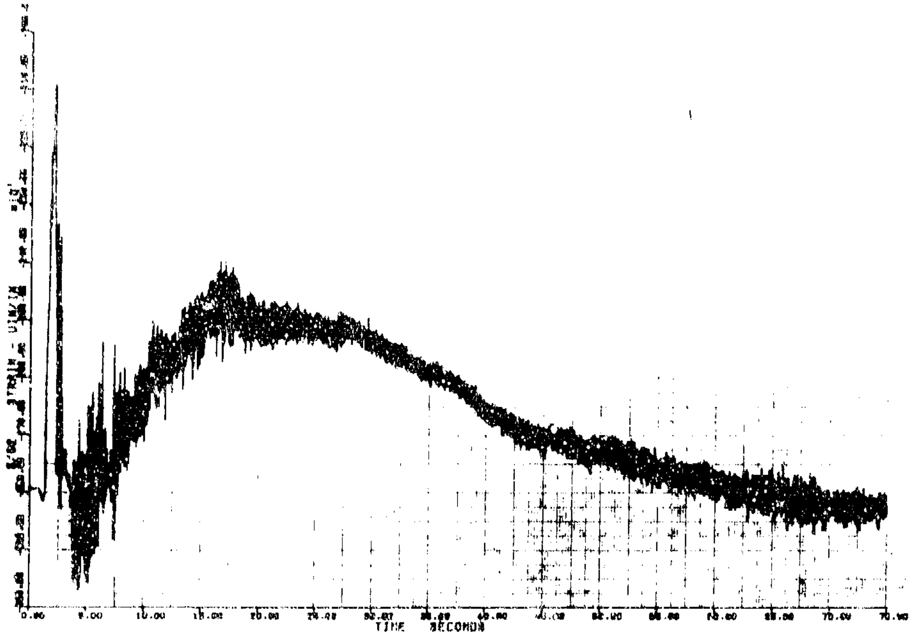

Figure 11[illegible]. Hoop Strain vs Time, S/G 2 (Lockring, 135°)

27237

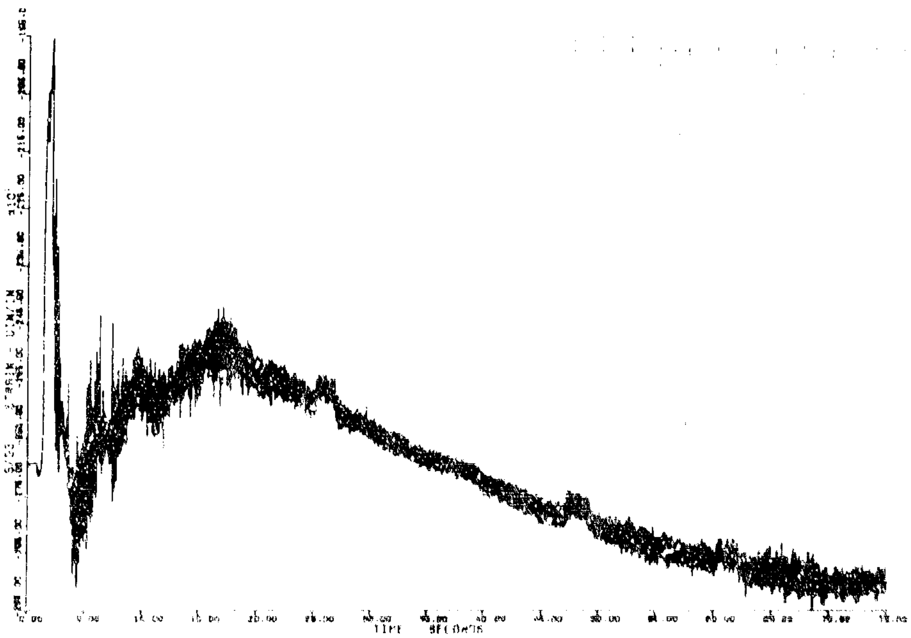

Figure [illegible]. Hoop Strain vs Time, S/G 3 (Lockring, 225°)

27238

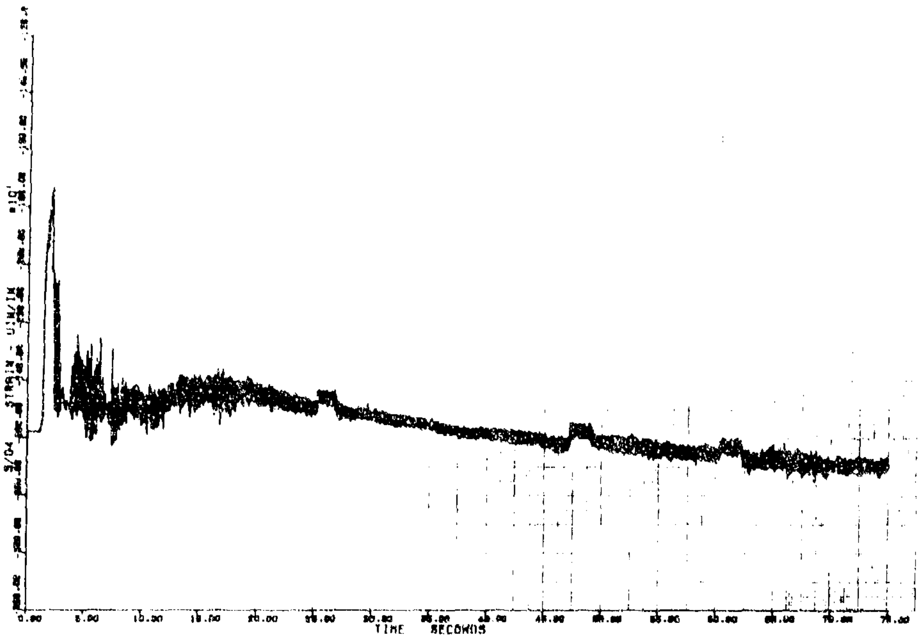

Figure 116. Hoop Strain vs Time, S/G 4 (Lockring, 315°)

27239

The condition of the posttest entrance and throat is presented in Figure 118. The entrance erosion pattern was substantially improved from that of nozzle S/N 1, proving the effectiveness of the sacrificial entrance. In addition, the sacrificial entrance virtually eliminated erosion in the splitline region.

The posttest actuation system shown in Figure 119 shows the rubber insulation bonded to the actuator cylinders partially burned away. The actuators were, however, not sufficiently heated to be considered a contributor to the high torque measured during the firing. Reuse of the actuators is feasible with only minor refurbishment. No electrical wires, hydraulic lines or other associated actuation hardware were damaged.

The nozzle, after removal of the actuation system and some cleaning, is shown in Figure 120. The steel adapter ring, adapter insulator, compliance ring and the exit cone are all reusable. C-34 graphite cement in the ball-to-exit threads prevented the exit from being unscrewed, which is normal. Therefore, the ball was cut from the exit forward of the threads to enable potential

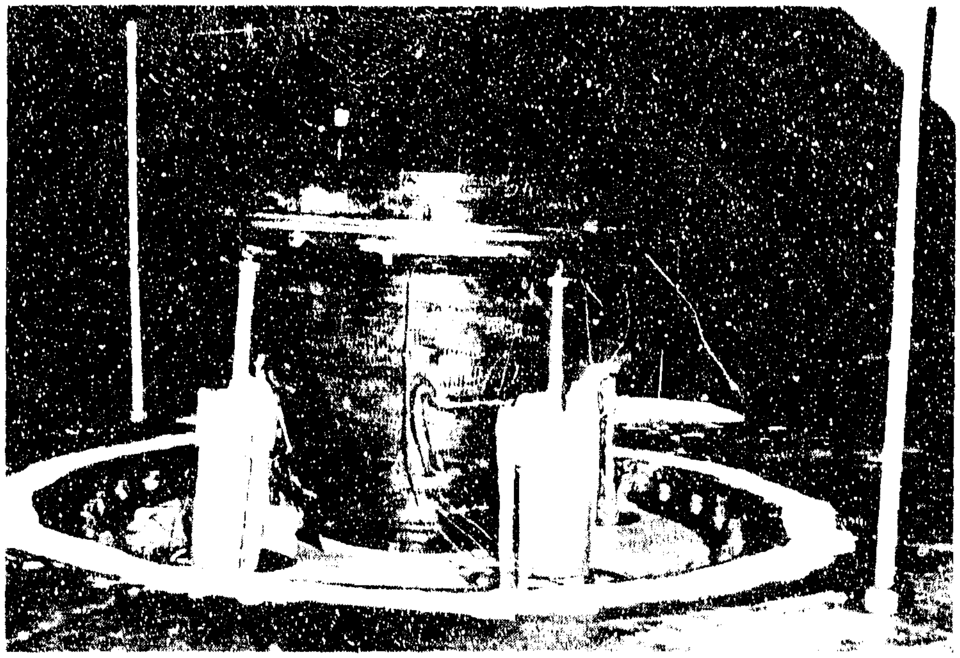

14187-1

Prefire

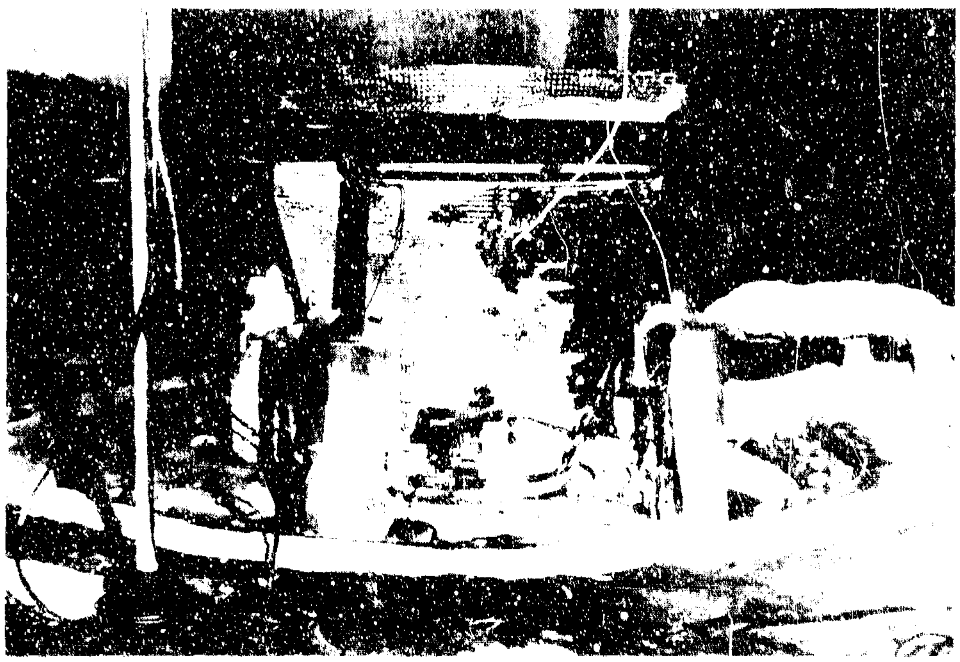

14187-6

Postfire

Figure 117. Comparison of the Prefire and Postfire View of Nozzle S/N 2

27,210

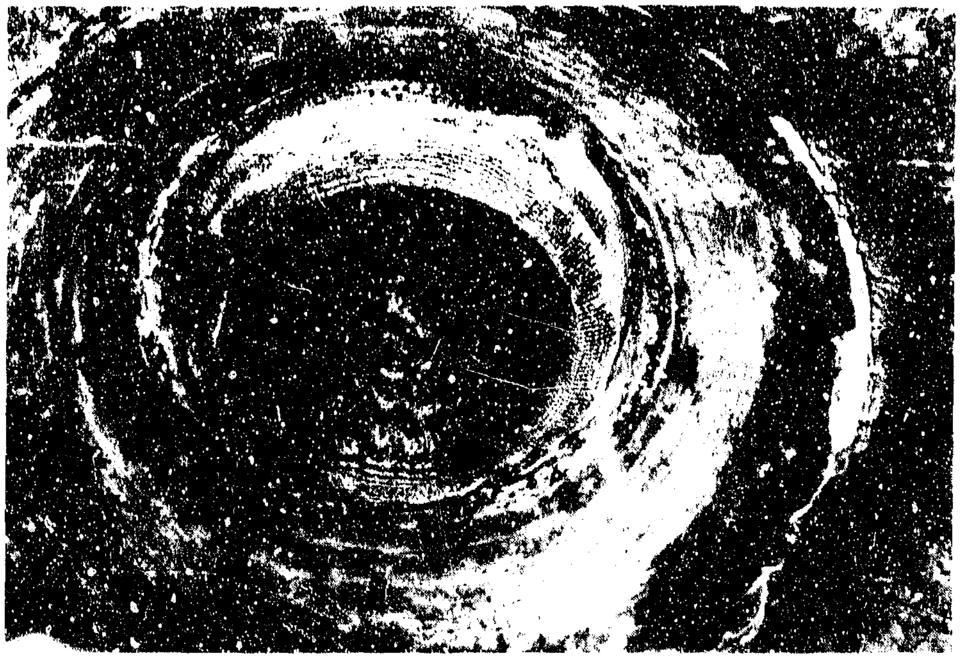

14187-2

Entrance

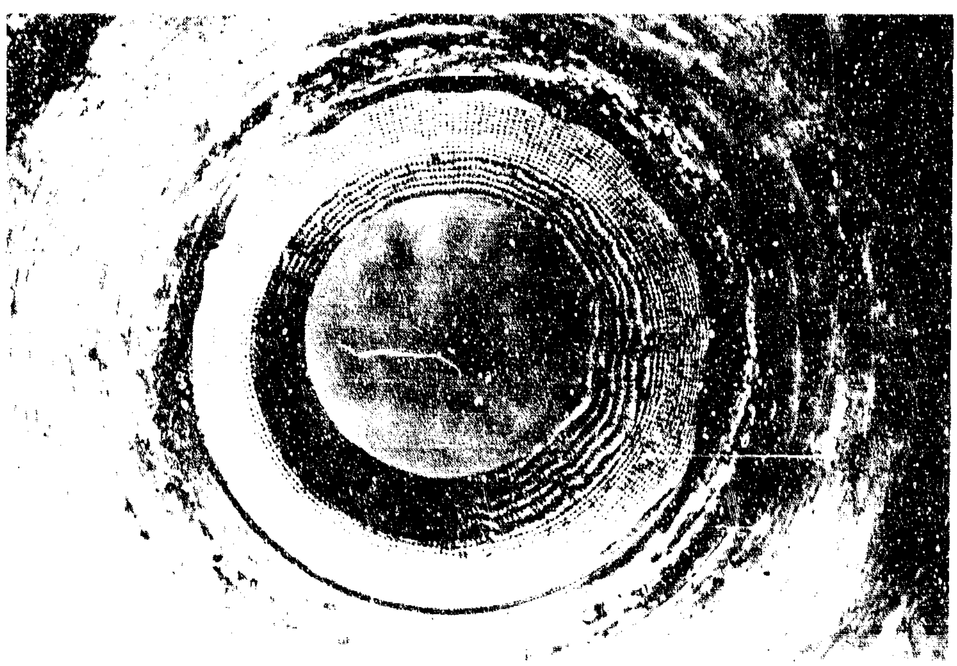

14187-7

Throat

Figure 118. Posttest Views of Entrance and Throat, Nozzle S/N 2

27,281

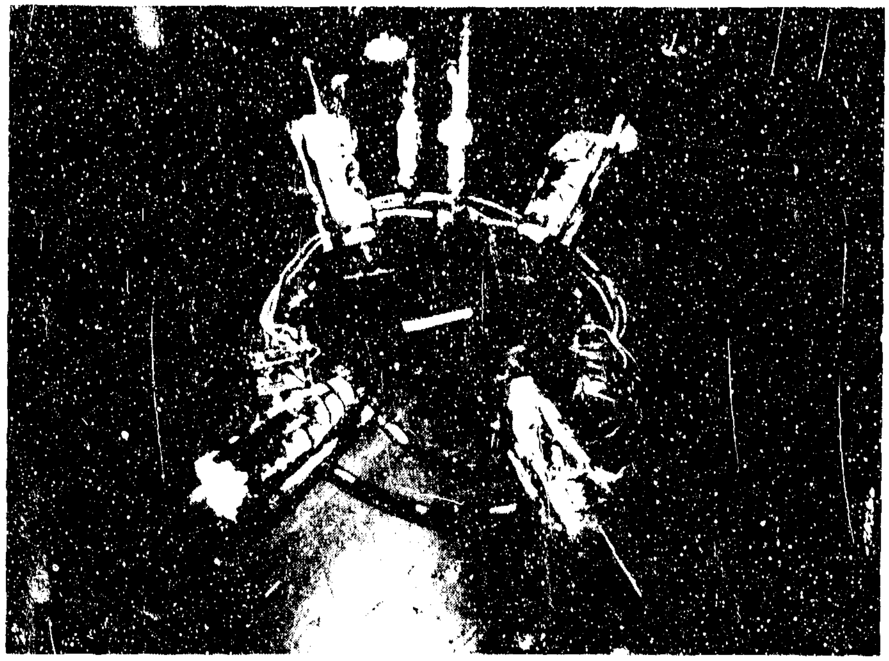

14137-13

Figure 119. Posttest Actuation System, Nozzle S/N 2

27242

14137-15

Figure 120. Posttest Nozzle S/N 2 Following Removal of Actuation Hardware

27245

subsequent reuse of the exit. Upon removal of the exit cone, the remaining nozzle components were disassembled.

Two views of the fired ball are presented in Figures 121 and 122. Note the discoloration, alumina deposition and wear patterns due to flow and alumina abrasion that resulted from the annular flow early in the firing. A close-up view of the alumina deposition on the ball and between the ball and lockring is presented in Figure 123. Another indication of the severity of the annular flow is evident in Figure 121. An eroded step can be seen at the lower part of the ball (aft end) where the surface was once conical. This damaged region extended from 0 to 180 deg only, with the maximum impingement at 90 deg corresponding to the region of maximum flow observed during the test.

An overall view of the socket and a close-up of the alumina deposition found on it is shown in Figure 124. The groove on the OD of the socket was incorporated for strain gage instrumentation. A close-up view of the extensive alumina plating found on the spherical surface of the carbon-phenolic lockring is presented in Figure 125. Because of the increased gap, the lockring did not swell into the ball, as occurred with the pherolic lockring of the subscale nozzle. The socket may also be reusable with minor refurbishment.

Figure 121. Posttest Ball, Nozzle S/N 2, Side View (0 to 180 deg)

14137-11

Figure 122. Posttest Ball, Nozzle S/N 2, Entrance View

27145

14137-1

Figure 123. Close-Up View of Alumina Deposition on the Ball and Lockring, Nozzle S/N 2

27146

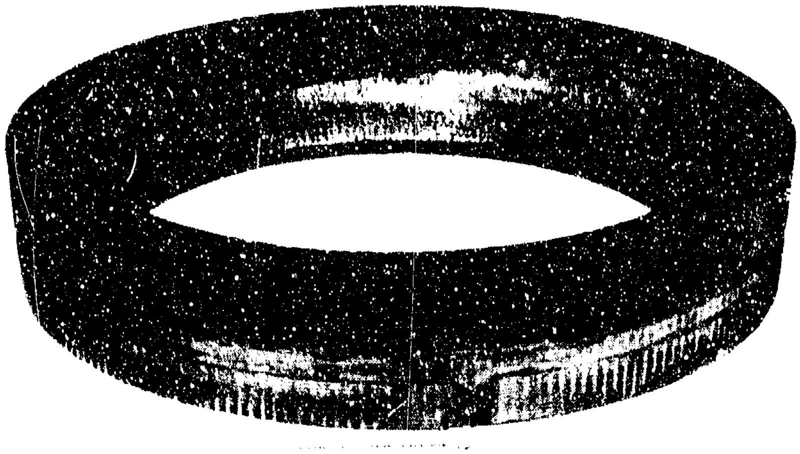

14137-9

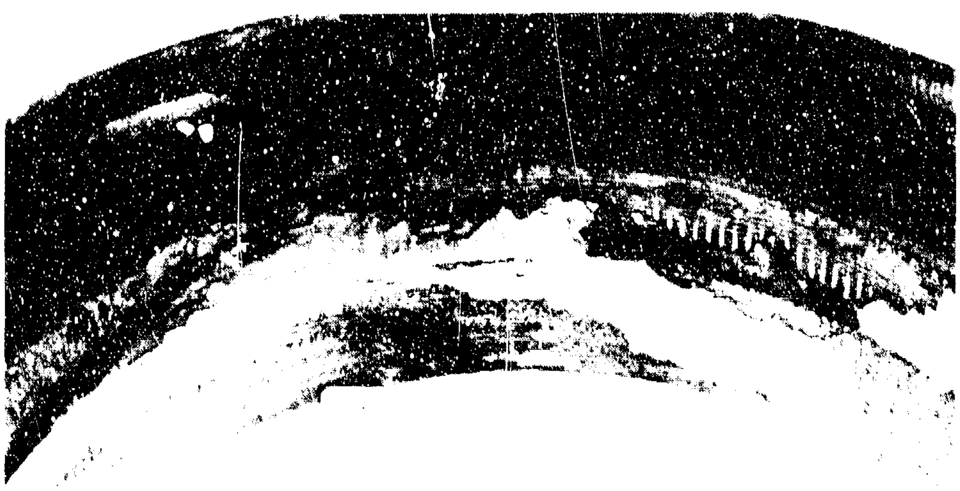

141[illegible] 2

Figure 124. Overall View of Posttest Socket and Close Up of Alumina Deposition, Nozzle S/N 2

.7197

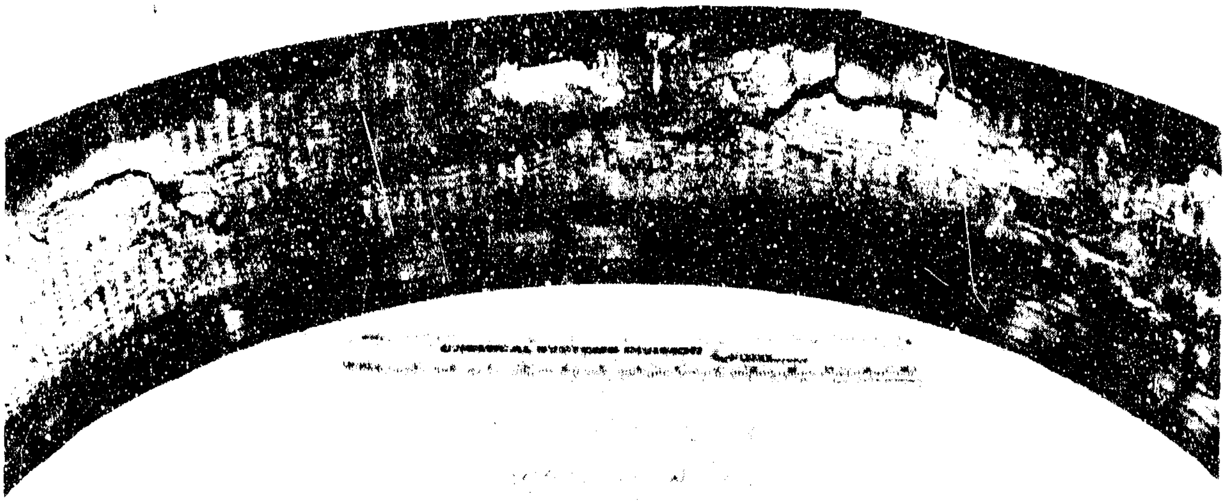

14137-8

Figure 125. Close-Up View of Alumina Deposition on the Lockring, Nozzle S/N 2

27148

Two views of the exit cone with the aft portion of the ball still threaded to the cone are shown in Figure 126. The exit cone was in excellent condition and is reusable after machining off the remaining aft ball.

The measured nozzle erosion profile is presented in Figure 127.

14137-7

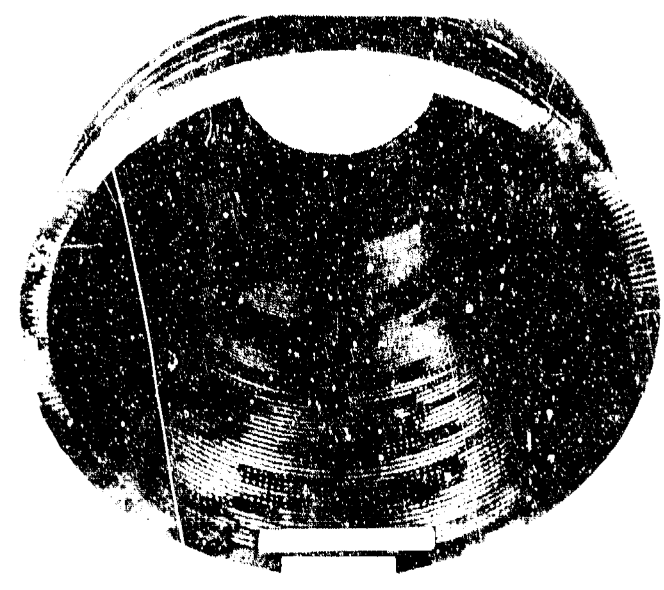

14137-5

Figure 1.6. Posttest Views of Exit Cone, Nozzle 2N 2

27169

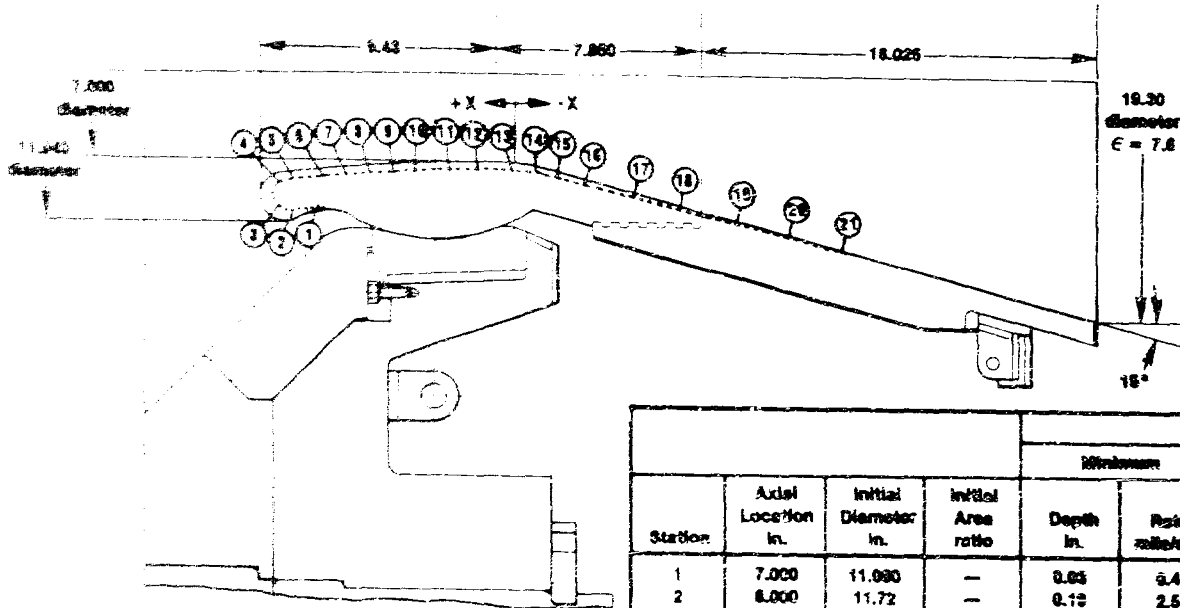

Motor Operating Conditions	
Propellant	UTP-12,687
Average pressure	5?? psia
Action time	74.6 sec

Measured average ballistic throat erosion rate — 4.7 mils/sec

				Ablation					
				Minimum		Average		Maximum	
Station	Axial Location in.	Initial Diameter in.	Initial Area ratio	Depth in.	Rate mils/sec	Depth, in.	Rate, mils/sec	Depth, in.	Rate, mils/sec
1	7.000	11.080	—	0.05	3.4	0.08	5.3	0.09	1.2
2	8.000	11.72	—	0.13	2.5	0.27	3.6	0.41	5.5
3	8.580	11.88	—	0.57	7.6	0.70	9.4	0.88	12.8
4	8.580	7.920	1.28	0.31	4.2	0.37	5.9	0.38	5.1
5	8.000	7.799	1.24	0.27	3.6	0.31	4.2	0.33	4.4
6	7.000	7.612	1.18	0.33	4.4	0.27	5.0	0.30	5.2
7	6.000	7.440	1.13	0.37	5.0	0.41	5.5	0.44	5.5
8	5.000	7.312	1.09	0.40	5.4	0.42	5.6	0.46	6.0
9	4.000	7.200	1.06	0.29	5.2	0.43	5.8	0.46	6.0
10	3.000	7.112	1.03	0.38	5.1	0.41	5.2	0.42	5.8
11	2.000	7.080	1.01	0.35	4.7	0.39	5.1	0.41	5.6
12	1.000	7.012	1.00	0.33	4.4	0.36	4.8	0.39	5.2
13	0.000	7.000	1.00	0.28	3.9	0.31	4.2	0.36	4.8
14	-1.000	7.144	1.04	0.21	2.8	0.26	3.5	0.27	3.8
15	-2.000	7.578	1.17	0.11	1.5	0.15	2.0	0.17	2.3
16	-3.5	8.220	1.41	—	—	0.12	1.6	—	—
17	-5.5	9.380	1.80	—	—	0.11	1.5	—	—
18	-7.5	10.460	2.23	—	—	0.10	1.3	—	—
19	-9.5	11.570	2.73	—	—	0.08	1.2	—	—
20	-11.5	12.800	3.24	—	—	0.06	0.7	—	—
21	-13.5	13.880	3.82	—	—	0.025	NR.	—	—

Figure 127. Postfire Erosion Profile, Nozzle S/N 2

27150

9.0 OBSERVATIONS/CONCLUSIONS

At the start of this program the hot ball and socket (HBS) integral nozzle and thrust vector control (TVC) system had been established as state-of-the-art in tactical size by the completely successful test of a 2-in. throat diameter, 15-deg nozzle for the Naval Surface Weapons Center (NSWC). Despite significant scale-up challenges, great strides have been made with only two large test firings toward the goal of providing an improved, simple, and reliable TVC system to allow advancements in future large motor propulsion systems. It is apparent from lack of complete success in large motors that further development is warranted.

It is probable that 7-in. nozzle S/N 2 would have been 100% successful, as evidenced by the posttest condition, had the associated actuators been modified to allow immediate seating of the ball on the socket. The problems associated with nozzle S/N 2 are summarized as follows:

- The actuation system was unable to instantaneously relieve hydraulic fluid from the actuator cylinders, and prevented the ball from translating 0.30-in. and sealing on the socket for about 5 sec
- During nearly 5 sec of annular flow around the ball, aluminum oxide liberally plated on the ball, socket and lockring
- The aluminum oxide solidified after one successful vector event, stalling the system.

The problems associated with nozzle S/N 1 were primarily attributed to inadequacies in the 3D carbon-carbon (C-C) exit cone material. Fabrication of this cone, the largest ever of its kind, was a major undertaking four years ago. Since that time, as demonstrated by nozzle S/N 2, great improvements have been made. Large 3D C-C exit cones are now state-of-the-art.

10.0 ACCOMPLISHMENTS

Significant accomplishments under this program include:

- Demonstration of the capability of a large (7-in. D_t) HBS nozzle to survive the severe thermal/structural environment associated with advanced upper stage test conditions
- Demonstration of the tenacity of 3D C-C as evidenced by survival in an unexpectedly adverse environment during the 5-sec of annular flow around the ball, and under subsequent stall forces experienced during the remaining planned duration
- Demonstration of a large C-C ball and socket to provide a non-leaking interface once seated
- Demonstration of the effectiveness of the sacrificial entrance to reduce entrance and splitline erosion.

In addition to these demonstrated accomplishments, significant knowledge and experience was acquired under this program relevant to the design of carbon-carbon (C-C) nozzles. Although the experience gained is applicable to C-C nozzles in general, the benefits are particularly associated with C-C TVC nozzles. As a result of the partial failure of nozzle S/N 1, attention was focused on several key design elements which may have not been considered otherwise. Included were:

- Carbon-carbon threaded joints
- Splitline entrance erosion
- Hoop tensile failure of the socket

The thread design of the ball-to-exit cone joint was a significant contributor to the exit failure of nozzle S/N 1. Careful attention is warranted in future designs to ensure that a thread form machined in C-C is compatible with the reinforcement spacing of the material. If a thread form consists of less than one unit cell of reinforcements, the thread strength will be considerably reduced from that expected. Also, compatibility of properties (i.e., density, fiber type and weave characteristics) between the mating 3D C-C ball and exit is desirable to enhance reliability thereby alleviating the potential for problems such as thermal expansion induced stresses typical of a non-homogeneous interface. An extensive study of non-threaded joints was also conducted (reference 3). The alternatives evaluated were not found to offer an overall advantage to the 7-in. hot ball and socket nozzle design but may be advantageous under a different set o conditions.

Excessive splitline entrance erosion as associated with nozzle S/N 1 was corrected with the incorporation of a "sacrificial entrance" which inhibited direct impingement and subsequent erosion in the splitline. By contour controlling the entrance, a separated flow region was created providing recirculation of flow. This experience can be applied to any future nozzles where concern about entrance splitline erosion exists.

Due to the hoop tensile failure of the S/N 1 socket, several modifications improving this region were implemented. The structurally critical socket was changed from the previous conical frustra design to a more reliable high hoop fraction cylindrical construction, thereby providing a construction of more predictable characteristics. Also, ramp retention and tighter tolerances on the OD of the socket were incorporated.

Other areas of knowledge which were enhanced by this program include C-C property testing and instrumentation. Extensive tag-end property testing of the 3-D C-C ball, socket and exit cone provided further structural and thermal data needed and desired by analysts. This work also provided an opportunity to refine test methods and data interpretation for the complex C-C material.

Instrumentation of large nozzles was advanced with the implementation of indepth thermocouples in nozzle S/N 2. The quality of data was suprisingly good with no adverse effects on nozzle performance.

11.0 RECOMMENDATIONS

Since the problems with nozzle S/N 2 were attributed only to the actuation system, the design modifications recommended to subsequently ensure a completely successful large motor demonstration are focused on the actuation system. Modification of the actuators to provide an aft biased load would enable the ball to be seated aft on the socket at ignition, eliminating the problems associated with axial translation. By maintaining a positive load on the socket, the forward lockring previously required for pre-ignition steering checks can be eliminated. An advantage recognized by the removal of the lockring is that there is no longer a small gap at the forward end susceptible to accummulation of aluminum oxide. Increasing the annular space around the ball will allow rapid heating of the surfaces, preventing aluminum oxide deposition as occurred on the previous cooler, insulated surfaces. The suggested nozzle redesign incorporating these improvements in the splitline is presented in Figure 128. Note that the recommended improvements further simplify the system.

The recommended modification of the existing actuators is presented in Figure 129. The modification requires the incorporation of glands to enable sealing and pressurization of the cavity on the push side of the piston with nitrogen gas. By pressurizing GN_2 slightly higher than the hydraulic pressure on the pull side of the piston, an aft bias load is created, maintaining a positive seat of the ball on the socket. It is recognized that torque will be slightly increased with the aft bias load of the actuators. However, development of the blowoff load as chamber pressure rises can be sensed, and the GN_2 can be bled out, returning the actuators to a pull-only mode so that there is no increase in torque during motor operation.

Most of the hardware used for nozzle S/N 2, including the exit cone, can be reused (as discussed in section 8.4.5) for a cost effective, fully successful firing of a third large nozzle.

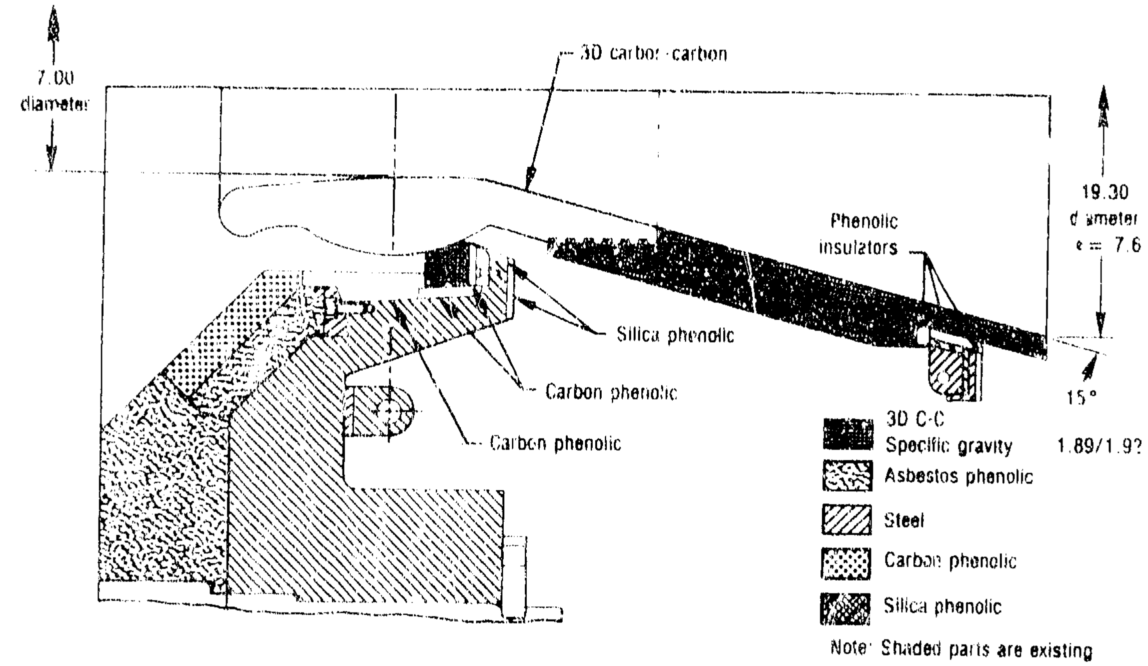

Figure 128. Suggested Redesign, Hot Ball and Socket Nozzle S/N 3
27151

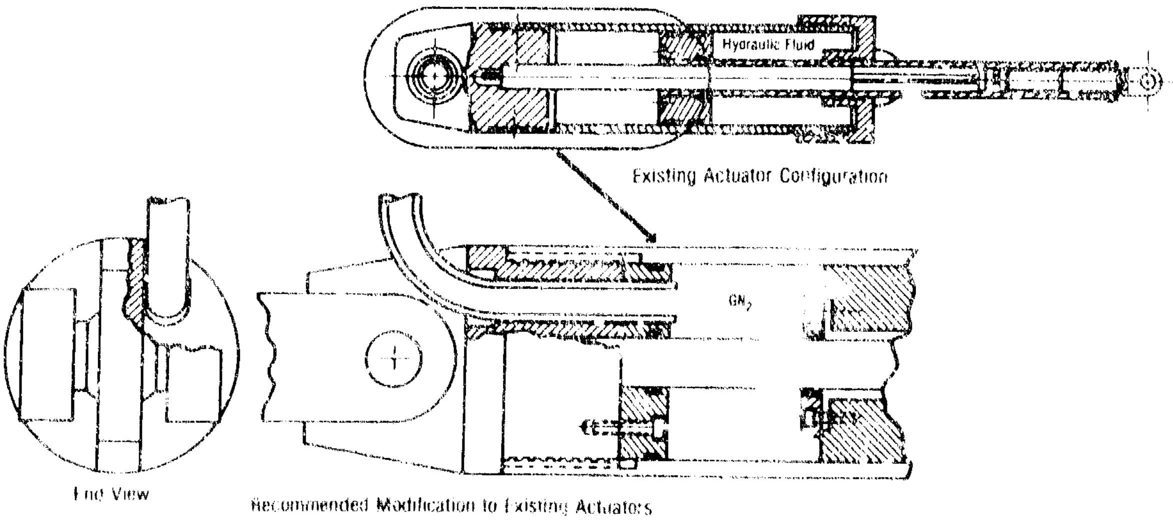

Figure 129. Recommended Modifications to Existing Pull-Only Actuators
27152

REFERENCES

1. Ellis, R. A. et al., "Hot Ball and Socket Nozzle TVC System: Static Test Report and Failure Analysis," CSD 2632-79-51, November 1979, AFRPL contract F04611-77-C-0017.

2. Baetz, J. G., "Carbon-Carbon Characterization Studies Test Report, CSD Hot Ball and Socket Nozzle - Material B," November 1979, AFRPL contract F04611-77-C-0017.

3. "Design Analysis Report, Nozzle S/N 2," CSD 2632-80-55, July 1980, AFRPL contract F04611-77-C-0017.

4. Ellis R. A., Kearney, W. J., "Strategic Missile Materials Technology (SMMT) Program, Carbon-Carbon Subscale Nozzles" CSD Final Report 2655-79-4, August 1979. NSWC contract N60921-77-C-0240.

5. "Final Report - Mechanical and Thermal Properties Hot Ball and Socket; P/N 5622 - Socket, P/N 5623 - Ball, P/N 5624 - Exit Cone: Fiber Materials, Inc., October 1981, CSD purchase order 224200.

Appendix A

ADDITIONAL TVC
DATA PLOTS
NOZZLE S/N 2

Figure A-1. Yaw Command versus Time

Figure A-2. Yaw Command Monitor versus Time

Figure A-3. Yaw Position versus Time

Figure A-4. Yaw Plus Pot Voltage versus Time

Figure A-5. Yaw Minus Pot Voltage versus Time

Figure A-6. Yaw Servovalve Current versus Time

Figure A-7. Pitch Command versus Time

Figure A-8. Pitch Command Monitor versus Time

Figure A-9. Pitch Position versus Time

Figure A-10. Pitch Plus Pot Voltage versus Time

Figure A-11. Pitch Minus Pot Voltage versus Time

Figure A-12. Pitch Servovalve Current versus Time

Figure A-13. Pitch Torque versus Time

Figure A-14. Axial Position versus Time

Figure A-15. Hydraulic Supply Flow Rate versus Time

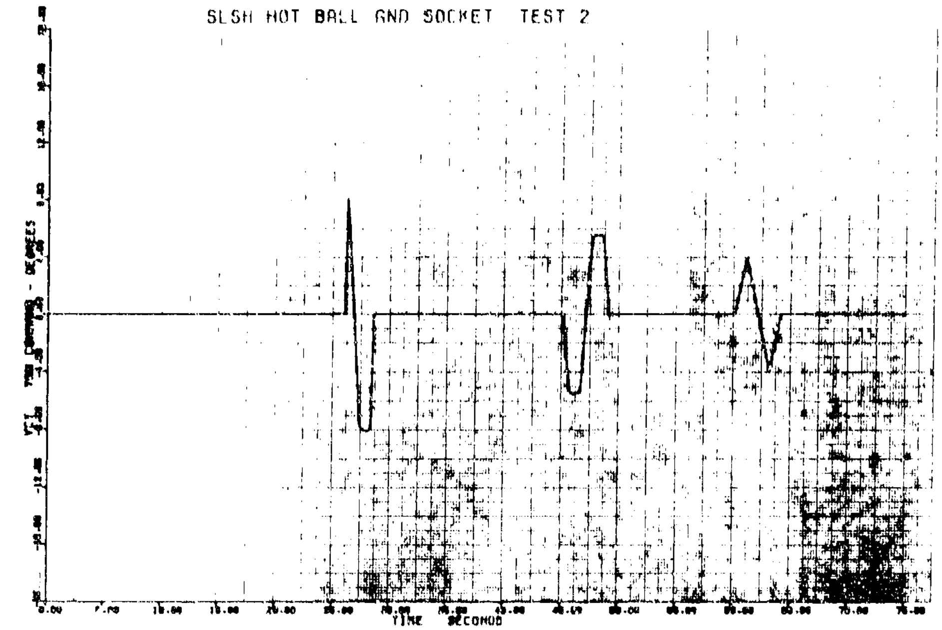

Figure A-1. Yaw Command vs Time

27161

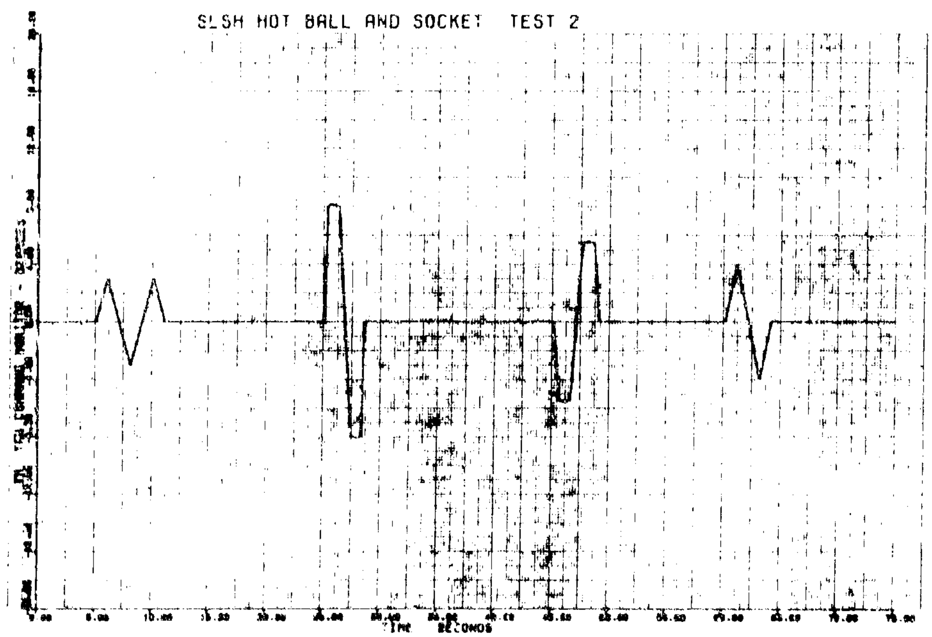

Figure A-2. Yaw Command Monitor vs Time

27162

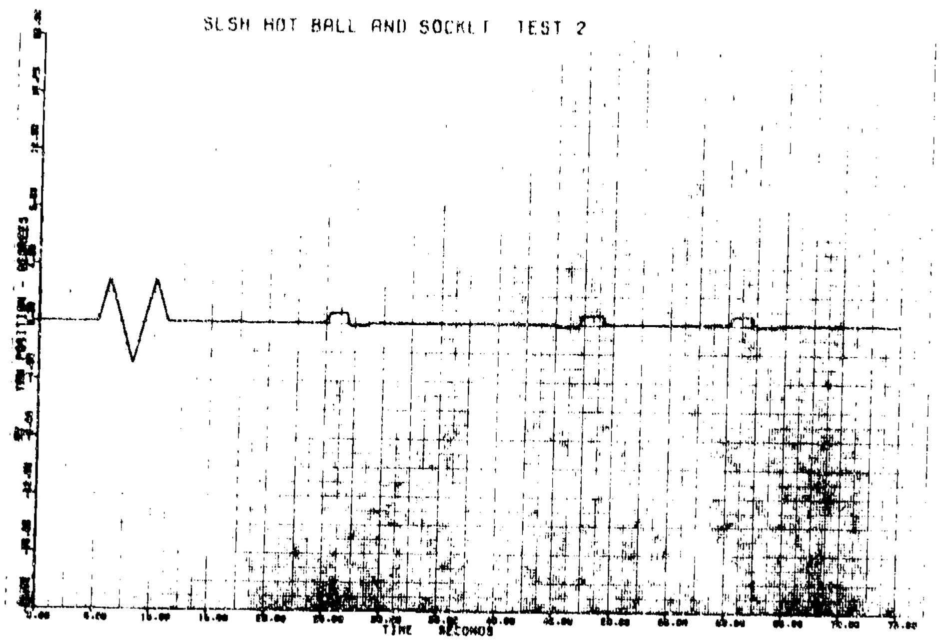

Figure A-3. Yaw Position vs Time

27163

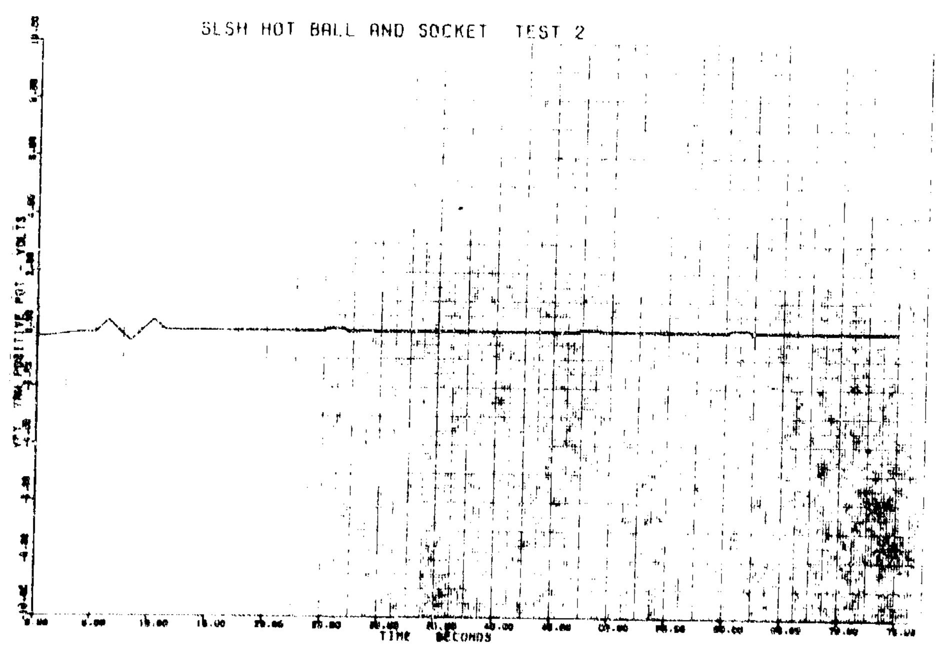

Figure A-4. Yaw Plus Pot Voltage vs Time

27164

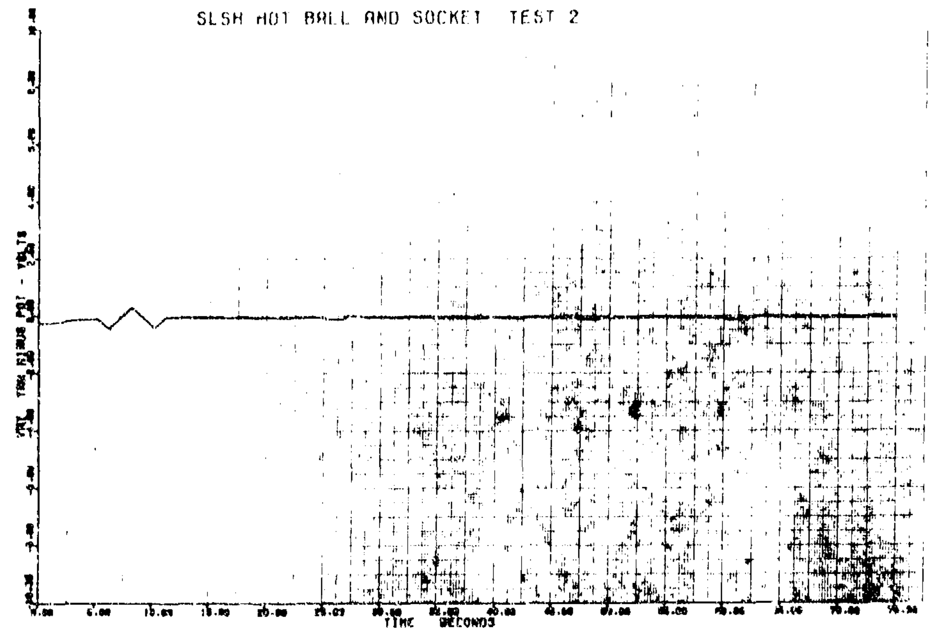

Figure A-5. Yaw Minus Pot Voltage vs Time

27165

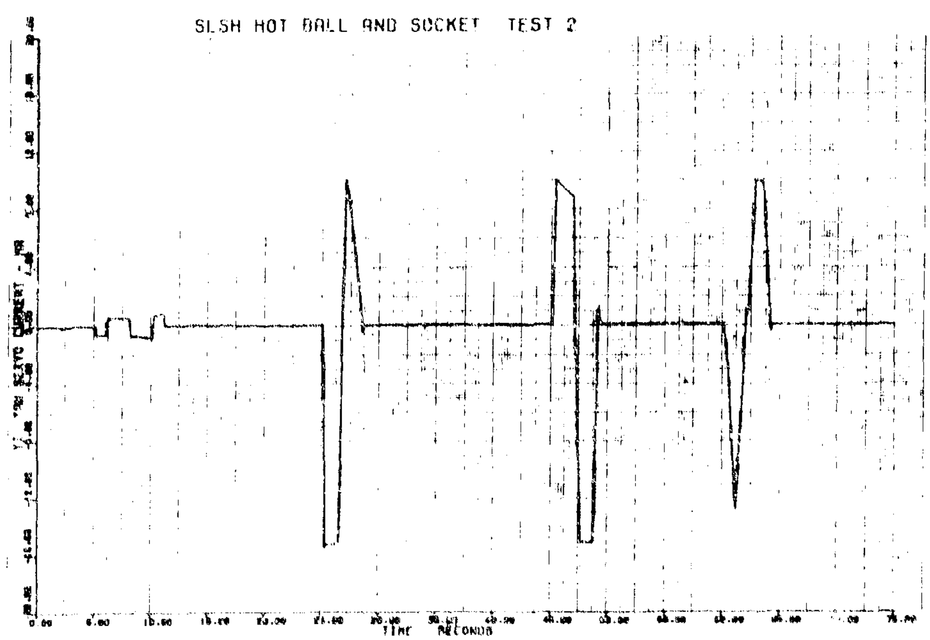

Figure A-6. Yaw Servovalve Current vs Time

27166

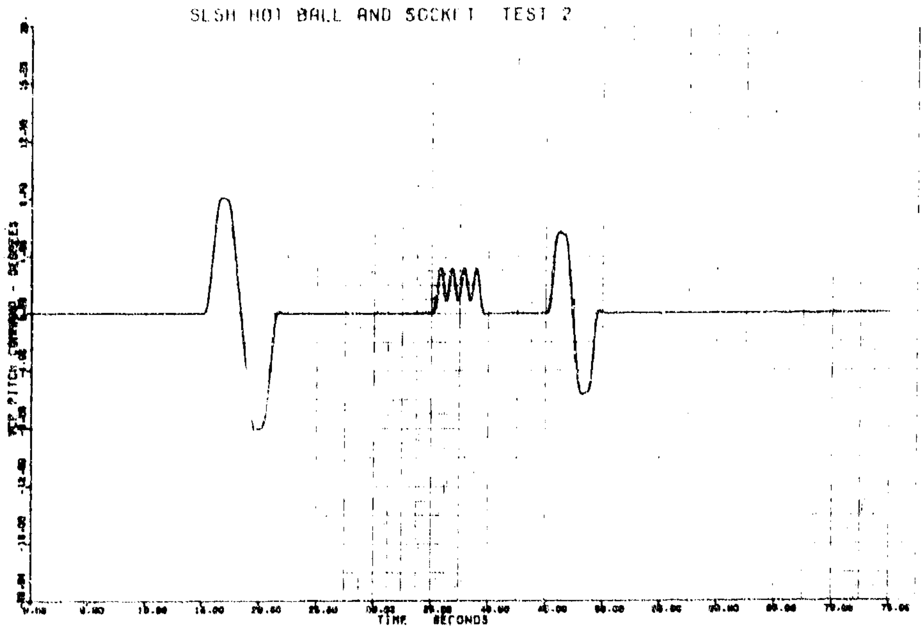

Figure A-7. Pitch Command vs Time

27168

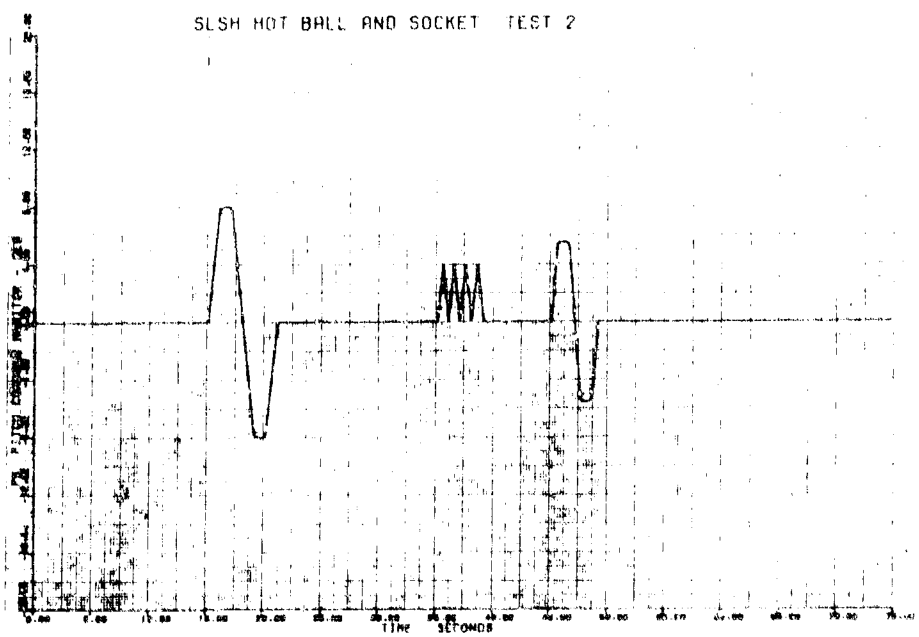

Figure A-8. Pitch Command Monitor vs Time

27169

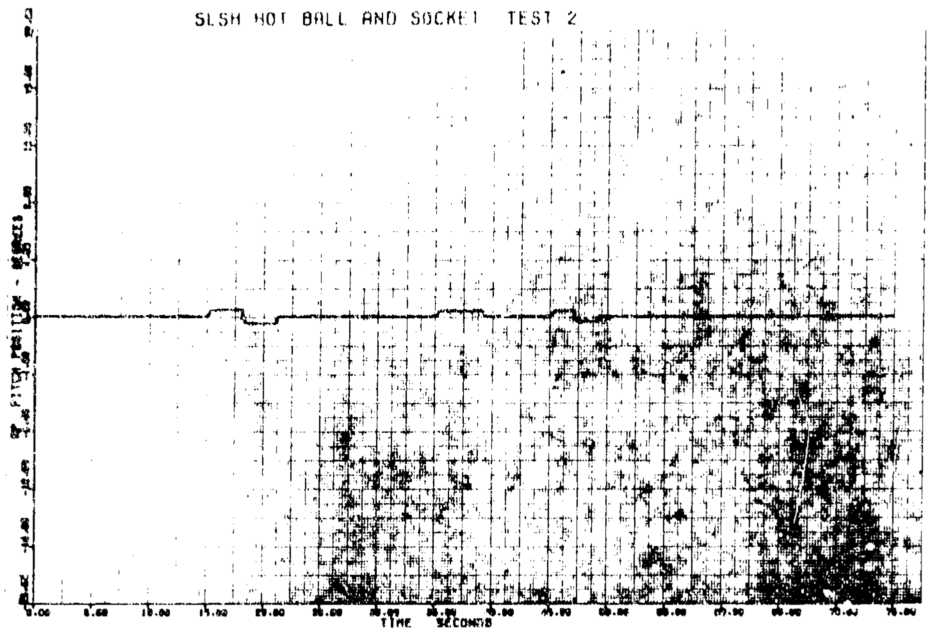

Figure A-9. Pitch Position vs Time

27170

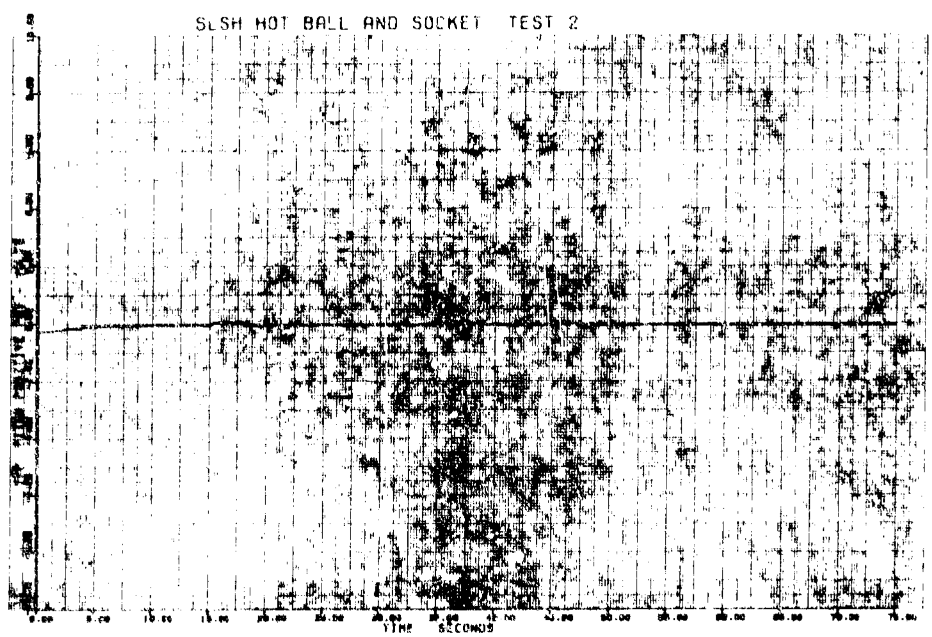

Figure A-10. Pitch Plus Pot Voltage vs Time

27171

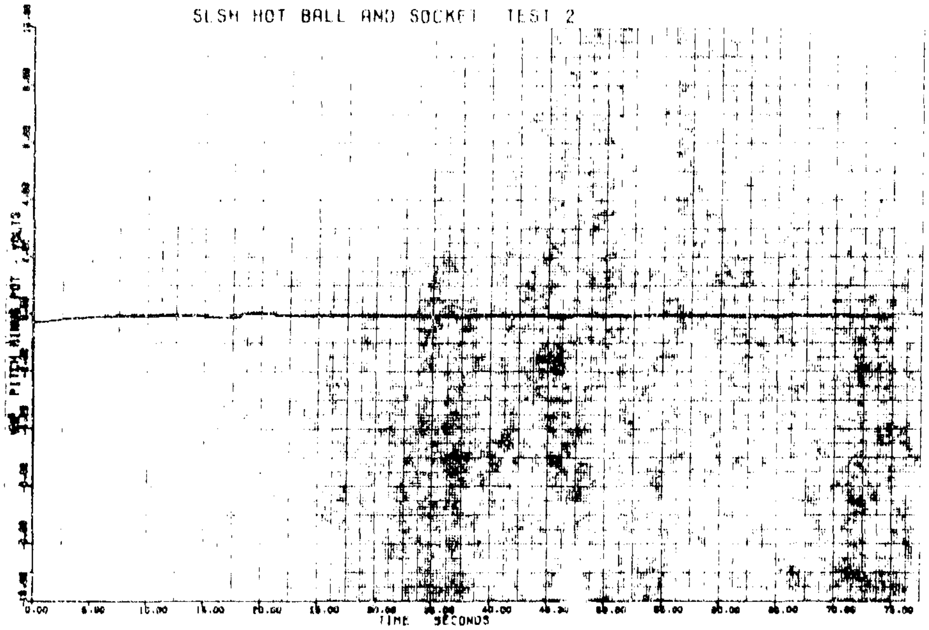

Figure A-11. Pitch Minus Pot Voltage vs Time

27172

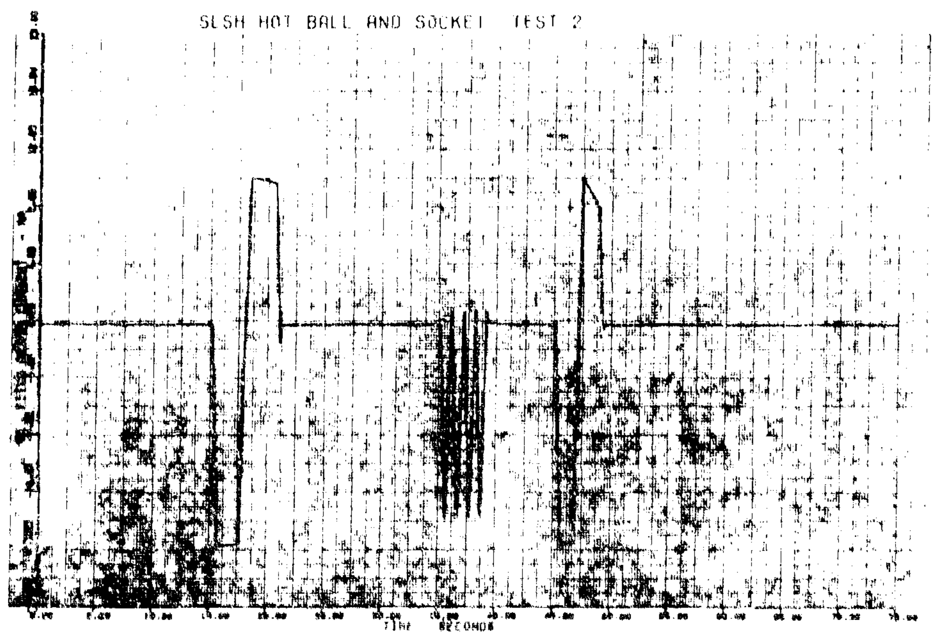

Figure A-12. Pitch Servovalve Current vs Time

27173

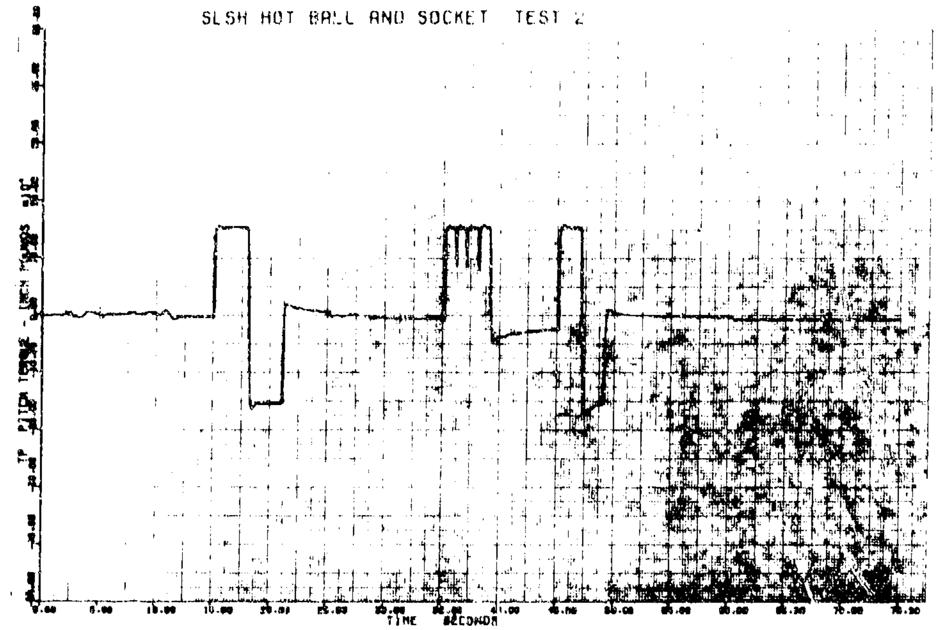

Figure A-13. Pitch Torque vs Time

27174

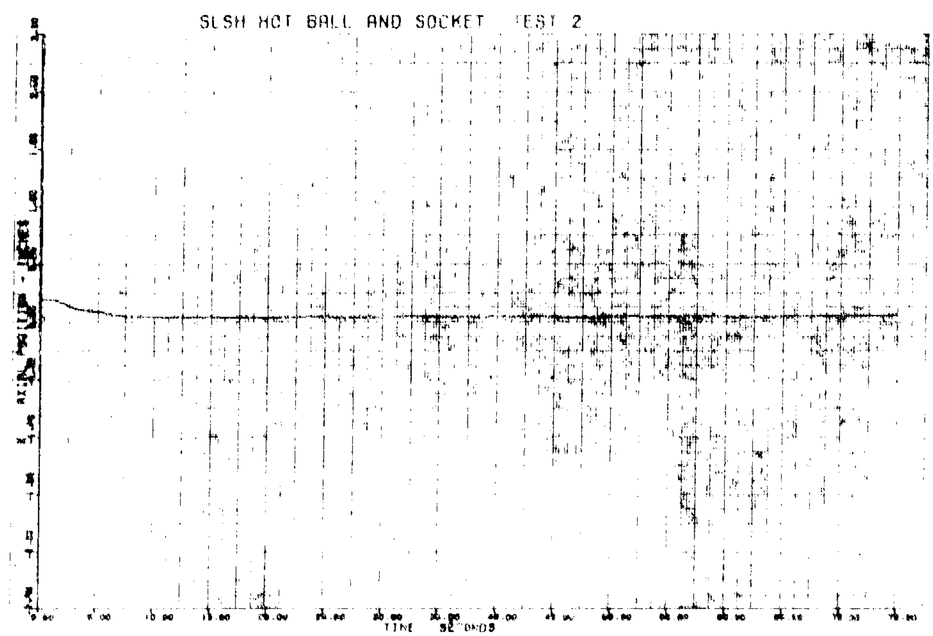

Figure A-14. Axial Position vs Time

27175

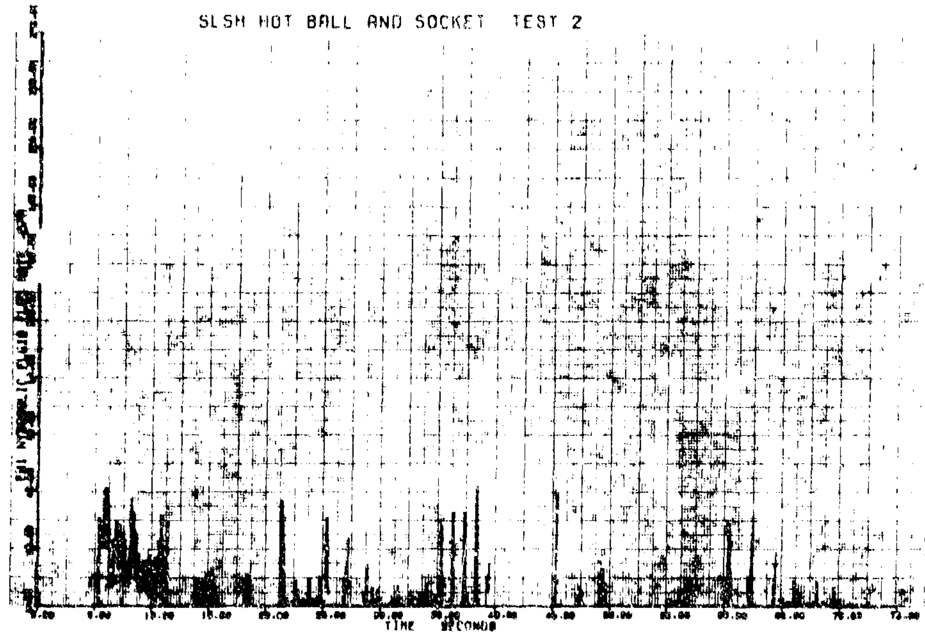

Figure A-15. Hydraulic Supply Flowrate vs Time

27176

Appendix B

ADDITIONAL MEASURED STRAIN VS TIME PLOTS
AND TEMPERATURE VS TIME PLOTS, NOZZLE S/N 2

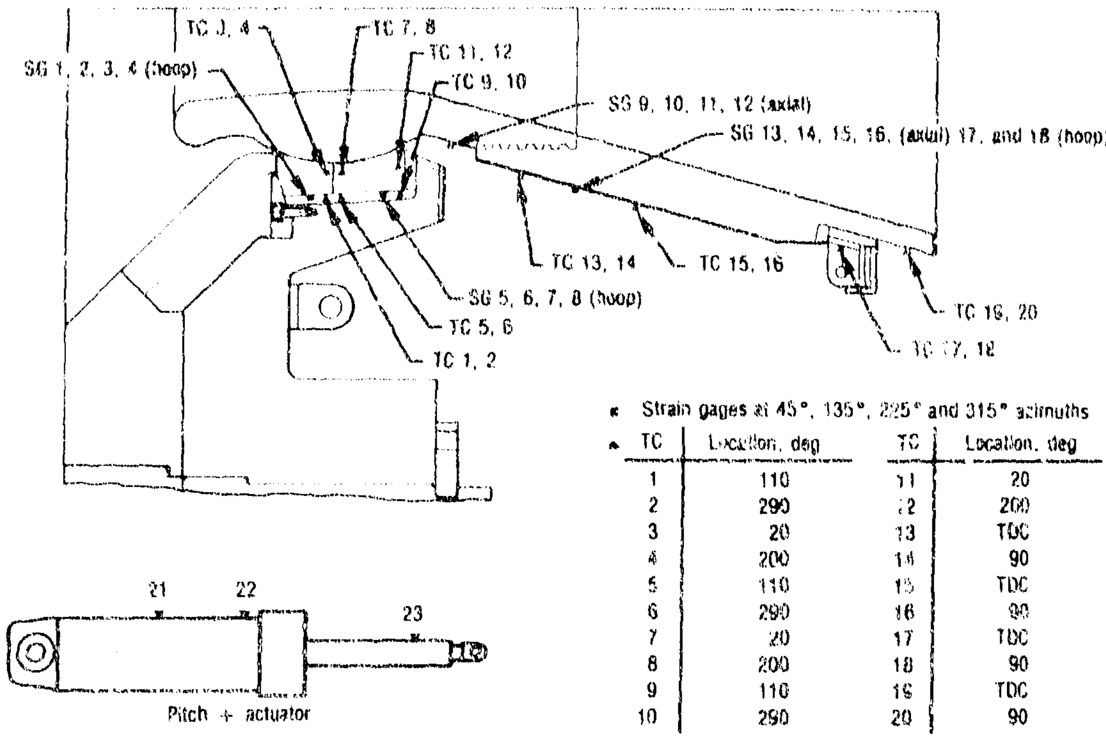

* Strain gages at 45°, 135°, 225° and 315° azimuths

TC	Location, deg	TC	Location, deg
1	110	11	20
2	290	12	200
3	20	13	TDC
4	200	14	90
5	110	15	TDC
6	290	16	90
7	20	17	TDC
8	200	18	90
9	110	19	TDC
10	290	20	90

Figure B-1. Thermocouple and Strain Gage Locations Nozzle S/N 2

18145

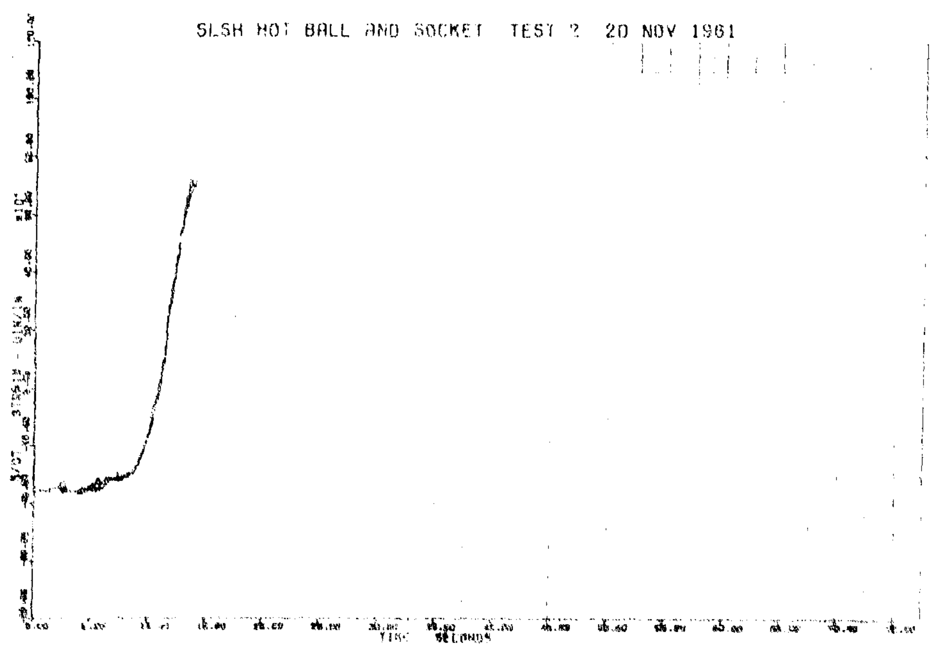

Figure B-2. Strain vs Time S/G 7

27177

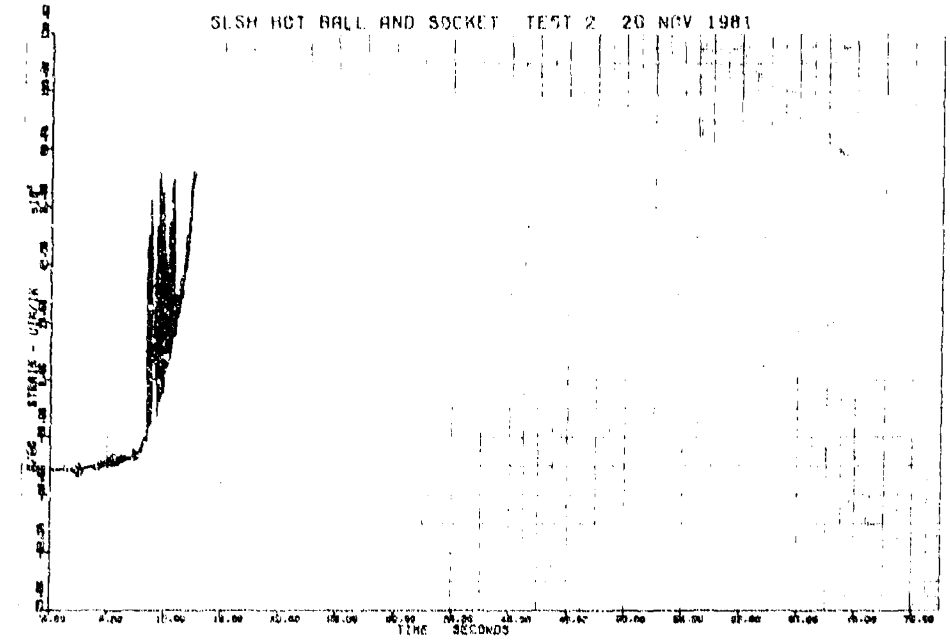

Figure B-3. Strain vs Time S/G 8

27178

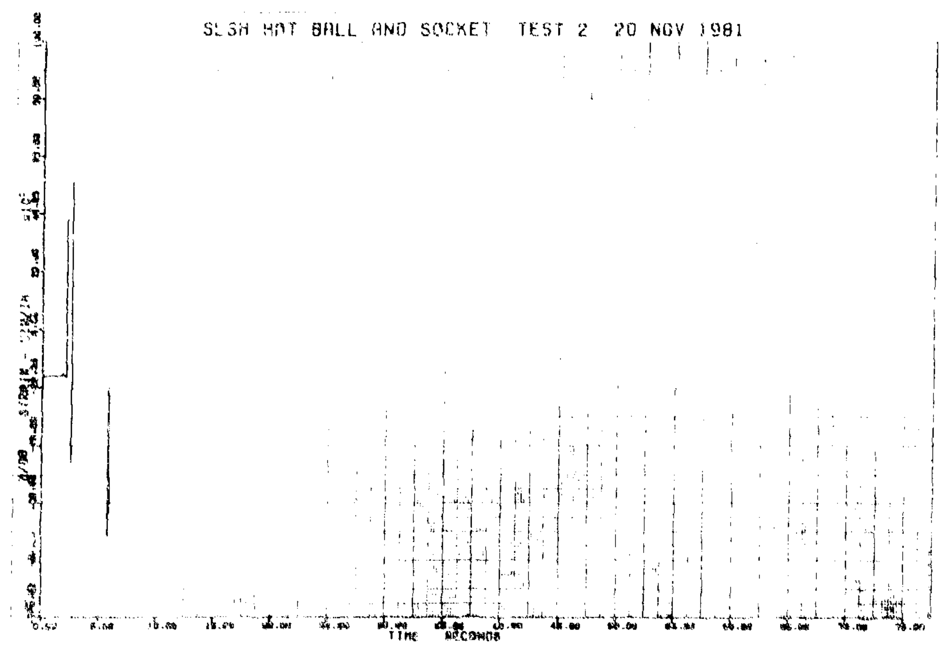

Figure B-4. Strain vs Time S/G 9

27179

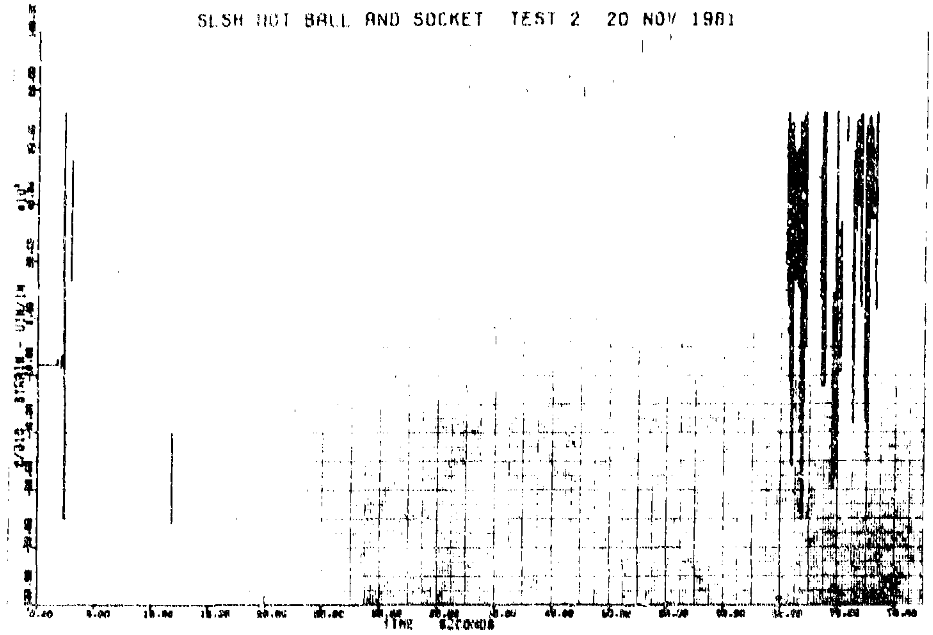

Figure B-5. Strain vs Time S/G 10

27180

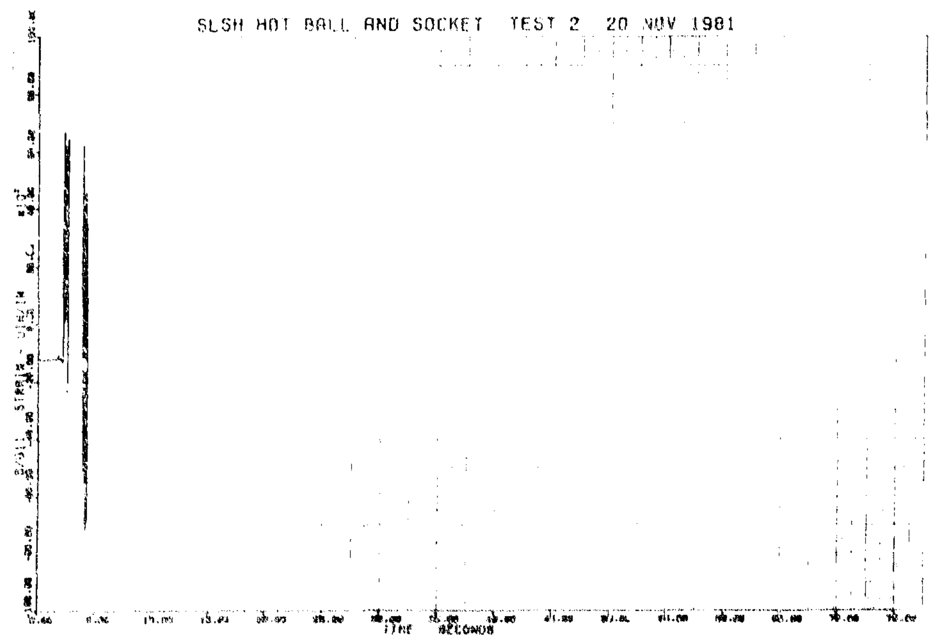

Figure B-6. Strain vs Time S/G 11

27181

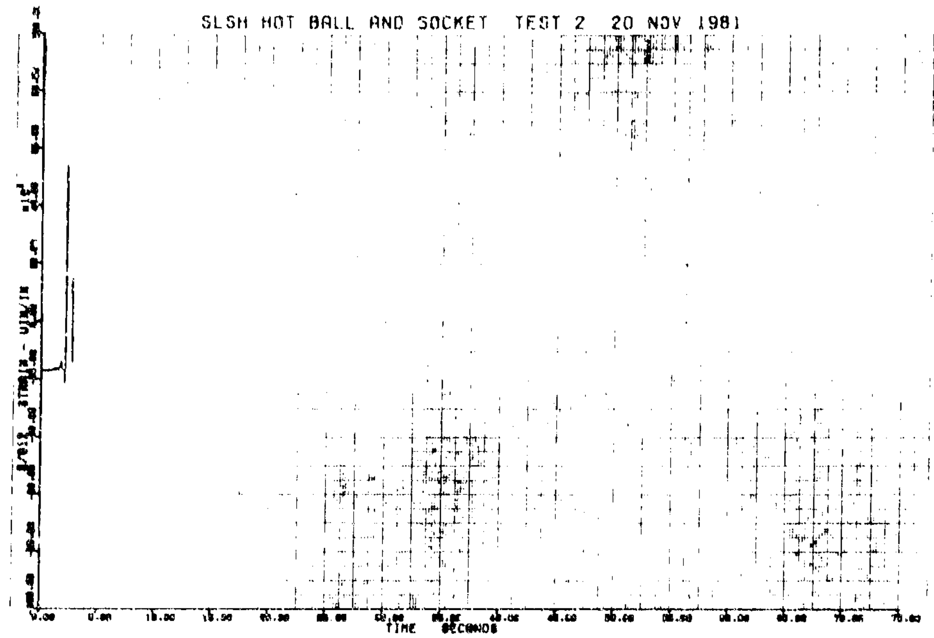

Figure B-7. Strain vs Time S/G 12

27182

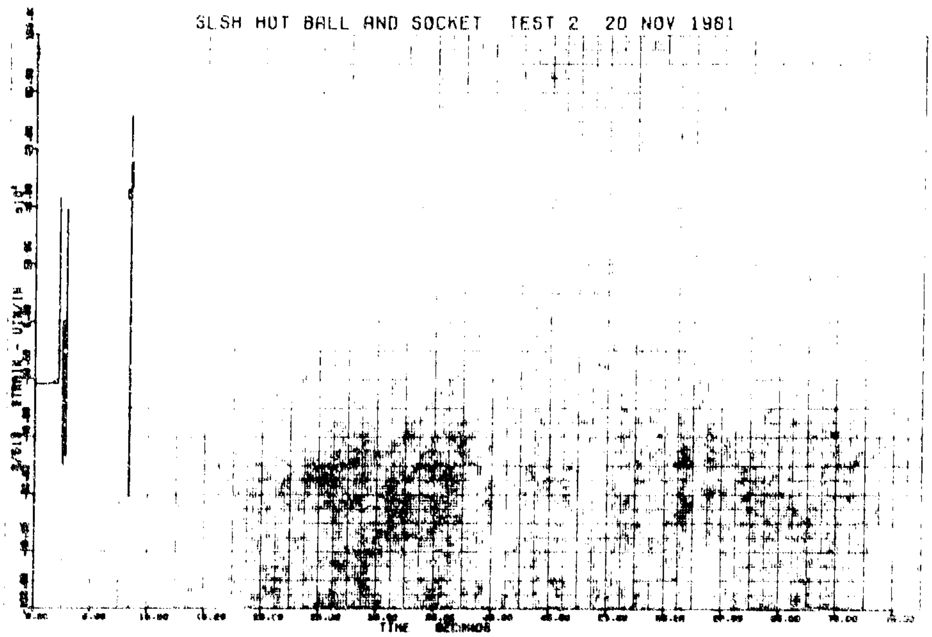

Figure B-8. Strain vs Time S/G 13

27183

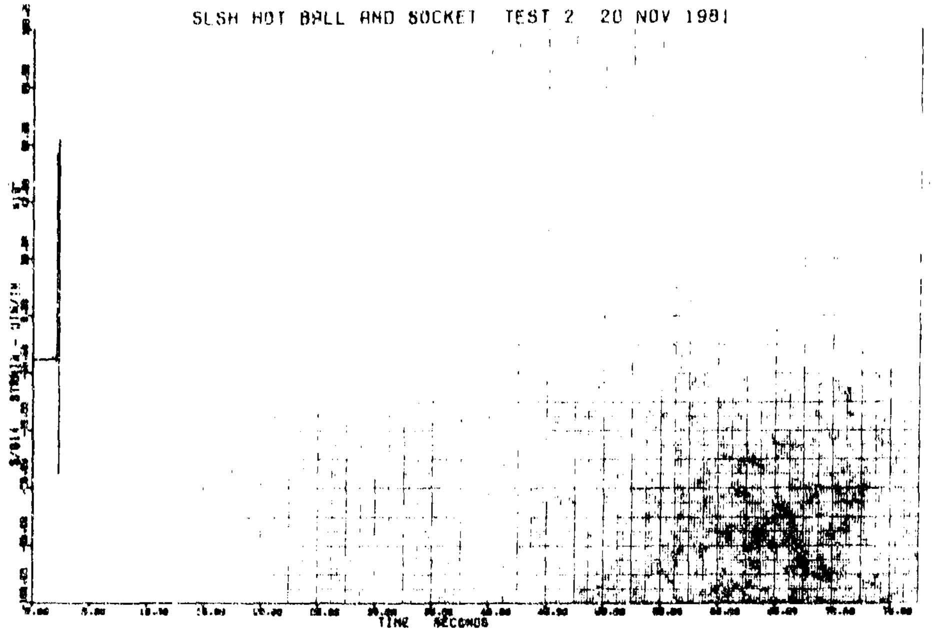

Figure B-9. Strain vs Time S/G 14

27184

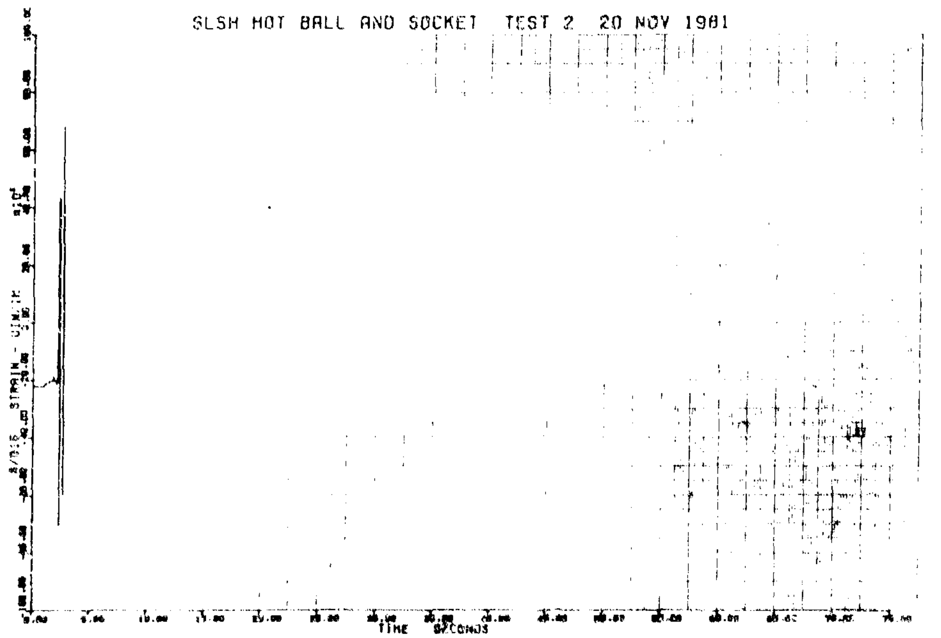

Figure B- Strain vs Time S/G 15

27187

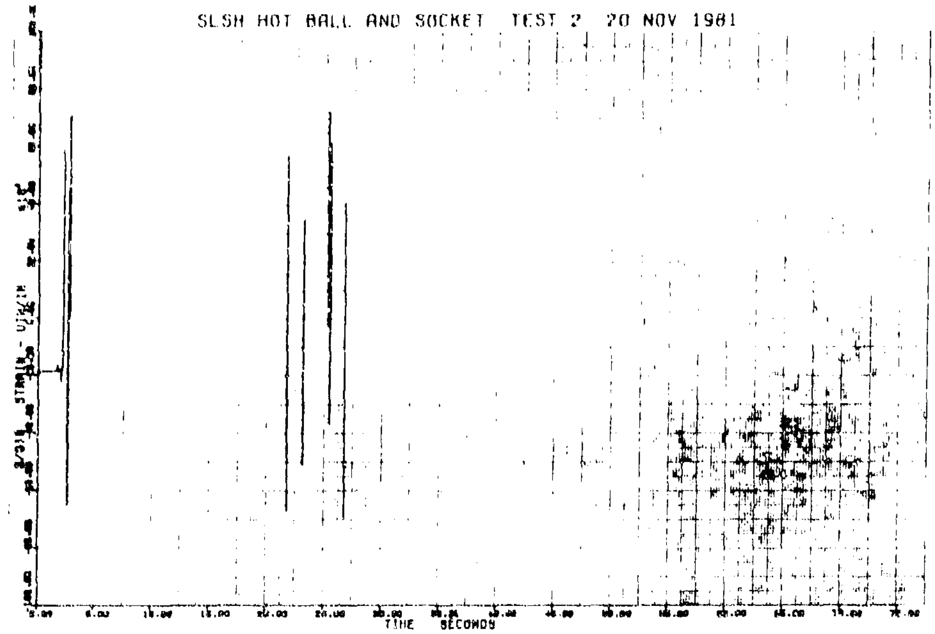

Figure B-11. Strain vs Time S/G 16

27188

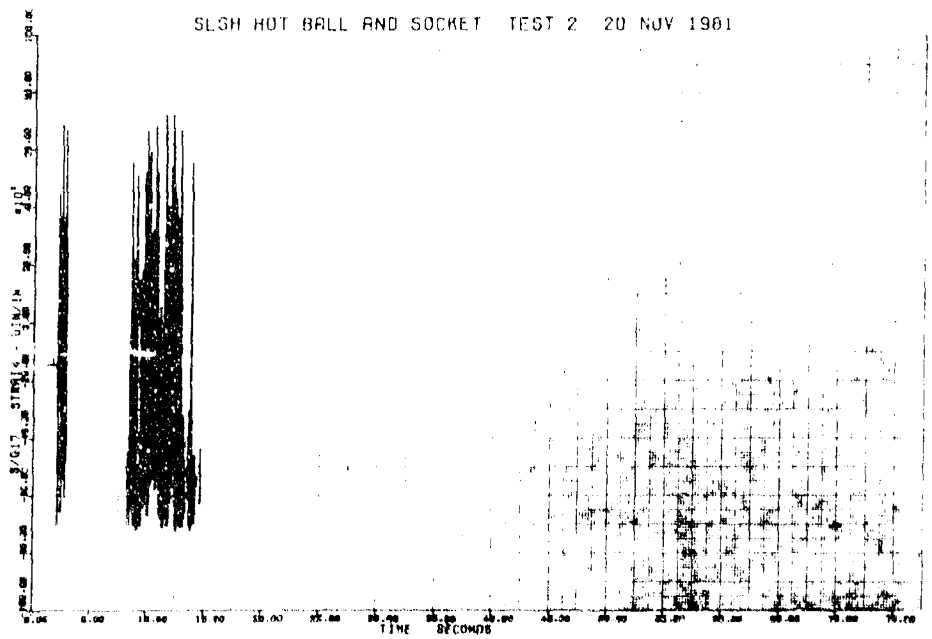

Figure B-12. Strain vs Time S/G 17

27189

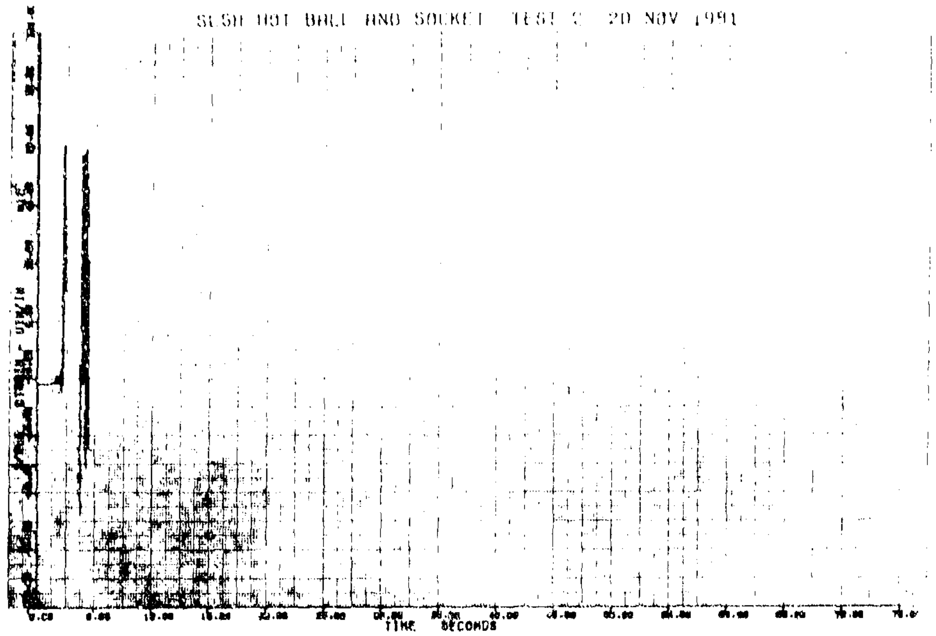

Figure B-13. Strain vs Time S/G 18

27190

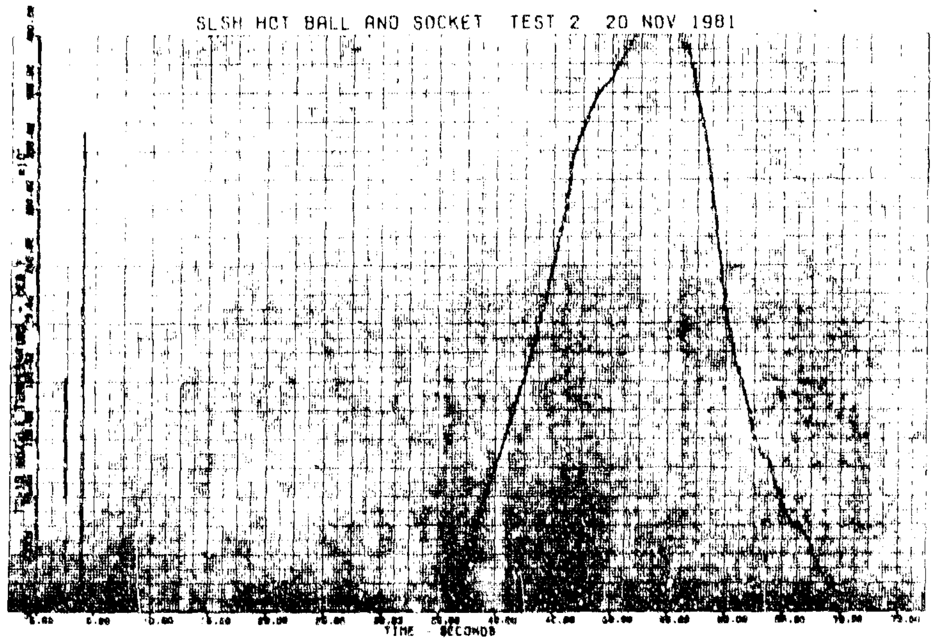

Figure B-14. Temperature vs Time, TC 13

27185

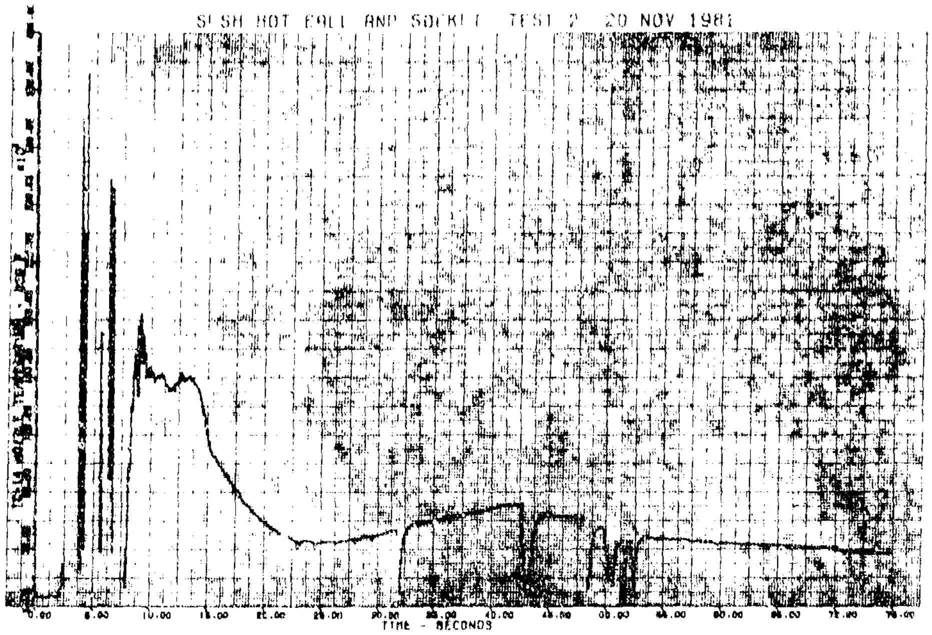

Figure B-15. Temperature vs Time, TC 14

27186

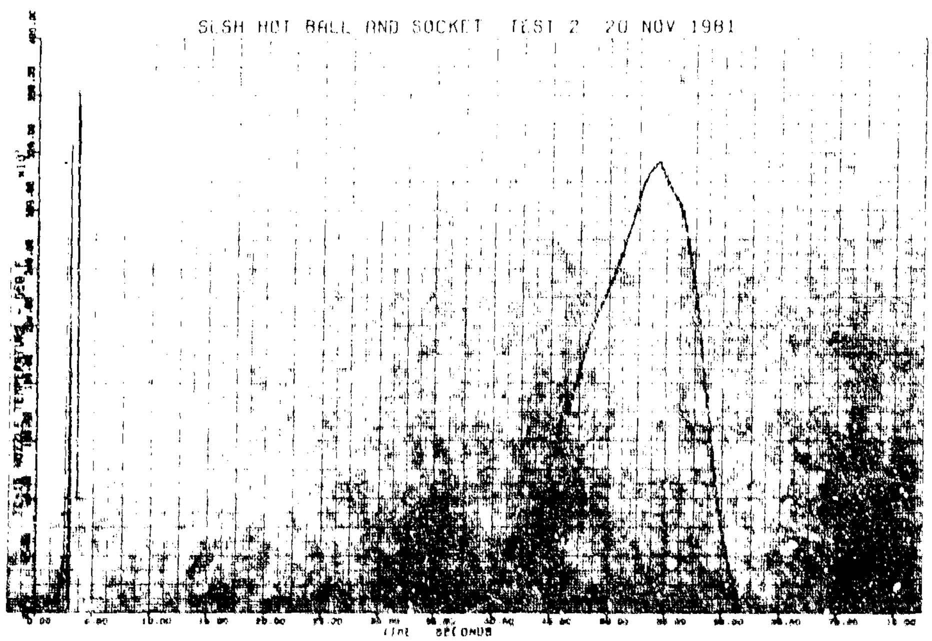

Figure B-16. Temperature vs Time, TC 15

27191

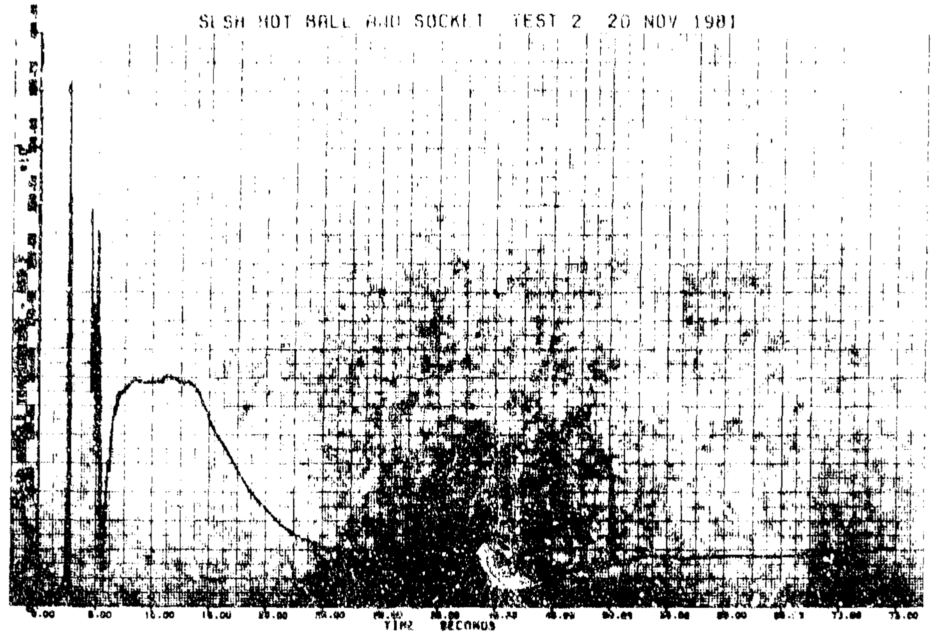

Figure B-17. Temperature vs Time, TC 16

27192

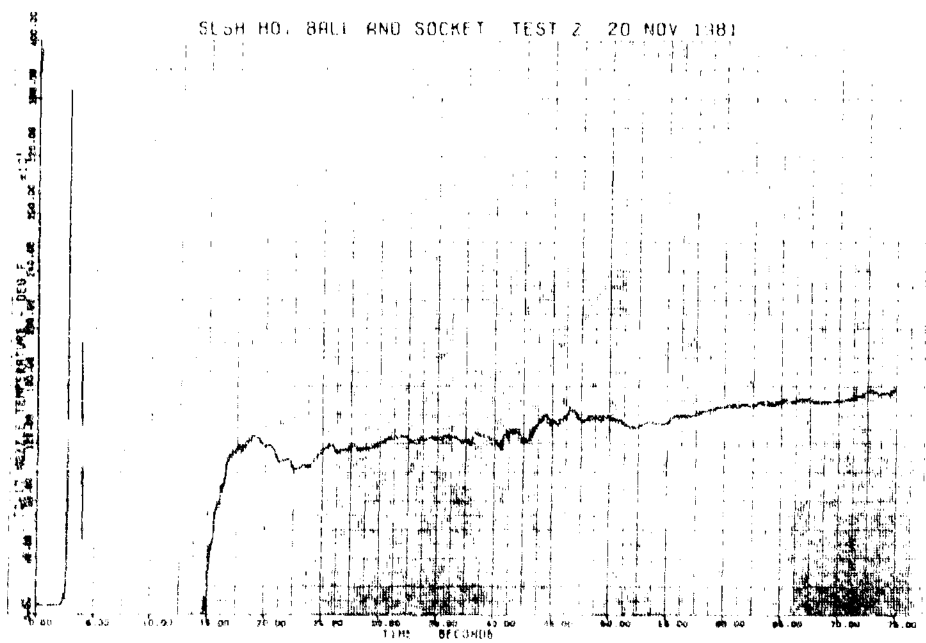

Figure B-18. Temperature vs Time, TC 17

27193

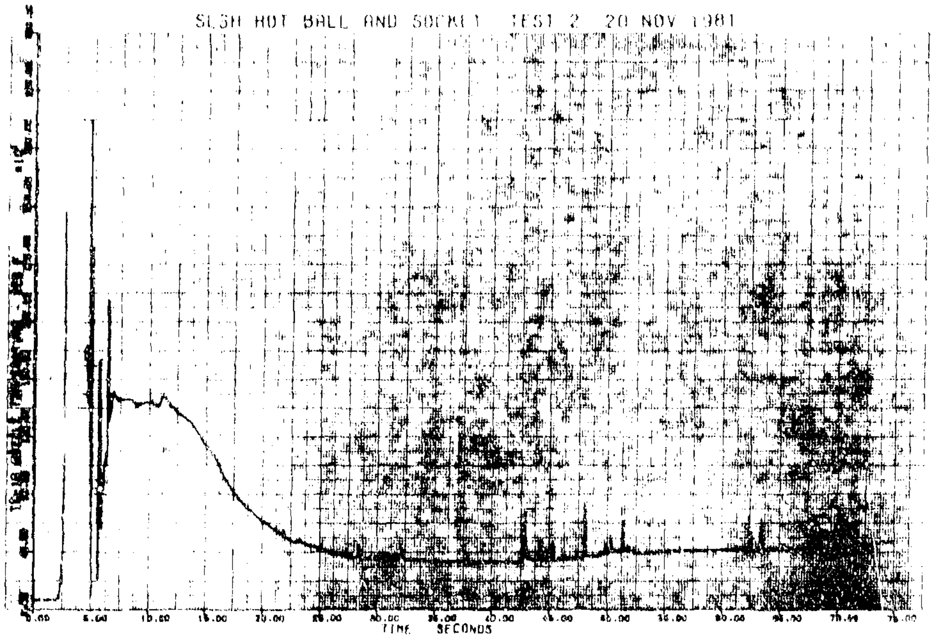

Figure B-19. Temperature vs Time, TC 18

27194

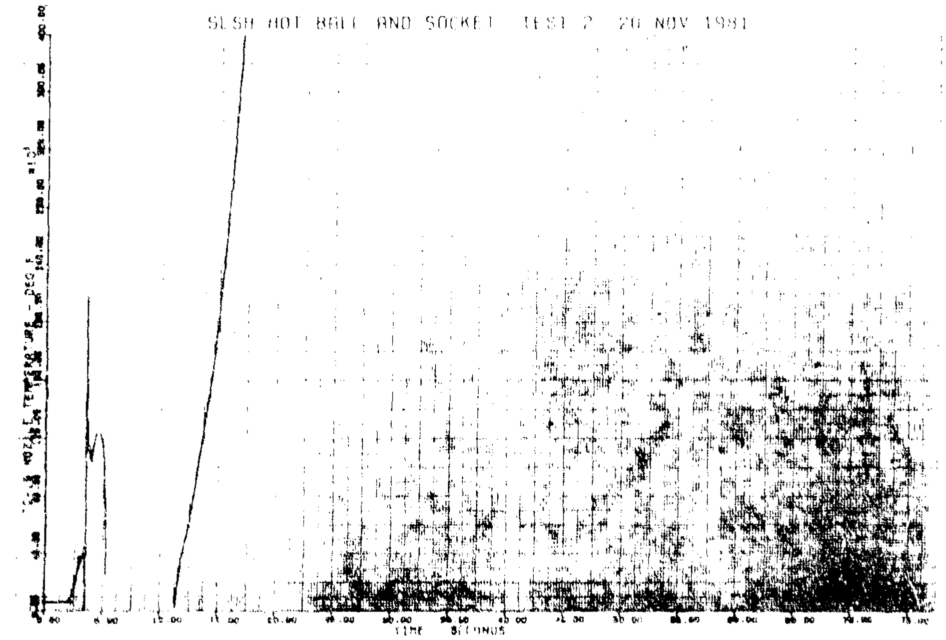

Figure B-20. Temperature vs Time, TC 19

27195

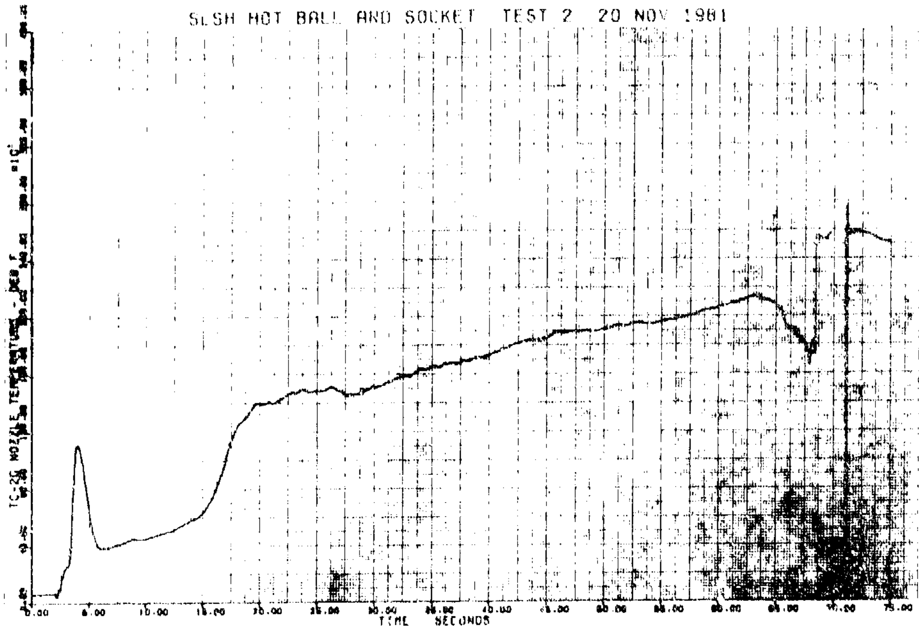

Figure B-21. Temperature vs Time, TC 20

27196